Appendixes

Supporting information

Appendix 1 Supporting information of Chapter 1

Appendix 2 Supporting information of Chapter 2

Appendix 3 Supporting information of Chapter 3

Appendix 4 Supporting information of Chapter 4

Appendix 1

Supporting information of Chapter 1

A1.1 Experimental section. General instrumentation

Elemental analyses (C, H, N) were performed on a Leco CHNS-932 microanalyser.

Thermogravimetric analysis (TG/DTA) were performed on a TG-Q500 TA Instruments thermal analyser from room temperature to 800 °C under a synthetic air atmosphere (79 % N_2/21 % O_2) at a heating rate of 10 °C min^{-1}.

FT-IR spectra of the ligand and prepared coordination compound were collected in the region of 400–4000 cm^{-1} on a Nicolet 6700 FTIR (Fourier transform infrared) spectrophotometer (Thermo Phisher Scientific, TX, USA) KBr pellets.

Photoluminescence measurements at low temperature were done in an Edinburgh Instruments FLS920 spectrometer using a close cycle helium cryostat enclosed, in an applied vacuum (10^{-7} bar). For steady state measurements in the UV-Vis range an IK3552R-G HeCd continuous laser (325 nm) was used as excitation source, whereas a Müller-Elektronik-Optik SVX1450 Xe lamp was employed to collect the excitation spectra. LDH-P-C-370 laser diode of PicoQuant was employed for recording the decay curves corresponding to the lifetimes of ns range.

Chiroptical properties: CD spectra were recorded at 25 °C on a Jasco J-815 or on an Olis DSM172 equipped with a Hamamatsu 150 W xenon arc lamp as light source. 1 cm path-length cuvettes and the following parameters were used for data acquisition on Jasco J-815: data pitch 0.5 nm; digital integration time (D.I.T.) 1 sec; scanning speed 200 nm/min; bandwidth 1 nm; accumulations 4. HT voltage was controlled (HT ≤ 800) to give reliable ellipticity values over the investigated wavelength range. CD raw data were processed with Jasco Spectra Manager 2 (Jasco) and Origin 9.5 (OriginLab Corp.). In case of compounds Cd-L_tyr (**1.8**) and Cd-D_tyr (**1.9**) 1 mm length cuvette was employed.

Circularly polarized luminescence (CPL) measurements were performed on an Olis DSM172 spectrophotometer equipped with fixed wavelengths LED (300 nm) as light source. A Hamamatsu photon counting detector for CPL measurements. Different settings and data processing were selected and carried out with the aim of ruling out the presence of any artefacts due to anisotropies.

Relaxation time measurements. Proton relaxation times T_1 and T_2 were measured at 60 MHz in a Bruker Minispec mq60 TD-NMR spectrometer working at clinical MRI field (1.4 T). Mn_gly (**1**) solutions of paramagnetic compound **1.1** was prepared at concentrations (1, 0.5, 0.1 mM relative to Mn^{2+}) were analysed. Three different measurements of T_1 and T_2 were performed for each sample and each concentration. Relaxativity values r_1 and r_2 were obtained from the slopes of the curves $1/T_1$ and $1/T_2$ *vs*. the concentration of Mn^{2+} expressed in mM. MRI

scans were carried out in a preclinical 7-T magnet (Agilent, Palo Alto, CA, USA) interfaced to Avance III electronics, using a quadrature transmit-receive coil (Bruker, Ettlingen, Germany). T_1 values were estimated from images acquired using the rapid acquisition with relaxation enhancement (RARE) sequence with inversion recovery (IT = 50, 200, 400, 800, 1500, 3000, 5500, 8000, 12,000 ms, TE = 7.0 ms, echo train length 2, data matrix size 128 × 64, field of view 30 × 15 mm^2, slice thickness = 3 mm, 1 scan).

The **X-ray powder diffraction** (XRPD) patterns were collected at 25 °C on a Phillips X'PERT powder diffractometer with Cu-Kα radiation (λ = 1.5418 Å) over the range $5 < 2\theta < 50^o$ with a step size of 0.02° and an acquisition time of 2.5 s per step. Indexation of the diffraction profiles were made by means of the FULLPROF program (pattern- matching analysis) based on the space group and the cell parameters found by single crystal X-ray diffraction.[1]

X-ray data collection of suitable single crystals were done at 100(2) K on a Bruker D8 VENTURE area detector equipped with graphite monochromated Mo−Kα radiation (λ = 0.71073 Å) by applying the ω-scan method. The data reduction was performed with the APEX270 software and corrected for absorption using SADABS.[2] Crystal structures were solved by direct methods using the SIR97 program[3] and refined by full-matrix least-squares on F2 including all reflections using anisotropic displacement parameters by means of the WINGX[4] crystallographic package. All hydrogen atoms were included as fixed contributions riding on attached atoms with isotropic thermal displacement parameters 1.2 times or 1.5 times those of their parent atoms for the organic ligands. Lattice solvent molecules could not be refined owing to their disordered disposition in the voids of the structures. so the electron density at the voids was subtracted from the reflection data by the SQUEEZE procedure as implemented in PLATON program[5] during the refinement.

A1.2 Chemical characterization

A1.2.1 Elemental Analysis

Table A1.1. Elemental analysis of compound **1.1**–**1.9**.

Compound	Formula	Molecular weight	Calc.	Found.
Mn_gly (**1.1**)	$C_{10}H_{26}Mn_2N_{10}O_{10}$	556.27	C: 21.67; H: 4.36; Mn: 19.82; N: 25.27; O: 28.87;	C: 21.65; H: 4.38; Mn: 19.85; N: 25.29; O: 28.82;
Zn-L_val (**1.2**)	$C_8H_{13}N_5O_2Zn$	276.60	C: 34.99; H: 4.77; N: 25.50; O: 11.65; Zn: 23.08;	C: 35.03; H: 4.77; N: 25.52; O: 11.65; Zn: 23.11;
Zn-D_val (**1.3**)	$C_8H_{13}N_5O_2Zn$	276.60	C: 34.99; H: 4.77; N: 25.50; O: 11.65; Zn: 23.08;	C: 35.06; H: 4.73; N: 25.48; O: 11.66; Zn: 23.10;
Zn-L_phen (**1.4**)	$C_{12}H_{13}N_5O_2Zn$	324.64	C: 44.67; H: 4.06; N: 21.71; O: 9.92; Zn: 19.64;	C: 44.69; H: 4.10; N: 21.73; O: 9.98; Zn: 19.66;
Zn-D_phen (**1.5**)	$C_{12}H_{13}N_5O_2Zn$	324.64	C: 44.67; H: 4.06; N: 21.71; O: 9.92; Zn: 19.64;	C: 44.72; H: 4.09; N: 21.72; O: 9.95; Zn: 19.72;
Zn-L_tyr (**1.6**)	$C_{12}H_{15}N_5O_4Zn$	356.62	C: 40.41; H: 4.24; N: 19.64; O: 17.94; Zn: 17.77	C: 40.44; H: 4.26; N: 19.63; O: 17.96; Zn: 17.72
Zn-D_tyr (**1.7**)	$C_{12}H_{15}N_5O_4Zn$	356.62	C: 40.41; H: 4.24; N: 19.64; O: 17.94; Zn: 17.77	C: 40.49; H: 4.21; N: 19.68; O: 17.99; Zn: 17.74
Cd-L_tyr (**1.8**)	$C_{12}H_{15}N_5O_4Cd$	405.68	C: 35.53; H: 3.73; N: 17.26; O: 15.78; Cd: 27.71	C: 35.55; H: 3.81; N: 17.30; O: 15.80; Cd: 27.74
Cd-D_tyr (**1.9**)	$C_{12}H_{15}N_5O_4Cd$	405.68	C: 35.53; H: 3.73; N: 17.26; O: 15.78; Cd: 27.71	C: 35.58; H: 3.72; N: 17.21; O: 15.82; Cd: 27.69

A1.2.2 FT-IR spectroscopy

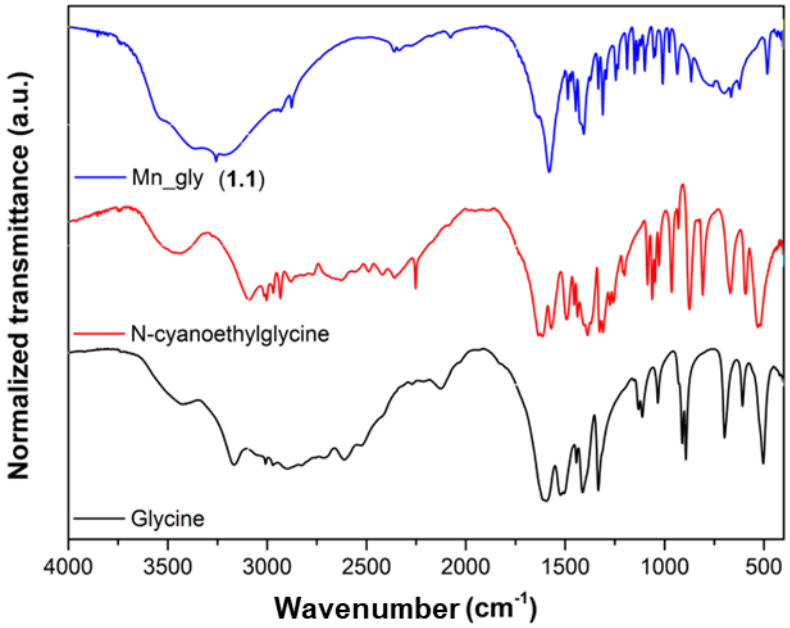

Figure A1.1. Figure of the infrared spectra of glycine, N-cyanoethylglycine, and compound **1.1**.

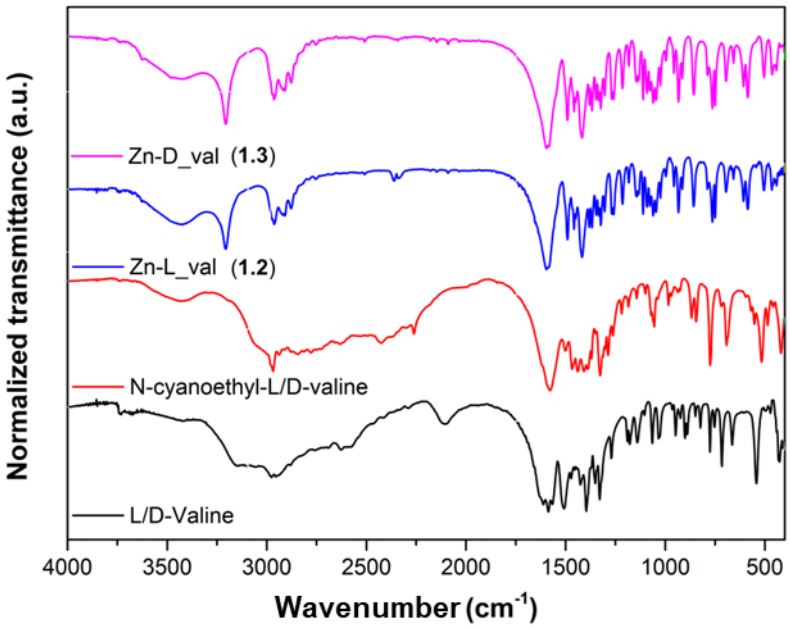

Figure A1.2. Figure of the infrared spectra of L/D-.valine, N-cyanoethyl-L/D-valine and compounds **1.2** and **1.3**

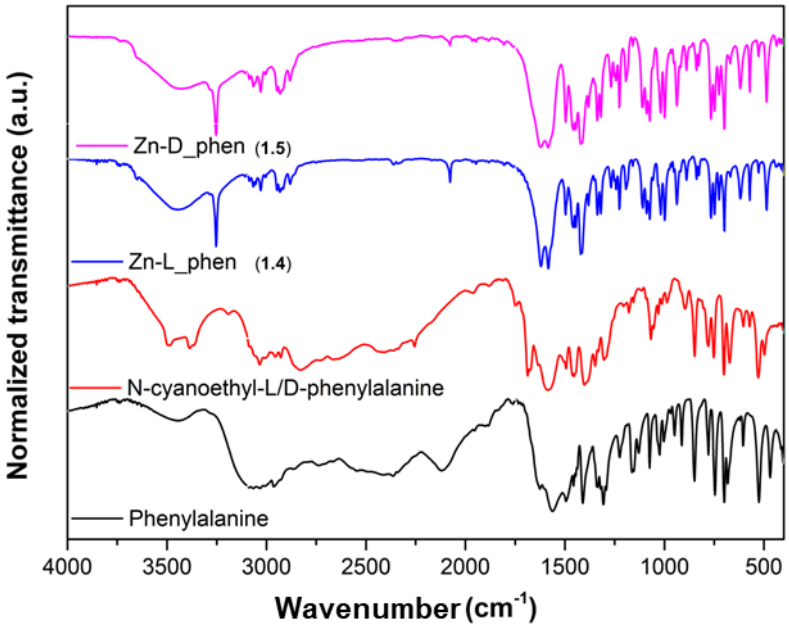

Figure A1.3. Figure of the infrared spectra of L/D-phenylalanine, N-cyanoethyl-L/D-phenylalanine and compounds **1.4** and **1.5.**

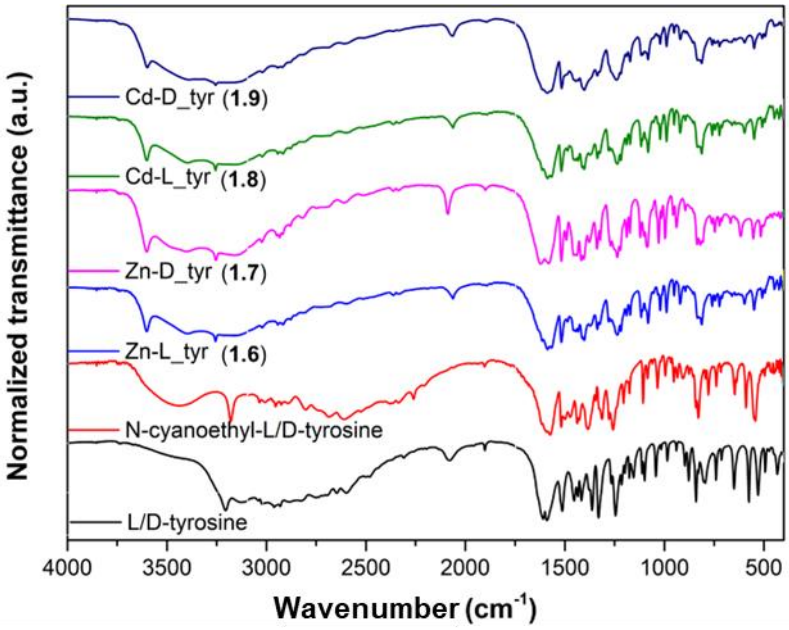

Figure A1.4. Figure of the infrared spectra of L/D-.tyrosine, N-cyanoethyl-L/D-tyrosine and compounds **1.6-1.9.**

A1.3 Crystallographic data

Table A1.2. Crystallographic data and structure refinement details of compounds.

Compound	Mn_gly (1.1)	Zn-L_val (1.2)	Zn-D_val (1.3)	Zn-D_phen (1.5)	Zn-L_tyr (1.6)	Zn-D_tyr (1.7)
Formula	$C_{10}H_{26}N_{10}O_{10}Mn_2$	$C_8H_{13}N_5O_2Zn$	$C_8H_{13}N_5O_2Zn$	$C_{12}H_{13}N_5O_2Zn$	$C_{12}H_{15}N_5O_4Zn$	$C_{12}H_{15}N_5O_4Zn$
M_r	556.27	276.60	276.60	324.64	358.66	358.66
Crystal system	monoclinic	orthorhombic	orthorhombic	monoclinic	orthorhombic	orthorhombic
Space group (no.)	$P2_1/c$	$P2_12_12_1$	$P2_12_12_1$	$P2_1$	$P2_12_12_1$	$P2_12_12_1$
a(Å)	7.4487(4)	9.8513(5)	9.84150(10)	8.4042(7)	7.775(5)	7.7416(5)
b(Å)	12.8875(7)	10.2910(5)	10.29580(10)	7.0871(6)	8.131(4)	8.1157(5)
c(Å)	12.2672(6)	10.7406(6)	10.73980(10)	11.4564(8)	22.863(12)	22.8643(16)
α(°)	90	90	90	90	90	90
β(°)	116.755(3)	90	90	98.231(3)	90	90
γ(°)	90	90	90	90	90	90
V(Å^3)	1051.52(10)	1088.88(10)	1088.222(18)	675.33(9)	1445.4(14)	1436.53(16)
Z	2	4	4	2	4	4
ρ_{calc} g/cm^3	1.751	1.687	1.688	1.597	1.648	1.658
μ/mm^{-1}	1.273	2.249	2.251	1.827	1.726	1.736
F(000)	568.0	568.0	568.0	332.0	736.0	736.0
Crystal size/mm^3	0.21 × 0.20 × 0.08	0.23 × 0.16 × 0.08	0.24 × 0.17 × 0.07	0.22 × 0.17 × 0.12	0.29 × 0.16 × 0.14	0.28 × 0.18 × 0.13
Radiation	MoKα (λ = 0.71073)	MoKα (λ = 0.71073)	MoKα (λ = 0.71073)	MoKα (λ = 0.71073)	MoKα (λ = 0.71073)	MoKα (λ = 0.71073)
2θ range for data collection/°	4.88 to 57.512	5.482 to 56.7	5.482 to 54.692	4.898 to 54.528	5.318 to 52.806	5.326 to 57.396
Index ranges	-10 ≤ h ≤ 10. -17 ≤ k ≤ 17. -16 ≤ l ≤ 16	-7 ≤ h ≤ 13. -12 ≤ k ≤ 13. -13 ≤ l ≤ 12	-11 ≤ h ≤ 11. -13 ≤ k ≤ 13. -13 ≤ l ≤ 13	-10 ≤ h ≤ 10. -9 ≤ k ≤ 9. -14 ≤ l ≤ 14	-9 ≤ h ≤ 9. -10 ≤ k ≤ 9. -28 ≤ l ≤ 28	-10 ≤ h ≤ 10. -10 ≤ k ≤ 10. -28 ≤ l ≤ 30
Reflections collected	52897	6556	7635	14675	14301	15421

Independent reflections	2714 [R_{int} = 0.0394. R_{sigma} = 0.0124]	2487 [R_{int} = 0.0141. R_{sigma} = 0.0290]	2236 [R_{int} = 0.0238. R_{sigma} = 0.0241]	2990 [R_{int} = 0.0724. R_{sigma} = 0.0504]	2906 [R_{int} = 0.0950. R_{sigma} = 0.0668]	3664 [R_{int} = 0.0368. R_{sigma} = 0.0398]
Data/restraints/parameters	2714/0/193	2487/0/148	2236/0/146	2990/1/181	2906/0/208	3664/0/203
Goodness-of-fit on F^2	1.082	1.076	0.944	1.047	1.000	1.176
Final R indexes [I>=2σ (I)]	R_1 = 0.0307. wR_2 = 0.0751	R_1 = 0.0153. wR_2 = 0.0387	R_1 = 0.0175. wR_2 = 0.0434	R_1 = 0.0268. wR_2 = 0.0571	R_1 = 0.0221. wR_2 = 0.0440	R_1 = 0.0288. wR_2 = 0.0623
Final R indexes [all data]	R_1 = 0.0337. wR_2 = 0.0775	R_1 = 0.0157. wR_2 = 0.0388	R_1 = 0.0181. wR_2 = 0.0438	R_1 = 0.0342. wR_2 = 0.0592	R_1 = 0.0386. wR_2 = 0.0456	R_1 = 0.0323. wR_2 = 0.0635
Largest diff. peak/hole / e $Å^{-3}$	1.01/-0.73	0.37/-0.73	0.31/-0.23	0.51/-0.34	0.33/-0.63	0.32/-0.70
Flack parameter	-	0.014(10)	0.994(13)	-0.006(8)	0.021(15)	0.029(6)

Table A1.3. Table of the selected bond lengths (Å) and angles (°) for compound **1.1**-**1.7**.

Mn_gly (1.1)			**Zn-L_val (1.2)**			**Zn-D_val (1.3)**		
Mn1	O11	2.1644(13)	Zn1	N1	2.0450(17)	Zn1	N1	2.005(2)
Mn1	O1W	2.1709(13)	Zn1	N4[1]	2.0067(17)	Zn1	N4	2.046(2)
Mn1	O2W	2.2373(14)	Zn1	N8	2.1258(16)	Zn1	N8	2.128(2)
Mn1	N8	2.3004(15)	Zn1	O11	2.1325(14)	Zn1	O11	2.1295(17)
Mn1	N1	2.2345(14)	Zn1	O12[2]	2.0816(14)	Zn1	O11	2.1295(17)
Mn1	N2[1]	2.2456(15)						
[1]1-x. -1-y. 1-z			[1]1/2-x. 1-y. 1/2+z; [2]-1/2+x. 1/2-y. 2-z					

Zn-D_phen (1.5)			**Zn-L_tyr (1.6)**			**Zn-D_tyr (1.7)**		
Zn1	O11	1.978(2)	Zn1	O12	2.162(2)	Zn1	O12[1]	2.1555(19)
Zn1	N4	2.141(3)	Zn1	O11[1]	1.964(2)	Zn1	O11	1.963(2)
Zn1	O12	2.117(3)	Zn1	N4[2]	2.156(3)	Zn1	N4[2]	2.150(3)
Zn1	N8	2.126(3)	Zn1	N8	2.112(2)	Zn1	N8[1]	2.114(2)
Zn1	N1	2.014(3)	Zn1	N1	2.019(3)	Zn1	N1[1]	2.017(3)
			Zn1	O12	2.162(2)	Zn1	O12[1]	2.1555(19)
			[1]1/2+x. 1/2-y. -z; [2]1/2+x.-1/2-y.-z			[1]1/2+x.1/2-y.1-z; [2]+x.-1+y.+z		

	Atom 1	Atom 2	Atom 3	Angle 2.1.3 [°]		Atom 1	Atom 2	Atom 3	Angle 2.1.3 [°]
Mn_gly	O11	Mn1	O1W	90.70(5)					
	O11	Mn1	O2W	91.10(5)					
	O11	Mn1	N8	74.85(5)					
	O11	Mn1	N1	160.37(5)					
	O11	Mn1	N2[1]	95.51(5)					
	O1W	Mn1	O2W	176.40(5)					
	O1W	Mn1	N8	93.05(5)					
	O1W	Mn1	N1	90.81(5)					
	O1W	Mn1	N2[1]	89.04(5)					
	O2W	Mn1	N8	90.42(5)					
	O2W	Mn1	N2[1]	87.69(5)					
	N1	Mn1	O2W	88.54(5)					
	N1	Mn1	N8	85.53(5)					
	N1	Mn1	N2[1]	104.09(5)					
	N2[1]	Mn1	N8	170.14(5)					
	[1]1-x. -1-y. 1-z								
Zn-L_val	N1	Zn1	N8	143.98(7)	**Zn-D_val**	N1	Zn1	N8	96.67(9)
	N1	Zn1	O11	88.03(6)		N1	Zn1	O11	97.28(8)
	N1	Zn1	O12[1]	90.72(6)		N1	Zn1	O12	100.83(8)
	N4[2]	Zn1	N1	117.97(7)		N4	Zn1	N1	117.97(9)
	N4[2]	Zn1	N8	96.81(7)		N4	Zn1	N8	144.10(8)
	N4[2]	Zn1	O11	97.25(6)		N4	Zn1	O11	88.04(8)
	N4[2]	Zn1	O12[1]	100.75(6)		N4	Zn1	O12	90.72(8)
	N8	Zn1	O11	77.95(6)		N8	Zn1	O11	77.89(7)
	O12[1]	Zn1	N8	91.76(6)		O12	Zn1	N8	91.77(7)
	O12[1]	Zn1	O11	160.22(5)		O12	Zn1	O11	160.09(7)
	[1]-1/2+x. 1/2-y. 2-z; [2]1/2-x. 1-y. 1/2+z;								

					Zn-D_phen	O11	Zn1	N4	96.84(11)
						O11	Zn1	O12	92.46(11)
						O11	Zn1	N8	158.14(11)
						O11	Zn1	N1	104.17(11)
						O12	Zn1	N4	161.90(10)
						O12	Zn1	N8	78.20(11)
						N8	Zn1	N4	87.60(11)
						N1	Zn1	N4	90.54(13)
						N1	Zn1	O12	102.21(13)
						N1	Zn1	N8	97.16(12)
Zn-L_tyr	$O11^{1}$	Zn1	O12	93.13(10)	**Zn-D_tyr**	O11	Zn1	$O12^{1}$	93.07(9)
	$O11^{1}$	Zn1	$N4^{2}$	95.91(9)		O11	Zn1	$N4^{2}$	96.03(9)
	$O11^{1}$	Zn1	N8	153.54(9)		O11	Zn1	$N8^{1}$	153.59(10)
	$O11^{1}$	Zn1	N1	107.73(10)		O11	Zn1	$N1^{1}$	107.28(10)
	$N4^{2}$	Zn1	O12	164.12(10)		$N4^{2}$	Zn1	$O12^{1}$	163.89(10)
	N8	Zn1	O12	77.86(11)		$N8^{1}$	Zn1	$O12^{1}$	77.92(10)
	N8	Zn1	$N4^{2}$	88.33(9)		$N8^{1}$	Zn1	$N4^{2}$	88.13(10)
	N1	Zn1	O12	97.86(10)		$N1^{1}$	Zn1	$O12^{1}$	98.00(10)
	N1	Zn1	$N4^{2}$	91.80(11)		$N1^{1}$	Zn1	$N4^{2}$	91.96(11)
	N1	Zn1	N8	98.19(10)		$N1^{1}$	Zn1	$N8^{1}$	98.60(10)
	^{1}1/2+x. 1/2-y.-z; ^{2}1/2+x.-1/2-y. -z					^{1} 1/2+x. 1/2-y.1-z; ^{2}x. -1+y. +z			

Table A1.4. Hydrogen bonding interactions (Å. °)

	D-H···A[b]	***D-H***	***H···A***	***D···A***	***D-H···A***
Mn_gly (1.1)	O1W-H1WA...O12 (i)	0.76(3)	1.92(3)	2.6800(19)	170(3)
	O1W-H1WB...O3W	0.81(3)	1.88(3)	2.692(2)	178(3)
	O2W-H2WB...O12 (ii)	0.90(3)	1.76(3)	2.660(2)	174(3)
	O2W-H2WA...N4 (iii)	0.78(3)	2.05(3)	2.827(2)	169(3)
	O3W-H3WA...N3 (iv)	0.79(3)	2.08(3)	2.863(2)	168(3)
Zn-L_tyr (1.6)	O19-H19...O1W (vi)	0.82	1.90	2.651(4)	150.8
Zn-D_tyr (1.7)	O19-H19...O1W	0.84	1.82	2.640 (3)	164.7

[a]Symmetry codes: (i) -x+1. y-1/2. -z+1/2; (ii) x. -y-1/2. z+1/2; (iii) x+1. y. z; (iv) -x. -y-1. -z+1 (vi) 1/2-x.-y.1/2+z

[b]D: donor. A: acceptor.

A1.4 Powder X-ray diffraction analysis

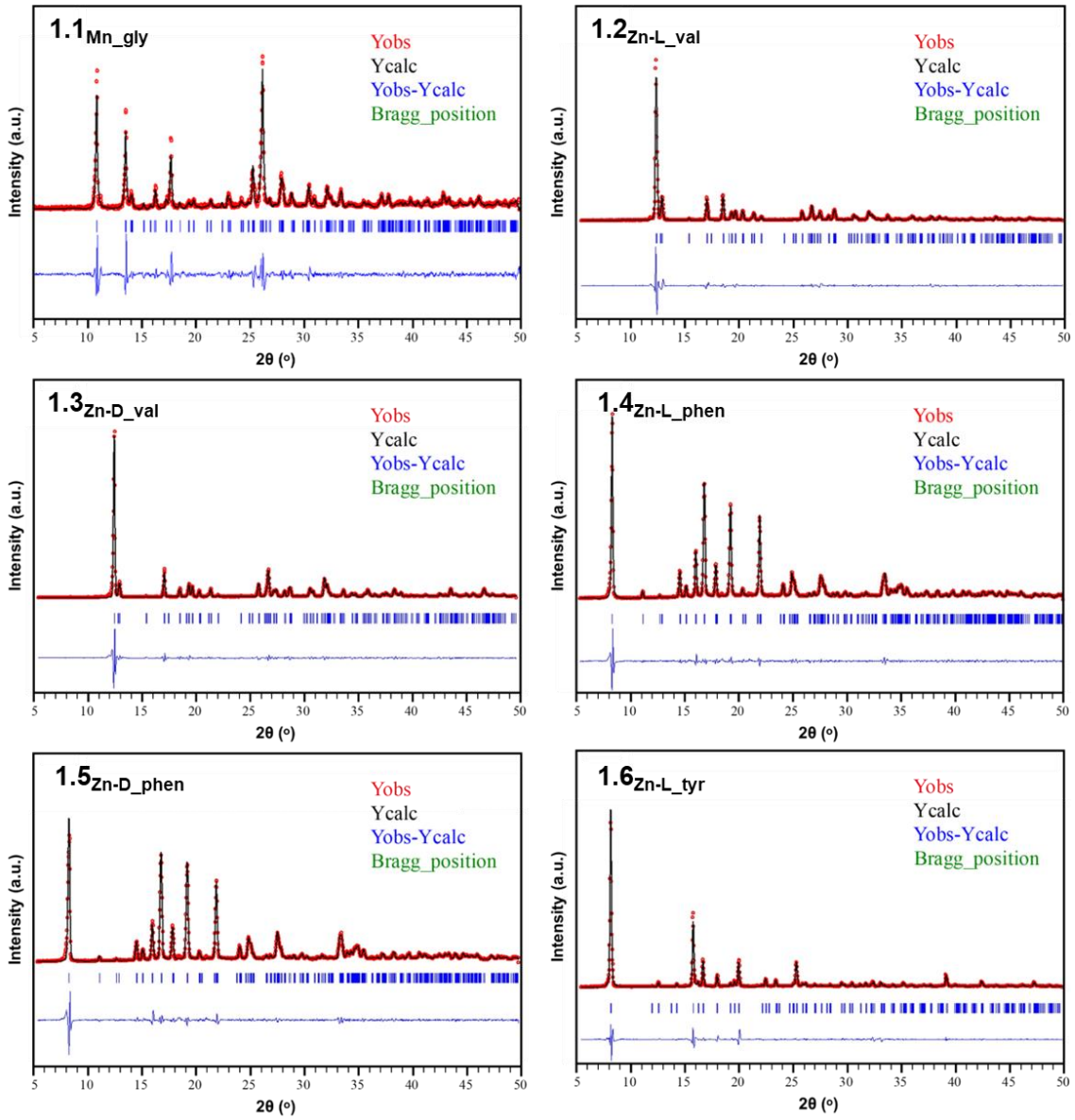

Figure A1.5. Figure of the pattern matching analysis and experimental PXRD for complexes **1.1**-**1.6**.

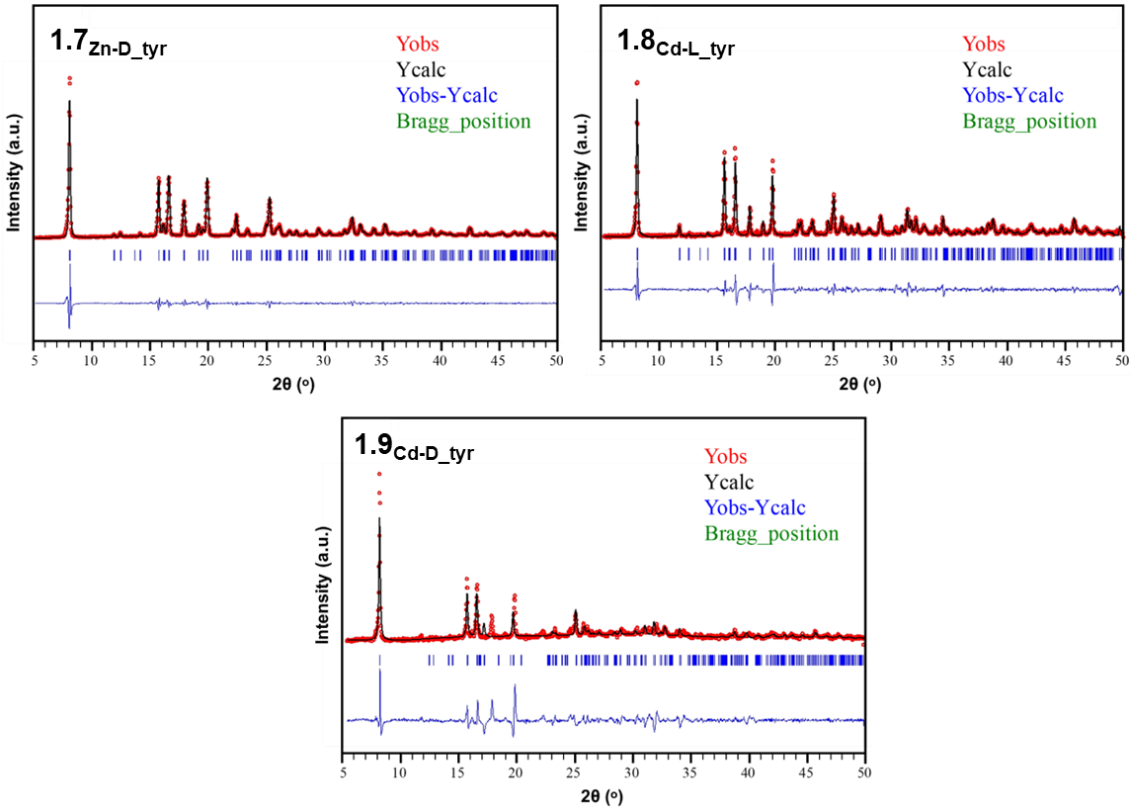

Figure A1.6. Figure of the pattern matching analysis and experimental PXRD for complexes **1.7**-**1.9**.

A1.5 Continuous Shape Measurements

Table A1.5. Continuous Shape Measurements for the MN_3O_3 coordination environment.

Codes		
HP-6	D_{6h}	Hexagon
PPY-6	C_{5v}	Pentagonal pyramid
OC-6	O_h	Octahedron
TPR-6	D_{3h}	Trigonal prism
JPPY-6	C_{5v}	Johnson pentagonal pyramid J2

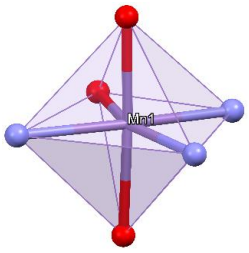

Structure [MnN_3O_3]	HP-6	PPY-6	OC-6	TPR-6	JPPY-6
Mn_gly (**1.1**)	33.464	25.371	**1.030**	12.467	29.058

Table A1.6. Continuous Shape Measurements for the MN_3O_2 coordination environment**.**

Codes		
PP-5	1 D5h	Pentagon
vOC-5	2 C4v	Vacant octahedron
TBPY-5	3 D3h	Trigonal bipyramid
SPY-5	4 C4v	Spherical square pyramid
JTBPY-5	5 D3h	Johnson trigonal bipyramid J12

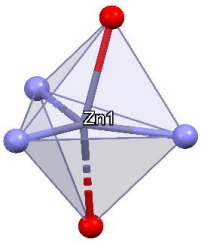

Structure [MnN_3O_2]	PP-5	vOC-5	TBPY-5	SPY-5	JTBPY-5
Zn-L/D_val (**1.2**/**1.3**)	29.182	2.086	3.432	**0.887**	5.786
Zn-L/D_phen (**1.4**/**1.5**)	30.929	1.050	5.087	**0.974**	6.754
Zn-L/D_tyr (**1.6**/**1.7**)	30.929	1.296	3.824	**1.124**	5.326

A1.6 Thermal analysis

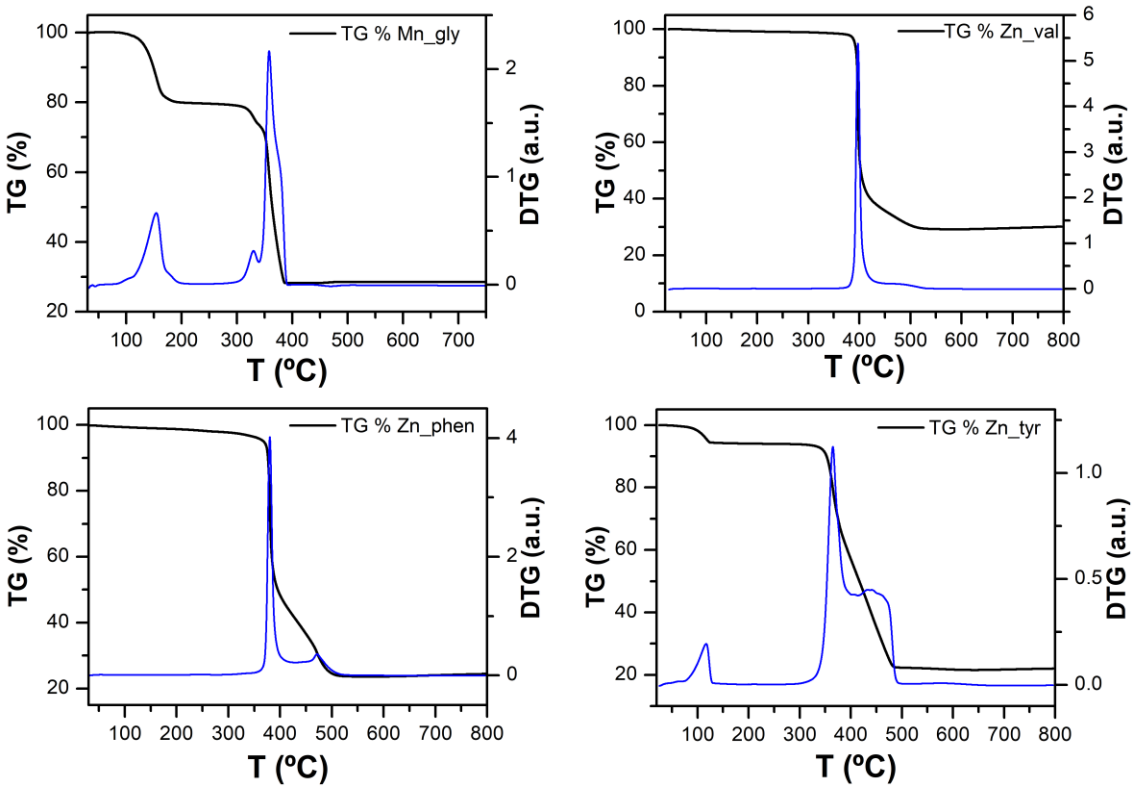

Figure A1.7. Figure of TG/DTG analysis of compounds Mn_gly, Zn_val, Zn_phen and Zn_tyr.

A1.7 Additional views of the structure

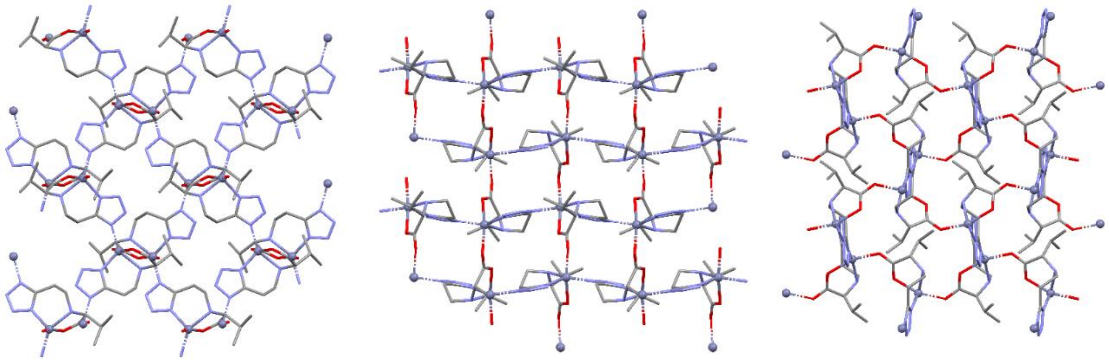

Figure A1.8. Perspective view along *a*. *b* and *c* axis from left to right of compound **1.2**$_{\text{Zn-L\_val}}$.

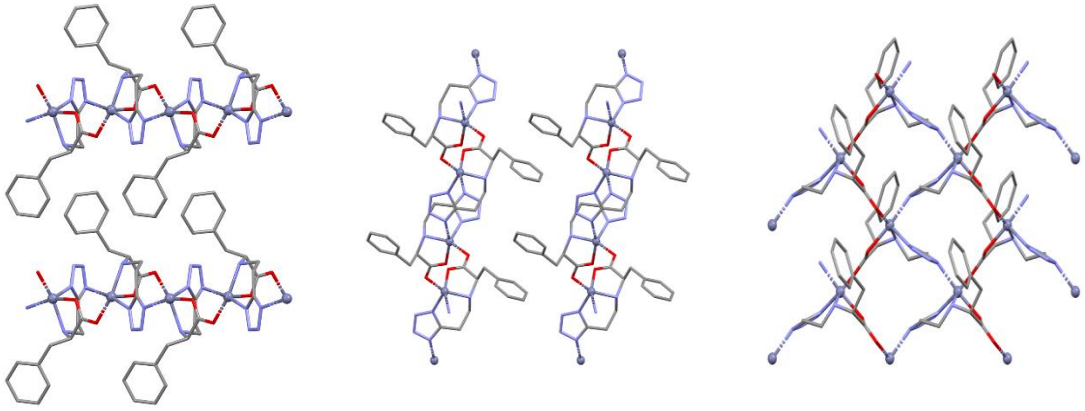

Figure A1.9. Perspective view along *a*. *b* and *c* axis from left to right of compound **1.5**$_{\text{Zn-D\_phen}}$.

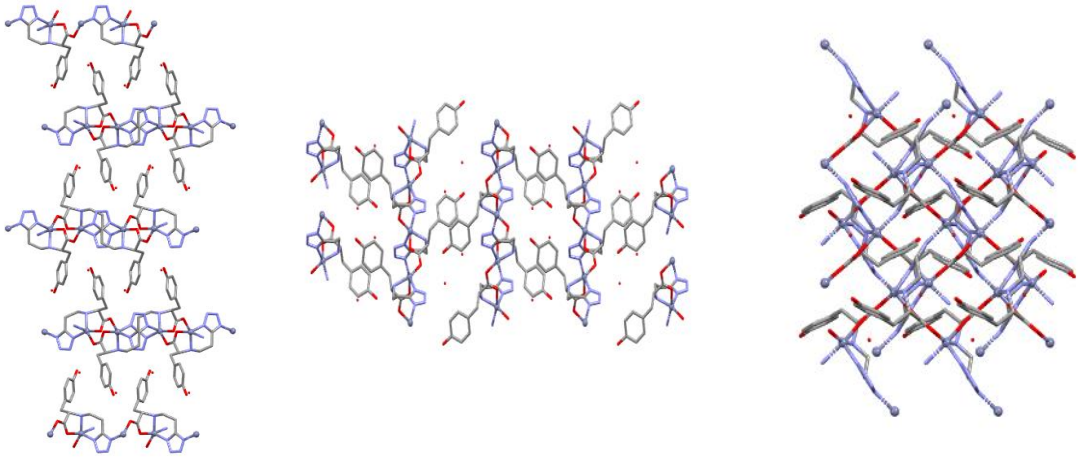

Figure A1.10. Perspective view along *a*. *b* and *c* axis from left to right of compound **1.6**$_{\text{Zn-L\_tyr}}$.

A1.8 Photoluminescent properties

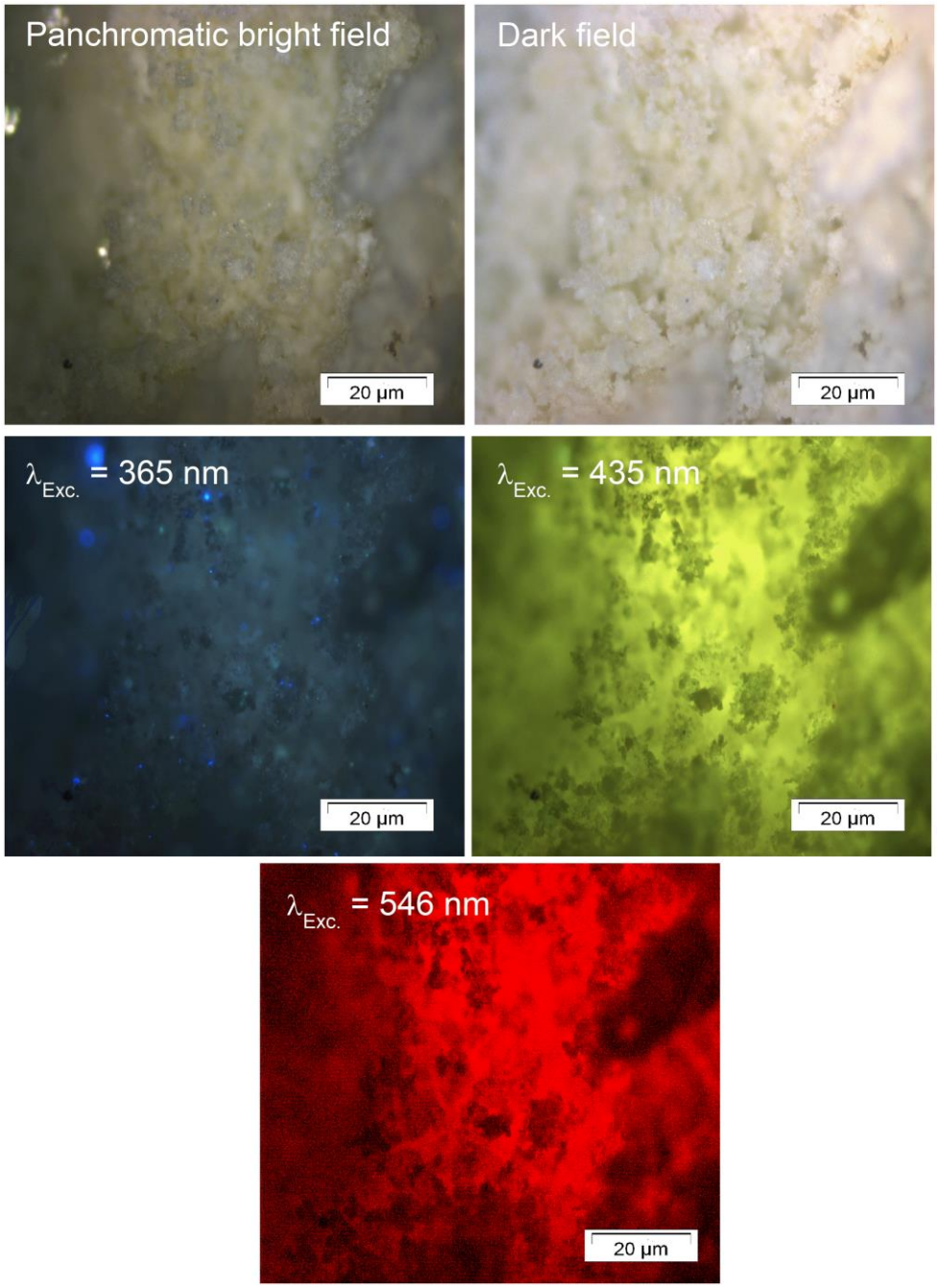

Figure A1.11. Ambient temperature micro-photoluminescence images taken on polycrystalline sample of compound Zn-L_tyr (**1.6**) at different excitation lines.

A1.9 Relaxativity measurements

Table A1.7. Raw data of measured relaxativity at 1.4 T. 0 mM concentration corresponds to milli-Q H_2O relaxation time.

Concentration (mM)	T_1 (ms)	T_1 error	T_2 (ms)	T_2 error
1	411.00	1.0	56.25	0.02
	411.07	0.9	56.22	0.02
	412.50	0.9	56.23	0.02
0.5	713	2	99.89	0.03
	715	2	99.84	0.03
	715	2	99.92	0.03
0.1	2028	5	456.86	0.04
	2040	5	457.39	0.04
	2046	5	457.92	0.04
0	3790	10	3306	0.7
	3830	10	3304	0.7
	3820	10	3302	0.7

Table A1.8. Raw data of measured relaxativity at 7 T. 0 mM concentration corresponds to milli-Q H_2O relaxation time.

Concentration (mM)	T_1 (ms)	T_1 error	T_2 (ms)	T_2 error
1	265	4	21	1
0.5	447	8	32	1
0.1	1298	25	107	1
0	2127	51	256	2
1 of $MnCl_2$	203	1	13	1

A1.10 Chiroptical properties. Statistical analysis of the CPL data

Table A1.9. Integrated areas of the CPL spectra and the corresponding statistic parameters

	Areas		
Data Set	**Zn-L_phen (1.4)**	**Zn-D_phen (1.5)**	**Racemic mixture**
1	-0.165	0.047	4.37E-04
2	-0.119	0.070	8.68E-04
3	-0.138	0.055	1.05E-03
4	-0.137	0.039	-9.24E-04
5	-0.136	0.075	2.01E-03
6	-0.151	0.017	1.78E-03
7	-0.110	0.059	2.10E-03
8	-0.122	0.062	-1.05E-03
9	-0.141	0.062	-2.40E-03
10	-0.129	0.053	2.40E-03
Average area	-0.135	0.054	0.001
Standard deviation (s)	0.016	0.017	0.002
Variance s^2	2.59E-04	2.78E-04	2.58E-06

Table A1.10. F-test two sample for variances corresponding to Zn-L_phen (**1.4**)

Zn-L_phen (1.4)		
F-Test two sample for Variances	*Variable 1*	*Variable 2*
Mean	-0.13	6.27E-04
Variance	0.00	2.58E-06
Observations	10.00	10
Degrees of freedom	9.00	9
F	**100.41**	
P(F<=f) one tail	0.00	
F Critical one tail	**3.18**	

Table A1.11. *F-test* two sample for variances corresponding to Zn-D_phen (**1.5**)

Zn-D_phen (1.5)		
F-Test two sample for Variances	*Variable 1*	*Variable 2*
Mean	0.05	6.27E-04
Variance	0.00	2.58E-06
Observations	10.00	10
Degrees of freedom	9.00	9
F	**107.99**	
P(F<=f) one tail	0.00	
F Critical one tail	**3.18**	

Table A1.12*. t-student* test for two sample assuming equal variances for Zn-L_phen (**1.4**)

Zn-L_phen (1.4)		
t-Test: Two-Sample Assuming Equal Variances	*Variable 1*	*Variable 2*
Mean	-0.13	6.27E-04
Variance	0.00	2.58E-06
Observations	10.00	10.00
Pooled Variance	0.00	
Hypothesized Mean Difference	0.00	
Degrees of freedom	18.00	
t Stat	**-26.48**	
P(T<=t) one-tail	0.00	
T Critical one-tail	1.73	
P(T<=t) two-tail	0.00	
t Critical two-tail	2.10	

Table A1.13. *t-student* test for two sample assuming equal variances for Zn-D_phen (**1.5**)

Zn-D_phen (1.5)		
t-Test: Two-Sample Assuming Equal Variances	*Method A*	*Method B*
Mean	0.05	0.00063
Variance	0.00	2.6E-06
Observations	10.00	10
Pooled Variance	0.00	

Hypothesized Mean Difference	0.00
Degrees of freedom	18.00
t Stat	**10.02**
P(T<=t) one-tail	0.00
T Critical one-tail	1.73
P(T<=t) two-tail	0.00
t Critical two-tail	2.10

Appendix 2

Supporting information of Chapter 2

A2.1 Experimental section. General instrumentation

Elemental analyses (C, H, N) were performed on a Leco CHNS-932 microanalyser. Infrared (IR) spectra (400-4000 cm^{-1}) were recorded on a Nicolet FT-IR 6700 spectrometer in KBr pellets.

Thermogravimetric analysis (TG/DTA) were performed on a TG-Q500 TA Instruments thermal analyser from room temperature to 800 °C under a synthetic air atmosphere (79 % N_2/21 % O_2) at a heating rate of 10 °C min^{-1}.

Scanning electron microscopy (SEM) images were acquired using either a Hitachi S4100 field emission gun tungsten filament instrument working at 25 kV or a high-resolution Hitachi SU-70 working at 4 kV. Samples were prepared by deposition on aluminium sample holders followed by carbon coating using an Emitech K950X carbon evaporator. EDS (energy dispersive X-ray spectroscopy) data and SEM mapping images were recorded using the latter microscope working at 15 kV and using either a Bruker Quantax 400 or an Esprit 1.9 EDS microanalysis system.

Magnetic susceptibility measurements were performed on polycrystalline samples of the complexes with a Quantum Design SQUID MPMS-7T susceptometer at an applied magnetic field of 1000 G. The susceptibility data were corrected for diamagnetism estimated from Pascal's tables,[6] the temperature-independent paramagnetism and magnetisation of the sample holder. The ac measurements were performed on a physical property measurement system quantum design model 6000 magnetometer under a 3.5 G ac field and frequencies ranging from 60 to 10000 Hz.

Photoluminescence Spectroscopy. The emission and excitation spectra were recorded at ambient-temperature and 12 K using a Fluorolog®-3Horiba Scientific (Model FL3-2T) spectroscope, with a modular double grating excitation spectrometer (fitted with a 1200 grooves/mm grating blazed at 330 nm) and a TRIAX 320 single emission monochromator (fitted with a 1200 grooves/mm grating blazed at 500 nm, reciprocal linear density of 2.6 $nm \cdot mm^{-1}$), coupled to a R928 Hamamatsu photomultiplier, using the front face acquisition mode. The excitation source was a 450 W Xe arc lamp. The emission spectra were corrected for detection and optical spectral response of the spectrofluorimeter and the excitation spectra were corrected for the spectral distribution of the lamp intensity using a photodiode reference detector. Time-resolved measurements have been carried out using a 1934D3 phosphorimeter coupled to the Fluorolog®-3, and a Xe-Hg flash lamp (6 μs/pulse half width and 20-30 μs tail) was used as the excitation source. The low temperature measurements (12 K) were performed using a helium-closed cycle cryostat with vacuum system measuring ca. 5×10^{-6} mbar and a Lakeshore 330 auto-tuning temperature controller with a resistance heater.

N_2 (77 and 273 K) and CO_2 (273 and 298 K) **physisorption** data were measured in a Quantachrome Autosorb-iQ MP, Prior to measurements, all samples were outgassed under vacuum at 150 °C for 6 hours. To estimate CO_2 adsorption enthalpies (Q_{st}), the isotherms were fitted to the modified Clausius−Clapeyron equation.

X-ray data collection of suitable single crystals were done at 100(2) K on a Bruker D8 VENTURE area detector equipped with graphite monochromated Mo−Kα radiation (λ = 0.71073 Å) by applying the ω-scan method. The data reduction was performed with the APEX270 software and corrected for absorption using SADABS.[2] Crystal structures were solved by direct methods using the SIR97 program[3] and refined by full-matrix least-squares on F2 including all reflections using anisotropic displacement parameters by means of the WINGX[4] crystallographic package. All hydrogen atoms were included as fixed contributions riding on attached atoms with isotropic thermal displacement parameters 1.2 times or 1.5 times those of their parent atoms for the organic ligands. Lattice solvent molecules could not be refined owing to their disordered disposition in the voids of the structures, so the electron density at the voids was subtracted from the reflection data by the SQUEEZE procedure as implemented in PLATON program[5] during the refinement.

The **X-ray powder diffraction** (XRPD) patterns were collected at 25 °C on a Phillips X'PERT powder diffractometer with Cu-Kα radiation (λ = 1.5418 Å) over the range $5 < 2\theta < 50^{o}$ with a step size of 0.02° and an acquisition time of 2.5 s per step. Indexation of the diffraction profiles were made by means of the FULLPROF program (pattern- matching analysis) based on the space group and the cell parameters found by single crystal X-ray diffraction.[1]

Variable-temperature powder X-ray diffraction measurements were conducted on a Bruker D8 Advance diffractometer, using polycrystalline sample of compound **2.7_{Dy}** under ambient atmosphere with heating rate of 5 °C·min^{-1} and measuring a complete diffractogram every 20 °C up to 510 °C, and every 50 °C from 510 °C up to 710 °C.

Catalytic studies: All experiments involving moisture-sensitive compounds were performed under an inert atmosphere of N_2 using standard techniques. Unless otherwise indicated, reagents and substrates were purchased from commercial sources and used as received. Solvents not required to be dry were purchased as technical grade and used as received. Conversion values relative to the limiting reagent were calculated from the ^{1}H NMR spectra of the reaction crudes. Isolated products were obtained after centrifugation (8000 rpm, 3 min) and washed with dichloromethane (2 x 0.5 mL) in order to remove the catalyst or column chromatography in silica gel using hexane as eluent.

NMR measurements: NMR spectra were measured in a Bruker Avance III 300 spectrometer equipped with a direct double SmartProbe BBFO $^{1}H/BB(^{19}F)$ probe. Chemical shifts are reported in parts per million (ppm) relative to residual solvent peak ($CDCl_3$, ^{1}H: 7.26 ppm; ^{13}C: 77.16 ppm). Coupling constants are reported in Hertz. Multiplicity is reported with the usual abbreviations (s: singlet, bs: broad singlet, d: doublet, dd: doublet of doublets, ddd: doublet of

doublet of doublets, t: triplet, td: triplet of doublets, q: quartet, dq: doublet of quartet, p: pentet, sex: sextet, hept: heptet, m: multiplet).

Dynamic water vapour sorption (DVS) measurements were performed on a DVS Resolution water vapour analyzer (Surface Measurement Systems™), at 25 °C and from 0 to 95 % RH, with steps of 10 % RH, using 200 SCCM N2 (N50, purity ≥ 99.999%) as carrier gas. Both the sorption and desorption curves were recorded by setting a stability criterion for the mass change (gravimetric precision of 0.1 μg) as the minimum in the variation of the mass over the time variation (d*m*/d*t*) of 0.002 % min^{-1}, or a maximum stage time at each RH of 360 min (in the case when the d*m*/d*t* minimum was not attained). Prior to the measurements, the sample of **2.6$_{Tb}$** was pretreated *in situ* in at 75 °C for 2 h at 0% RH and then at 25 °C for 1 h at 0 % RH, to ensure dehumidification for an initial reference state. An equivalent treatment was used for samples **2.6$_{Tb}$@PSF** and **2.6$_{Tb}$@PMMA** but with the first isothermal dwell at 60 °C to prevent softening of the polymer matrices.

The electrical conductivity (σ) of pelletized sample **2.6$_{Tb}$** and **composite membranes (2.6$_{Tb}$@PSF** and **2.6$_{Tb}$@PMMA)** were studied by impedance spectroscopy using an Agilent E4980A Precision LCR meter. Disc shaped sample 1 was obtained after pressing the powder in a uniaxial press at 10 MPa, and then isostatically at 200 MPa. Silver electrodes were applied on both sides of the pellet and membranes (with an area of approximately 1x1 cm^2) by painting a commercial paste (Agar Scientific). Samples were placed on ceramic tubular sample holders (equipped with platinum wires for current collection) inside a climatic chamber (ACS DY110) in order to carry out the measurements under variable temperature (40-94 °C) and relative humidity (RH, 20-95%). The impedance spectra were collected between 20 Hz and 2 MHz with a test signal amplitude of 100 mV. The current collection was ensured by separate platinum wires for voltage and current. The spectra were analyzed with ZView (Version 2.6b, Scribner Associates) to assess the ohmic resistance (R), which was then normalized to the samples geometry to calculate the conductivity using Equation A2.1:

$$\sigma = L(RA)^{-1} \qquad \textbf{Equation A2.1}$$

where L is the sample thickness and A is the surface area of the electrodes. The maximum relative error in the conductivity data is estimated to be of the order of 4% through the conventional chain rule of differentiation of Equation A2.1 and the uncertainties in the measured parameters (ΔR = 0.1% to 0.3% of *R*, $\Delta L = \pm 0.002\ cm, \Delta A = \pm\ 0.005\ cm$).

A2.2 Chemical characterization

A2.2.1 Elemental analysis

Table A2.1. Elemental analysis of compounds **2.2$_{Nd}$-2.11$_{Yb}$**

Compound	Formula	Molecular weight	Calc.	Found.
2.1	$C_7H_5NO_3Co$	210.05	C: 40.03; H: 2.40; N: 6.67; O: 22.85; Co: 28.06	C: 40.09; H: 2.45; N: 6.64; O: 22.83; Co: 28.12
2.2	$C_{51}H_{64}N_9O_{29}Nd_5$	1988.31	C: 30.80; H: 3.24; N: 6.34; O: 23.34; Nd: 36.27	C: 30.82; H: 3.21; N: 6.35; O: 23.37; Nd: 36.24
2.3	$C_{51}H_{64}N_9O_{29}Sm_5$	2019.11	C: 30.34; H: 3.19; N: 6.24; O: 22.98; Sm: 37.24;	C: 30.33; H: 3.21; N: 6.26; O: 22.97; Sm: 37.25;
2.4	$C_{51}H_{64}N_9O_{29}Eu_5$	2026.91	C: 30.22; H: 3.18; N: 6.22; O: 22.89; Eu: 37.49;	C: 30.23; H: 3.19; N: 6.22; O: 22.91; Eu: 37.49;
2.5	$C_{51}H_{64}N_9O_{29}Gd_5$	2053.36	C: 29.83; H: 3.14; N: 6.14; O: 22.60; Gd: 38.29;	C: 29.82; H: 3.13; N: 6.16; O: 22.60; Gd: 38.30;
2.6	$C_{51}H_{64}N_9O_{29}Tb_5$	2061.74	C: 29.71; H: 3.13; N: 6.11; O: 22.50; Tb: 38.54;	C: 29.72; H: 3.13; N: 6.13; O: 22.54; Tb: 38.55;
2.7	$C_{51}H_{64}N_9O_{29}Dy_5$	2079.61	C: 29.46; H: 3.10; N: 6.06; O: 22.31; Dy: 39.07;	C: 29.48; H: 3.12; N: 6.05; O: 22.33; Dy: 39.07;
2.8	$C_{51}H_{64}N_9O_{29}Ho_5$	2091.76	C: 29.28; H: 3.08; N: 6.03; O: 22.18; Ho: 39.42;	C: 29.29; H: 3.11; N: 6.05; O: 22.20; Ho: 39.43;
2.9	$C_{51}H_{64}N_9O_{29}Er_5$	2103.41	C: 29.12; H: 3.07; N: 5.99; O: 22.06; Er: 39.76;	C: 29.12; H: 3.10; N: 6.00; O: 22.08; Er: 39.82;
2.10	$C_{51}H_{64}N_9O_{29}Tm_5$	2111.78	C: 29.01; H: 3.05; N: 5.97; O: 21.97; Tm: 40.00;	C: 29.03; H: 3.06; N: 5.97; O: 21.97; Tm: 40.02;
2.11	$C_{51}H_{64}N_9O_{29}Yb_5$	2132.31	C: 28.73; H: 3.03; N: 5.91; O: 21.76; Yb: 40.58;	C: 28.74; H: 3.06; N: 5.93; O: 21.76; Yb: 40.56;
2.12	$C_{51}H_{64}N_9O_{29}Y_5$	1711.64	C: 35.79; H: 3.77; N: 7.36; O: 27.11; Y: 25.97	C: 35.82; H: 3.74; N: 7.41; O: 27.16; Y: 26.02
2.19	$C_{57}H_{74}N_{11}O_{29}Eu_5$	2137	C: 32.04; H: 3.49; N: 7.21; O: 21.71; Eu: 35.55	C: 31.98; H: 3.51; N: 7.19; O: 21.68; Eu: 35.54

A2.2.2 Determination of the metal content by ICP-AES

Table A2.2. ICP-AES results of compounds **2.16-2.18.**

	Content			Percentage		
Compounds	Yor Gd mg L^{-1} (mM)	Tb mg L^{-1} (mM)	Eu mg L^{-1} (mM)	Y or Gd %	Tb %	Eu%
2.16$_{Y\text{-}Tb\text{-}Eu5\%}$	491 mg L^{-1} (5.52 mM)	869 mg L^{-1} (5.47 mM)	73.8 mg L^{-1} (0.49 mM)	48.1	47.7	4.2
2.17$_{Y\text{-}Tb\text{-}Eu10\%}$	463 mg L^{-1} (5.20 mM)	756 mg L^{-1} (4.75 mM)	132 mg L^{-1} (0.87 mM)	48.1	43.9	8.0
2.18$_{Gd\text{-}Tb\text{-}Eu10\%}$	838 mg L^{-1} (5.33 mM)	746 mg L^{-1} (4.69 mM)	142 mg L^{-1} (0.93 mM)	48.6	42.9	8.5

A2.2.3 FT-IR spectroscopy

FTIR spectra of compound **2.1$_{Co}$** exhibit broad and intense band around 3439 cm^{-1} that corresponds to the O–H bond vibration of the of 3-amino-4-hydroxybenzoate free ligand, The bands between 3331 cm^{-1} and 2928–2857 cm^{-1} can be attributed to aromatic ring's C–H bond vibrations of the ligand. The intense vibrations in the 1668–1430 cm^{-1} region are referred to both the asymmetric stretching vibrations of the carboxylate groups and the aromatic C–C and C–N bonds. The symmetric stretching vibrations of the carboxylate groups appear in the lower range of 1391–1297 cm^{-1}. The remaining bands that are found at lower frequency can be attributed to the distortions originated in the aromatic ring and the carboxylate groups of the ligands. The vibration bands of the M–O and M–N bonds are observed below 670 cm^{-1}.

FTIR spectra of compound **2.7$_{Dy}$** display a narrow peak at around 3625 cm^{-1}, attributed to the N-H stretching vibration of amine group, which is practically hided below the intense broad band around 3412 cm^{-1} attributed to O–H bond vibration of the of 3-amino-4-hydroxybenzoate free ligand.

At lower frequency, a set of intense bands are visible between 3207 cm^{-1} and 2921–2830 cm^{-1} which corresponds to aromatic ring's C–H bond vibrations of the ligand The intense vibrations in the 1661–1433 cm^{-1} region are referred to both the asymmetric stretching vibrations of the carboxylate groups and the aromatic C–C and C–N bonds. The symmetric stretching vibrations of the carboxylate groups appear in the lower range of 1381–1281 cm^{-1}. The remaining bands that are found at lower frequency can be attributed to the distortions originated in the aromatic ring and the carboxylate groups of the ligands. The vibration bands of the M-O and M-N bonds are observed below 646 cm^{-1}.

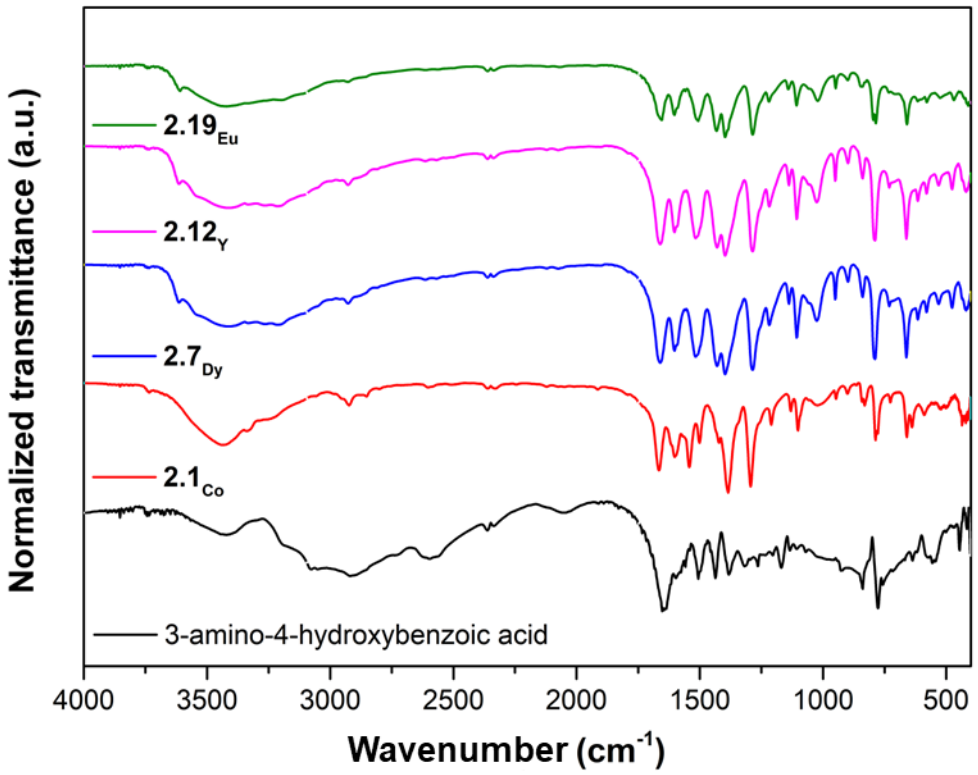

Figure A2.1. Infrared spectra of the ligand and compound **2.7$_{Dy}$.**

A2.3 Crystallographic data

Table A2.3. Crystallographic data and structure refinement details of compounds **2.1** and **2.7**.

Compound	**2.1_{Co}**	**2.7_{Dy}**	**2.12_{Y}**	**2.19_{Eu}**
Formula	$C_7H_5NO_3Co$	$C_{51}H_{51}N_9O_{24}Dy_5$	$C_{51}H_{54}N_9O_{24}Y_5$	$C_{57}H_{74}N_{11}O_{29}Eu_5$
M_r	210.05	1986.51	1711.63	2137
Crystal system	tetragonal	hexagonal	hexagonal	hexagonal
Space group (no.)	*$P4_2$(77)*	*P*63/*m*	*$P6_3$/m (176)*	*$P6_3$/m (176)*
a(Å)	9.1366(2)	15.4579(11)	14.730(3)	15.8816(3)
b(Å)	9.1366(2)	15.4579(11)	14.730	15.8816(3)
c(Å)	6.6080(3)	17.0864(13)	17.616(5)	16.9930(6)
α(°)	90	90	90	90
β(°)	90	90	90	90
γ(°)	90	120	120	120
V(Å^3)	551.62(3)	3535.8(6)	3310.1(17)	3311.84(19)
Z	2	4	2	2
ρ_{calc}g/cm^3	1.265	1.866	1.627	2.566
μ/mm^{-1}	12.007	5.293	4.415	4.298
F(000)	210.0	1884.0	1620.0	2880.0
Crystal size/mm^3	0.700 × 0.124 × 0.080	0.27 × 0.24 × 0.22	0.660 × 0.164 × 0.090	0.660 × 0.164 × 0.090
Radiation	CuKα (λ = 1.54178)	MoKα (λ = 0.71073)	MoKα (λ = 0.71073)	MoKα (λ = 0.71073)
2θ range for data collection/°	16.556 to 132.752	3.866 to 50.038	4.624 to 46.716	5.662 to 54.968
Index ranges	-10 ≤ h ≤ 10, -10 ≤ k ≤ 10, -7 ≤ l ≤ 7	-18 ≤ h ≤ 17. -18 ≤ k ≤ 18. -20 ≤ l ≤ 20	-16 ≤ h ≤ 16, -16 ≤ k ≤ 16, -19 ≤ l ≤ 19	-20 ≤ h ≤ 20, -20 ≤ k ≤ 20, -22 ≤ l ≤ 21
Reflections collected	6346	23375	12689	36732
Independent reflections	933 [R_{int} = 0.0284, R_{sigma} = 0.0180]	2170 [R_{int} = 0.1243. R_{sigma} = 0.0634]	1674 [R_{int} = 0.0936, R_{sigma} = 0.0933]	2937 [R_{int} = 0.0444, R_{sigma} = 0.0174]
Data/restraints/parameters	933/70/106	2170/57/160	1674/24/147	2937/0/122
Goodness-of-fit on F^2	1.152	1.016	1.146	1.080
Final R indexes [I>=2σ (I)]	R_1 = 0.0562, wR_2 = 0.1643	R_1 = 0.0394. wR_2 = 0.0837	R_1 = 0.0480, wR_2 = 0.1361	R_1 = 0.0176, wR_2 = 0.0649
Final R indexes [all data]	R_1 = 0.0716, wR_2 = 0.1833	R_1 = 0.0666. wR_2 = 0.0944	R_1 = 0.0852, wR_2 = 0.1592	R_1 = 0.0201, wR_2 = 0.0487
Largest diff. peak/hole / e Å^{-3}	0.76/-0.29	1.09/-1.31	1.38/-1.36	1.07/-0.66

Table A2.4. Table of the selected bond lengths (Å) for compound **2.1$_{Co}$**, **2.7$_{Dy}$**, **2.12$_{Y}$** and **2.19$_{Eu}$**

Complex		**2.1$_{Co}$**			**2.7$_{Dy}$**			**2.12$_{Y}$**			**2.19$_{Eu}$**
Atom1-2		**Length/Å**	**Atom1-2**		**Length/Å**	**Atom1-2**		**Length/Å**	**Atom1-2**		**Length/Å**
Co1	O2	1.8610(157)	Dy1	Dy1[1]	3.4984(12)	Y1	O3	2.536(5)	Eu1	Eu1[1]	3.5922(4)
	O3	1.9145(173)	Dy1	Dy2[2]	3.9242(6)	Y1	N1	2.517(6)	Eu1	O1	2.5265(17)
	O1	1.9367(242)	Dy1	Dy2	3.9242(6)	Y1	O1H	2.349(4)	Eu1	O1[2]	2.5266(17)
	O1	2.0802(241)	Dy1	O1H[3]	2.366(5)	Y2	O1	2.425(5)	Eu1	O1[3]	2.5265(17)
	N1	2.4091(169)	Dy1	O1H	2.366(5)	Y2	O2	2.396(5)	Eu1	N1	2.546(2)
	O2	3.1768(204)	Dy1	O1H[2]	2.366(5)	Y2	O3	2.349(5)	Eu1	N1[3]	2.546(2)
	Co1	3.304(14)	Dy1	O3	2.513(6)	Y2	O1D	2.305(7)	Eu1	N1[2]	2.546(2)
	O3	3.3833(160)	Dy1	O3[2]	2.513(6)	Y2	O1H	2.348(6)	Eu1	Eu2[2]	3.94656(18)
	N1	3.5469(246)	Dy1	O3[3]	2.513(6)				Eu1	Eu2	3.94655(18)
			Dy1	N1	2.509(7)				Eu1	O4[3]	2.4145(16)
			Dy1	N1[3]	2.510(7)				Eu1	O4	2.4145(16)
			Dy1	N1[2]	2.510(7)				Eu1	O4[2]	2.4485(18)
			Dy2	O1[4]	2.394(6)				Eu2	O2[4]	2.4485(18)
			Dy2	O1[5]	2.394(6)				Eu2	O2[5]	2.4675(18)
			Dy2	O1H	2.337(7)				Eu2	O3[5]	2.4675(18)
			Dy2	O2[4]	2.417(6)				Eu2	O3[4]	2.349(2)
			Dy2	O2[5]	2.417(6)				Eu2	O4	2.385(3)
			Dy2	O3	2.371(5)				Eu2	O5	2.3837(16)
			Dy2	O3[1]	2.371(5)				Eu2	O1	2.4485(18)
			Dy2	O4	2.327(11)						
			[1]+x,+y,3/2-z; [2]1-y,1+x-y,+z; [3]+y-x,1-x,+z; [4]+y,1-x+y,1/2+z; [5]+y,1-x+y,1-z						[1]+x,+y,3/2-z; [2]1-y,1+x-y,+z; [3]+y-x,1-x,+z; [4]+y,1-x+y,1-z; [5]+y,1-x+y,1/2+z		

						2.1_{Co}					
Atom 1	**Atom 2**	**Atom 3**	**Angle 2,1,3 [º]**	**Atom 1**	**Atom 2**	**Atom 3**	**Angle 2,1,3 [º]**	**Atom 1**	**Atom 2**	**Atom 3**	**Angle 2,1,3 [º]**
Co1	O2	O2	139.187(637)	Co1	O3	O2	42.354(546)	Co1	O1	N1	50.949(612)
	O2	O3	94.161(649)		O3	O3	101.962(494)		N1	N1	149.856(553)
	O2	O3	95.754(649)		O3	N1	145.330(617)		N1	O2	77.203(570)
	O2	O1	106.728(634)		O3	N1	63.367(650)		N1	O2	77.692(570)
	O2	O1	105.999(634)		O1	O1	72.205(950)		N1	O3	71.828(489)
	O2	O1	36.326(586)		O1	O1	132.495(760)		N1	O3	138.316(482)
	O2	O1	102.862(572)		O1	O1	132.495(761)		N1	N1	101.321(585)
	O2	N1	35.482(597)		O1	N1	77.979(585)		O2	O2	66.605(494)
	O2	N1	174.648(608)		O1	N1	77.765(584)		O2	O3	133.980(407)
	O2	O2	106.943(625)		O1	O2	2.823(657)		O2	O3	134.715(407)
	O2	O3	36.354(555)		O1	O2	69.404(785)		O2	N1	105.715(470)
	O2	O3	102.835(569)		O1	O3	132.406(585)		O2	N1	172.315(478)
	O2	N1	75.025(610)		O1	O3	132.616(586)		O3	O3	66.490(319)
	O2	N1	74.452(610)		O1	N1	102.914(694)		O3	N1	50.654(394)
	O2	O2	106.943(624)		O1	N1	175.118(651)		O3	N1	51.046(394)
	O3	O3	151.303(735)		O1	O1	66.541(828)		N1	N1	81.966(489)
	O3	O1	111.754(615)		O1	N1	71.802(491)				
	O3	O1	39.549(648)		O1	N1	138.342(510)				
	O3	O1	101.828(571)		O1	O2	134.064(643)				
	O3	O1	102.089(570)		O1	O2	134.598(640)				
	O3	N1	85.908(764)		O1	O3	0.134(467)				
	O3	N1	86.702(766)		O1	O3	66.515(628)				
	O3	O2	108.950(533)		O1	N1	50.778(611)				

2.7_{Dy}											
Atom 1	**Atom 2**	**Atom 3**	**Angle 2,1,3 [º]**	**Atom 1**	**Atom 2**	**Atom 3**	**Angle 2,1,3 [º]**	**Atom 1**	**Atom 2**	**Atom 3**	**Angle 2,1,3 [º]**
Dy1	Dy2	Dy1[1]	52.943(18)	N1[3]	Dy1	Dy2	158.59(18)	O1H	Dy1	N1[2]	88.4(2)
Dy1[1]	Dy1	Dy2[2]	63.527(9)	N1[3]	Dy1	O3[2]	68.7(2)	O1H	Dy1	N1	132.4(2)
Dy1[1]	Dy1	Dy2	63.528(9)	N1[3]	Dy1	O3	138.0(2)	O1H	Dy2	Dy1	33.69(10)
Dy1[1]	O1H	Dy1	95.3(3)	N1[3]	Dy1	O3[3]	64.6(2)	O1H	Dy2	Dy1[1]	33.69(10)
Dy2	O1H	Dy1	113.1(2)	N1[3]	Dy1	N1	82.5(3)	O1H	Dy2	O1[4]	76.4(2)
Dy2	O1H	Dy1[1]	113.1(2)	N1[3]	Dy1	N1[2]	82.5(3)	O1H	Dy2	O1[5]	76.4(2)
Dy2	O3	Dy1	106.89(19)	O1[4]	Dy2	Dy1	109.19(15)	O1H	Dy2	O2[4]	128.35(19)
Dy2[2]	Dy1	Dy2	101.651(11)	O1[4]	Dy2	Dy1[1]	76.71(17)	O1H	Dy2	O2[5]	128.35(19)
N1	Dy1	Dy1[1]	130.44(18)	O1[4]	Dy2	O1[5]	77.6(3)	O1H	Dy2	O3[1]	71.48(17)
N1	Dy1	Dy2[2]	158.59(18)	O1[4]	Dy2	O2[5]	101.9(2)	O1H	Dy2	O3	71.48(17)
N1	Dy1	Dy2	99.55(17)	O1[4]	Dy2	O2[4]	53.7(2)	O1H[2]	Dy1	Dy1[1]	42.34(13)
N1	Dy1	O3	64.6(2)	O1[5]	Dy2	Dy1	76.71(17)	O1H[2]	Dy1	Dy2	101.91(14)
N1	Dy1	O3[3]	68.7(2)	O1[5]	Dy2	Dy1[1]	109.19(15)	O1H[2]	Dy1	O1H[3]	71.4(2)
N1	Dy1	O3[2]	138.0(2)	O1[5]	Dy2	O2[5]	53.7(2)	O1H[2]	Dy1	O3[3]	74.5(2)
N1[2]	Dy1	Dy1[1]	130.44(19)	O1[5]	Dy2	O2[4]	101.9(2)	O1H[2]	Dy1	O3	133.58(17)
N1[2]	Dy1	Dy2[2]	99.55(17)	O1H	Dy1	Dy1[1]	42.34(13)	O1H[2]	Dy1	O3[2]	68.5(2)
N1[2]	Dy1	Dy2	76.73(17)	O1H	Dy1	Dy2[2]	69.01(17)	O1H[2]	Dy1	N1	142.4(2)
N1[2]	Dy1	O3	68.7(2)	O1H	Dy1	Dy2	33.21(16)	O1H[2]	Dy1	N1[3]	88.4(2)
N1[2]	Dy1	O3[2]	64.6(2)	O1H	Dy1	O1H[3]	71.4(2)	O1H[2]	Dy1	N1[2]	132.4(2)
N1[2]	Dy1	O3[3]	138.0(2)	O1H	Dy1	O3[3]	133.59(17)	O1H[3]	Dy1	Dy1[1]	42.34(13)
N1[2]	Dy1	N1	82.5(3)	O1H	Dy1	O3[2]	74.5(2)	O1H[3]	Dy1	Dy2	69.01(17)
N1[3]	Dy1	Dy1[1]	130.44(19)	O1H	Dy1	O3	68.5(2)	O1H[3]	Dy1	Dy2[2]	101.91(14)
N1[3]	Dy1	Dy2[2]	76.73(17)	O1H	Dy1	N1[3]	142.4(2)	O1H[3]	Dy1	O3	74.5(2)

2.7_{Dy}								2.12_{Y}					
Atom 1	**Atom 2**	**Atom 3**	**Angle 2,1,3 [º]**	**Atom 1**	**Atom 2**	**Atom 3**	**Angle 2,1,3 [º]**	**Atom 1**	**Atom 2**	**Atom 3**	**Angle 2,1,3 [º]**		
O1H[3]	Dy1	O3[2]	133.59(17)	O3[1]	Dy2	O1[4]	82.1(2)	N1	Y1	N1	81.5(2)		
O1H[3]	Dy1	O3[3]	68.5(2)	O3[1]	Dy2	O1[5]	145.2(2)	N1	Y1	O3	64.60(17)	69.44(18)	137.62(19)
O1H[3]	Dy1	N12	142.4(2)	O3[1]	Dy2	O2[4]	88.0(2)	O1	Y2	O1	78.4(3)		
O1H3	Dy1	N1	88.4(2)	O3[1]	Dy2	O2[5]	160.2(2)	O1D	Y2	O1H	136.7(3)		
O1H[3]	Dy1	N1[3]	132.4(2)	O3[2]	Dy1	Dy1[1]	91.44(12)	O1D	Y2	O3	81.1(2)		
O2[4]	Dy2	Dy1	162.03(15)	O3[2]	Dy1	Dy2	97.41(13)	O1D	Y2	O2	133.58(17)		
O2[4]	Dy2	Dy1[1]	112.49(16)	O3[2]	Dy1	Dy2[2]	35.32(12)	O1D	Y2	O1	82.5(2)		
O2[4]	Dy2	O25	79.3(3)	O3[2]	Dy1	O3	119.938(12)	O1H	Y1	O1H	71.50(18)		
O2[5]	Dy2	Dy1	112.49(16)	O3[2]	Dy1	O3[3]	119.938(12)	O1H	Y1	N1	88.96(19)	132.1(2)	143.3(2)
O2[5]	Dy2	Dy1[1]	162.03(15)	O3[3]	Dy1	Dy1[1]	91.44(12)	O1H	Y1	O3	68.09(18)	74.49(19)	133.41(16)
O3	Dy1	Dy1[1]	91.44(12)	O3[3]	Dy1	Dy2	136.10(12)	O1H	Y1	Y1	42.43(11)		
O3	Dy1	Dy2[2]	136.10(12)	O3[3]	Dy1	Dy2[2]	97.41(13)	O1H	Y2	O3	71.35(15)		
O3	Dy1	Dy2	35.32(12)	O4	Dy2	Dy1[1]	111.9(8)	O1H	Y2	O2	75.35(18)		
O3	Dy1	O3[3]	119.937(11)	O4	Dy2	Dy1	112.3(4)	O1H	Y2	O1	128.22(16)		
O3	Dy2	Dy1	37.79(13)	O4	Dy2	O1[4]	132.7(7)	O2	Y2	O2	77.7(3)		
O3	Dy2	Dy1[1]	83.76(14)	O4	Dy2	O1[5]	133.4(10)	O2	Y2	O1	54.29(18)	102.08(19)	
O3	Dy2	O1[4]	145.2(2)	O4	Dy2	O1H	136.4(5)	O3	Y1	O3	119.956(9)		
O3	Dy2	O1[5]	82.1(2)	O4	Dy2	O2[5]	82.5(9)	O3	Y2	O3	99.1(2)		
O3	Dy2	O2[4]	160.2(2)	O4	Dy2	O2[4]	82.0(5)	O3	Y2	O2	81.82(18)	136.01(11)	
O3	Dy2	O2[5]	88.0(2)	O4	Dy2	O3[1]	80.7(9)	O3	Y2	O1	88.86(18)		
O3	Dy2	O3[1]	99.7(3)	O4	Dy2	O3	81.3(6)	Y2	O3	Y1	107.03(17)	144.31(18)	
O3[1]	Dy2	Dy1[1]	37.80(13)					Y2	O1H	Y1	113.5(2)	160.43(18)	
O3[1]	Dy2	Dy1	83.76(14)										

[1]+x,+y,3/2-z; [2]+y,1-x+y,1/2+z; [3]+y,1-x+y,1-z; [4]1-y,1+x-y,+z; [5]+y-x,1-x,+z; [6]1-y+x,+x,1-z

2.19_{Eu}											
Atom	**Atom**	**Atom**	**Angle/˚**	**Atom**	**Atom**	**Atom**	**Angle/˚**	**Atom**	**Atom**	**Atom**	**Angle/˚**
Eu1[1]	Eu1	Eu2	62.928(3)	O1	Eu1	N1[3]	137.56(7)	O1[2]	Eu1	N1	137.56(7)
Eu1[1]	Eu1	Eu2[2]	62.927(3)	O1	Eu1	Eu2[2]	135.26(4)	O1[2]	Eu1	Eu2[2]	35.30(4)
Eu1[1]	Eu2	Eu1	54.144(6)	O1	Eu1	Eu2	35.30(4)	O1[2]	Eu1	Eu2	97.80(4)
Eu1[1]	O4	Eu1	96.13(8)	O1	Eu2	Eu1[1]	85.20(4)	O1[3]	Eu1	Eu1[1]	91.25(4)
Eu2	O1	Eu1	106.94(6)	O1	Eu2	Eu1	37.76(4)	O1[3]	Eu1	O1	119.954(3)
Eu2	O4	Eu1	111.88(7)	O1	Eu2	O1[1]	101.90(8)	O1[3]	Eu1	N1	69.02(6)
Eu2	O4	Eu1[1]	111.88(7)	O1	Eu2	O2[4]	81.96(6)	O1[3]	Eu1	N1[2]	137.56(7)
Eu2[2]	Eu1	Eu2	100.912(4)	O1	Eu2	O2[5]	145.29(6)	O1[3]	Eu1	N1[3]	64.98(6)
N1	Eu1	Eu1[1]	131.11(6)	O1	Eu2	O3[5]	159.95(6)	O1[3]	Eu1	Eu2	135.26(4)
N1	Eu1	Eu2[2]	158.99(5)	O1	Eu2	O3[4]	86.93(6)	O1[3]	Eu1	Eu2[2]	97.80(4)
N1	Eu1	Eu2	99.87(5)	O1	Eu2	O5	79.95(6)	O2[4]	Eu2	Eu1	77.08(5)
N1[2]	Eu1	Eu1[1]	131.11(6)	O1[1]	Eu2	Eu1[1]	37.76(4)	O2[4]	Eu2	Eu1[1]	109.88(4)
N1[2]	Eu1	N1	81.46(8)	O1[1]	Eu2	Eu1	85.20(4)	O2[4]	Eu2	O3[5]	101.11(6)
N1[2]	Eu1	Eu2	78.04(5)	O1[1]	Eu2	O2[5]	81.95(6)	O2[4]	Eu2	O3[4]	53.17(6)
N1[2]	Eu1	Eu2[2]	99.88(5)	O1[1]	Eu2	O2[4]	145.29(6)	O2[5]	Eu2	Eu1	109.88(4)
N1[3]	Eu1	Eu1[1]	131.11(6)	O1[1]	Eu2	O3[4]	159.95(6)	O2[5]	Eu2	Eu1[1]	77.08(5)
N1[3]	Eu1	N1[2]	81.46(8)	O1[1]	Eu2	O3[5]	86.92(6)	O2[5]	Eu2	O2[4]	76.54(9)
N1[3]	Eu1	N1	81.46(8)	O1[1]	Eu2	O5	79.96(6)	O2[5]	Eu2	O3[5]	53.17(6)
N1[3]	Eu1	Eu2[2]	78.04(5)	O1[2]	Eu1	Eu1[1]	91.25(4)	O2[5]	Eu2	O3[4]	101.11(6)
N1[3]	Eu1	Eu2	158.99(5)	O1[2]	Eu1	O1[3]	119.951(3)	O3[4]	Eu2	Eu1	111.75(4)
O1	Eu1	Eu1[1]	91.25(4)	O1[2]	Eu1	O1	119.953(3)	O3[4]	Eu2	Eu1[1]	162.29(4)
O1	Eu1	N1[2]	69.02(6)	O1[2]	Eu1	N1[2]	64.98(6)	O3[5]	Eu2	Eu1	162.29(4)
O1	Eu1	N1	64.98(6)	O1[2]	Eu1	N1[3]	69.02(6)	O3[5]	Eu2	Eu1[1]	111.75(4)

[1]+x,+y,3/2-z; [2]1-y,1+x-y,+z; [3]+y-x,1-x,+z; [4]+y,1-x+y,1-z; [5]+y,1-x+y,1/2+z; [6]1-y+x,+x,1-z

Table A2.5. Hydrogen bonding interactions (Å. º) of compound **2.7$_{Dy}$**

D-H···A[a]	*D-H*	*H···A*	*D···A*	*D-H···A*
N1-H1A···O1[1]	0.91	2.10	2.951 (10)	155.8
[1]1-x,1-y,1-z		[a]**D: donor. A: acceptor.**		

A2.4 Powder X-ray diffraction analysis

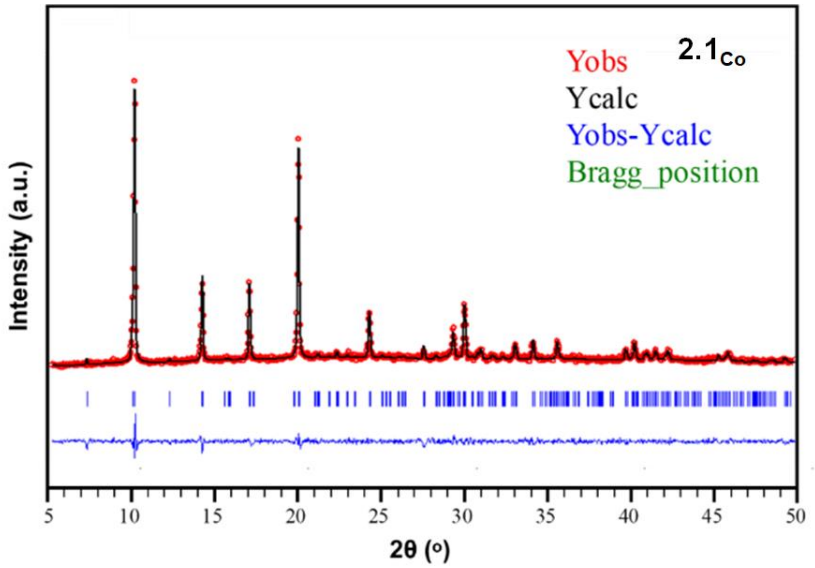

Figure A2.2. Figure of the pattern matching analysis and experimental PXRD for complex **2.1$_{Co}$.**

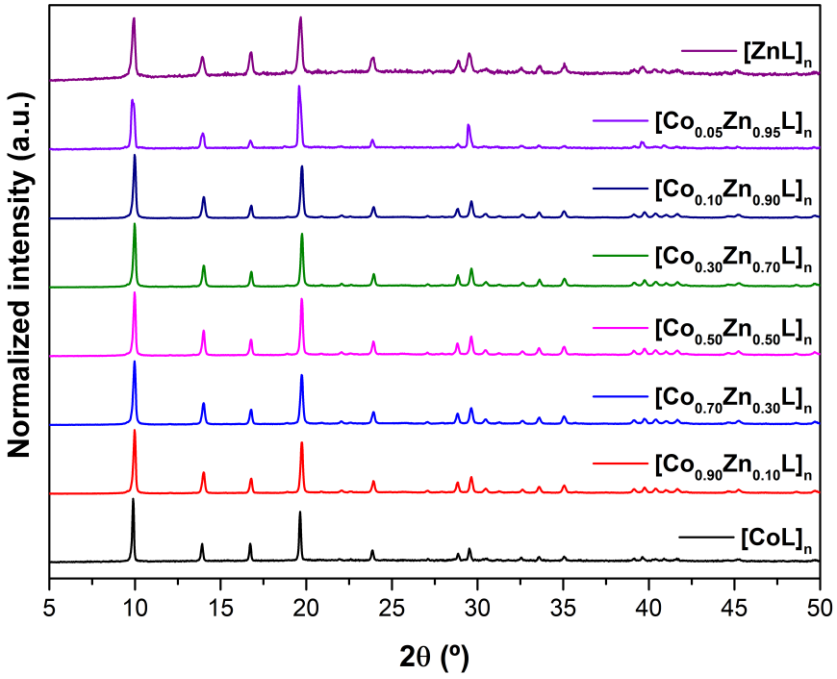

Figure A2.3. Experimental PXRD of $[Co_xZn_{1-x}L]_n$ heterometallic samples.

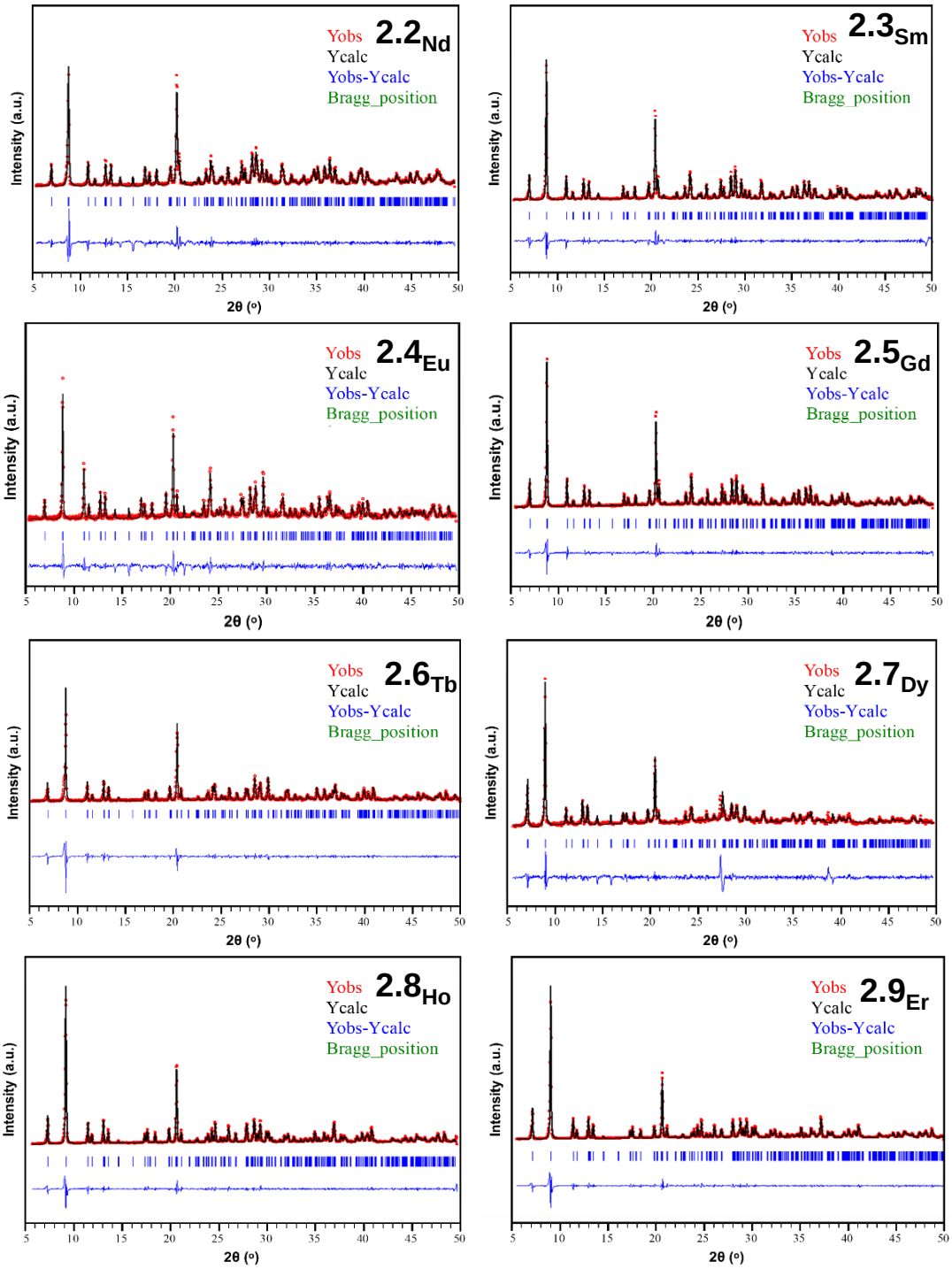
Yobs
Ycalc
Yobs-Ycalc
Bragg_position
2.2Nd
2.3Sm
2.4Eu
2.5Gd
2.6Tb
2.7Dy
2.8Ho
2.9Er
Intensity (a.u.)
2θ (°)

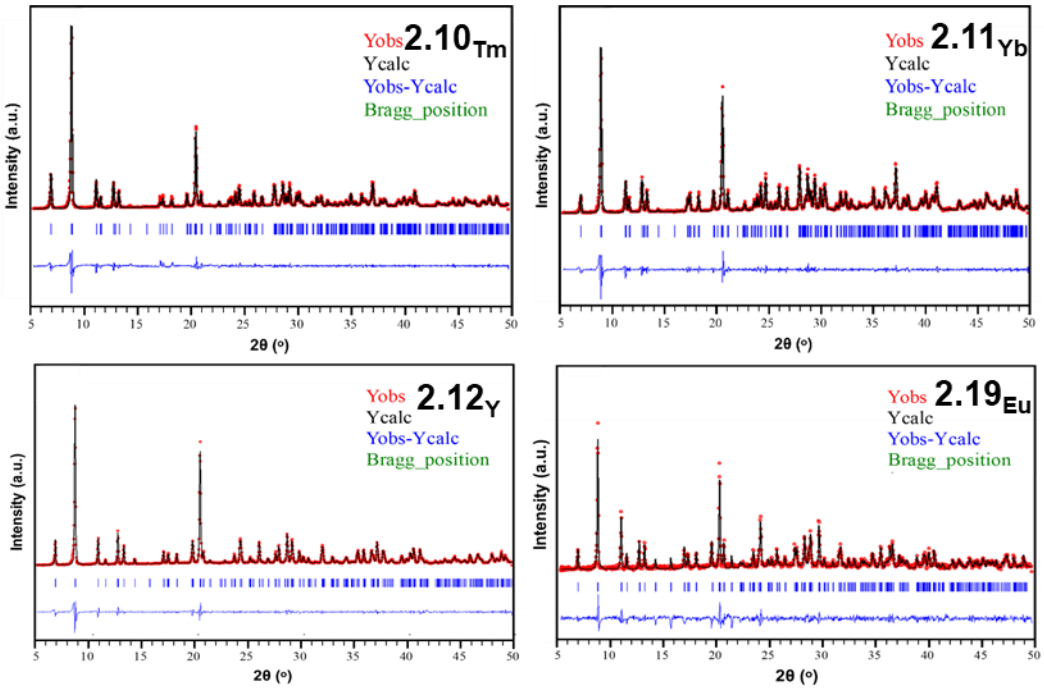

Figure A2.4. Figure of the pattern matching analysis and experimental PXRD for complexes **2.2-2.11.**

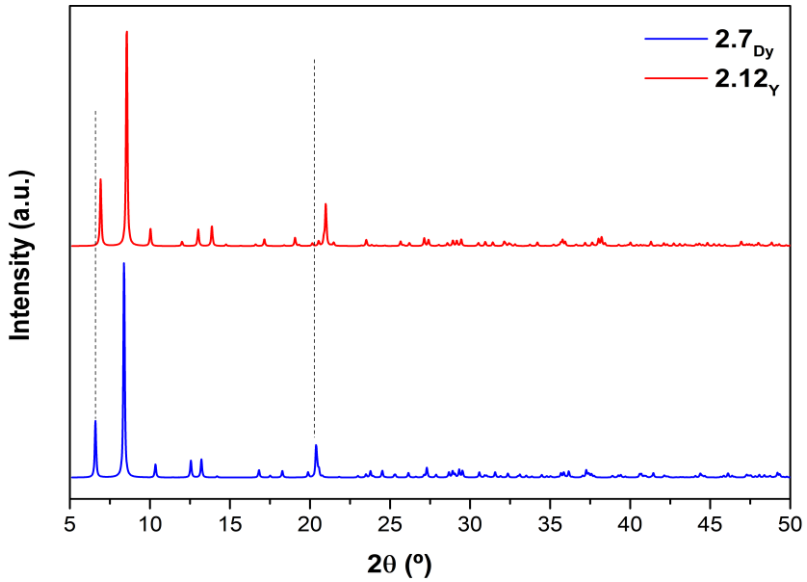

Figure A2.5. Figure of the theoretical simulated-PXRD for complexes **2.7$_{Dy}$** and **2.12$_{Y}$.**

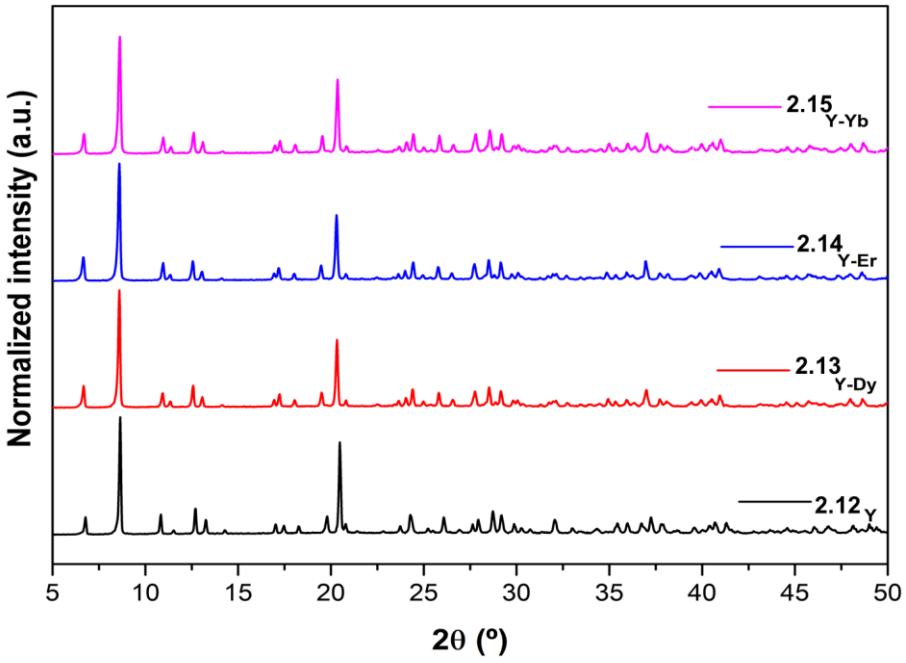

Figure A2.6. PXRD for complexes **2.12-2.15.**

When the quaternary compounds (containing yttrium. europium and terbium ions and the ligand) are characterized, it is observed that, depending on the Y^{3+} to Ln^{3+} doping proportion. PXRD patterns present diffraction maxima corresponding to both pure compounds **2.12** and **2.2-2.11.** This fact, *a priori*, is indicative of a crystal phase segregation, although it makes no much sense given the isostructural nature of the compounds. Nevertheless, SEM mapping experiments have shown that even if mixture of two type of crystals could happen, the three elements are randomly distributed along a single crystal (Figure A2.17 and Figure A2.18).

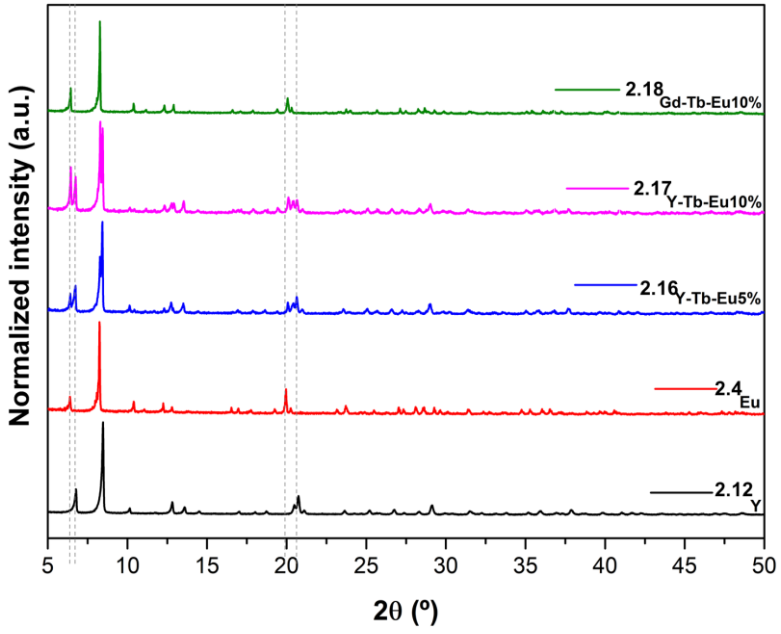

Figure A2.7. PXRD for complexes **2.4, 2.12, 2.12, 2.16-2.18.**

A2.5 Continuous Shape Measurements

CShMs for the coordination environment of compound **2.1** and **2.7**. The lowest SHAPE values for each ion are shown highlighted in bold, indicating best fits.

Table A2.6. Table of the continuous Shape Measurements for the CoO_4 coordination environment.

SP-4	D_{4h}	Square
T-4	Td	Tetrahedron
SS-4	C_{2v}	Seesaw
vTBPY-4	C_{3v}	Vacant trigonal bipyramid

Complex	SP-4	T-4	SS-4	vTBPY-
2.1$_{Co}$	30.170	**1.878**	4.528	2.270

Table A2.7. Table of the continuous Shape Measurements for the CoN_2O_4 coordination environment.

HP-6	D_{6h}	Hexagon
PPY-6	C_{5v}	Pentagonal pyramid
OC-6	O_h	Octahedron
TPR-6	D_{3h}	Trigonal prism
JPPY-6	C_{5v}	Johnson pentagonal pyramid J2

Complex	HP-6	PPY-6	OC-6	TPR-6	JPPY-6
2.1$_{Co}$	34.045	12.509	12.883	**7.490**	15.585

Table A2.8. Table of the continuous Shape Measurements for the LnN_3O_6 coordination environment.

EP-9	D_{9h}	Enneagon
OPY-9	C_{8v}	Octagonal pyramid
HBPY-9	D_{7h}	Heptagonal bipyramid
JTC-9	C_{3v}	Johnson triangular cupola J3
JCCU-9	C_{4v}	Capped cube J8
CCU-9	C_{4v}	Spherical-relaxed capped cube
JCSAPR-9	C_{4v}	Capped square antiprism J10
CSAPR-9	C_{4v}	Spherical capped square antiprism
JTCTPR-9	D_{3h}	Tricapped trigonal prism J51
TCTPR-9	D_{3h}	Spherical tricapped trigonal prism
JTDIC-9	C_{3v}	Tridiminished icosahedron J63

HH-9	C_{2v}	Hula-hoop
MFF-9	C_s	Muffin

Complex	JCSAPR-9	CSAPR-9	JTCTPR-9	TCTPR-9	MFF-9
2.7$_{Dy}$ (Dy1)	2.280	1.243	2.073	**0.890**	1.630
2.12$_{Y}$ (Y1)	2.372	1.493	1.855	**0.829**	2.180
2.19$_{Eu}$ (Eu1)	2.315	1.361	1.904	**0.666**	2.050

Table A2.9. Table of the continuous Shape Measurements for the LnO_8 coordination environment

OP-8	D_{8h}	Octagon
HPY-8	C_{7v}	Heptagonal pyramid
HBPY-8	D_{6h}	Hexagonal bipyramid
CU-8	O_h	Cube
SAPR-8	D_{4d}	Square antiprism
TDD-8	D_{2d}	Triangular dodecahedron
JGBF-8	D_{2d}	Johnson - Gyrobifastigium (J26)
JETBPY-8	D_{3h}	Johnson - Elongated triangular bipyramid (J14)
JBTP-8	C_{2v}	Johnson - Biaugmented trigonal prism (J50)
BTPR-8	C_{2v}	Biaugmented trigonal prism
JSD-8	D_{2d}	Snub disphenoid (J84)
TT-8	T_d	Triakis tetrahedron
ETBPY-8	D_{3h}	Elongated trigonal bipyramid

Complex	SAPR-8	TDD-8	JBTPR-8	BTPR-8	JSD-8
2.7$_{Dy}$ (Dy2)	2.973	**2.770**	3.784	3.342	5.612
2.12$_{Y}$ (Y2)	2.927	**2.713**	3.638	3.183	5.487
2.19$_{Eu}$ (Eu2)	2.700	**2.649**	3.578	3.183	5.448

A2.6 Thermal analysis

Thermogravimetric analyses have been performed over polycrystalline sample in compound **2.1, 2.7, 2.12** and **2.19** in order to check the stability of the product.

The TG curves for **2.1** and **2.7** has been collected before and after solvent exchange with MeOH. Solvent exchange procedure has been accomplished as an approach to replace lattice-solvent molecules (dimethylformamide and water) to ease material activation to posteriorly analyse its adsorptive-capacity. Powder X-ray diffraction confirmed that compounds **2.1** and **2.7** remains stable after solvent exchange with MeOH as it can be seen in Figure A2.8 and Figure A2.9, down.

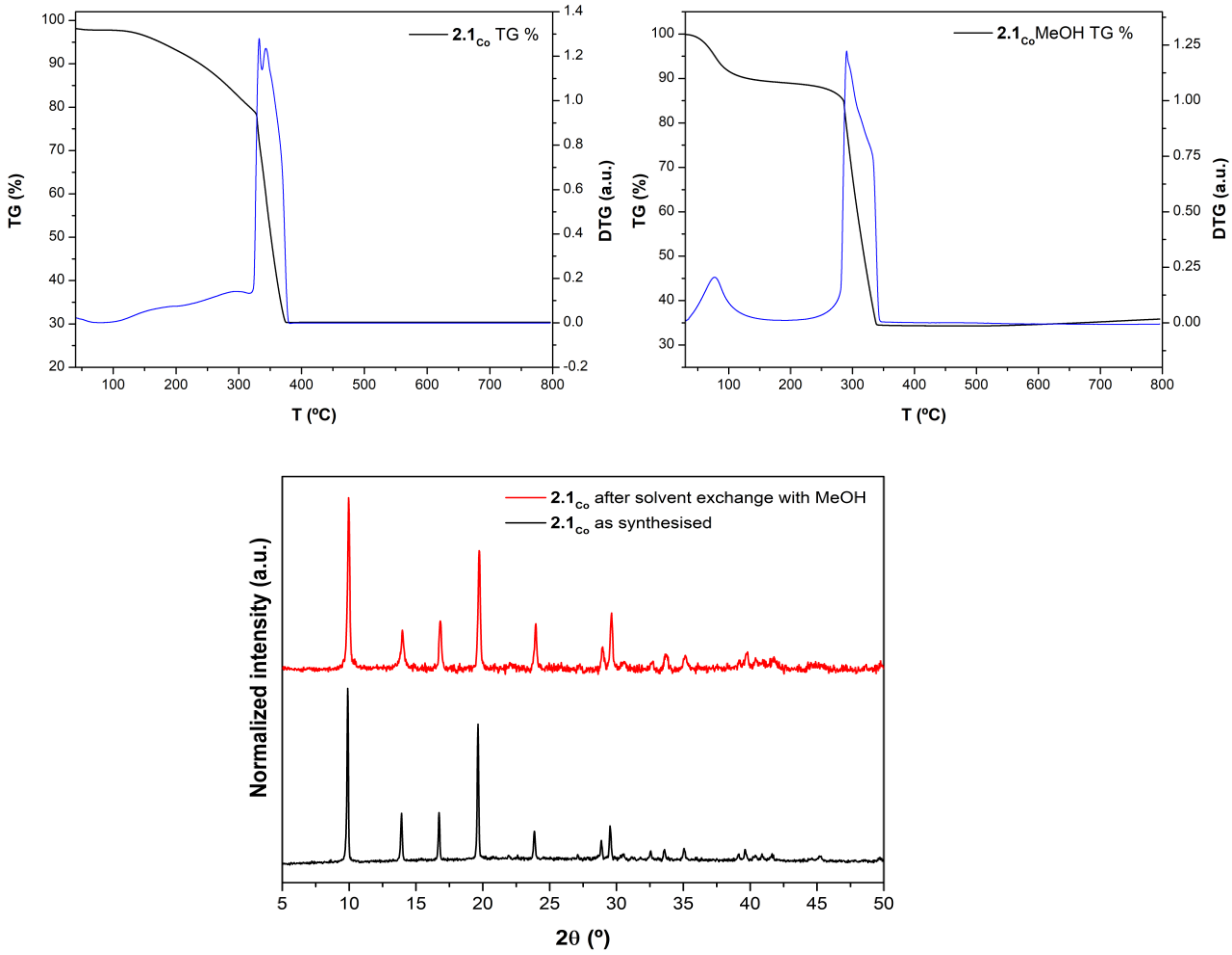

Figure A2.8. Figure of TG/DTG analysis of compound **2.1** (left -up, as synthesised, right -up, after solvent exchange with MeOH) and figure of the experimental PXRD for complex **2.1** before and after solvent exchange with MeOH (down).

More concretely, TG curve of Co_MOF (**2.1**) shows two main steps of weight loses. The first step concerns to the progressive loss of the solvent lattice molecules (DMF and H_2O) which are released from room temperature up to 300ºC. Then, an abrupt descent can be seen that

corresponds to the collapse of the crystal structure. From the shape of the TG curve, it seems that solvent molecules stabilise the structure and their removal promote crystal structure decomposition. However, TG curve of Co_MOF (**2.1**) after solvent exchange with methanol (this procedure has been carried out suspending three times the material in MeOH for an hour) shows two well defined steps. The first step comprises the loss of lattice solvent molecules, which occurs at 100 ºC, and agrees with an efficient DMF to MeOH exchange. Subsequently, from 110 ºC to 300 ºC the TG curve of the compound describes a plateau, where the empty skeleton of the MOF is gotten. Finally, at 300 ºC ligand decomposition occurs and involves the collapse of the crystal structure, evolving to Co_3O_4 that is obtained at 800 ºC as the final residue.

The TG curves has been collected for compound **2.7$_{Dy}$** before and after solvent exchange with MeOH. This procedure has been carried out suspending the material in MeOH for 16 h. The thermal behaviour of the bulk $[Dy_5L_6(OH)_3(DMF)_3]\cdot 5H_2O$, compound **2.7$_{Dy}$**, as synthesised materials were also investigated between ambient temperature and ca. 800 ºC in order to study its thermal stability. Due to the isotypical nature of the compounds the following paragraph discussion will be solely focused on compound **2.7$_{Dy}$**. Three main regions are appreciable in the TG curve. The first weight loss, between ambient temperature and up to 300 ºC concerns to the progressive loss of solvent molecules, firstly, lattice, water molecules and then coordinated DMF molecules. Above this temperature there is an abrupt descent that corresponds to the collapse of the crystal structure. From the shape of the TG curve, it seems that solvent molecules stabilise the structure and their removal promote crystal structure decomposition. In the final step as a consequence of the decomposition of the organic content metal oxide is obtained.

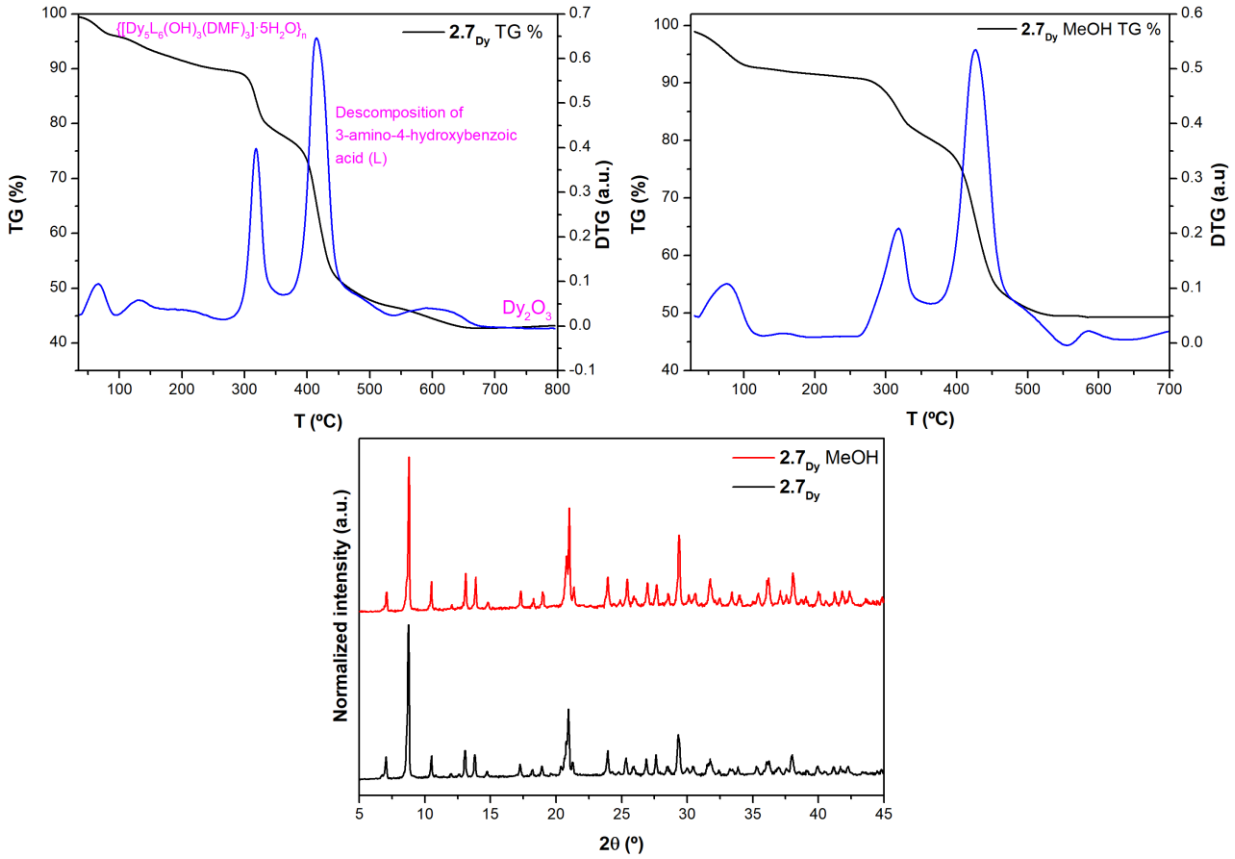

Figure A2.9. Figure of TG/DTG analysis of compound **2.7$_{Dy}$** (up-left, as synthesised). after solvent exchange with MeOH during 16 h (up-right) and figure of the experimental PXRD for complex **2.7$_{Dy}$** before and after solvent exchange with MeOH (down).

After solvent exchange with MeOH, TG curve performed in **2.7$_{Dy}$**_MeOH shows a plateau at around 100 ºC suggesting that solvent molecules (DMF and water) have been properly replaced with MeOH which would evaporate up to the indicated temperature. Around 100-200 ºC it seems that the MOF desolvatated skeleton is obtained. Finally, as another evidence for the proper solvent exchange, final-residue Dy_2O_3 percentage has increased by 6 %. It is expected since DMF and water molecules are heavier and have higher boiling points than MeOH.

Thermogravimetric analyses have been performed over polycrystalline sample in compounds **2.12$_{Y}$** show two main steps of weight loses. The first steps concerns to the release of the water lattice molecules which are released from room temperature up to 275 ºC. Then, it starts the loss of coordinated DMF molecules, which is somewhat overlapped with the third step corresponding to the decomposition of the ligands. The latter involves the collapse of the crystal structure, evolving to Y_2O_3 that is obtained at 800 ºC as the final residue. On its part, thermogravimetric analyses have been performed over polycrystalline sample in compounds **2.19** exhibit two main steps of weight loses. The first steps concern to the release of the solvent molecules which are released from room temperature up to 275 ºC. The second step refers to the

decomposition of the ligands which involves the collapse of the crystal structure, evolving, to Eu_2O_3 obtained at 800 ºC as the final residue.

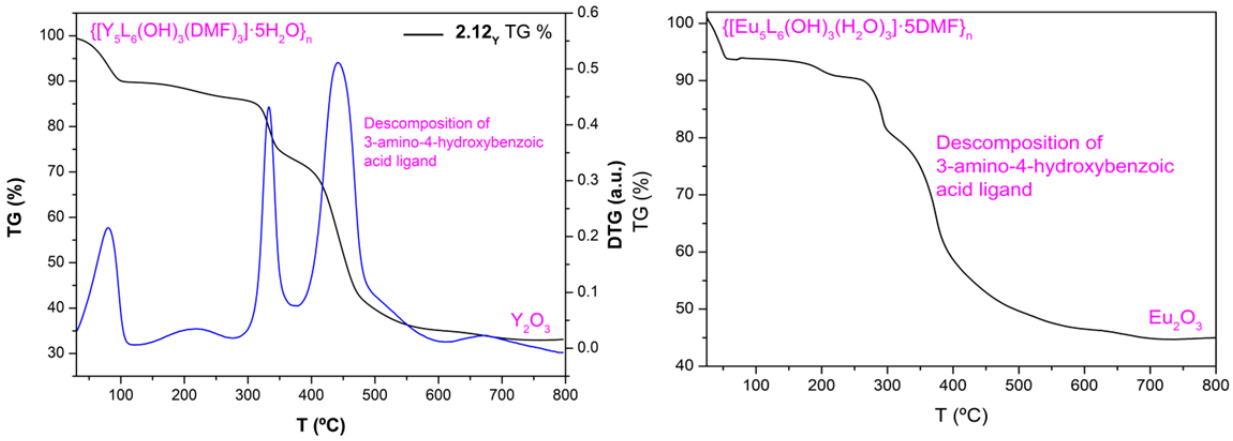

Figure A2.10. Figure of TG analysis of compounds **2.12$_Y$** (left) and **2.19$_{Eu}$** (right).

A2.7 Thermal evolution

Thermal evolution of **2.1$_{Co}$** shows that the compound maintains its crystallinity up to 300 ºC. These results come in line with thermogravimetric analysis, where it could be seen that above this temperature structure collapses and evolves into the metallic residue Co_3O_4 at around 800 ºC.

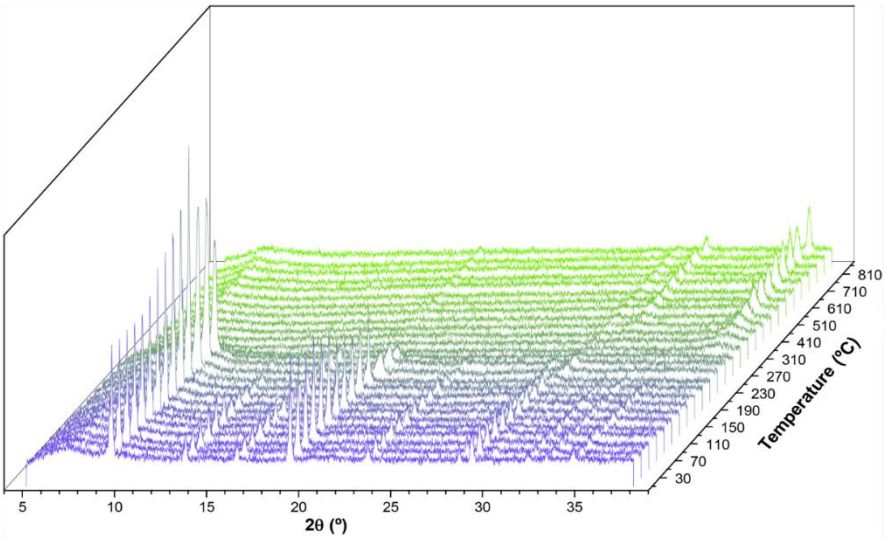

Figure A2.11. Thermal evolution of compound **2.1$_{Co}$**.

Thermal evolution of compound **2.7$_{Dy}$** shows that the compound maintains its crystallinity up to 230 ºC. These results come in line with thermogravimetric analysis, where it could be seen that above this temperature structure collapses and evolves into the metallic residue Dy_2O_3 at around 800 ºC.

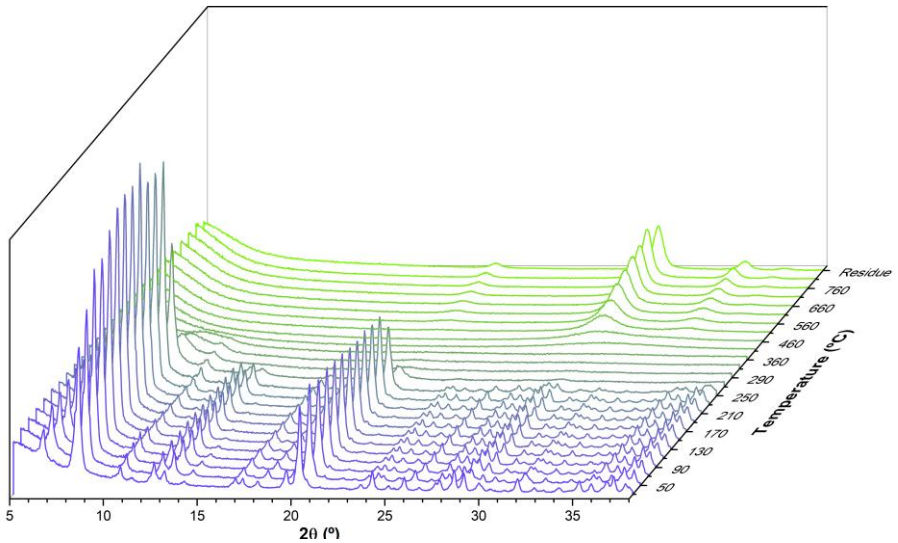

Figure A2.12. Thermal evolution of compound **2.7$_{Dy}$.**

A2.8 Additional views of the structure

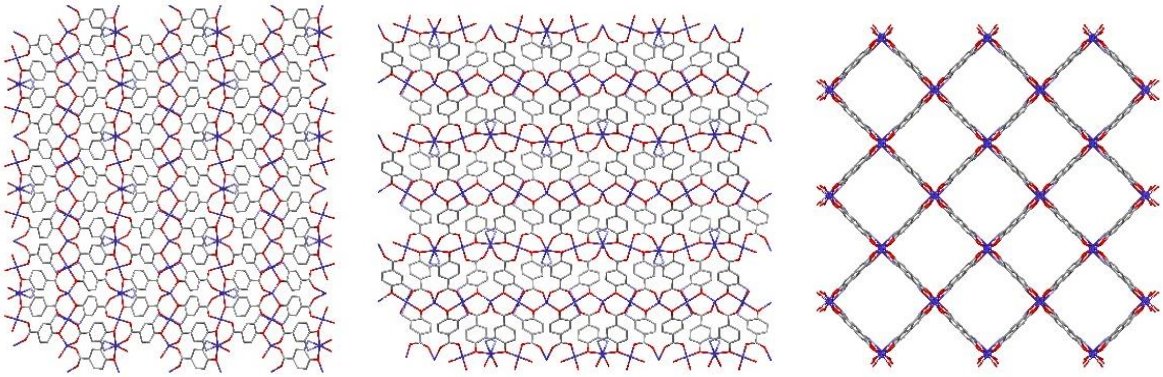

Compound 2.1

Figure A2.13. View along *a, b* and *c* axis (from left to right) of complex **2.1**$_{Co}$.

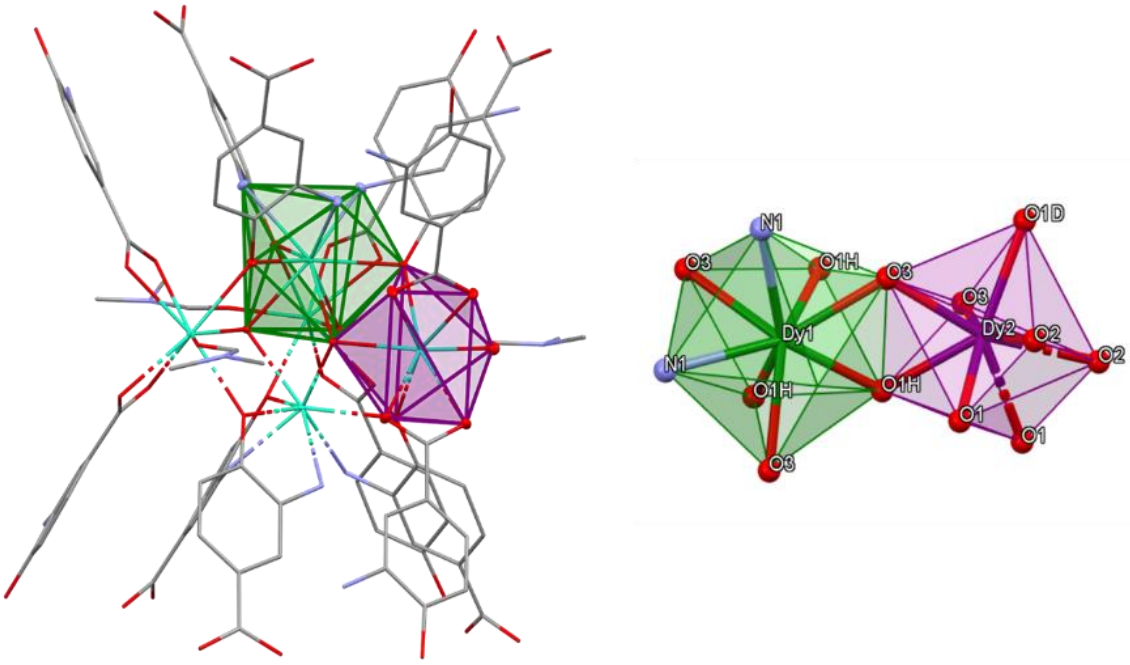

Figure A2.14. View of pentametallic nodous showing Dy1 and Dy2 coordination polyhedral.

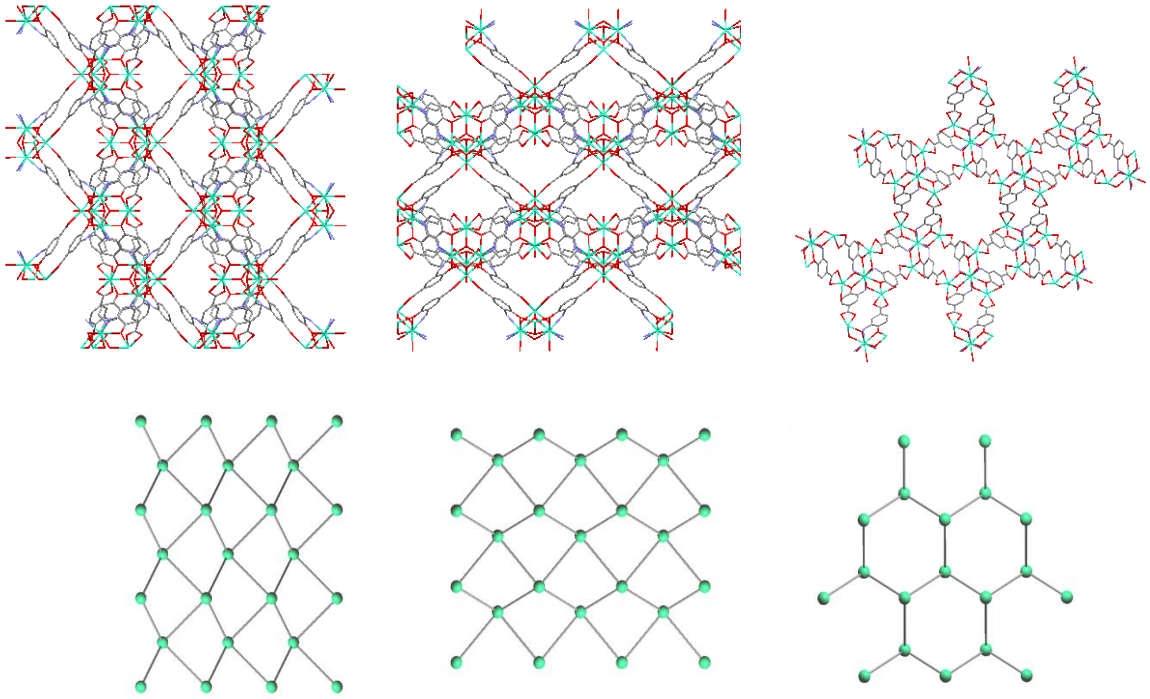

Compound 2.7

Figure A2.15. View along *a, b* and *c* axis (from left to right) of complex the topological representation along *a*. *b* and *c* axis (down).

A2.9 Scanning electron Microscopy

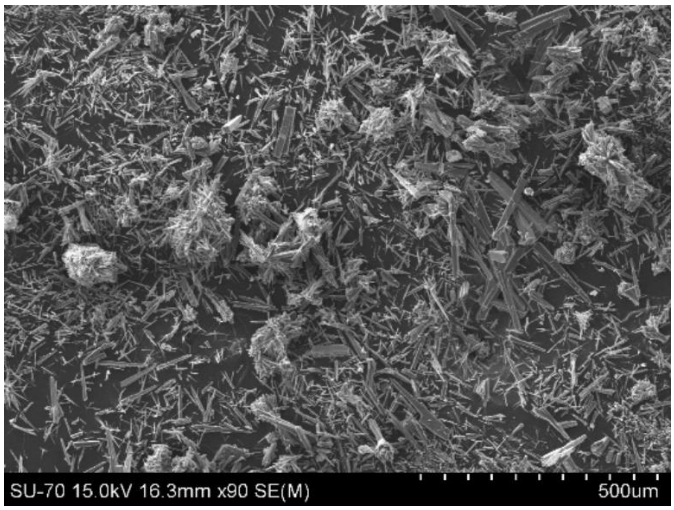

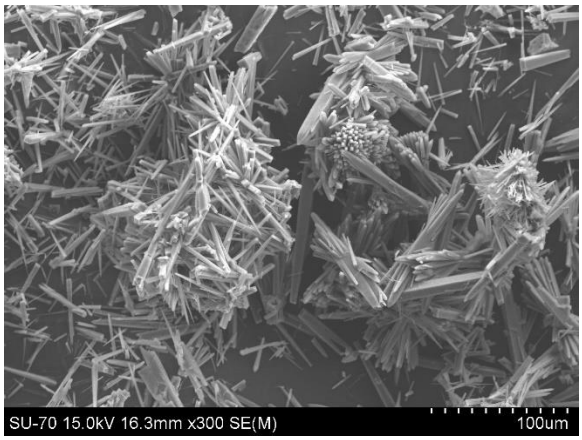

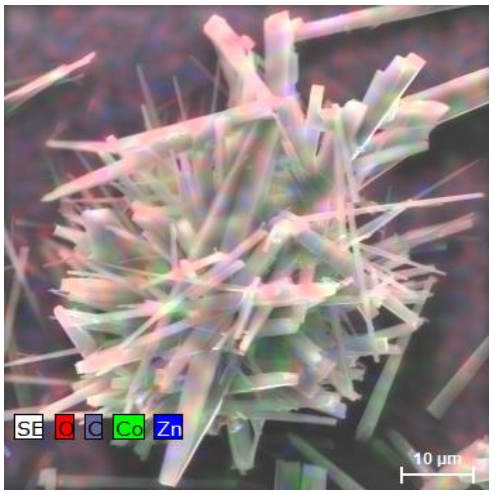

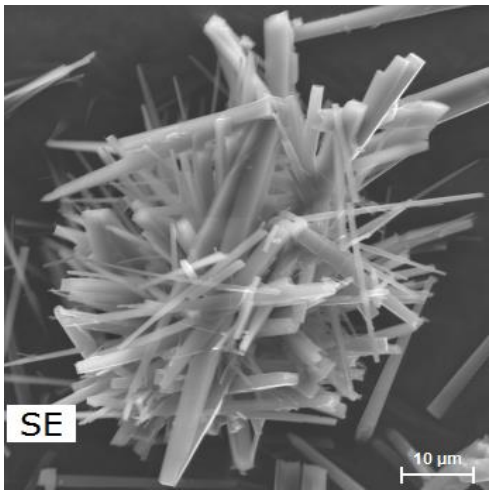

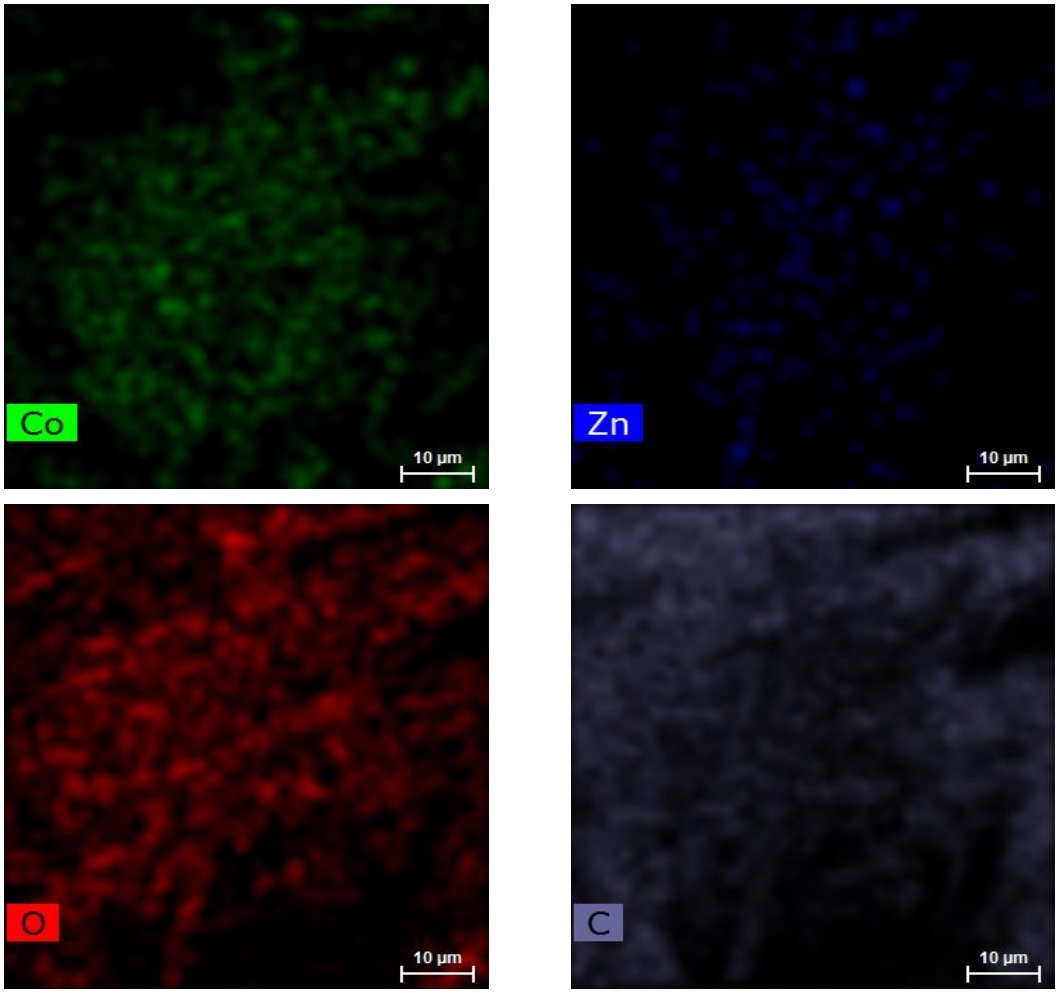

Figure A2.16. SEM-EDS spectrum performed in single crystal of $[Co_{0.9}Zn_{0.1}L]_n$.

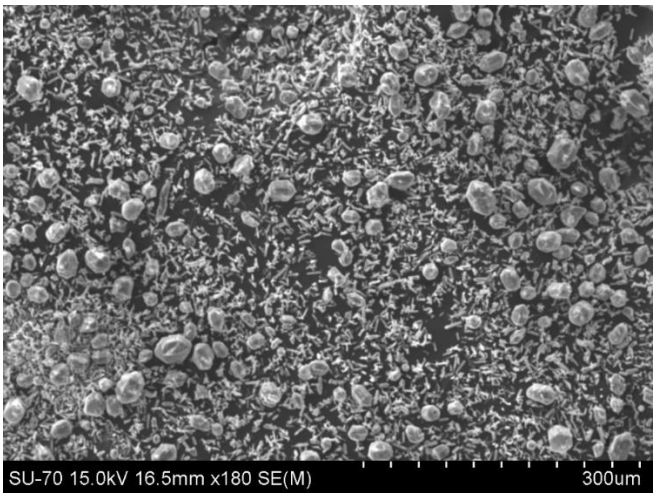

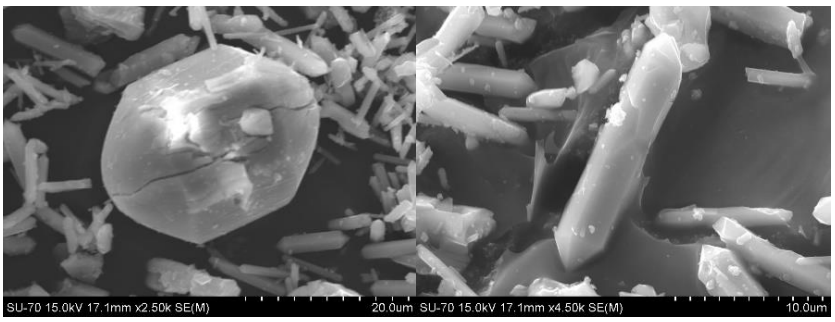

Figure A2.17. SEM images of compound **2.17$_{\text{Y-Tb-Eu10\%}}$** where two types of crystal are distinguished.

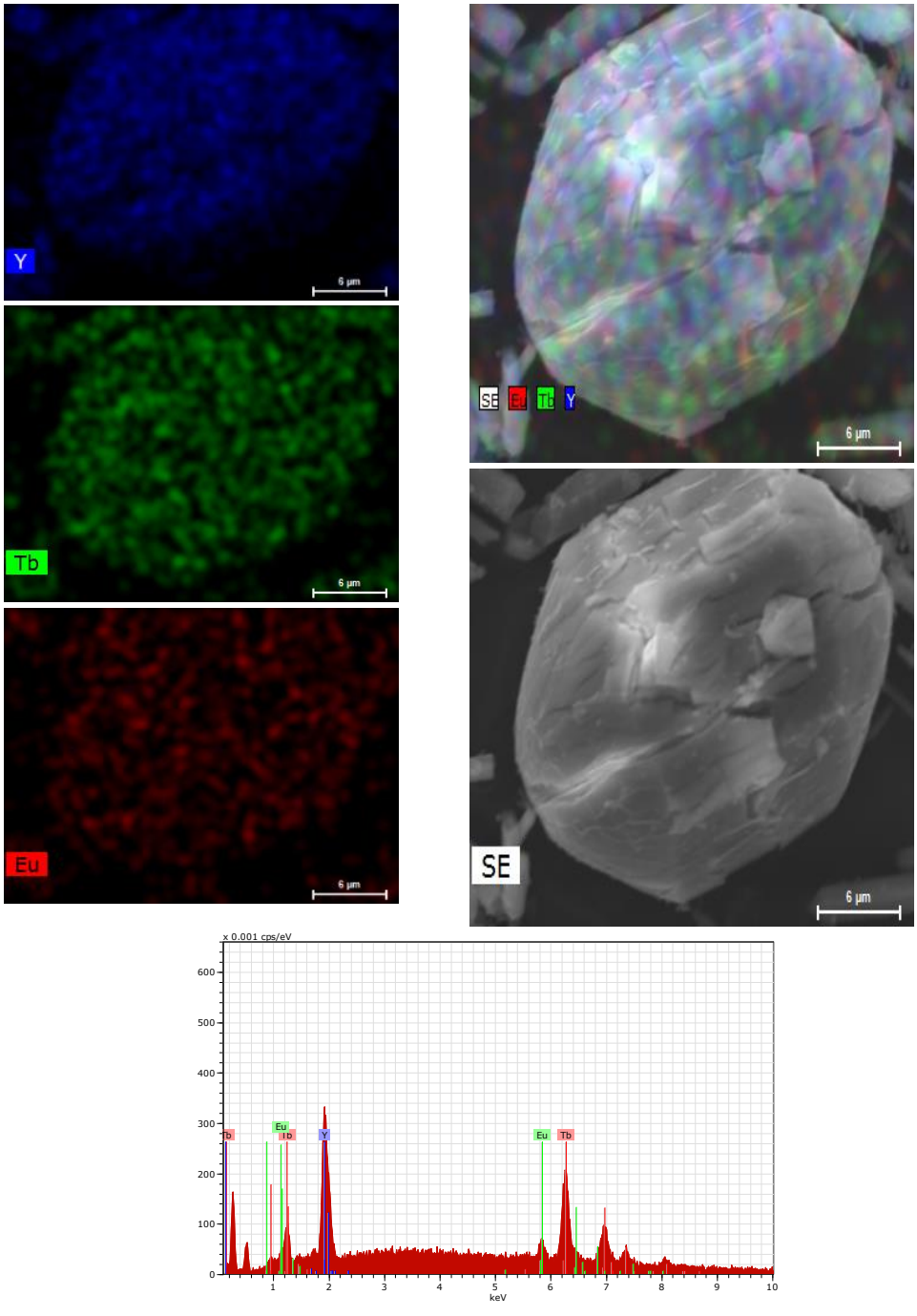

Spectrum: crystal type 1

Element	Series	unn. C [wt.%]	norm. C [wt.%]	Atom. C [at.%]	Error (3 Sigma) [wt.%]
Terbium	L-series	37.80	56.13	**43.91**	3.78
Europium	L-series	6.10	9.05	**7.41**	0.84
Yttrium	L-series	23.44	34.81	**48.68**	3.04
Total:		67.34	100.00	100.00	

Figure A2.18. SEM image, EDS spectrum and elemental quantitative data representative of the crystal type 1 of compound **2.17**$_{\text{Y-Tb-Eu10\%}}$.

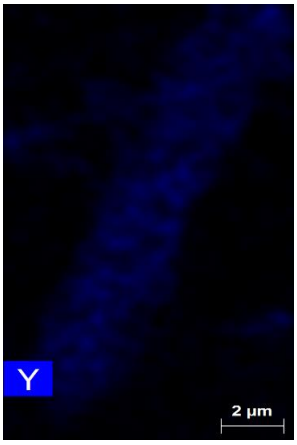
Y
2 µm

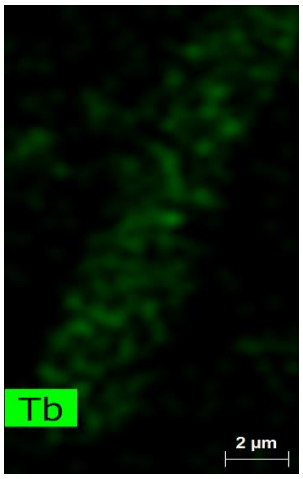
Tb
2 µm

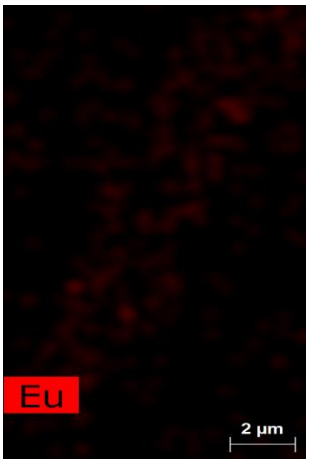
Eu
2 µm


SE
Eu
Tb
Y
2 µm

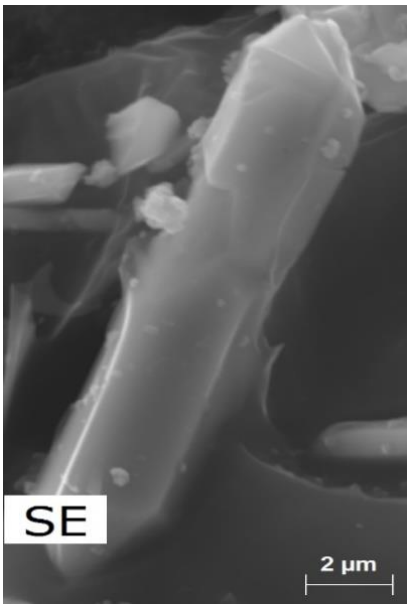
SE
2 µm

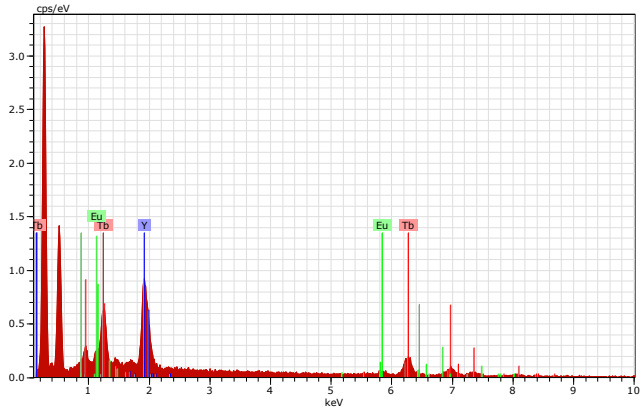

Spectrum: crystal type 2

Element	Series	unn. C [wt.%]	norm. C [wt.%]	Atom. C [at.%]	Error (3 Sigma) [wt.%]
Terbium	L-series	39.37	55.08	**42.75**	4.18
Europium	L-series	6.29	8.81	**7.15**	1.01
Yttrium	L-series	25.81	36.11	**50.10**	3.23
Total:		71.47	100.00	100.00	

Figure A2.19. SEM image, EDS spectrum and elemental quantitative data representative of the crystal type 2 of compound **2.17**$_{\text{Y-Tb-Eu10\%}}$.

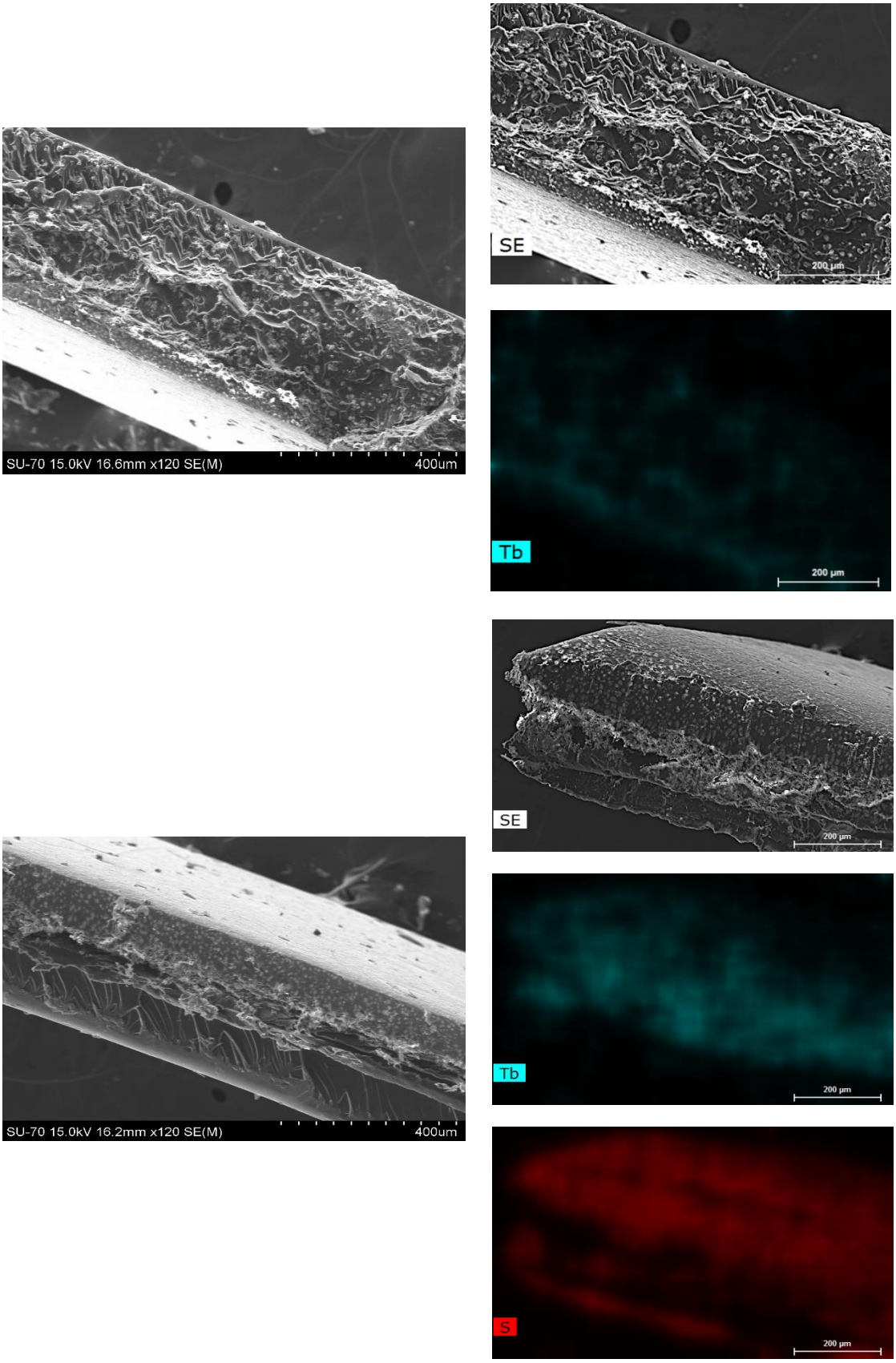

Figure A2.20. Cross section EDS mapping of **2.6$_{Tb}$@PMMA** (up) and **2.6$_{Tb}$ @PSF** (buttom) membranes.

A2.10 *Ac* magnetic susceptibility measurements

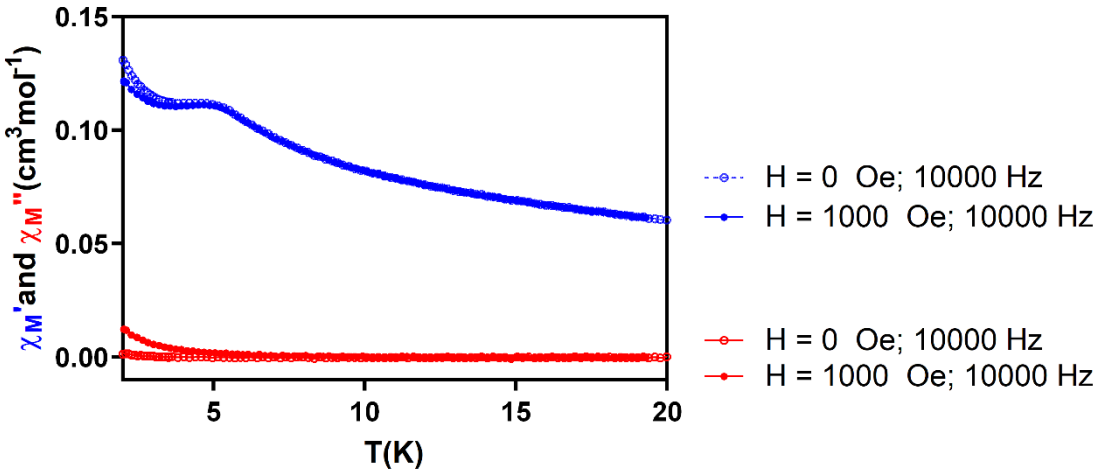

Figure A2.21. Temperature dependence of in-phase (blue) and out of phase (red) components of the *ac* susceptibility in a *dc* applied field of 1000 Oe for **2.1$_{Co}$**.

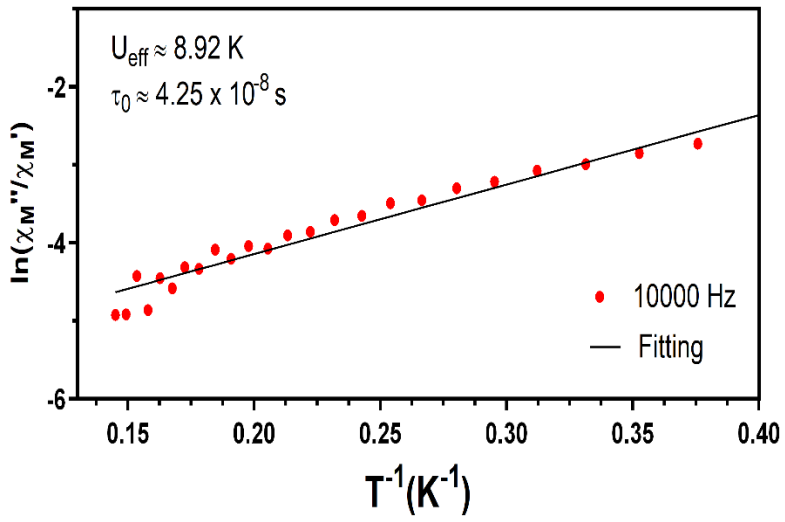

Figure A2.22. Plot of ln(χ_M''/χ_M') versus 1/T at 10000 Hz for compound **2.1$_{Co}$** under an applied field of 1000 Oe. The solid lines represent the linear fit with ln(χ_M''/χ_M') = ln($2\pi\nu\tau_0$)+ E_a/k_BT.

Table A2.10. NEVPT2- calculated on the fully optimized structures D, E/D, g-tensor and energy-separation between KD1-KD2 and KD1-KD3.

Parameters	TPR	Td
D (D_{KD1-2}, D_{KD1-3})/ cm^{-1}	-58.7 (-48.6, 46.7)	-31.4 (25.2, -28.1)
E/D	0.21	0.18
g_{xx}, g_{yy}, g_{zz}	2.08, 2.45, 2.93	2.16, 2.28, 2.6
ΔE(1–2), ΔE(1–3) / cm^{-1}	2367.2, 5325.4	3432.7, 4453.7

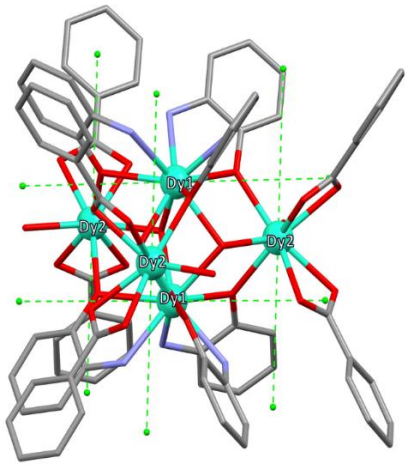

Figure A2.23. Magnetic axes of the Dy^{III} ions calculated with the Magellan software for compound **2.7**.[7]

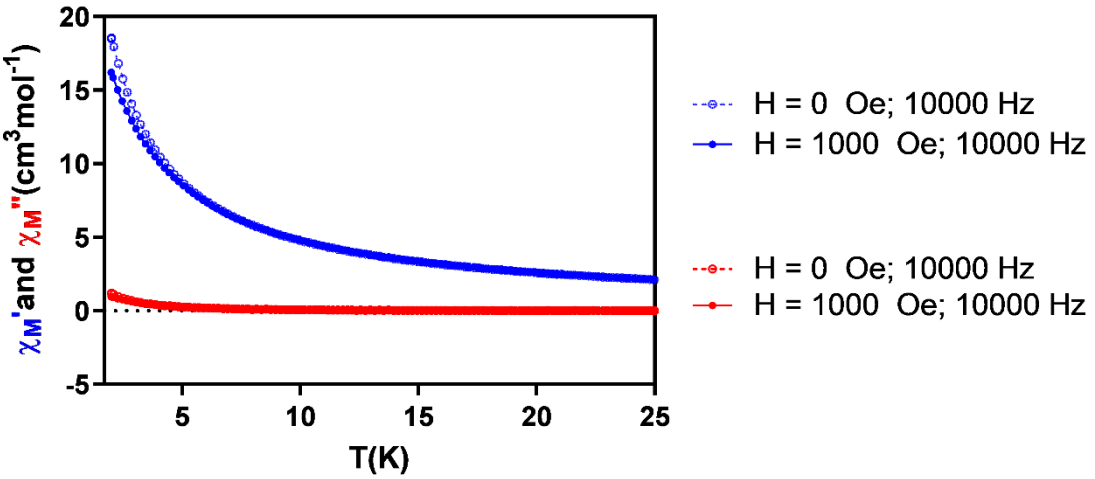

Figure A2.24. Temperature dependence of in-phase (red) and out-of-phase (blue) components of the *ac* susceptibility in a zero applied dc field for **2.7**$_{Dy}$.

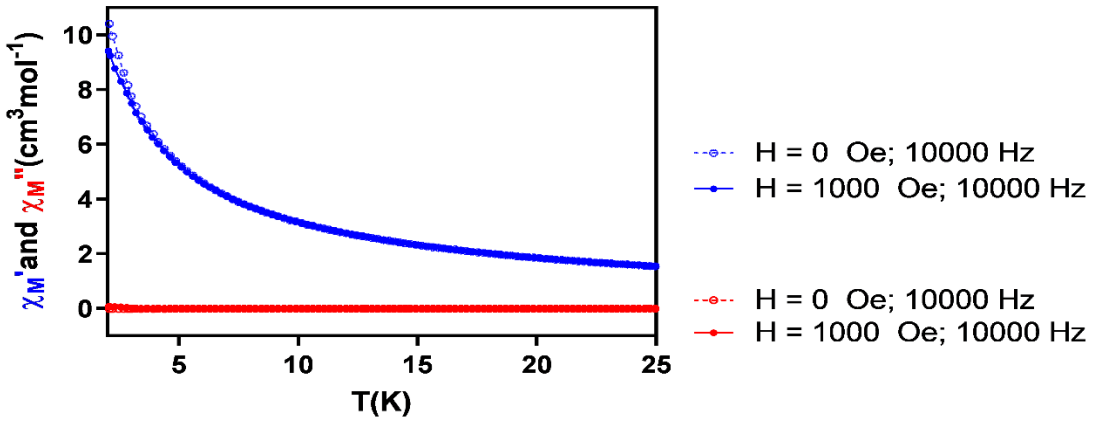

Figure A2.25. Temperature dependence of in-phase (red) and out-of-phase (blue) components of the ac susceptibility in a zero applied dc field for **2.9**$_{Er}$.

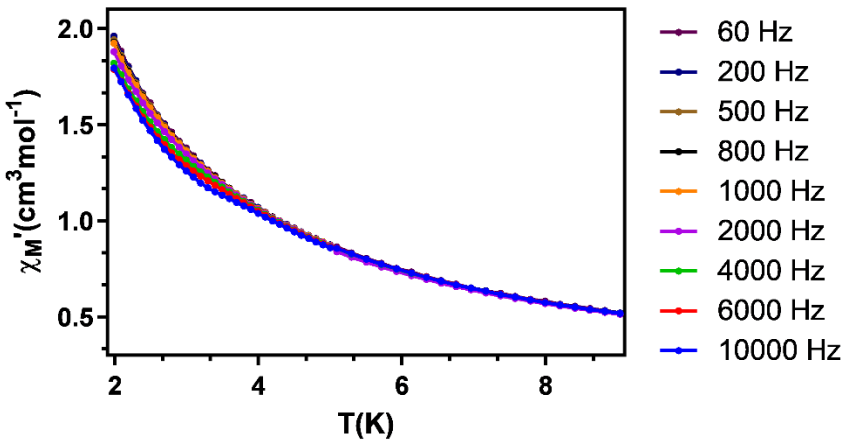

Figure A2.26. Temperature dependence of in-phase components of the *ac* susceptibility in a *dc* applied field of 1000 Oe for **2.11**$_{Yb}$.

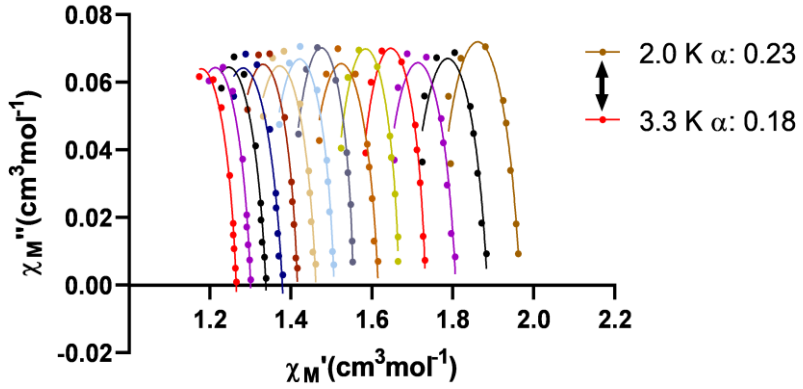

Figure A2.27. Cole-Cole plots in a *dc* applied field of 1000 Oe for **2.11**$_{Yb}$.

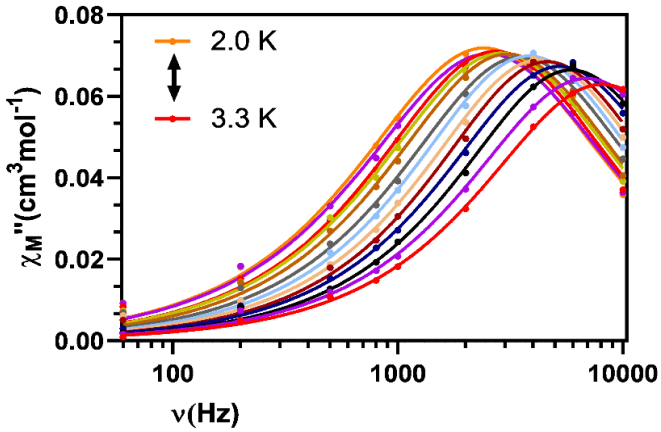

Figure A2.28. Variable-temperature frequency dependence of the χ_M'' signal under 1000 Oe applied field for **2.11**$_{Yb}$. Solid lines represent the best fitting of the experimental data to the Debye model.

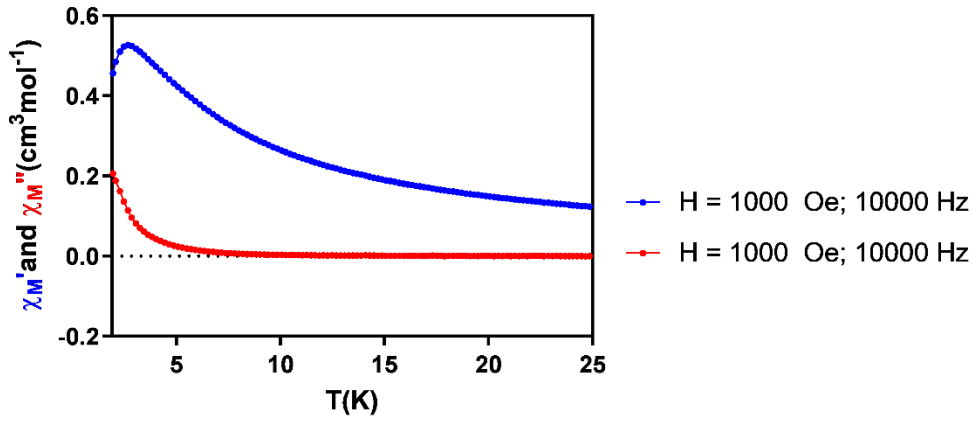

Figure A2.29. Temperature dependence of in-phase (blue) and out of phase (red) components of the *ac* susceptibility in a *dc* applied field of 1000 Oe for **2.13**$_{\text{Y-Dy}}$.

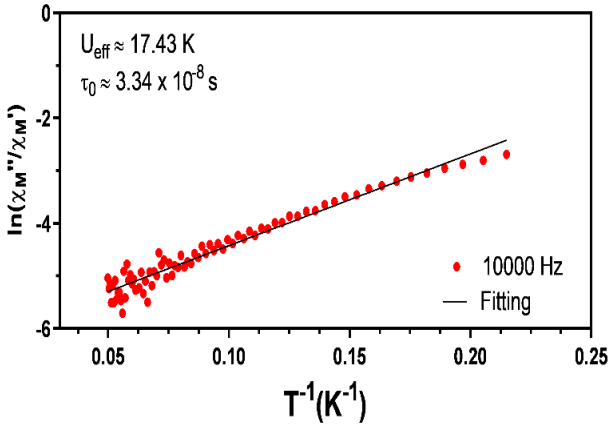

Figure A2.30. Plot of ln(χ_M''/χ_M') versus 1/T at 10000 Hz for compound **2.13**$_{\text{Y-Dy}}$ under an applied field of 1000 Oe. The solid lines represent the linear fit with ln(χ_M''/χ_M') = ln($2\pi\nu\tau_0$)+ E_a/k_BT.

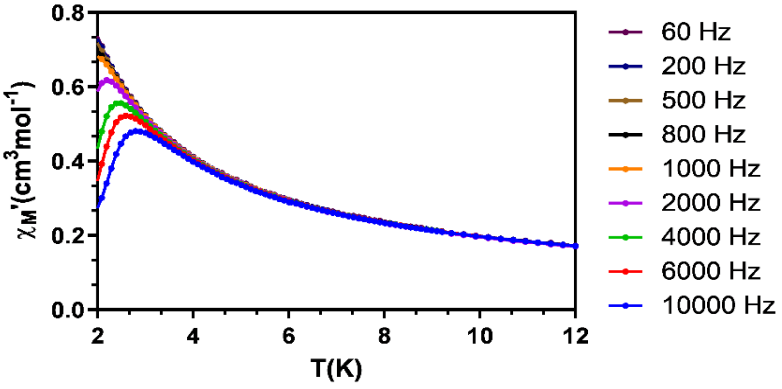

Figure A2.31. Temperature dependence of in-phase components of the *ac* susceptibility in a *dc* applied field of 1000 Oe for **2.14**$_{\text{Y-Er}}$.

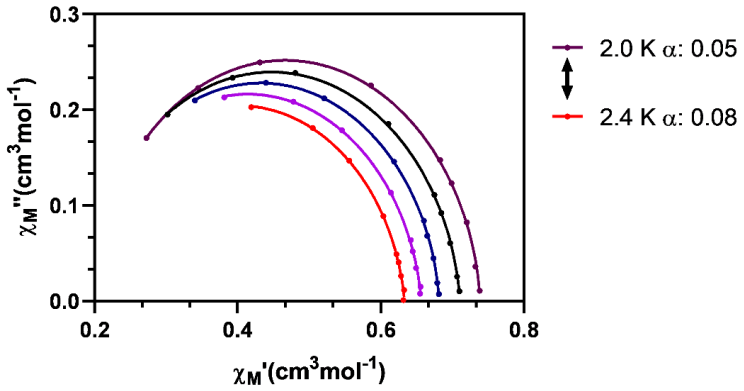

Figure A2.32. Cole-Cole plots in a *dc* applied field of 1000 Oe for **2.14**$_{\text{Y-Er}}$.

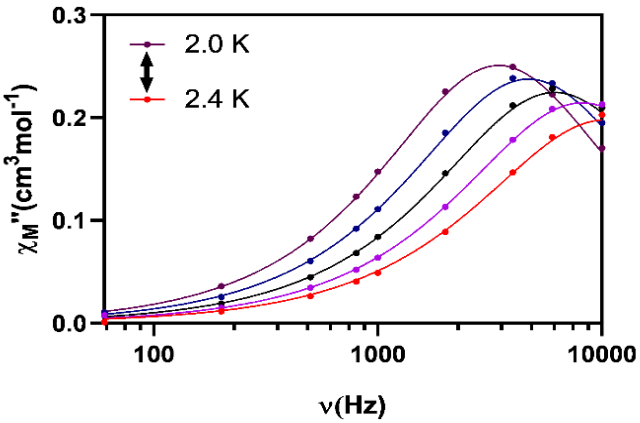

Figure A2.33. Variable-temperature frequency dependence of the χ_M'' signal under 1000 Oe applied field for **2.14**$_{\text{Y-Er}}$. Solid lines represent the best fitting of the experimental data to the Debye model.

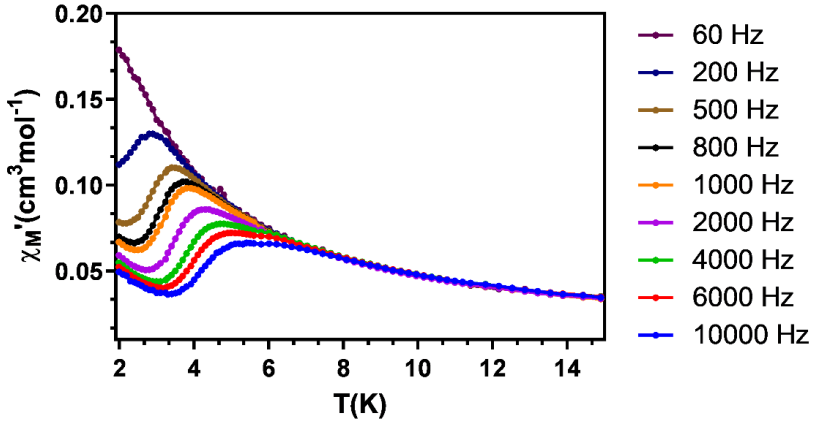

Figure A2.34. Temperature dependence of in-phase components of the *ac* susceptibility in a *dc* applied field of 1000 Oe for **2.15**$_{\text{Y-Yb}}$.

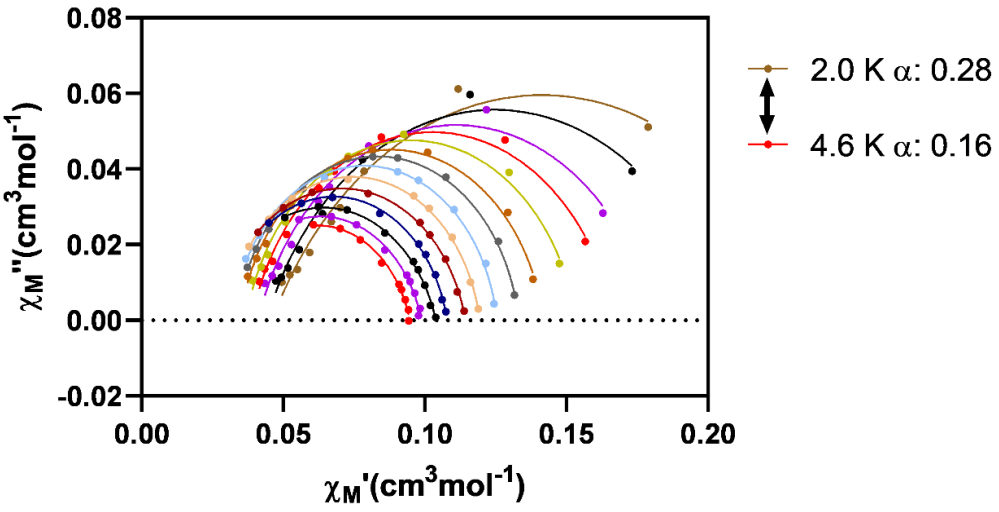

Figure A2.35. Cole-Cole plots in a *dc* applied field of 1000 Oe for **2.15**$_{Y\text{-}Yb}$.

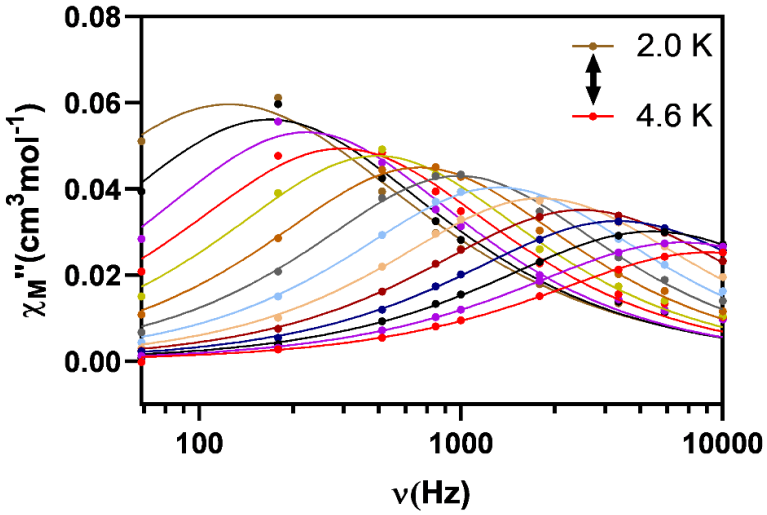

Figure A2.36. Variable-temperature frequency dependence of the χ_M'' signal under 1000 Oe applied field for **2.15**$_{Y\text{-}Yb}$. Solid lines represent the best fitting of the experimental data to the Debye model.

A2.11 Diffuse reflectance measurements

Absorption spectrum of 3-amino-4-hydroxybenzoic acid ligand, pure Co^{II} and Zn^{II} homometallic compounds and $[Co_{0.05}Zn_{0.95}L]_n$ heterometallic compound show absorption bands in the range of 220–800 nm. Three main regions can be differentiated, the first one from 220–300 nm attributed to the ligand 3-amino-4-hydroxybenzoic acid ligand π–π* transitions, the shoulder at around 310 nm (clearly observed for both homometallic and heterometallic compounds) corresponds to metal-to-ligand charge transfer (MLCT) transitions. Moreover, the bands with a broad and structured shape covering the 400–700 nm region, are attributed to spin-allowed d-d transitions found in heterometallic $[Co_{0.05}Zn_{0.95}L]_n$ and homometallic Co^{II} compounds.

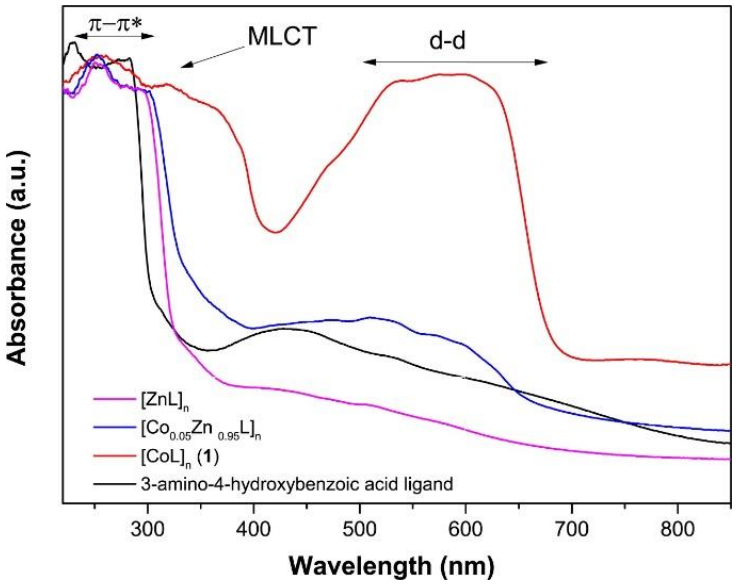

Figure A2.37. Diffuse reflectance of 3-amino-4-hydroxybenzoic acid ligand, homometallic Co_MOF (**2.1**), and Zn compounds and heterometallic $[Co_{0.05}Zn_{0.95}L]_n$ heterometallic sample.

A2.12 Photoluminescence measurements

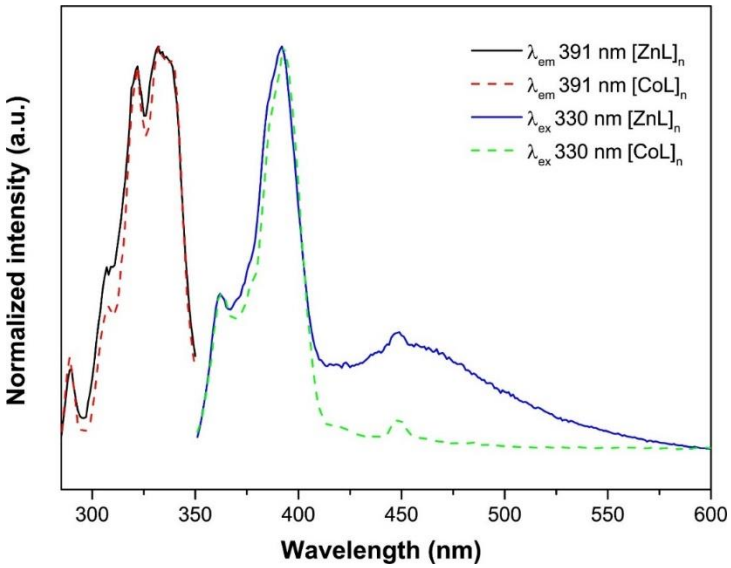

Figure A2.38. Figure caption of the experimental room temperature photoluminescence excitation and emission spectra under λ_{em} = 391 nm and λ_{ex} = 330 nm, respectively for compounds 1 and isostructural Zn^{II} homometallic counterpart.

The normalized excitation and emission spectra of compound **2.1** and isostructural $[ZnL]_n$ compounds are sown in Figure A2.38.

The excitation spectra have been measured for both homometallic compounds by monitoring the emission maxima, at 391 nm. As observed in Figure A2.37, the excitation spectra show a band covering the 275–350 nm range in which four peaks (sited at ca. 288, 310, 322 and 334 nm) are distinguished.

Ambient temperature emission spectra monitored at the excitation maxima, at 330 nm, show a main band with the maxima at 362 nm and 391 nm and a tail. In case of homometallic Zn^{II} compound a more prominent shoulder can be appreciable peaking at 447 nm.

Normalization of the spectra has been carried out in order to compare the position of the maxima in both structures more than to compare the relative intensity, which in case of Co^{II} was, as expected, relatively weaker.

Table A2.11. Comparison of lifetime values of compound **2.6$_{Tb}$** in bulk and PMMA membrane at ambient temperature (294 K) and low temperature (12 K).

Compound	τ_1 / ms	τ_2/ ms	<τ> / ms
2.6$_{Tb}$ (377)	0.08 ± 0.01	0.36 ± 0.01	0.29
2.6$_{Tb}$@PMMA at 294 K (315)	0.10 ± 0.01	0.40 ± 0.01	0.35
2.6$_{Tb}$@PMMA at 12 K (315)	0.09 ± 0.01	0.38 ± 0.01	0.33

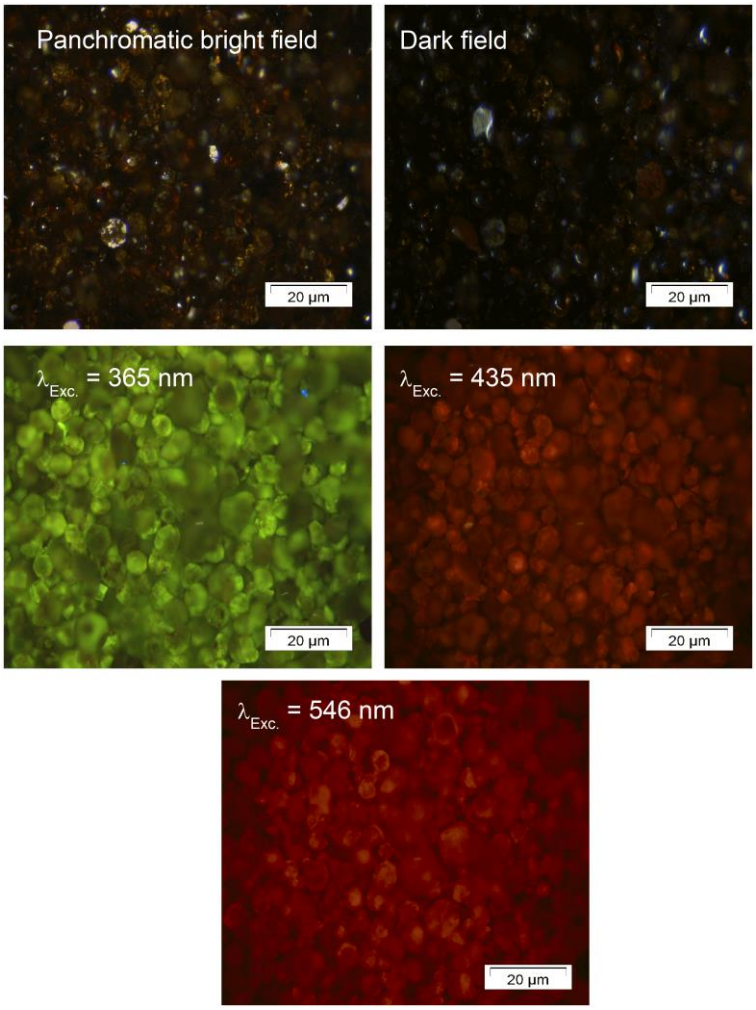

Figure A2.39. Ambient temperature micro-photoluminescence images taken on single-crystal of compound **2.6$_{Tb}$** at different excitation lines.

A2.13 Adsorption properties

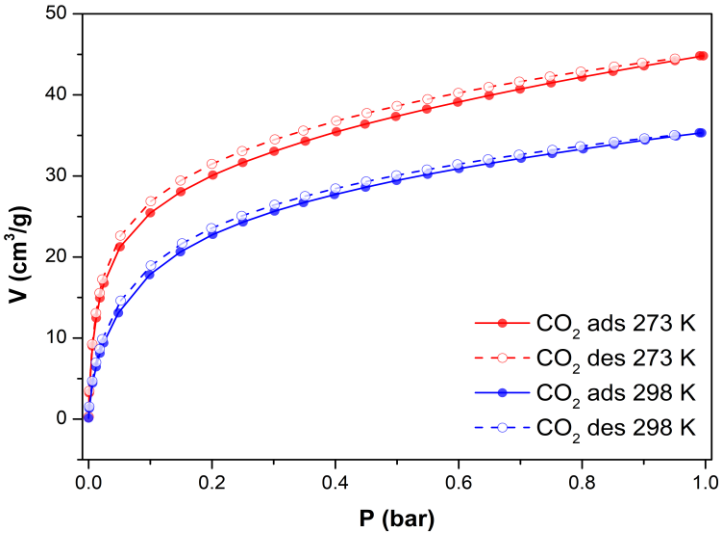

Figure A2.40. Isotherm of compound **2.7$_{Dy}$** in cm^3/g. The conversion to mmol/g has done taking into account that 1 mmol of any gas at stp (standard temperature and pressure conditions. according to the IUPAC. at 273 K and 1 bar pression conditions) occupies 22.414 cm^3 volume.

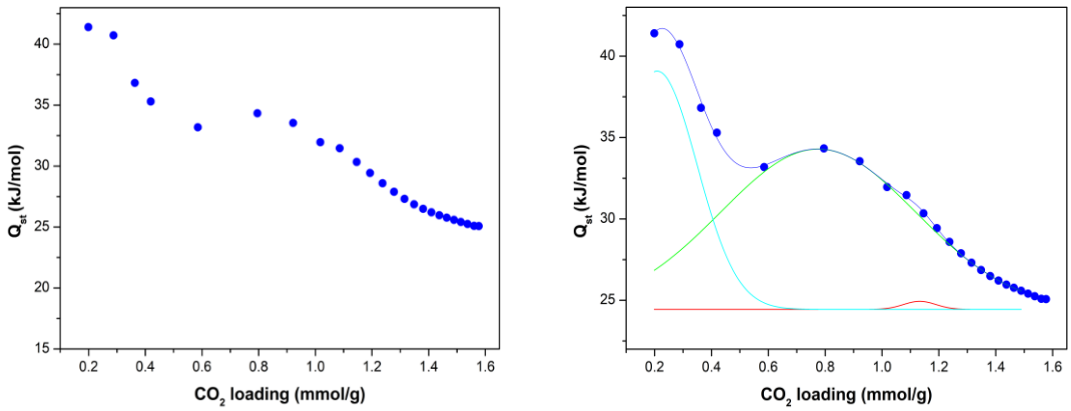

Figure A2.41. Isosteric heats of adsorption (Q_{st}) of CO_2 per Dy_5 cluster for compound **2.7$_{Dy}$** (left) and the deconvolution of the curve (right).

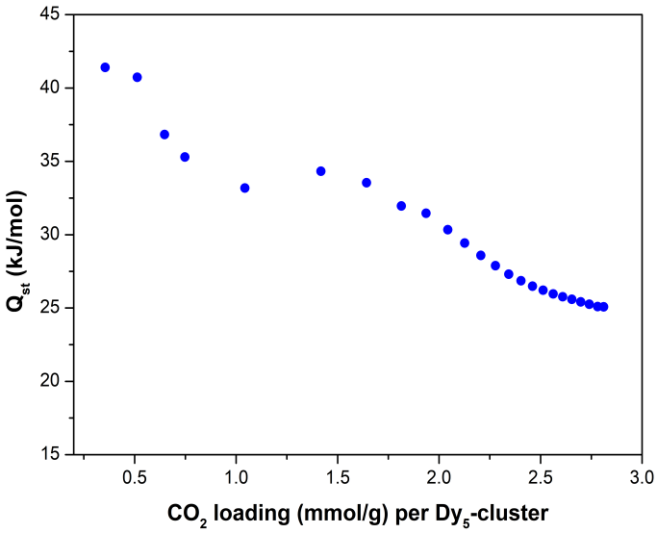

Figure A2.42. Isosteric heat of adsorption of CO_2 loading (mmol/g) per Dy_5 cluster.

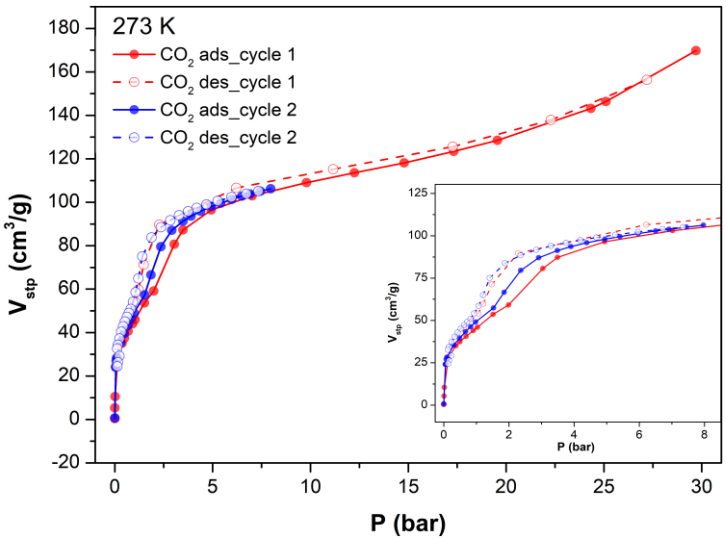

Figure A2.43. High pressure CO_2 adsorption-desorption regeneration cycles for compound **2.7** at 273 K**.**

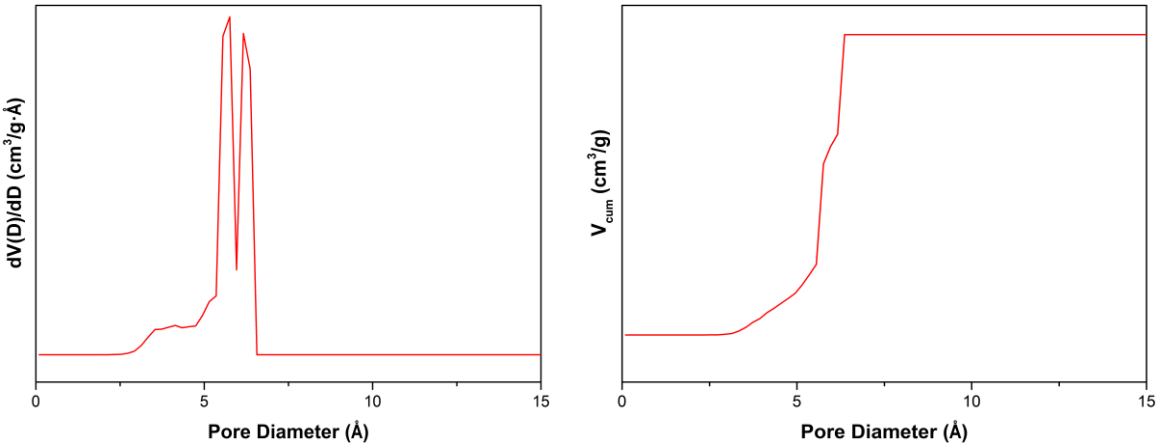

Figure A2.44. Derivative Geometric Pore Volume (pore size distribution) and cumulative volume in anhydrous compound **2.7**$_{Dy}$.

Table A2.12. Calculations performed by Monte Carlo procedure.[8,9]

Compound	Area & Vol			Pore diameter		
	S_{area} ($m^2 \cdot g^{-1}$)	V_{pore} ($cm^3 \cdot g^{-1}$)	Porosity (%)	Limiting (Å)	Maximun (Å)	Dimensionality
2.7_{Dy} anhydrous	713.2	0.319	50.9	4.89	6.35	3 D

A2.14 Catalytic activity. Characterization Data of Products.

Cyanosilylated carbonyl compounds catalysed by 2.12Y

2-Phenyl-2-((trimethylsilyl)oxy)acetonitrile (3a). This product has been previously reported.[10] ^{1}H NMR (300.13 MHz, $CDCl_3$): δ 7.50–7.35 (m, 5H, ArH), 5.50 (s, 1H, *CH*CN), 0.23 (s, 9H, TMS) ppm. ^{13}C NMR (75.48 MHz, $CDCl_3$): δ 136.2 (C_{ipso}), 129.3(ArCH), 128.9 (ArCH), 126.3 (ArCH), 119.1 (CN), 63.6 (CH), -0.29 (TMS) ppm.

2-(*p*-Tolyl)-2-((trimethylsilyl)oxy)acetonitrile (3b). This product has been previously reported.[11] ^{1}H NMR (300.13 MHz, $CDCl_3$): δ 7.37 (d, *J* = 7.9 Hz, 2H, ArH), 7.22 (d, *J* = 7.9 Hz, 2H, ArH), 5.47 (s, 1H, *CH*CN), 2.38 (s, 3H, CH_3), 0.23 (s, 9H, TMS) ppm. ^{13}C NMR (75.48 MHz, $CDCl_3$): δ 139.3 (C_{ipso}), 133.3 (C_{ispo}), 129.5 (ArCH), 126.3 (ArCH), 119.2 (CN), 63.5 (CH), 21.1 (CH_3), -0.29 (TMS) ppm.

2-(4-Methoxyphenyl)-2-((trimethylsilyl)oxy)acetonitrile (3c). This product has been previously reported.[12] ^{1}H NMR (300.13 MHz, $CDCl_3$): δ 7.38 (d, *J* = 8.6 Hz, 2H, ArH), 6.92 (d, *J* = 8.6 Hz, 2H, ArH), 5.43 (s, 1H, *CH*CN), 3.82 (s, 3H, OMe), -0.21 (s, 9H, TMS) ppm. ^{13}C NMR (75.48 MHz, $CDCl_3$): δ 160.3 (C_{ipso}), 128.3 (C_{ipso}), 127.9 (ArCH), 119.3 (CN), 114.2 (ArCH), 63.3 (CH), 55.3 (OCH_3), -0.24 (TMS) ppm.

2-(4-(Dimethylamino)phenyl)-2-((trimethylsilyl)oxy)acetonitrile (3d). ^{1}H NMR (300.13 MHz, $CDCl_3$): δ 7.31 (d, *J* = 8.7 Hz, 2H, ArH), 6.71 (d, *J* = 8.7 Hz, 2H, ArH), 5.39 (s, 1H, *CH*CN), 2.98 (s, 6H, N*Me*$_2$), 0.19 (s, 9H, TMS) ppm. ^{13}C NMR (75.48 MHz, $CDCl_3$): δ 151.1 (C_{ipso}), 127.8 (ArCH), 123.6 (C_{ipso}), 119.6 (CN), 112.1 (ArCH), 63.7 (CH), 40.3 (CH_3), -0.16 (TMS) ppm. IR (ATR): v 2959 (CH_3), 2230 (C≡N), 1621 (C=N), 1531 (C=C), 1371 (C-N), 1257 (C-O), 1061 (C-O), 835 cm^{-1}. Elemental Analysis calc. for $C_{13}H_{20}N_2OSi$: C 62.86, N, 11.28, H 8.12; found: C 63.23, N 11.65, H 7.67.

2-(3-Fluorophenyl)-2-((trimethylsilyl)oxy)acetonitrile (3e). This product has been previously reported.[13] ^{1}H NMR (300.13 MHz, $CDCl_3$): δ 7.45–7.35 (m, 1H, ArH), 7.25–7.15 (m, 2H, ArH), 7.10–7.05 (m, 1H, ArH), 5.50 (s, 1H, *CH*CN), 0.25 (s, 9H, TMS) ppm. ^{13}C NMR (75.48 MHz, $CDCl_3$): δ 162.8 (d, C_{ipso}, $^{1}J_{C\text{-}F}$ = 247.7 Hz,), 138.6 (d, C_{ipso}, $^{3}J_{C\text{-}F}$ = 7.8 Hz,), 130.5 (d, ArCH, $^{3}J_{C\text{-}F}$ = 8.1 Hz,), 121.7 (d, ArCH, $^{4}J_{C\text{-}F}$ = 3.0 Hz,), 118.7 (CN), 116.3 (d, ArCH, $^{2}J_{C\text{-}F}$ = 21.2 Hz,), 113.3 (d, ArCH, $^{2}J_{C\text{-}F}$ = 23.4 Hz,), 62.8 (d, CH, $^{4}J_{C\text{-}F}$ = 2.1 Hz,), -0.4 (TMS) ppm. ^{19}F-NMR (282.4 MHz, $CDCl_3$): δ -111.4 ppm.

2-(4-Chlorophenyl)-2-((trimethylsilyl)oxy)acetonitrile (3f). This product has been previously reported.[14] ^{1}H NMR (300.13 MHz, $CDCl_3$): δ 7.45–7.40 (m, 5H, ArH), 5.49 (s, 1H, *CH*CN), 0.26 (s, 9H, TMS) ppm. ^{13}C NMR (75.48 MHz, $CDCl_3$): δ 135.3 (C_{ipso}), 134.8 (C_{ipso}), 129.1 (ArCH), 127.7 (ArCH), 118.8 (CN), 63.0 (CH), -0.30 (TMS) ppm.

2-(4-Nitrophenyl)-2-((trimethylsilyl)oxy)acetonitrile (3g). This product has been previously reported.[14] ^{1}H NMR (300.13 MHz, $CDCl_3$): δ 8.29 (d, *J* = 8.8 Hz, 2H, ArH), 7.67 (d, *J* = 8.8 Hz, 2H, ArH), 5.59 (s, 1H, *CH*CN), 0.29 (s, 9H, TMS) ppm. ^{13}C NMR (75.48 MHz, $CDCl_3$): δ 148.4 (C*ipso*), 142.8 (C*ispo*), 127.0 (ArCH), 124.1 (ArCH), 118.1 (CN), 62.6 (CH), -0.40 (TMS) ppm.

2-(Pyridin-2-yl)-2-((trimethylsilyl)oxy)acetonitrile (3h). This product has been previously reported.[15] ^{1}H NMR (300.13 MHz, $CDCl_3$): δ 8.60–8.55 (m, 1H, ArH), 7.79 (dt, *J* = 7.7, 1.7 Hz, 1H, ArH), 7.59 (d, *J* = 7.7 Hz, 1H, ArH), 7.35–7.25 (m, 1H, ArH), 5.58 (s, 1H, *CH*CN), 0.26 (s, 9H, TMS) ppm. ^{13}C NMR (75.48 MHz, $CDCl_3$): δ 155.4 (C_{ipso}), 149.3 (ArCH), 137.5(ArCH), 124.0 (ArCH), 120.5 (ArCH), 118.6 (CN), 65.1 (CH), -0.37 (TMS) ppm.

2-(Quinolin-2-yl)-2-((trimethylsilyl)oxy)acetonitrile (3i). ^{1}H NMR (300.13 MHz, $CDCl_3$): δ 8.27 (d, *J* = 8.5 Hz, 1H, ArH), 8.09 (d, *J* = 8.5 Hz, 1H, ArH), 7.85 (d, *J* = 8.1 Hz, 1H, ArH), 7.80–7.70 (m, 2H, ArH), 7.60–7.55 (m, 1H, ArH), 5.75 (s, 1H, *CH*CN), 0.27 (s, TMS) ppm. ^{13}C NMR (75.48 MHz, $CDCl_3$): δ 155.4 (C_{ipso}), 147.2 (C_{ipso}), 137.9 (ArCH), 130.1 (ArCH), 129.3 (ArCH), 128.0 (C_{ipso}), 127.6 (ArCH), 127.3 (ArCH), 118.6 (CN), 117.8 (ArCH), 65.9 (CH), -0.31 (TMS) ppm. IR (ATR): v 3058 (Csp^2-H), 2959 (CH_3), 2170 (C≡N), 1593 (C=N), 1504 (C=C), 1254 (C-O), 1046 (C-O), 838, 774 cm^{-1}. Elemental Analysis calc. for $C_{14}H_{16}N_2OSi$: C 65.59, N, 10.93, H 6.29; found: C 64.85, N 10.66, H 5.98.

2-(Furan-2-yl)-2-((trimethylsilyl)oxy)acetonitrile (3j). This product has been previously reported.[16] ^{1}H NMR (300.13 MHz, $CDCl_3$): δ 7.45 (d, *J* = 1.7 Hz, 1H, CH), 6.54 (d, *J* = 3.3 Hz, 1H, CH), 6.40 (dd, *J* = 3.3, 1.7 Hz, 1H, CH), 5.54 (s, 1H, *CH*CN), 0.19 (s, 9H, TMS) ppm. ^{13}CNMR (75.48 MHz, $CDCl_3$): δ 148.2 (C), 143.8 (FurCH), 117.1 (CN), 110.8 (FurCH), 109.7 (FurCH), 57.4 (CH), -0.42 (TMS) ppm.

2-(Thiophen-2-yl)-2-((trimethylsilyl)oxy)acetonitrile (3k). This product has been previously reported.[16] ^{1}H NMR (300.13 MHz, $CDCl_3$): δ 7.37 (d, *J* = 5.3 Hz, 1H, CH), 7.20–7.15 (m, 1H, CH), 7.05–7.00 (m, 1H, CH), 5.73 (s, 1H, *CH*CN), 0.23 (s, 9H, TMS) ppm. ^{13}C NMR (75.48 MHz, $CDCl_3$): δ 139.5 (C), 127.2 (TiophCH), 126.9 (TiophCH), 126.3 (TiophCH), 118.3 (CN), 59.5 (CH), -0.31 (TMS) ppm.

2-((Trimethylsilyl)oxy)butanenitrile (3l). This product has been previously reported.[17] ^{1}H NMR (300.13 MHz, $CDCl_3$): δ 4.34 (t, J = 6.3 Hz, 1H, CH), 1.85–1.75 (m, 2H, CH_2), 1.04 (t, J = 7.4 Hz, 3H, CH_3), 0.21 (s, 9H, CH_3 x 3) ppm. ^{13}C NMR (75.48 MHz, $CDCl_3$): δ 119.9 (CN), 62.7 (CH), 29.6 (CH_2), 8.9 (CH_3), 0.4 (TMS) ppm.

(*E*)-4-Phenyl-2-((trimethylsilyl)oxy)but-3-enenitrile (3m). This product has been previously reported.[18] ^{1}H NMR (300.13 MHz, $CDCl_3$): δ 7.45–7.30 (m, 5H, ArH), 6.82 (d, *J* =

15.8 Hz, 1H, CH), 6.20 (dd, *J* = 15.8, 6.0 Hz, 1H, CH), 5.13 (d, *J* = 6.0 Hz, 1H, CH), 0.26 (s, 9H, TMS) ppm. ^{13}C NMR (75.48 MHz, $CDCl_3$): δ 135.0 (C_{ipso}). 133.9 (CH), 128.76 (ArCH), 128.71 (ArCH), 126.96 (ArCH), 123.5 (CH), 118.4 (CN), 62.2 (CH), 0.15 (TMS) ppm.

2-Phenyl-2-((trimethylsilyl)oxy)propanenitrile (3n). This product has been previously reported.[19] ^{1}H NMR (300.13 MHz, $CDCl_3$): δ 7.60–7.50 (m, 2H, ArH), 7.45–7.30 (m, 3H, ArH), 1.86 (s, 3H, CH_3), 0.18 (s, 9H, TMS) ppm. ^{13}C NMR (75.48 MHz, $CDCl_3$): δ 142.0 (C_{ipso}), 128.68 (ArCH), 128.66 (ArCH), 124.6 (ArCH), 121.6 (CN), 71.6 (C), 33.5 (CH_3), 1.03 (TMS) ppm.

2-(4-Isobutylphenyl)-2-((trimethylsilyl)oxy)propanenitrile (3o). This product has been previously reported.[20] ^{1}H NMR (300.13 MHz, $CDCl_3$): δ 7.44 (d, *J* = 8.2 Hz, 2H, ArH), 7.16 (d, *J* = 8.2 Hz, 2H, ArH), 2.49 (d, *J* = 7.2 Hz, 2H, CH_2), 1.90–1.80 (m, 4H, CH, CH_3), 0.90 (d, *J* = 6.6 Hz, 6H, 2 x CH_3), 0.16 (s, 9H, TMS) ppm. ^{13}C NMR (75.48 MHz, $CDCl_3$): δ 142.3 (C_{ipso}), 139.2 (C_{ipso}), 129.3 (ArCH), 124.5 (ArCH), 121.8 (CN), 71.5 (C), 44.9 (CH_2), 33.4 (CH_3), 30.1 (CH_3), 22.3 (CH_3), 1.04 (TMS) ppm.

2,2-Diphenyl-2-((trimethylsilyl)oxy)acetonitrile (3p). This product has been previously reported.[21] ^{1}H NMR (300.13 MHz, $CDCl_3$): δ 7.55–7.50 (m, 4H, ArH), 7.40–7.35 (m, 6H, ArH), 0.15 (s, 9H, TMS) ppm. ^{13}C NMR (75.48 MHz, $CDCl_3$): δ 141.9 (C_{ipso}), 128.6 (ArCH), 128.5 (ArCH), 125.9 (ArCH), 120.7 (CN), 76.3 (C), 0.9 (TMS) ppm.

2-Methyl-2-((trimethylsilyl)oxy)butanenitrile (3q). This product has been previously reported.[22] ^{1}H NMR (300.13 MHz, $CDCl_3$): δ 1.85–1.65 (m, 2H, CH_2), 1.55 (s, 3H, CH_3), 1.04 (t, *J* = 7.4 Hz, 3H, CH_3CH_2), 0.23 (s, 9H, TMS) ppm. ^{13}C NMR (75.48 MHz, $CDCl_3$): δ 121.9 (CN), 70.2 (C), 36.4 (CH_2), 28.4 (CH_3), 8.6 (CH_3), 1.21 (TMS) ppm.

1-((Trimethylsilyl)oxy)cyclohexane-1-carbonitrile (3r). This product has been previously reported.[23] ^{1}H NMR (300.13 MHz, $CDCl_3$): δ 2.10–2.00 (m, 2H, CH_2), 1.75–1.70 (m, 2H, CH_2), 1.70–1.45 (m, 6H, CH_2 x 3), 1.30–1.20 (m, 2H, CH_2), 0.23 (s, 9H, TMS) ppm. ^{13}C NMR (75.48 MHz, $CDCl_3$): δ 121.9 (CN), 70.6 (C), 39.3 (CH_2), 24.5 (CH_2), 22.6 (CH_2), 1.38 (TMS) ppm.

1-((Trimethylsilyl)oxy)-1,2,3,4-tetrahydronaphthalene-1-carbonitrile (3s). This product has been previously reported.[23] ^{1}H NMR (300.13 MHz, $CDCl_3$): δ 7.70–7.60 (m, 1H, ArH), 7.30–7.20 (m, 2H, ArH), 7.15–7.05 (m, 1H, ArH), 2.85–2.80 (m, 2H), 2.40–2.30 (m, 1H), 2.25–2.15 (m, 1H), 2.10–1.95 (m, 2H), 0.21 (s, 9H, TMS) ppm. ^{13}C NMR (75.48 MHz, $CDCl_3$): δ 136.1 (C_{ipso}), 135.7 (C_{ipso}), 129.3 (ArCH), 129.1 (ArCH), 128.0 (ArCH), 126.6 (ArCH), 122.1 (CN), 69.6 (C), 37.7 (CH_2), 28.3 (CH_2), 18.7 (CH_2), 1.3 (TMS) ppm.

2-((Trimethylsilyl)oxy)adamantane-2-carbonitrile (3t). This product has been previously reported.[24,25] ^{1}H NMR (300.13 MHz, $CDCl_3$): δ 2.20–2.00 (m, 6H), 1.95–1.80 (m, 3H), 1.80–1.65 (m, 3H), 1.60–1.50 (m, 2H), 0.25 (s, 9H, TMS) ppm. ^{13}C NMR (75.48 MHz, $CDCl_3$): δ 122.1

(CN), 74.7 (C), 38.1 (CH), 37.2 (CH_2), 34.7 (CH_2), 30.9 (CH_2), 26.3 (CH), 26.1 (CH), 1.2 (TMS) ppm.

2,2-Dicyclohexyl-2-((trimethylsilyl)oxy)acetonitrile (3u). ^{1}H NMR (300.13 MHz, $CDCl_3$): δ 1.90–1.75 (m, 8H), 1.70–1.60 (m, 4H), 1.30–1.05 (m, 10H, CH_2), 0.23 (s, 9H, TMS) ppm. ^{13}C NMR (75.48 MHz, $CDCl_3$): δ 120.5 (CN), 80.6 (C), 43.6 (CH), 28.3 (CH_2), 26.4 (CH_2), 26.2 (CH_2), 26.1 (CH_2), 1.9 (TMS) ppm. IR (ATR): v 2931 (CH_2), 2858 (CH_2), 1451, 1249, 1123, 1023, 842, 766 cm^{-1}. Elemental Analysis calc. for $C_{17}H_{31}NOSi$: C 69.56, N 4.77, H 10.65; found: C 69.62, N 4.68, H 10.21.

Cyanosilylated carbonyl compounds catalysed by 2.19$_{Eu}$

2-Phenyl-2-((trimethylsilyl)oxy)acetonitrile (4a). This product has been previously reported.[10] ^{1}H NMR (300.13 MHz, $CDCl_3$): δ 7.50–7.35 (m, 5H, ArH), 5.50 (s, 1H, *CH*CN), 0.23 (s, 9H, TMS) ppm. ^{13}C NMR (75.48 MHz, $CDCl_3$): δ 136.2 (C_{ipso}), 129.3(ArCH), 128.9 (ArCH), 126.3 (ArCH), 119.1 (CN), 63.6 (CH), -0.29 (TMS) ppm.

2-(4-Methoxyphenyl)-2-((trimethylsilyl)oxy)acetonitrile (4b). This product has been previously reported.[12] ^{1}H NMR (300.13 MHz, $CDCl_3$): δ 7.38 (d, *J* = 8.6 Hz, 2H, ArH), 6.92 (d, *J* = 8.6 Hz, 2H, ArH), 5.43 (s, 1H, *CH*CN), 3.82 (s, 3H, OMe), -0.21 (s, 9H, TMS) ppm. ^{13}C NMR (75.48 MHz, $CDCl_3$): δ 160.3 (C_{ipso}), 128.3 (C_{ipso}), 127.9 (ArCH), 119.3 (CN), 114.2 (ArCH), 63.3 (CH), 55.3 (OCH_3), -0.24 (TMS) ppm.

2-(4-Chlorophenyl)-2-((trimethylsilyl)oxy)acetonitrile (4c). This product has been previously reported.[14] ^{1}H NMR (300.13 MHz, $CDCl_3$): δ 7.45–7.40 (m, 5H, ArH), 5.49 (s, 1H, *CH*CN), 0.26 (s, 9H, TMS) ppm. ^{13}C NMR (75.48 MHz, $CDCl_3$): δ 135.3 (C_{ipso}), 134.8 (C_{ipso}), 129.1 (ArCH), 127.7 (ArCH), 118.8 (CN), 63.0 (CH), -0.30 (TMS) ppm.

2-Phenyl-2-((trimethylsilyl)oxy)propanenitrile (4d). This product has been previously reported.[19] ^{1}H NMR (300.13 MHz, $CDCl_3$): δ 7.60–7.50 (m, 2H, ArH), 7.45–7.30 (m, 3H, ArH), 1.86 (s, 3H, CH_3), 0.18 (s, 9H, TMS) ppm. ^{13}C NMR (75.48 MHz, $CDCl_3$): δ 142.0 (C_{ipso}), 128.68 (ArCH), 128.66 (ArCH), 124.6 (ArCH), 121.6 (CN), 71.6 (C), 33.5 (CH_3), 1.03 (TMS) ppm.

2-(4-Methoxyphenyl)-2-((trimethylsilyl)oxy)propanenitrile (4e). This product has been previously reported.[22] ^{1}H NMR (300.13 MHz, $CDCl_3$): δ 7.46 (d, *J* = 8.7 Hz, 2H, ArH), 6.91 (d, *J* = 8.7 Hz, 2H, ArH), 3.82 (s, 3H, OMe), 1.85 (s, 3H, CH_3), 0.16 (s, 9H, TMS) ppm. ^{13}C NMR (75.48 MHz, $CDCl_3$): δ 159.7 (C_{ipso}), 133.9 (C_{ipso}), 126.0 (ArCH), 121.7 (CN), 113.8 (ArCH), 71.2 (C), 55.2 (OCH_3), 33.3 (CH_3), 1.00 (TMS) ppm.

2-(4-Isobutylphenyl)-2-((trimethylsilyl)oxy)propanenitrile (4f). This product has been previously reported.[20] ^{1}H NMR (300.13 MHz, $CDCl_3$): δ 7.44 (d, *J* = 8.2 Hz, 2H, ArH), 7.16 (d, *J*

= 8.2 Hz, 2H, ArH), 2.49 (d, *J* = 7.2 Hz, 2H, CH_2), 1.90–1.80 (m, 4H, CH, CH_3), 0.90 (d, *J* = 6.6 Hz, 6H, 2 x CH_3), 0.16 (s, 9H, TMS) ppm. ^{13}C NMR (75.48 MHz, $CDCl_3$): δ 142.3 (C_{ipso}), 139.2 (C_{ipso}), 129.3 (ArCH), 124.5 (ArCH), 121.8 (CN), 71.5 (C), 44.9 (CH_2), 33.4 (CH_3), 30.1 (CH_3), 22.3 (CH_3), 1.04 (TMS) ppm.

2-(4-Chlorophenyl)-2-((trimethylsilyl)oxy)propanenitrile (4g). This product has been previously reported.[22] ^{1}H NMR (300.13 MHz, $CDCl_3$): δ 7.48 (d, *J* = 8.5 Hz, 2H, ArH), 7.37 (d, *J* = 8.5 Hz, 2H, ArH), 1.83 (s, 3H, CH_3), 0.19 (s, 9H, TMS) ppm. ^{13}C NMR (75.48 MHz, $CDCl_3$): δ 140.6 (C_{ipso}), 134.5 (C_{ipso}), 128.8 (ArCH), 126.0 (ArCH), 121.2 (CN), 71.0 (C), 33.4 (CH_3), 1.00 (TMS) ppm.

2-(3-Chlorophenyl)-2-((trimethylsilyl)oxy)propanenitrile (4h). This product has been previously reported.[26] ^{1}H NMR (300.13 MHz, $CDCl_3$): δ 7.55 (s, 1H, ArH), 7.50–7.40 (m, 1H, ArH), 7.40–7.30 (m, 2H, ArH), 1.87 (s, 3H, CH_3), 0.23 (s, 9H, TMS) ppm. ^{13}C NMR (75.48 MHz, $CDCl_3$): δ 144.1 (C_{ipso}), 134.7 (C_{ipso}), 130.0 (ArCH), 128.8 (ArCH), 124.9 (ArCH), 122.58 (ArCH), 121.1 (CN), 71.0 (C), 33.5 (CH_3), 1.03 (TMS) ppm.

2-(2-Chlorophenyl)-2-((trimethylsilyl)oxy)propanenitrile (4i). This product has been previously reported.[27] ^{1}H NMR (300.13 MHz, $CDCl_3$): δ 7.75–7.70 (m, 1H, ArH), 7.45–7.40 (m, 1H, ArH), 7.35–7.30 (m, 2H, ArH), 2.00 (s, 3H, CH_3), 0.29 (s, 9H, TMS) ppm. ^{13}C NMR (75.48 MHz, $CDCl_3$): δ 138.0 (C_{ipso}), 131.5 (ArCH), 131.2 (C_{ipso}), 129.9 (ArCH), 127.0 (ArCH), 126.9 (ArCH), 120.4 (CN), 70.2 (C), 29.7 (CH_3), 1.14 (TMS) ppm.

2-(2,4-Difluorophenyl)-2-((trimethylsilyl)oxy)propanenitrile (**4j**). This product has been previously reported.[28] ^{1}H NMR (500.13 MHz, $CDCl_3$): δ 7.56 (td, *J* = 8.8, 6.4 Hz, 1H, ArH), 6.95–6.90 (m, 1H, ArH), 6.86 (ddd, *J* = 11.1, 8.8, 2.5 Hz, 1H, ArH), 1.92 (s, 3H, CH_3), 0.27 (s, 9H, TMS) ppm. ^{13}C NMR (125.77 MHz, $CDCl_3$): δ 163.2 (dd, *J* = 250.8, 12.0 Hz, C_{ipso}-F), 159.4 (dd, *J* = 252.5, 12.0 Hz, C_{ipso}-F), 127.8 (dd, *J* = 9.7, 4.3 Hz, ArCH), 125.0 (dd, *J* = 11.2, 3.9 Hz, C_{ipso}-F), 120.4 (CN), 111.2 (d, *J* = 21.2 Hz, ArCH), 104.9 (t, *J* = 25.6 Hz, ArCH), 68.0 (d, *J* = 2.0 Hz, C), 30.8 (d, *J* = 2.9 Hz, CH_3), 1.08 (TMS) ppm.

2-(Pyridin-2-yl)-2-((trimethylsilyl)oxy)propanenitrile (4k). This product has been previously reported.[29] ^{1}H NMR (300.13 MHz, $CDCl_3$): δ 8.62 (d, *J* = 4.7 Hz, 1H, ArH), 7.77 (t, *J* = 7.8 Hz, 1H, ArH), 7.60 (d, J = 7.8 Hz, 1H, ArH), 7.30–7.25 (m, 1H, ArH), 1.93 (s, 3H, CH_3), 0.26 (s, 9H, TMS) ppm. ^{13}C NMR (75.48 MHz, $CDCl_3$): δ 160.0 (C_{ipso}), 149.0 (ArCH), 137.2 (ArCH), 123.4 (ArCH), 121.3 (CN), 118.9 (ArCH), 72.9 (C), 31.2 (CH_3), 1.06 (TMS) ppm.

3,3,3-Trifluoro-2-(4-fluorophenyl)-2-((trimethylsilyl)oxy)propanenitrile (**4l**). ^{1}H NMR (500.13 MHz, $CDCl_3$): δ 7.65 (dd, *J* = 8.0, 5.2 Hz, 2H ArH), 7.25–7.20 (m, 2H, ArH), 0.26 (s, 9H, TMS) ppm. ^{13}C NMR (125.77 MHz, $CDCl_3$): δ 164.0 (d, *J* = 251.2Hz, C_{ipso}-F), 129.0 (d, *J* = 9.0 Hz, *C*H-CH-C-F), 128.5 (d, *J* = 3.3 Hz, C_{ipso}), 121.5 (q, *J* = 285.5 Hz, CF_3), 115.9 (d, *J* = 22.2 Hz,

*C*H-C-F), 115.6 (CN), 74.5 (q, *J* = 34.4 Hz, C-CF_3), 0.60 (TMS) ppm. ^{19}F NMR (470.54 MHz, $CDCl_3$): δ -80.2 (CF_3), -109.8 ($C_{ipso}F$) ppm. IR (ATR): v 2966 (CF_3), 1606, 1509, 1415 (C=C), 1259 (C-O), 1185, 1144, 846, 817, 756 cm^{-1}. Elemental Analysis calc. for $C_{12}H_{13}F_4NOSi$: C 49.5, N 4.8, H 4.5, found: C 49.1, N 4.7, H 4.4.

2,2-Diphenyl-2-((trimethylsilyl)oxy)acetonitrile (4m). This product has been previously reported.[21] ^{1}H NMR (300.13 MHz, $CDCl_3$): δ 7.55–7.50 (m, 4H, ArH), 7.40–7.35 (m, 6H, ArH), 0.15 (s, 9H, TMS) ppm. ^{13}C NMR (75.48 MHz, $CDCl_3$): δ 141.9 (C_{ipso}), 128.6 (ArCH), 128.5 (ArCH), 125.9 (ArCH), 120.7 (CN), 76.3 (C), 0.9 (TMS) ppm.

2-Phenyl-2-(*o*-tolyl)-2-((trimethylsilyl)oxy)acetonitrile (**4n**). ^{1}H NMR (500.13 MHz, $CDCl_3$): δ 7.95–7.90 (m, 1H, ArH), 7.45–7.40 (m, 2H, ArH), 7.40–7.35 (m, 3H, ArH), 7.35–7.30 (m, 2H, ArH), 7.15–7.10 (m, 1H, ArH), 2.00 (s, 3H, CH_3), 0.11 (s, 9H, TMS) ppm. ^{13}C NMR (125.77 MHz, $CDCl_3$): δ 140.9 (C_{ipso}), 138.3 (C_{ipso}), 136.3 (C_{ipso}), 132.5 (ArCH), 129.1 (ArCH), 128.7 (ArCH), 128.5 (ArCH), 126.9 (ArCH), 126.4 (ArCH), 125.7 (ArCH), 120.1 (CN), 76.4 (C), 20.5 (CH_3), 0.84 (TMS) ppm. **IR (ATR):** v 3063, 3028 (=C-H), 2959 (CH3), 1601, 1489 (C=C), 1266, 1253 (C-O), 1070, 1055, 1031, 872, 840 cm^{-1}. **Elemental Analysis calc. fo**r $C_{18}H_{21}NOSi$: C 73.2, N 4.7, H 7.2, found: C 69.35, N 4.56, H 6.48.

(*E*)-2,4-Diphenyl-2-((trimethylsilyl)oxy)but-3-enenitrile (4**o**). This product has been previously reported.[30] ^{1}H NMR (300.13 MHz, $CDCl_3$): δ 7.60 (d, *J* = 7.4 Hz, 2H, ArH), 7.45–7.25 (m, 8H, ArH), 7.03 (d, *J* = 15.9 Hz, 1H, CH), 6.21 (d, *J* = 15.9 Hz, 1H, CH), 0.27 (s, 9H, TMS) ppm. ^{13}C NMR (75.48 MHz, $CDCl_3$): δ 140.3 (C_{ipso}), 135.1 (C_{ipso}), 130.9, 128.9, 128.8, 128.71, 128.67, 127.0, 125.4, 119.6 (CN), 75.0 (C), 1.27 (TMS) ppm.

2,2-Dicyclohexyl-2-((trimethylsilyl)oxy)acetonitrile (4p). This product has been previously reported.[31] ^{1}H NMR (300.13 MHz, $CDCl_3$): δ 1.90–1.75 (m, 8H), 1.70–1.60 (m, 4H), 1.30–1.05 (m, 10H, CH_2), 0.23 (s, 9H, TMS) ppm. ^{13}C NMR (75.48 MHz, $CDCl_3$): δ 120.5 (CN), 80.6 (C), 43.6 (CH), 28.3 (CH_2), 26.4 (CH_2), 26.2 (CH_2), 26.1 (CH_2), 1.9 (TMS) ppm. IR (ATR): v 2931 (CH_2), 2858 (CH_2), 1451, 1249, 1123, 1023, 842, 766 cm^{-1}.

2-Methyl-2-((trimethylsilyl)oxy)butanenitrile (4q). This product has been previously reported.[22] ^{1}H NMR (300.13 MHz, $CDCl_3$): δ 1.85–1.65 (m, 2H, CH_2), 1.55 (s, 3H, CH_3), 1.04 (t, *J* = 7.4 Hz, 3H, *C*$H_3$$CH_2$), 0.23 (s, 9H, TMS) ppm. ^{13}C NMR (75.48 MHz, $CDCl_3$): δ 121.9 (CN), 70.2 (C), 36.4 (CH_2), 28.4 (CH_3), 8.6 (CH_3), 1.21 (TMS) ppm.

1-((Trimethylsilyl)oxy)cyclohexane-1-carbonitrile (4r). This product has been previously reported.[22] ^{1}H NMR (300.13 MHz, $CDCl_3$): δ 2.10–2.00 (m, 2H, CH_2), 1.75–1.70 (m, 2H, CH_2), 1.70–1.45 (m, 6H, CH_2 x 3), 1.30–1.20 (m, 2H, CH_2), 0.23 (s, 9H, TMS) ppm. ^{13}C NMR (75.48 MHz, $CDCl_3$): δ 121.9 (CN), 70.6 (C), 39.3 (CH_2), 24.5 (CH_2), 22.6 (CH_2), 1.38 (TMS) ppm.

1-((Trimethylsilyl)oxy)-1,2,3,4-tetrahydronaphthalene-1-carbonitrile (4s). This product has been previously reported.[23] ^{1}H NMR (300.13 MHz, $CDCl_3$): δ 7.70–7.60 (m, 1H, ArH), 7.30–7.20 (m, 2H, ArH), 7.15–7.05 (m, 1H, ArH), 2.85–2.80 (m, 2H), 2.40–2.30 (m, 1H), 2.25–2.15 (m, 1H), 2.10–1.95 (m, 2H), 0.21 (s, 9H, TMS) ppm. ^{13}C NMR (75.48 MHz, $CDCl_3$): δ 136.1 (C_{ipso}), 135.7 (C_{ipso}), 129.3 (ArCH), 129.1 (ArCH), 128.0 (ArCH), 126.6 (ArCH), 122.1 (CN), 69.6 (C), 37.7 (CH_2), 28.3 (CH_2), 18.7 (CH_2), 1.3 (TMS) ppm.

2-((Trimethylsilyl)oxy)adamantane-2-carbonitrile (4t). This product has been previously reported.[24,25] ^{1}H NMR (300.13 MHz, $CDCl_3$): δ 2.20–2.00 (m, 6H), 1.95–1.80 (m, 3H), 1.80–1.65 (m, 3H), 1.60–1.50 (m, 2H), 0.25 (s, 9H, TMS) ppm. ^{13}C NMR (75.48 MHz, $CDCl_3$): δ 122.1 (CN), 74.7 (C), 38.1 (CH), 37.2 (CH_2), 34.7 (CH_2), 30.9 (CH_2), 26.3 (CH), 26.1 (CH), 1.2 (TMS) ppm.

A2.15 Transformation into pellets and membranes

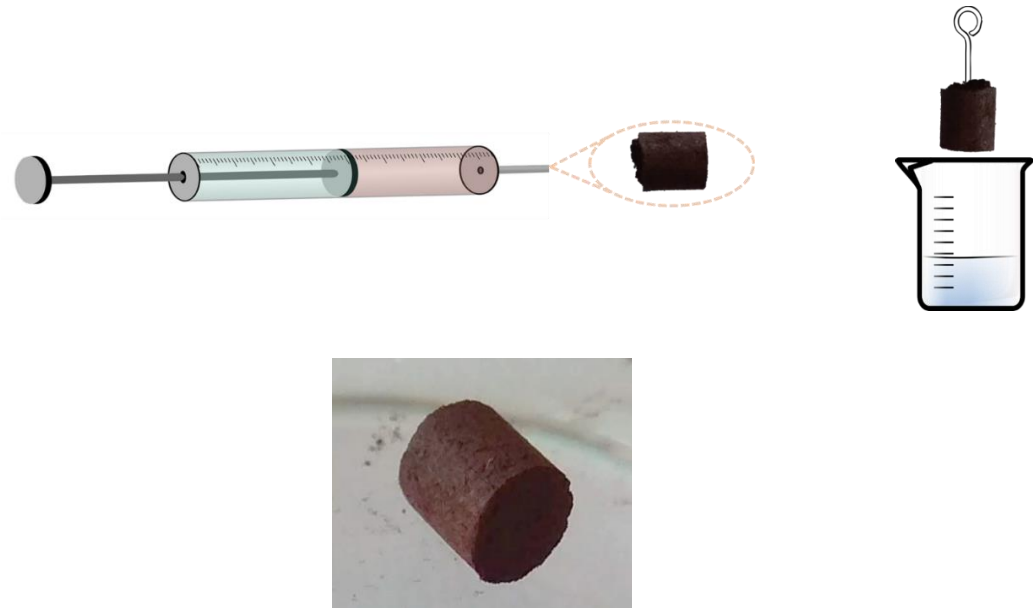

Figure A2.45. Schematic representation of how pellets preparations have been performed with the home-made extrusion apparatus and how the coating of the pellets was done (up) and picture of an uncoated pellet of compound **2.6$_{Tb}$** (down).

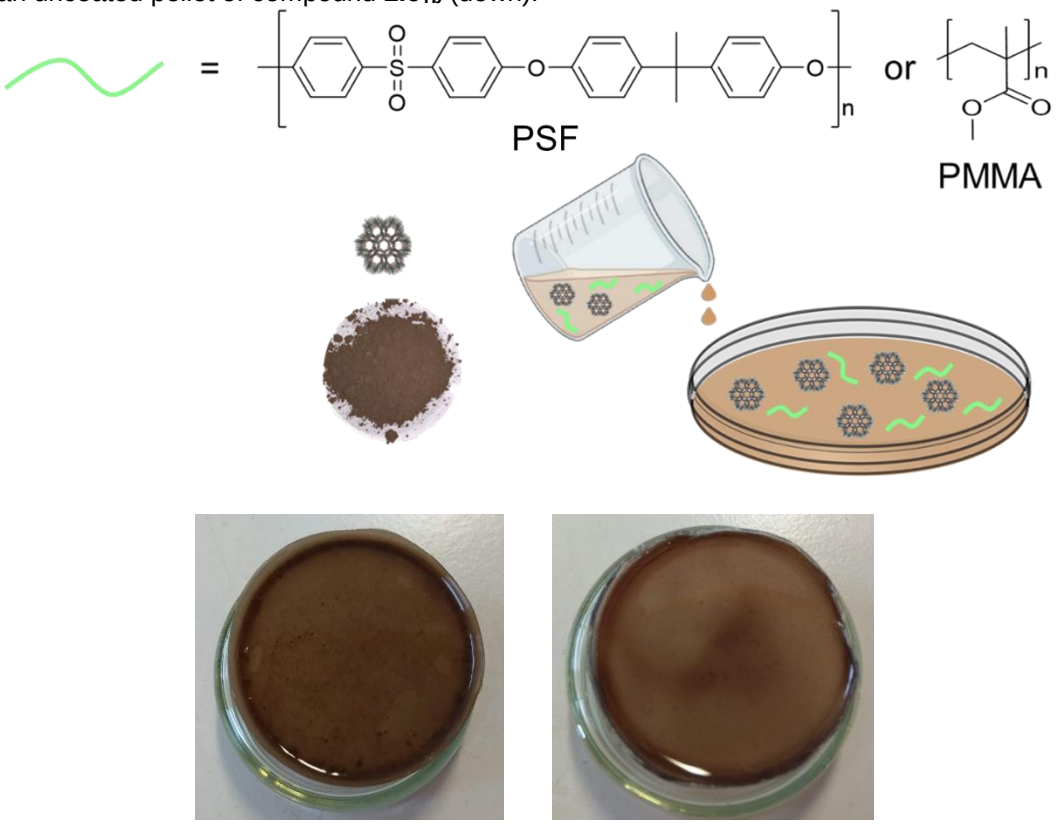

Figure A2.46. Schematic representation of how membrane preparations has been performed (up) and picture compound **2.6$_{Tb}$** immobilized in polymethyl methacrylate (PMMA) and polysulphone (PSF) membranes from left to right, respectively (down).

A2.15.1 Moisture stability

PXRD results exhibit that compound **2.6$_{Tb}$** is stable and keeps its structure after being transformed into pellets or membranes and being exposed for 72 h at 98 % RH. Contrary to what happens when material is directly put in contact with water, that evolves into another crystalline phase, long exposure to humidity do not provoke material transformation and remains stable. Due to the amorphous nature of the polymer, only the main intense peaks of compound **2.6$_{Tb}$** stands over the amorphous background in polysulphone based membrane's PXRD.

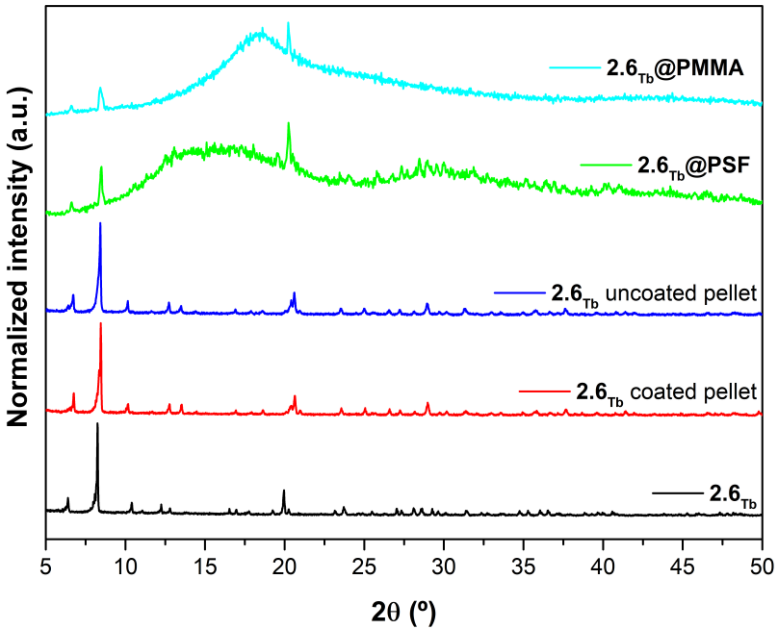

Figure A2.47. Powder X-ray diffractograms of the studied materials, as-synthesized and after processing into pellets and membranes.

A2.15.2 Temperature stability

Once carrying out humidity tests, pellets were subsequently treated to temperature cycles. For that purpose, four heating and cooling down cycles were performed and materials were characterised by PXRD analysis. Therefore, uncoated pellets and polysulphone with coated were first tested against 98 % relative humidity (RH) for 72 h and later tested their thermal stability. For this purpose, temperature cycles of heating to 125 ºC and cooling down to room temperature were carried out. After each cycle, a photograph of both pellets (coated and uncoated) was taken in order to check their integrity. Subsequently, PXRD analysis was performed after the second and forth cycle in coated and uncoated pellets.

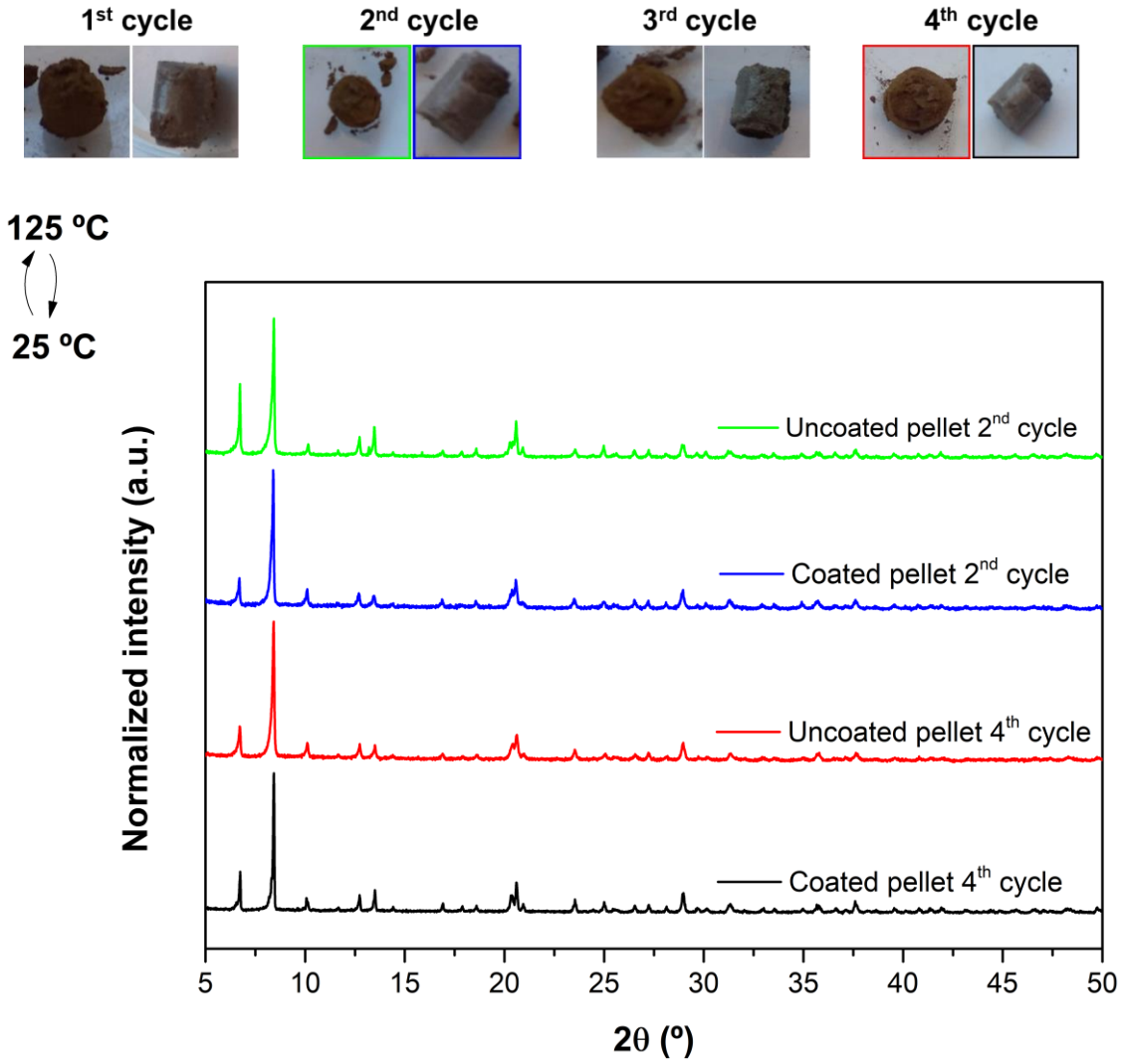

Figure A2.48. Powder X-ray diffractograms of the studied materials of compound **2.6$_{Tb}$**, as-synthesized and after processing into pellets.

Appendix 3

Supporting information of Chapter 3

A3.1 Experimental section. General instrumentation

Elemental analyses (C, H, N) were performed on a Leco CHNS-932 microanalyser. **Infrared** (FT-IR) spectra (400-4000 cm^{-1}) were recorded on a Nicolet FT-IR 6700 spectrometer in KBr pellets.

Thermogravimetric analysis (TG/DTA) were performed on a TG-Q500 TA Instruments thermal analyser from room temperature to 800 °C under a synthetic air atmosphere (79 % N_2/21 % O_2) at a heating rate of 10 °C min^{-1}.

X-ray data collection of suitable single crystals were done at 100(2) K on a Bruker D8 VENTURE area detector equipped with graphite monochromated Mo−Kα radiation (λ = 0.71073 Å) by applying the ω-scan method. The data reduction was performed with the APEX270 software and corrected for absorption using SADABS.[2] Crystal structures were solved by direct methods using the SIR97 program[3] and refined by full-matrix least-squares on F2 including all reflections using anisotropic displacement parameters by means of the WINGX[4] crystallographic package. Lattice solvent molecules could not be refined owing to their disordered disposition in the voids of the structures, so the electron density at the voids was subtracted from the reflection data by the SQUEEZE procedure as implemented in PLATON program[5] during the refinement.

X-ray powder diffraction (XRPD) patterns were collected at 25 °C on a Phillips X'PERT powder diffractometer with Cu-Kα radiation (λ = 1.5418 Å) over the range 5º < 2θ < 50º with a step size of 0.02º and an acquisition time of 2.5 s per step. Indexation of the diffraction profiles were made by means of the FULLPROF program (pattern- matching analysis) based on the space group and the cell parameters found by single crystal X-ray diffraction.

Variable-temperature powder X-ray diffraction measurements were conducted on a Bruker D8 Advance diffractometer, using polycrystalline sample of compound **2.7$_{Dy}$** under ambient atmosphere with heating rate of 5 °C·min^{-1} and measuring a complete diffractogram every 20 °C up to 510 °C, and every 50 °C from 510 °C up to 710 °C.

Scanning electron microscopy (SEM) images were acquired using either a Hitachi S4100 field emission gun tungsten filament instrument working at 25 kV or a high-resolution Hitachi SU-70 working at 4 kV. Samples were prepared by deposition on aluminium sample holders followed by carbon coating using an Emitech K950X carbon evaporator. EDS (energy dispersive X-ray spectroscopy) data and SEM mapping images were recorded using the latter microscope working at 15 kV and using either a Bruker Quantax 400 or an Esprit 1.9 EDS microanalysis system.

The **water vapour adsorption** isotherms were collected in a Dynamic Vapor Sorption apparatus from Surface Measurements Systems, using N_2 as the carrier gas (Air Liquide Alphagaz, less than 3 ppm H2O, total flow of 200 sccm). Dry aliquots (16 mg) were loaded in a steel pan and suspended in the measuring chamber. The experiment started with a 2 h pre-treatment at 125 ºC, to completely dry the sample, followed by the isotherm at 25 ºC with increasing and decreasing RH steps from 0 to 98 %. Each humidity step was kept until the rate of change of mass per fixed time (dm/dt) was lower than 0.002 %, for a period of at least 10 min.

A3.2 Chemical characterization

A3.2.1 Elemental Analysis

Table A3.1. Elemental analysis of compound **3.1**

Compound	Formula	Molecular weight	Calc.	Found.
3.1	$C_{20}H_{26}N_2O_{13}Cu_3$	692.5	C: 34.66; H: 3.78; N: 4.04; O: 30.01; Cu: 27.51	C: 34.75; H: 3.74; N: 4.03; O: 30.00; Cu: 27.62

A3.2.2 FT-IR spectroscopy

When FTIR spectra of is examined from left to right, from higher to smaller frequency, compound **3.1** exhibit an intense broad band around 3447 cm^{-1} assigned to O–H bond vibration of the of 3,4-dihydroxybenzoate free ligand. At lower frequency, a set of sharp and of medium intensity bands that corresponds to aromatic ring's C–H bond vibrations of the ligand are visible between 3073 cm^{-1} and 2989–2864 cm^{-1}. The following intense vibrations located in 1659–1426 cm^{-1} region are attributed to both the asymmetric stretching vibrations of the carboxylate groups and the aromatic C–C bonds. Moving to lower range of 1389–1252 cm^{-1}, symmetric stretching vibrations of the carboxylate groups appear in the spectrum. The remaining bands that are found at lower frequency can be attributed to the distortions originated in the aromatic ring and the carboxylate groups of the ligands.

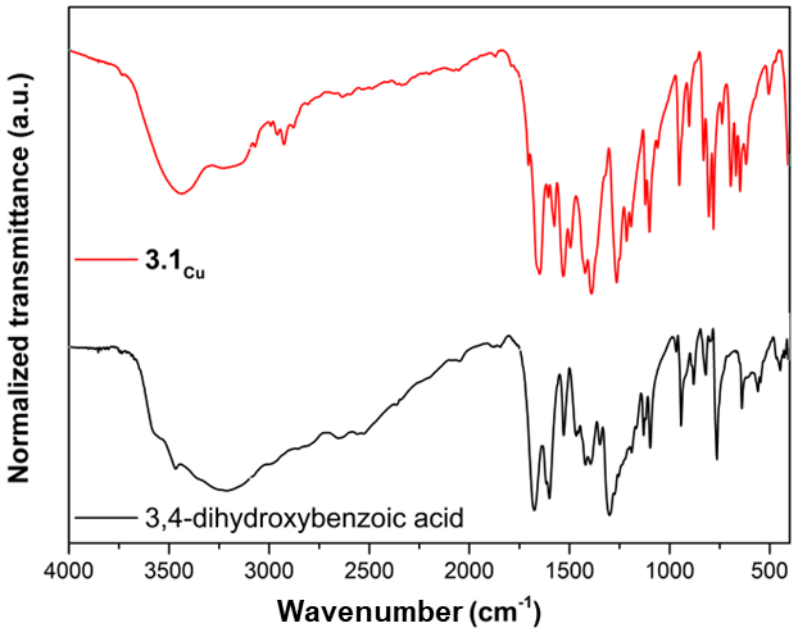

Figure A3.1. Infrared spectra of the ligand and compound **3.1.**

A3.3 Crystallographic data

Table A3.2. Crystallographic data and structure refinement details of compound **3.1**.

Compound	**3.1_{Cu}**
Formula	$C_{20}H_{26}N_2O_{13}Cu_3$
M_r	693
Crystal system	monoclinic
Space group (no.)	C2/c
a(Å)	20.2893(16)
b(Å)	8.6194(7)
c(Å)	16.7337(11)
α(°)	90
β(°)	126.632(2)
γ(°)	90
V(Å^3)	2348.4(3)
Z	8
ρ_{calc}g/cm^3	1.785
μ/mm^{-1}	2.749
F(000)	1254.0
Crystal size/mm^3	0.32 × 0.17 × 0.12
Radiation	MoKα (λ = 0.71073)
2θ range for data collection/°	5.062 to 50.756
Index ranges	-24 ≤ h ≤ 22, -10 ≤ k ≤ 10, -20 ≤ l ≤ 20
Reflections collected	17193
Independent reflections	2149 [R_{int} = 0.0229, R_{sigma} = 0.0123]
Data/restraints/parameters	2149/0/173
Goodness-of-fit on F^2	1.150
Final R indexes [I>=2σ (I)]	R_1 = 0.0349, wR_2 = 0.0928
Final R indexes [all data]	R_1 = 0.0382, wR_2 = 0.0947
Largest diff. peak/hole / e Å^{-3}	0.72/-0.47

Table A3.3. Table of the selected bond lengths (Å) and angles (°) for compound **3.1.**

Compound 3.1		
Atom	**Atom**	**Length/Å**
Cu1	Cu1[1]	3.0121(8)
Cu1	Cu2[2]	3.0461(4)
Cu1	O8	2.296(3)
Cu1	O1	1.946(2)
Cu1	O2[1]	1.952(2)
Cu1	O2	1.943(2)
Cu1	O4[3]	1.924(3)
Cu2	O1[4]	1.960(2)
Cu2	O1[5]	1.960(2)
Cu2	O3[6]	1.926(3)
Cu2	O3	1.926(3)

[1]1-x,+y,1/2-z; [2]3/2-x,-1/2+y,1/2-z; [3]-1/2+x,3/2-y,-1/2+z; [4]1/2+x,3/2-y,1/2+z; [5]3/2-x,1/2+y,1/2-z; [6]2-x,2-y,1-z

Atom 1	**Atom 2**	**Atom 3**	**Angle 2,1,3 [°]**
Cu1[1]	Cu1	Cu2[2]	141.692(17)
Cu1	O2	Cu1[1]	101.28(11)
O1	Cu1	O8	89.55(12)
O1	Cu1	O2[1]	161.21(10)
O2[1]	Cu1	Cu1[1]	39.25(7)
O2[1]	Cu1	O8	100.21(12)
O2	Cu1	O8	96.04(12)
O2	Cu1	O1	84.47(10)
O2	Cu1	O2[1]	78.60(11)
O4[3]	Cu1	Cu1[1]	136.74(8)
O4[3]	Cu1	Cu2[2]	80.35(8)
O4[3]	Cu1	O8	94.65(13)
O4[3]	Cu1	O1	95.96(11)
O4[3]	Cu1	O2	169.30(12)
O4[3]	Cu1	O2[1]	99.18(10)
Cu1[4]	Cu2	Cu1[5]	180.0
O1[5]	Cu2	O1[4]	180.00(13)
O3	Cu2	O1[4]	91.30(11)
O3	Cu2	O1[5]	88.69(11)
O3[6]	Cu2	O1[5]	91.30(11)
O3[6]	Cu2	O1[4]	88.70(11)
O3[6]	Cu2	O3	180.0

[1]1-x,+y,1/2-z; [2]3/2-x,-1/2+y,1/2-z; [3]-1/2+x,3/2-y,-1/2+z; [4]3/2-x,1/2+y,1/2-z; [5]1/2+x,3/2-y,1/2+z; [6]2-x,2-y,1-z

A3.4 Powder X-ray diffraction analysis

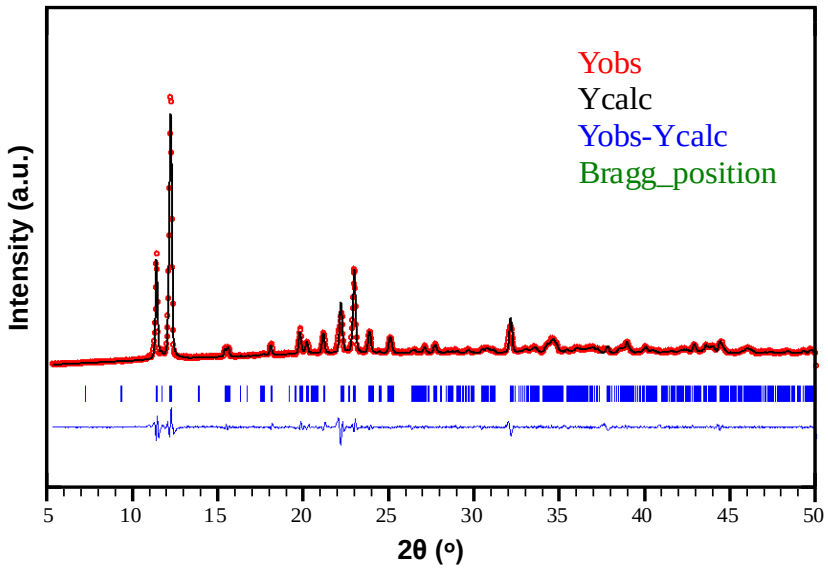

Figure A3.2. Figure of the pattern matching analysis and experimental PXRD for complex **3.1**.

Compound **3.1** stability was examined in various solvents. For that purpose, 100 mg of MOF were suspended in a 4 mL of solvent and left agitating for 16 h. Afterwards, material was filtered off and left drying before carrying on powder X-ray diffraction (PXRD) analysis.

According to the PXRD, compound **3.1** is stable in EtOH after 16 h keeping its structure, contrary to what it happens in MeOH and H_2O. In the latter case, compound **3.1** completely evolves into a different crystalline product. However, in the former case, in MeOH, PXRD reveals that even if compound **3.1** most important peaks are present in the diffractogram, several new peaks appear. The position of those new peaks come in accordance with the evolved crystalline product obtained after soaking compound **3.1** for 16 h in water.

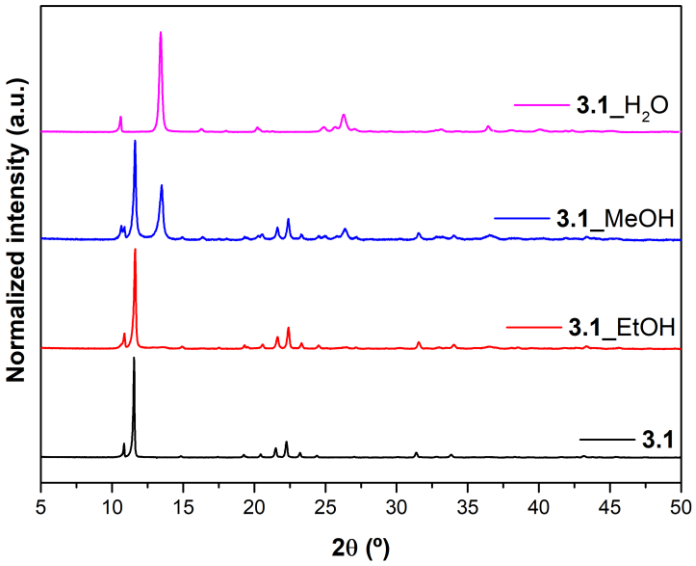

Figure A3.3. Experimental PXRD for complexes **3.1** after being soaked for 16 h in several solvents.

A3.5 Continuous Shape Measurements

Table A3.4. Table of the continuous Shape Measurements for the CuO_5 coordination environment.

PP-5	D_{5h}	Pentagon
vOC-5	C_4	Vacant octahedron (Johnson square pyramid, J1)
TBPY-5	D_{3h}	Trigonal bipyramid
SPY-5	C_{4v}	Square pyramid
JTBPY-5	D_{3h}	Johnson trigonal bipyramid (J12)

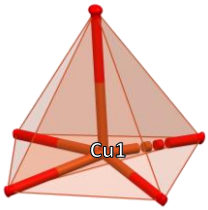

Complex 3.1	PP-5	vOC-5	TBPY-5	SPY-5	JTBPY-5
Cu1	29.740	1.653	6.289	**1.062**	9.155

Table A3.5. Table of the continuous Shape Measurements for the CuO_6 coordination environment.

HP-6	D_{6h}	Hexagon
PPY-6	C_{5v}	Pentagonal pyramid
OC-6	O_h	Octahedron
TPR-6	D_{3h}	Trigonal prism
JPPY-6	C_{5v}	Johnson pentagonal pyramid J2

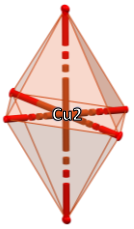

Complex 3.1	HP-6	PPY-6	OC-6	TPR-6	JPPY-6
Cu2	29.385	28.101	**2.417**	17.463	30.372

A3.6 Thermal analysis

Thermogravimetric analyses performed over polycrystalline sample in compound **3.1** enabled checking the stability of the product. TG curves has been collected for compound **3.1** for the as synthesised compound **3.1** and after solvent exchange with EtOH. In stability section, we saw that material remains stable after being soaked in EtOH and being this latter solvent more volatile than the solvents used in the synthesis of the material, we tried to accomplish solvent exchange procedure as an approach to replace solvent molecules (dimethylformamide and water molecules) to ease material activation to posteriorly analyse its adsorptive-capacity. For this purpose, as for stability tests, compound **3.1** was suspended in EtOH for 16 h, left solvent evaporated and carried on thermal analysis. Powder X-ray diffraction confirmed that**3. 1** remains stable after solvent exchange with MeOH as it can be seen in Figure A3.5, right.

The thermal behaviour of the as synthesised $[Cu_3L_2(DMF)_2]\cdot 3H_2O$, compound **3.1**, exhibits two main regions. The first weight of loss was progressive and went from ambient temperature to 200 ºC and corresponded to the loss of solvent molecules, firstly, lattice water molecules and then coordinated DMF molecules. Above this temperature, there is an abrupt loss corresponding to the complete collapse of the crystal structure. From the shape of the TG curve, it seems that solvent molecules stabilise the structure and their removal promote crystal structure decomposition. In the final step, as a consequence of the decomposition of the organic content metal oxide is obtained.

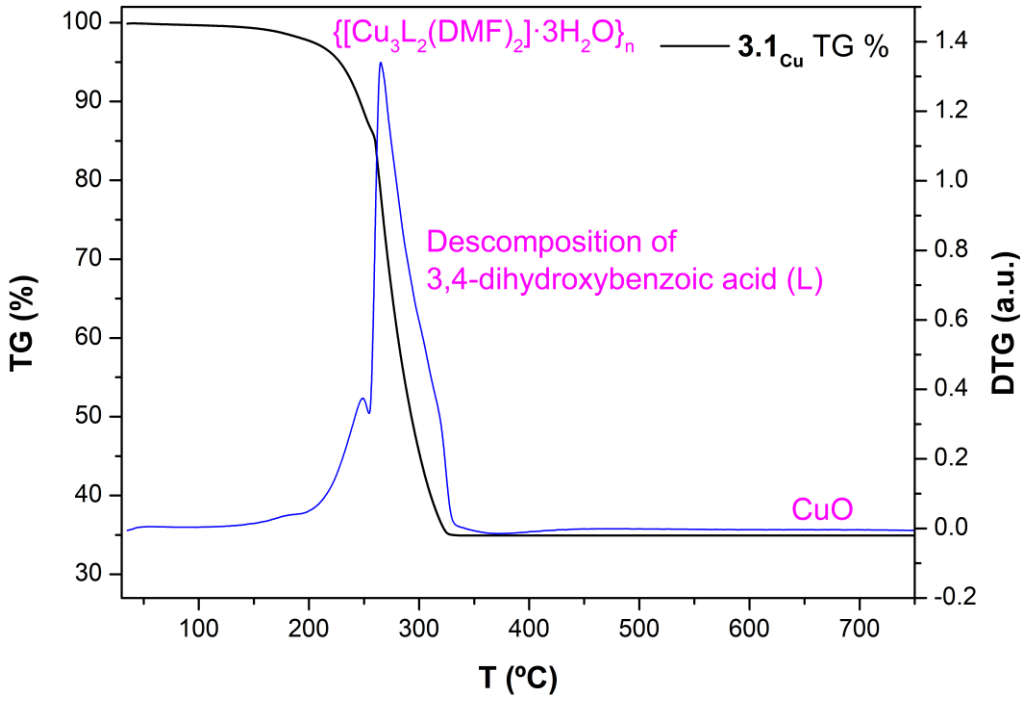

Figure A3.4. Figure of TG/DTG analysis of as synthesised compound **3.1**.

TG curve performed after solvent exchange with EtOH exhibits different pattern in comparison to the previous curve obtained with as synthesised compound **3.1** material. In this case, after solvent exchange procedure, the weight of loss occurs in three main regions. The first region comprises from the room temperature to 150 ºC and after an initial loss of weight occurring from 30 to 70 ºC a plateau is obtained around 80 ºC which goes up to 150 ºC. Then, from 150 ºC to 200 ºC a second loss of weight is visible in the spectra before the last abrupt loss corresponding to compound **3.1** degradation which occurs at 250 ºC. Above this temperature, CuO is obtained as final residue. The plateau obtained in the at around 80 ºC and the increase of final-residue percentage (in around 8 %) can be indicative of solvent molecules being fully or at least partly replaced by EtOH, being this solvent-exchange strategy a possible option to promote material activation at lower temperatures.

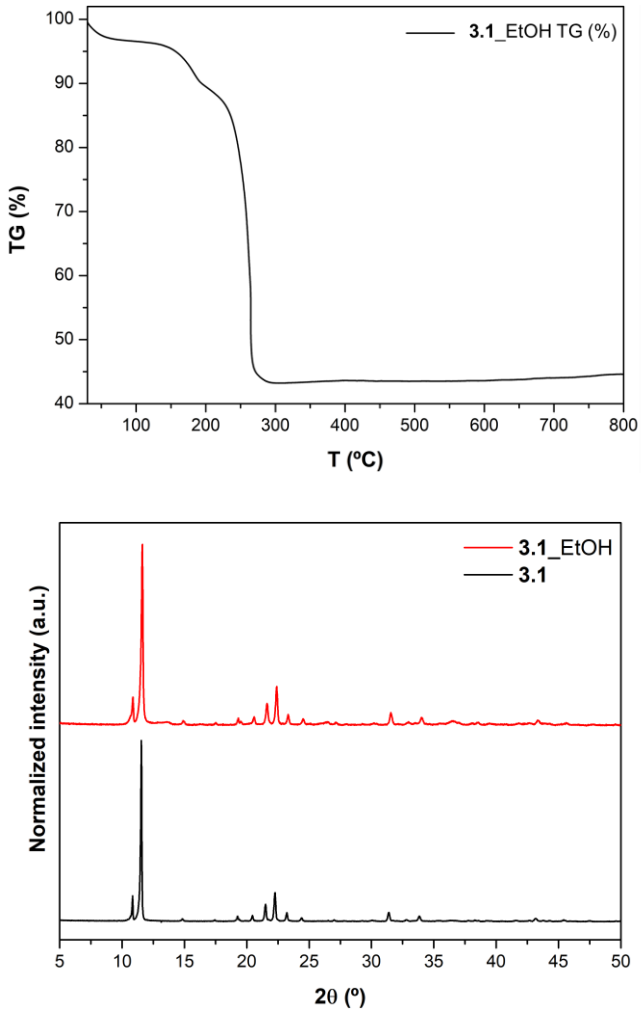

Figure A3.5. Figure of TG analysis of compound **3.1** performed after solvent exchange with EtOH during 16 h (up) and experimental PXRD for complex **3.1** before and after solvent exchange with EtOH (bottom).

A3.7 Thermal evolution

Thermal evolution of as synthesised compound **3.1** shows that the material keeps its initial phase crystallinity up to 110 ºC. Above this temperature, new peaks appear in the diffractogram indicating the transformation into a different crystalline phase; this second phase, maintains its crystallinity up to 210 ºC and it must be noted that is very similar to the phase obtained when material was soaked in H_2O. Finally, compound **3.1** collapses and evolves into metallic residue CuO, obtained around 800 ºC.

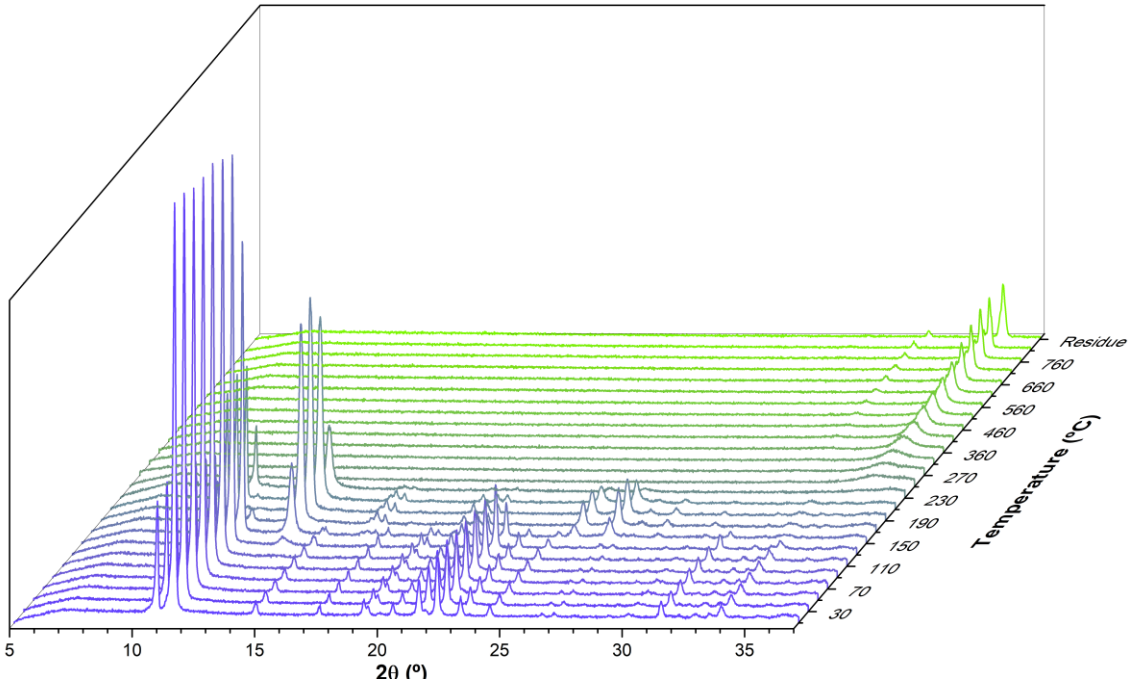

Figure A3.6. Thermal evolution of as synthesised compound **3.1.**

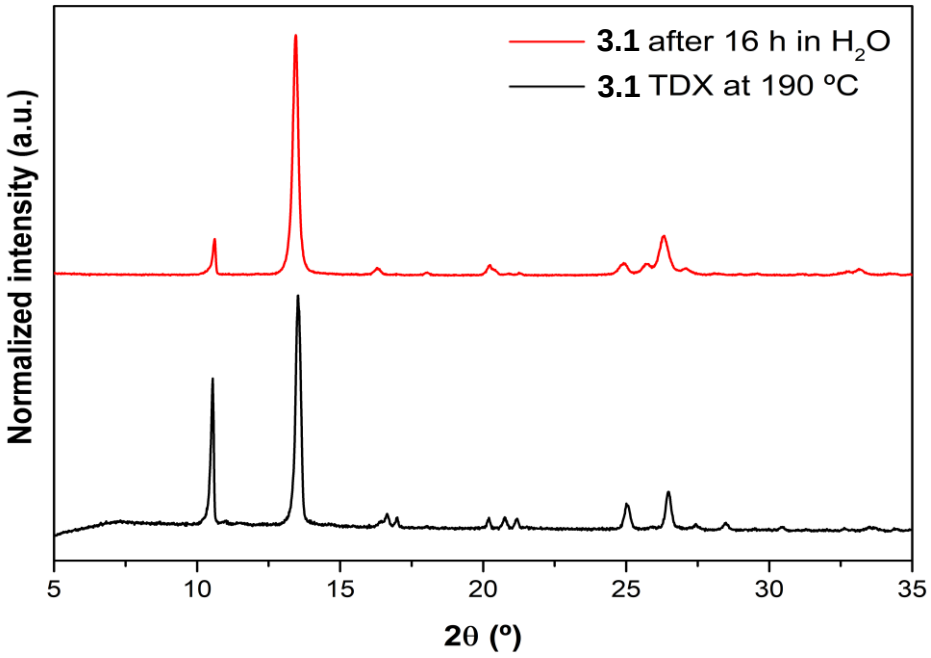

Figure A3.7. Similarity between the PXRD transformed phase of compound **3.1** obtained from thermal evolution at 190 ºC and the phase obtained soaking compound **3.1** in H_2O during 16 h.

A3.8 Additional views of the structure

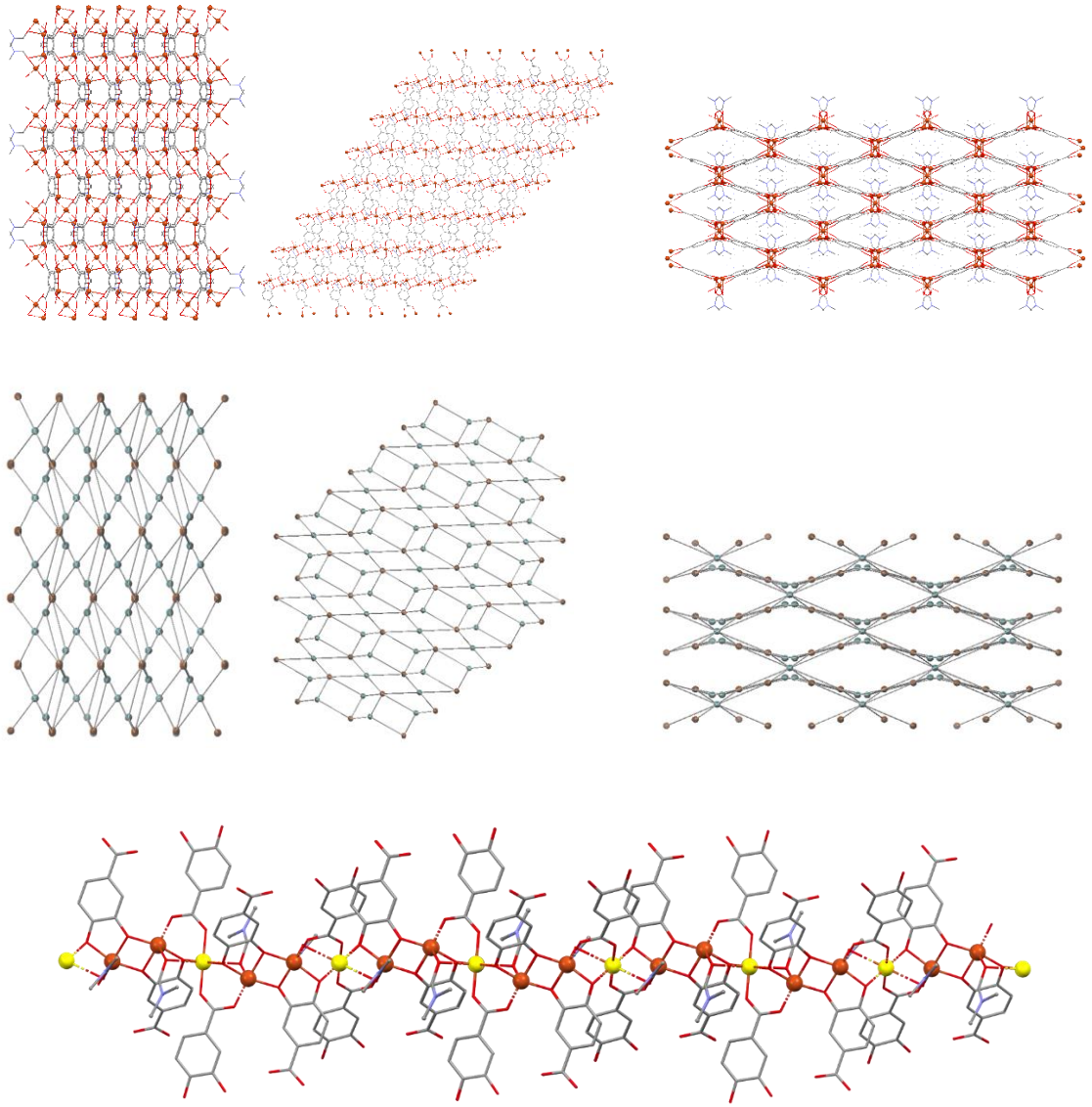

Figure A3.8. View along *a*, *b* and *c* crystallographic axis, the corresponding topological representation and view of “ABBA...” SBU.

A3.9 Scanning Electron Microscopy

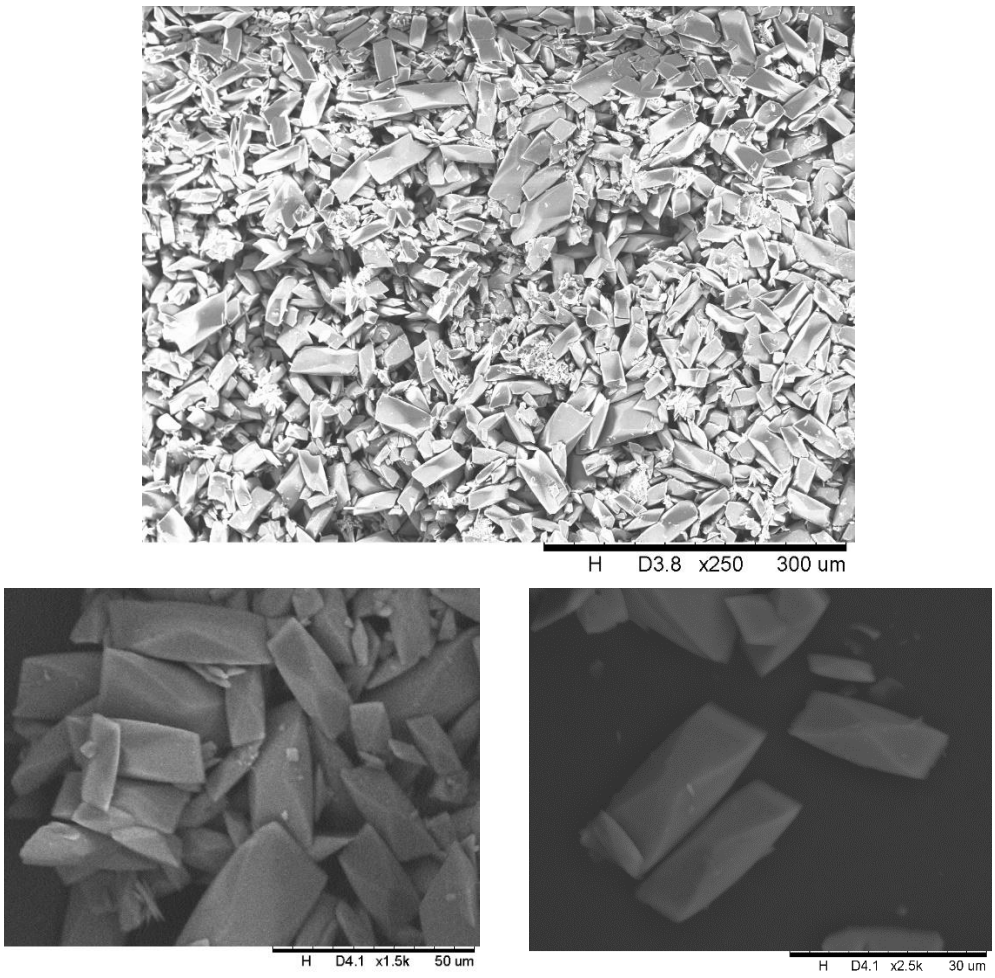

Figure A3.9. SEM images of compound **3.1**.

Appendix 4

Supporting information of Chapter 4

A4.1 Experimental section. General instrumentation

Elemental analyses (C, H, N) were performed on a Leco CHNS-932 microanalyser. **Infrared** (FT-IR) spectra (400-4000 cm^{-1}) were recorded on a Nicolet FT-IR 6700 spectrometer in KBr pellets.

Thermogravimetric analysis (TG/DTA) were performed on a TG-Q500 TA Instruments thermal analyser from room temperature to 800 °C under a synthetic air atmosphere (79 % N_2/21 % O_2) at a heating rate of 10 °C min^{-1}.

X-ray powder diffraction (XRPD) patterns were collected at 25 °C on a Phillips X'PERT powder diffractometer with Cu-Kα radiation (λ = 1.5418 Å) over the range 5º < 2θ < 50º with a step size of 0.02º and an acquisition time of 2.5 s per step. Indexation of the diffraction profiles were made by means of the FULLPROF program (pattern- matching analysis) based on the space group and the cell parameters found by single crystal X-ray diffraction.

Scanning electron microscopy (SEM) images were acquired using either a Hitachi S4100 field emission gun tungsten filament instrument working at 25 kV or a high-resolution Hitachi SU-70 working at 4 kV. Samples were prepared by deposition on aluminium sample holders followed by carbon coating using an Emitech K950X carbon evaporator. EDS (energy dispersive X-ray spectroscopy) data and SEM mapping images were recorded using the latter microscope working at 15 kV and using either a Bruker Quantax 400 or an Esprit 1.9 EDS microanalysis system.

GC-FID analysis carried out in a Bruker 430-GC-FID chromatograph (Bruker, Faculty of Science, University of Porto, Porto, Portugal). Hydrogen was used as a carrier gas (55 $cm \cdot s^{-1}$), and fused silica Supelco capillary columns SPB-5 (30 m × 0.25 mm i.d.; 25 µm film thickness) were used.

Photoluminescence Spectroscopy. The emission and excitation spectra were recorded at ambient-temperature and 12 K using a Fluorolog®-3Horiba Scientific (Model FL3-2T) spectroscope, with a modular double grating excitation spectrometer (fitted with a 1200 grooves/mm grating blazed at 330 nm) and a TRIAX 320 single emission monochromator (fitted with a 1200 grooves/mm grating blazed at 500 nm, reciprocal linear density of 2.6 $nm.mm^{-1}$), coupled to a R928 Hamamatsu photomultiplier, using the front face acquisition mode. The excitation source was a 450 W Xe arc lamp. The emission spectra were corrected for detection and optical spectral response of the spectrofluorometer and the excitation spectra were corrected for the spectral distribution of the lamp intensity using a photodiode reference detector. Time-resolved measurements have been carried out using a 1934D3 phosphorimeter coupled to the Fluorolog®-3, and a Xe-Hg flash lamp (6 µs/pulse half width and 20-30 µs tail) was used as the

excitation source. The low temperature measurements (12 K) were performed using a helium-closed cycle cryostat with vacuum system measuring ca. 5×10^{-6} mbar and a Lakeshore 330 auto-tuning temperature controller with a resistance heater.

A4.2 Chemical characterization

A4.2.1 Elemental Analysis

Table A4.1 Elemental analysis of compound **4.1**-**4.8**.

Compound	Formula	Molecular weight	Calc.	Found.
4.1$_{Ru-Nd}$	$C_{72}H_{36}O_{24}N_{12}Ru_2Nd_3$	2088.0	C: 41.42; H: 1.74; O: 18.39; N: 8.05; Ru: 9.68; Nd: 20.72;	C: 41.48; H: 1.82; O: 18.41; N: 8.12; Ru: 9.68; Nd: 20.76;
4.2$_{Ru-Sm}$	$C_{72}H_{36}O_{24}N_{12}Ru_2Sm_3$	2106.5	C: 41.05; H: 1.72; O: 18.23; N: 7.98; Ru: 9.60; Sm: 21.42;	C: 41.09; H: 1.84; O: 18.26; N: 8.01; Ru: 9.61; Sm: 21.37;
4.3$_{Ru-Eu}$	$C_{72}H_{36}O_{24}N_{12}Ru_2Eu_3$	2111.2	C: 40.96; H: 1.72; O: 18.19; N: 7.96; Ru: 9.57; Eu: 21.59;	C: 41.00; H: 1.74; O: 18.21; N: 7.93; Ru: 9.62; Eu: 21.68;
4.4$_{Ru-Gd}$	$C_{72}H_{36}O_{24}N_{12}Ru_2Gd_3$	2127.0	C: 40.66; H: 1.71; O: 18.05; N: 7.90; Ru: 9.50; Gd: 22.18;	C: 40.62; H: 1.75; O: 18.15; N: 7.93; Ru: 9.56; Gd: 22.22;
4.5$_{Ru-Tb}$	$C_{72}H_{36}O_{24}N_{12}Ru_2Tb_3$	2132.1	C: 40.56; H: 1.70; O: 18.01; N: 7.88; Ru: 9.48; Tb: 22.36;	C: 40.62; H: 1.68; O: 18.05; N: 7.92; Ru: 9.68; Tb: 22.48;
4.6$_{Ru-Dy}$	$C_{72}H_{36}O_{24}N_{12}Ru_2Dy_3$	2142.8	C: 40.36; H: 1.69; O: 17.92; N: 7.84; Ru: 9.43; Dy: 22.75;	C: 40.42; H: 1.64; O: 18.00; N: 7.84; Ru: 9.41; Dy: 22.76;
4.7$_{Ru-Er}$	$C_{72}H_{36}O_{24}N_{12}Ru_2Er_3$	2157.1	C: 40.09; H: 1.68; O: 17.80; N: 7.79; Ru: 9.37; Er: 23.26;	C: 40.12; H: 1.71; O: 17.86; N: 7.84; Ru: 9.41; Er: 23.21;
4.8$_{Ru-Yb}$	$C_{72}H_{36}O_{24}N_{12}Ru_2Yb_3$	2174.4	C: 39.77; H: 1.67; O: 17.66; N: 7.73; Ru: 9.30; Yb: 23.87;	C: 39.89; H: 1.71; O: 17.77; N: 7.74; Ru: 9.31; Yb: 23.84;

A4.2.2 Determination of the metal content by ICP-AES

Table A4.2. Determination of the metal content by ICP and Dy to Ru relationship.

Compound	Dy content in mgL^{-1}	Ru content in mgL^{-1}	Dy to Ru relationship
4.6$_{Ru-Dy}$	1652 (10.2 mM)	686 (6.8 mM)	± 1.5

A4.2.3 FT-IR spectroscopy

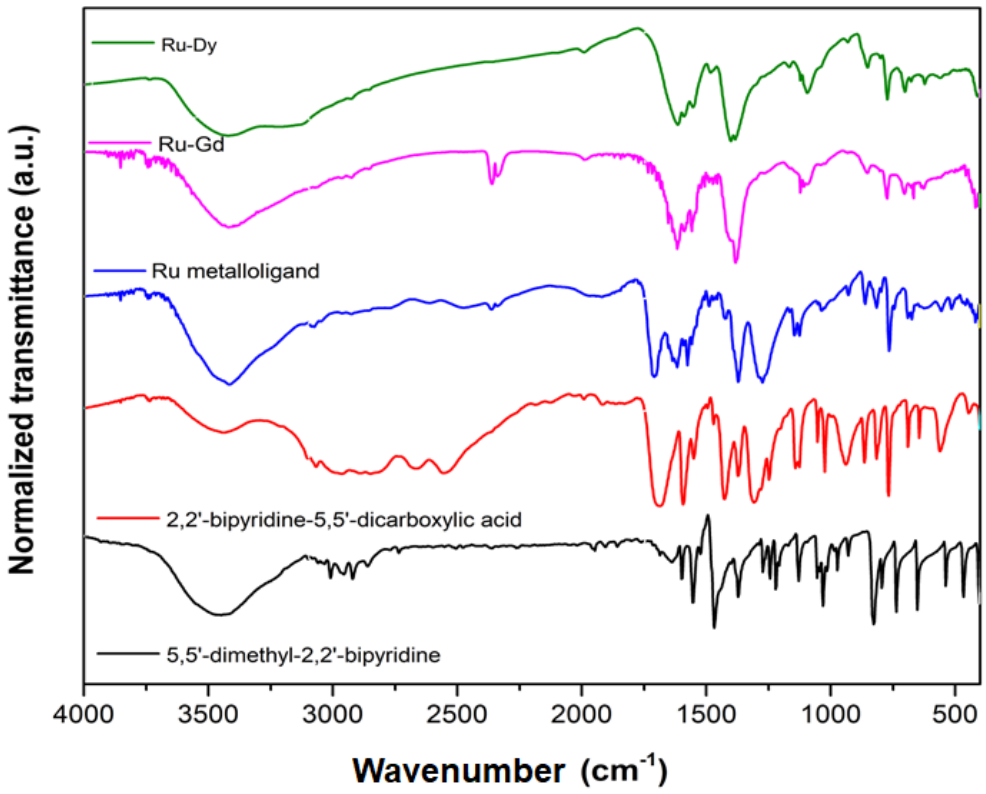

Figure A4.1. Infrared spectra of the 5,5'-dimehtyl-2,2'-bipyridine, 2,2'-bipyridine-5,5'-dicarboxylic acid, $[RuL_3]Cl_2$ metalloligand and compounds **4.4**$_{Ru\text{-}Gd}$ and **4.6**$_{Ru\text{-}Dy}$.

A4.2.4 ^{1}H-Nuclear Magnetic Resonance

2,2'-bipyridine-5,5'-dicarboxylic acid was prepared following the literature method consisting in the oxidation of 5,5'-dimethyl-2,2'-bipyridyl with $K_2Cr_2O_7$ in concentrated sulfuric acid. This product has been previously reported in bibliography.[32,33]

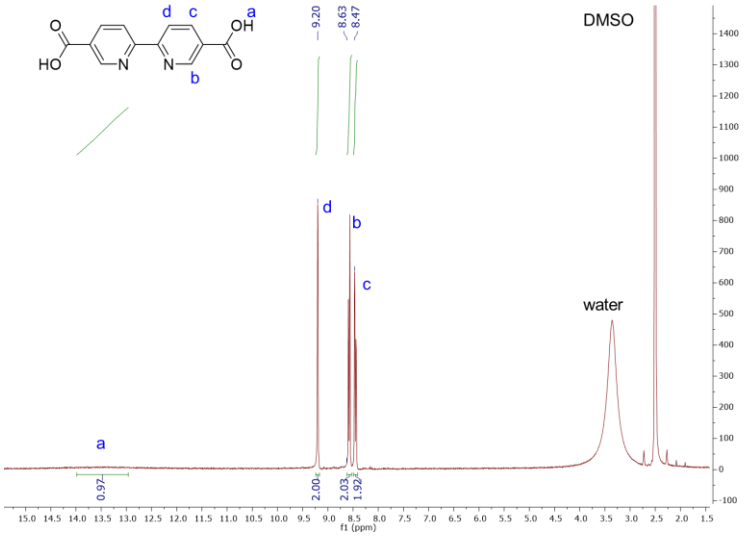

Figure A4.2. [1]H-NMR spectra of 2,2'-bipyridine-5,5'-dibarboxylic acid in DMSO-*d*$_6$.

This product has already been reported in bibliography and [1]H-NMR matches with the reported data.[34,35]

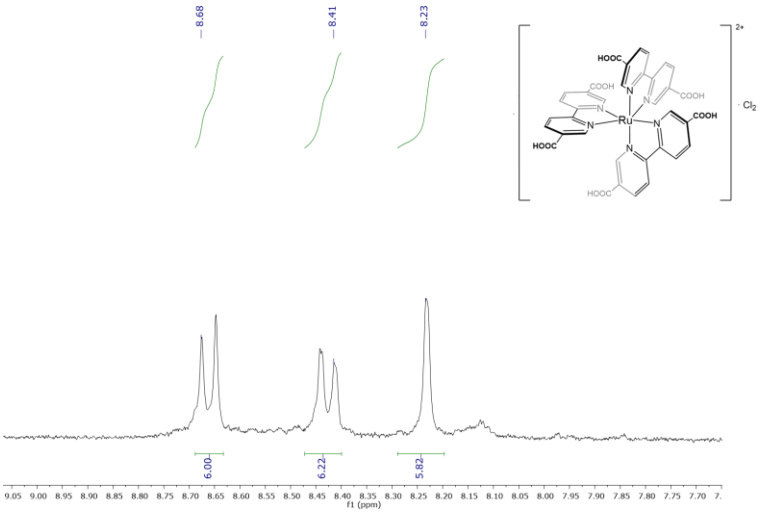

Figure A4.3. [1]H-NMR spectra of ruthenium(II) metalloligand in D_2O made alkaline with NaOD.

A4.3 Crystallographic data

Table A4.3. Crystallographic data and structure refinement details of compound **4.6$_{Ru-Dy}$**.

Compound	Ru-metalloligand	**4.6$_{Ru-Dy}$**
Formula	$C_{36}H_{26}N_6O_{14}Ru$	$C_{36}ClDy_2N_6O_{17}Ru$
M_r	867.7	1249.94
Crystal system	monoclinic	orthorhombic
Space group (no.)	C2/c	*Cmca*
a(Å)	22.904(5)	23.7721(8)
b(Å)	12.436(5)	18.7340(8)
c(Å)	14.584(5)	18.7634(7)
α(°)	90	90
β(°)	121.973(5)	90
γ(°)	90	90
V(Å^3)	3524(2)	8356.2(6)
Z	4	8
ρ_{calc}g/cm^3	1.636	1.987
μ/mm^{-1}	0.526	23.033
F(000)	1760	4696.0
Crystal size/mm^3	0.22 × 0.16 × 0.07	12 × 11 × 9
Radiation	MoKα (λ = 0.71073)	CuKα (λ = 1.54178)
2θ range for data collection/°	5.63 to 55.908	7.438 to 79.938
Index ranges	-29 ≤ h ≤ 30, -16 ≤ k ≤ 16, -19 ≤ l ≤ 19	-18 ≤ h ≤ 19, -15 ≤ k ≤ 15, -15 ≤ l ≤ 15
Reflections collected	28678	10398
Independent reflections	4230 [R_{int} = 0.0332, R_{sigma} = 0.0194]	1316 [R_{int} = 0.1268, R_{sigma} = 0.0643]
Data/restraints/parameters	4230/8/270	1316/0/153
Goodness-of-fit on F^2	1.104	1.722
Final R indexes [I>=2σ (I)]	R_1 = 0.0366, wR_2 = 0.1027	R_1 = 0.1432, wR_2 = 0.3759
Final R indexes [all data]	R_1 = 0.0414, wR_2 = 0.1075	R_1 = 0.1755, wR_2 = 0.4103
Largest diff. peak/hole / e Å^{-3}	1.51/-0.64	3.84/-1.6

Table A4.4. Table of the selected bond lengths (Å) for Ru-metalloligand and compound **4.6$_{Ru-Dy}$**.

Ru-metalloligand			Compound 4.6$_{Ru-Dy}$		
Atom	**Atom**	**Length/Å**	**Atom**	**Atom**	**Length/Å**
Ru1	N1[1]	2.067(2)	Dy1	O1	2.34(3)
Ru1	N1	2.067(2)	Dy1	O1[1]	2.34(3)
Ru1	N2	2.077(2)	Dy1	O2[2]	2.31(4)
Ru1	N2[1]	2.077(2)	Dy1	O2[3]	2.31(4)
Ru1	N3[1]	2.060(2)	Dy1	O4[4]	2.23(4)
Ru1	N1[1]	2.060(2)	Dy1	O4[5]	2.23(4)
[1]-x,+y,1/2-z			Dy2	Dy2[7]	3.879(17)
			Dy2	O7	2.41(5)
			Dy2	O5[1]	2.28(6)
			Dy2	O5	2.28(6)
			Dy2	O6[8]	2.34(6)
			Dy2	O6[7]	2.34(6)
			Ru1	N2	2.07(3)
			Ru1	N2[6]	2.07(3)
			Ru1	N1	2.07(3)
			Ru1	N1[6]	2.07(3)
			Ru1	N3	2.09(4)
			Ru1	N3[6]	2.09(4)
			[1]-x,+y,+z; [2]+x,1-y,-z; [3]-x,1-y,-z; [4]-1/2+x,1/2+y,+z; [5]1/2-x,1/2+y,+z; [6]1/2-x,+y,1/2-z; [7]-x,1-y,1-z; [8]+x,1-y,1-z		

Table A4.5. Table of the selected angles (°) for ruthenium metalloligand and compound **4.6$_{Ru-Dy}$**.

Ru-metalloligand				4.6$_{Ru-Dy}$							
Atom	**Atom**	**Atom**	**Angle/˚**	**Atom**	**Atom**	**Atom**	**Angle/˚**	**Atom**	**Atom**	**Atom**	**Angle/˚**
N1[1]	Ru1	N1	173.68(11)	N1	Ru1	N3[6]	92.2(13)	O4[4]	Dy1	O2[2]	88.2(14)
N1	Ru1	N2	78.30(8)	N1	Ru1	N3	94.9(13)	O4[4]	Dy1	O2[3]	149.8(14)
N1[1]	Ru1	N2	96.76(8)	N1[6]	Ru1	N1	171.1(17)	O4[5]	Dy1	O1	78.0(13)
N1[1]	Ru1	N2[1]	78.30(8)	N1[6]	Ru1	N3	92.2(13)	O4[5]	Dy1	O1[1]	131.5(13)
N1	Ru1	N2[1]	96.76(8)	N1[6]	Ru1	N3[6]	94.9(13)	O4[5]	Dy1	O2[2]	149.8(14)
N2[1]	Ru1	N2	79.12(11)	N2	Ru1	N1	79.7(12)	O4[5]	Dy1	O2[3]	88.2(14)
N3	Ru1	N1[1]	94.04(8)	N2	Ru1	N1[6]	93.6(12)	O4[5]	Dy1	O4[4]	87(2)
N3	Ru1	N1	90.85(8)	N2	Ru1	N3	173.6(13)	O5	Dy2	O7	134.5(15)
N3[1]	Ru1	N1	94.04(8)	N2	Ru1	N3[6]	99.9(13)	O5	Dy2	O6[8]	81(2)
N3[1]	Ru1	N1[1]	90.84(8)	N2[6]	Ru1	N2	83.9(15)	O5	Dy2	O6[7]	149(2)
N3	Ru1	N2	101.58(9)	N2[6]	Ru1	N1[6]	79.7(12)	O5[1]	Dy2	O7	134.5(15)
N3[1]	Ru1	N2[1]	101.58(9)	N2[6]	Ru1	N1	93.6(12)	O5[1]	Dy2	O5	91(3)
N3	Ru1	N2[1]	172.33(8)	N2[6]	Ru1	N3	99.9(13)	O5[1]	Dy2	O6[7]	81(2)
N3[1]	Ru1	N2	172.33(8)	N2[6]	Ru1	N3[6]	173.6(13)	O5[1]	Dy2	O6[8]	149(2)
N3	Ru1	N3[1]	78.76(12)	N3	Ru1	N3[6]	77(2)	O6[7]	Dy2	O7	60.5(17)
[1]-x,+y,1/2-z				O1	Dy1	O1[1]	78.8(14)	O6[8]	Dy2	O7	60.5(17)
				O2[2]	Dy1	O1	125.9(12)	O6[8]	Dy2	O6[7]	90(3)
				O2[2]	Dy1	O1[1]	76.0(12)	N1[6]	Ru1	N1	171.1(17)
				O2[2]	Dy1	O2[3]	81.3(18)	N1[6]	Ru1	N3	92.2(13)
				O2[3]	Dy1	O1[1]	125.9(12)	N1[6]	Ru1	N3[6]	94.9(13)
				O2[3]	Dy1	O1	76.0(12)				
				O4[4]	Dy1	O1	131.5(13)				
				O4[4]	Dy1	O1[1]	78.0(13)				
				1-x,+y,+z; 2-x,1-y,-z; 3+x,1-y,-z; 4-1/2+x,1/2+y,+z; 51/2-x,1/2+y,+z; 61/2-x,+y,1/2-z; 7-x,1-y,1-z; 8+x,1-y,1-z; 91/2+x,-1/2+y,+z							

A4.4 Diffuse reflectance

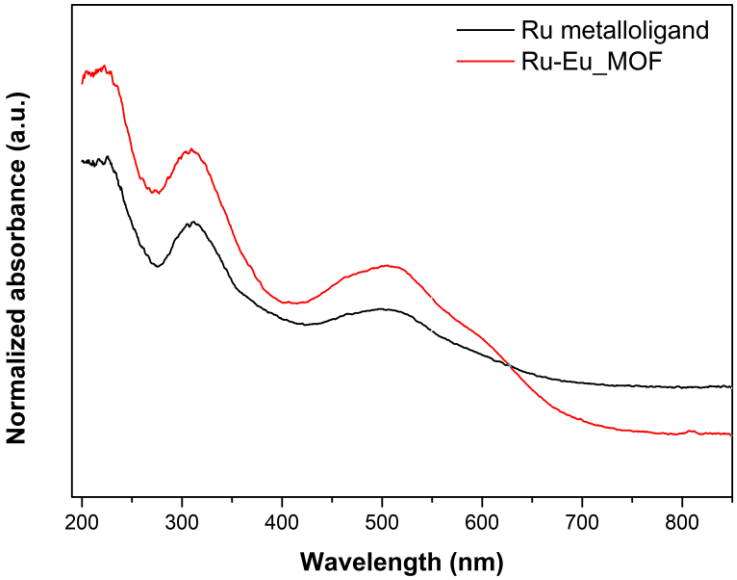

Figure A4.4. Normalized diffuse reflectance spectrum of $[RuL_3]Cl_2$ and compound **4.3**$_{\text{Ru-Eu}}$.

A4.5 Powder X-ray diffraction analysis

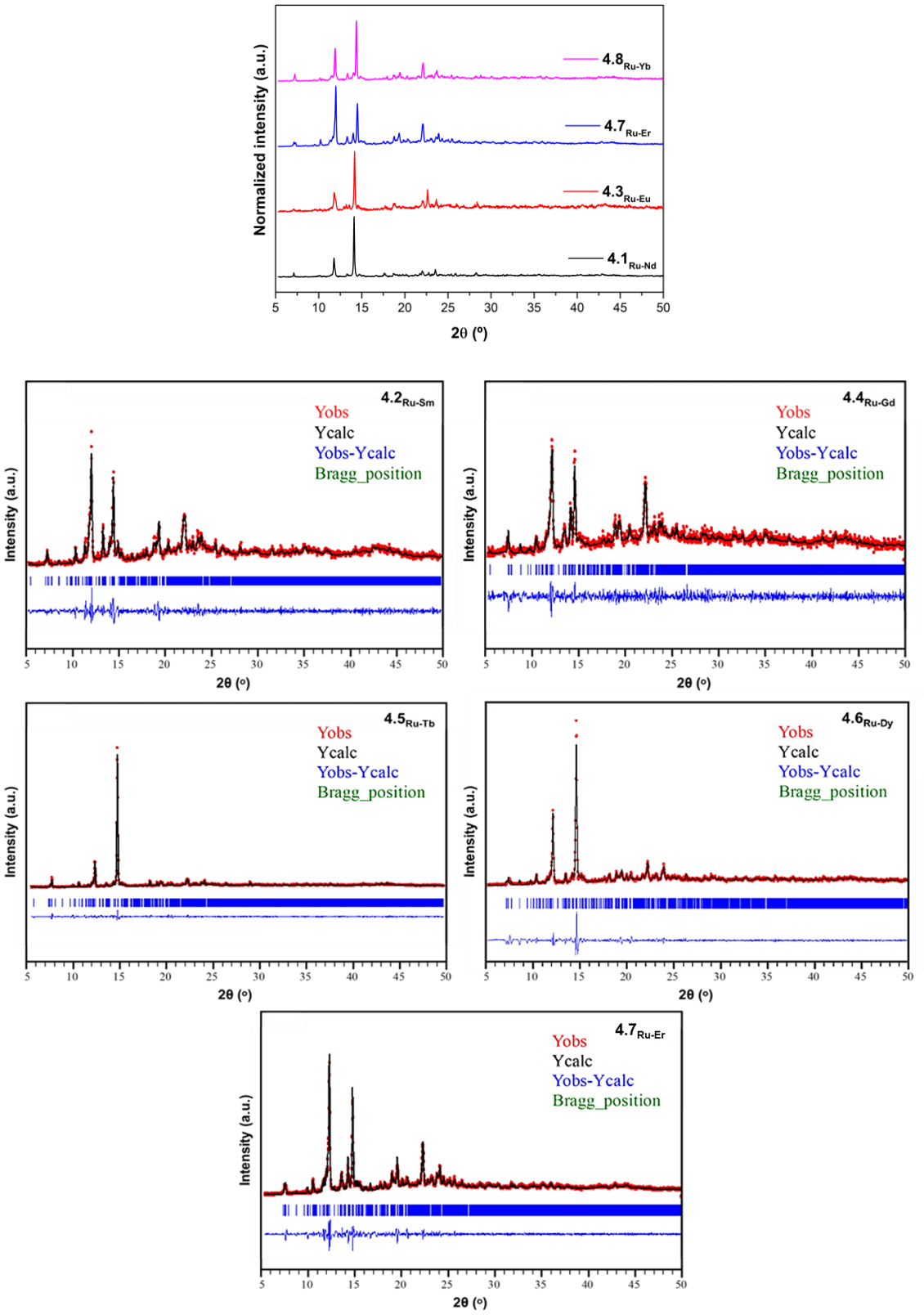

Figure A4.5. Pattern matching analysis and experimental PXRD for complexes **4.1**-**4.8**.

A4.6 Continuous Shape Measurements

CShMs for the coordination environment of **4.6$_{Ru-Dy}$**. The lowest SHAPE values for each ion is shown highlighted in grey, indicating best fits.

Table A4.6. Table of the continuous Shape Measurements for the RuN_6 andDyO_6 coordination environments.

HP-6	D_{6h}	Hexagon
PPY-6	C_{5v}	Pentagonal pyramid
OC-6	O_h	Octahedron
TPR-6	D_{3h}	Trigonal prism
JPPY-6	C_{5v}	Johnson pentagonal pyramid J2

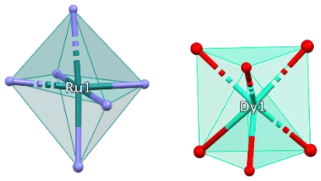

Complex 4.6$_{Ru-Dy}$	HP-6	PPY-6	OC-6	TPR-6	JPPY-6
Dy1	30.003	15.450	17.049	**0.379**	19.024
Ru1	26.975	27.199	**1.032**	14.844	30.469

Table A4.7. Table of the continuous Shape Measurements for the DyO_5 coordination environment.

PP-5	D_{5h}	Pentagon
vOC-5	C_4	Vacant octahedron (Johnson square pyramid, J1)
TBPY-5	D_{3h}	Trigonal bipyramid
SPY-5	C_{4v}	Square pyramid
JTBPY-5	D_{3h}	Johnson trigonal bipyramid (J12)

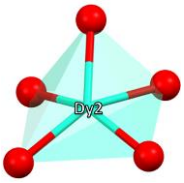

Complex 4.6$_{Ru-Dy}$	PP-5	vOC-5	TBPY-5	SPY-5	JTBPY-5
Dy2	13.456	10.115	14.337	**9.334**	15.973

A4.7 Thermal analysis

Thermogravimetric analyses have been performed over polycrystalline sample in compound **4.4** in order to check the stability of the products. The TG curves show three main steps of weight loses. The first steps concern to the release of coordinated solvent molecules which are released from room temperature up to 200 ºC. The second step refers to the decomposition of the ligands which involves the collapse of the crystal structure, evolving to mixture of Gd_2O_3 and RuO obtained at 700 ºC as the final residue.

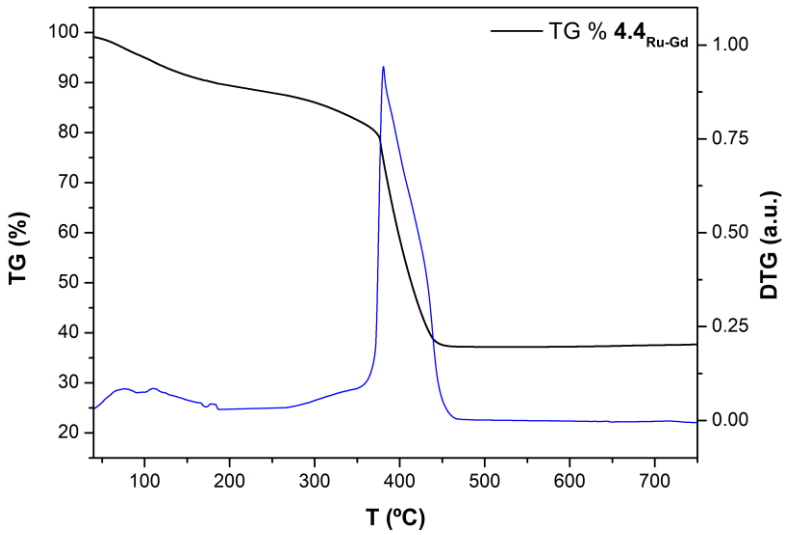

Figure A4.6. Figure of TG/DTG analysis of compound **4.4**$_{\text{Ru-Gd}}$.

A4.8 Thermal evolution

Thermal evolution has been measured to Ru-Dy_MOF and has showed that the material keeps its crystallinity up to around 200 ºC. At higher temperatures it stars degradation process until Dy_2O_3 is get as final residue.

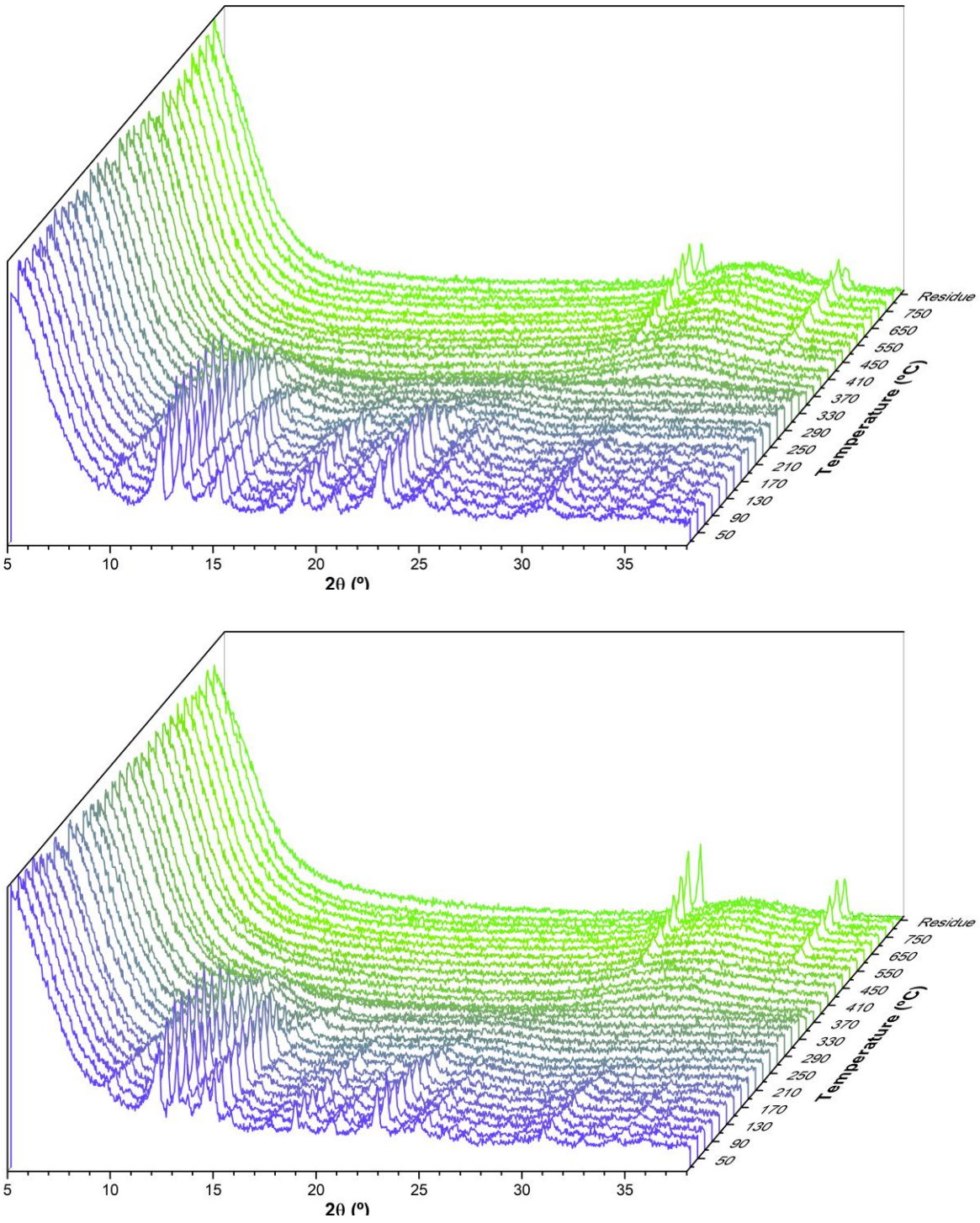

Figure A4.7. Thermal evolution of as synthesised compound **4.4**$_{\text{Ru-Gd}}$ (up) and **4.6**$_{\text{Ru-Dy}}$ (bottom).

A4.9 Additional views of the structure

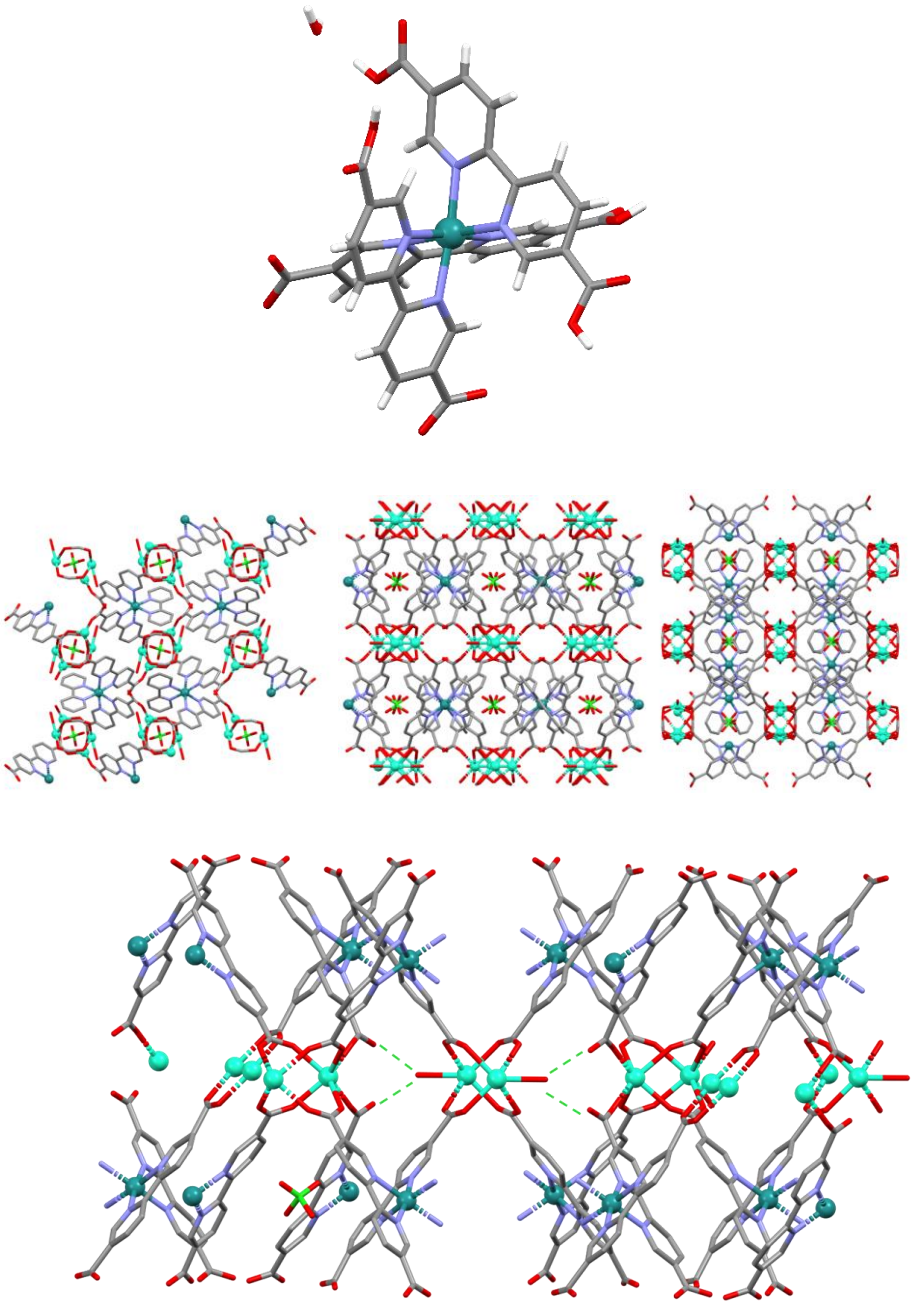

Figure A4.8. View of Ru-metalloligand single crystal (up) and compound **4.6**$_{\text{Ru-Dy}}$ along *a*, *b* and *c* crystallographic axis (middle) and "ABAB..." growing of SBU showing hydrogen bonding interaction (bottom)**.**

A4.10 Scanning Electron Microscopy

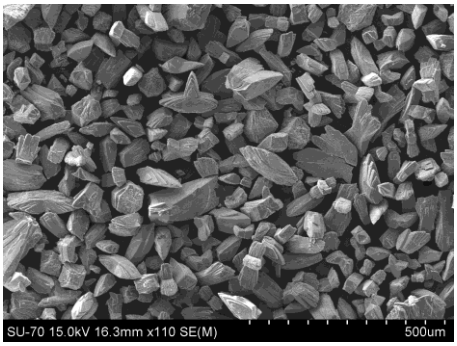

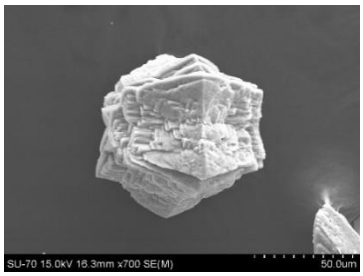

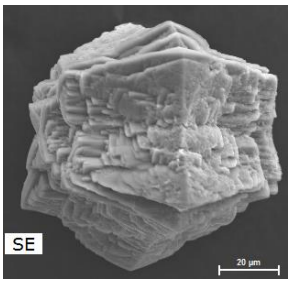

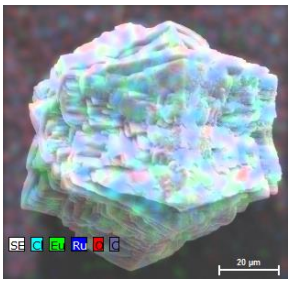

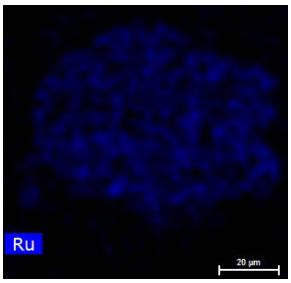

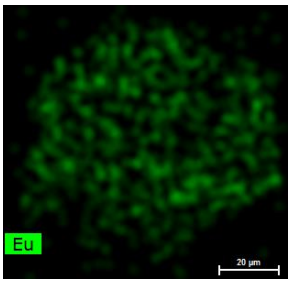

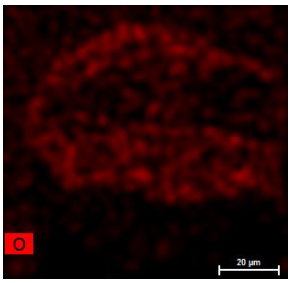

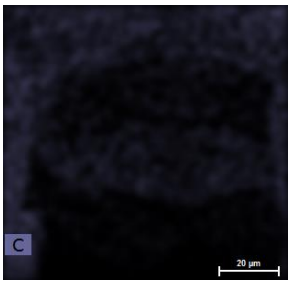

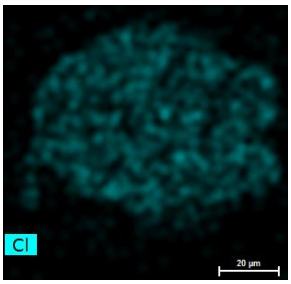

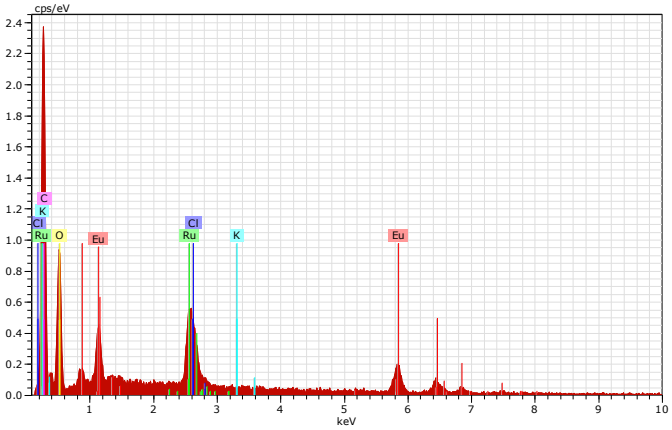

Spectrum: EE756

Element	Series	unn. C [wt.%]	norm. C [wt.%]	Atom. C [at.%]	Error (3 Sigma) [wt.%]
Europium	L-series	19.08	21.06	**2.61**	2.18
Ruthenium	L-series	8.82	9.74	**1.82**	1.10
Chlorine	K-series	2.99	3.30	**1.76**	0.46
Potassium	K-series	0.01	0.01	0.00	0.09
Carbon	K-series	37.53	41.41	**64.98**	16.30
Oxygen	K-series	22.18	24.48	**28.83**	11.04
	Total:	90.61	100.00	100.00	

Figure A4.9. SEM images of compound **4.3$_{Ru-Eu}$**.

A4.11 Extraction and Catalytic Oxidative Desulfurization

Table A4.8. Desulfurization of a multicomponent model diesel catalysed by heterogeneous **4.3$_{Ru-Eu}$** catalyst at three catalytic loadings.

Catalyst loading		**5 mg**		**10 mg**		**20 mg**	
	time/min	**Ppm sum**	**% Desulfuration**	**Ppm sum**	**% Desulfuration**	**Ppm sum**	**% Desulfuration**
Initial extraction	0	2338.84	0	2419.06	0	2419.06	0.00
	10	1101.86	52.89				
	20	1677.28	28.29	1185.87	50.98	1667.69	31.06
	40	935.23	60.01	1080.33	55.34	894.27	63.03
	70	647.09	72.33	992.65	58.97	1654.66	31.60
	130	1028.85	56.01	1504.76	37.80	1631.09	32.57
	190	1423.35	39.14	855.68	64.63	1792.47	25.90
	250	919.27	60.70	891.30	63.16	1094.59	54.75
	310	1391.90	40.49	906.27	62.54	1353.76	44.04

A4.12 Cellular cytotoxicity

Additionally, with this family of compounds cytotoxicity evaluation was performed. For that purpose, Adenocarcinoma cell line (Caco-2) was selected and cell viability assays conducted. This cell line is widely used as model of the intestinal epithelial barrier and is originally derived from a colon carcinoma.[36]

Compounds **4.4** and **4.6** in 1 to 0.8 mg·mL^{-1} MOF concentration were incubated for 72 h with the aforementioned cells and regardless the concentration cell viability do not decreases what confirms the lack of cytotoxicity of the synthesised materials.

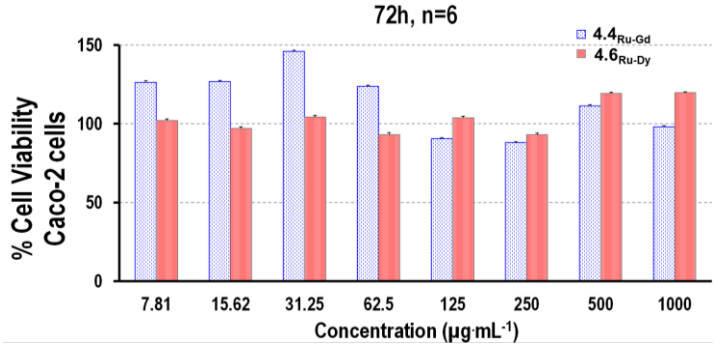

Figure A4.10. The cell viability of Caco-2 cells after being incubated with compounds 4.4 and 4.6 for 72 h at various MOF concentrations.

Subsequently, analogous experiments were conducted with metalloligand and gadolinium and dysprosium metallic salts exhibiting similar behaviour. Results exhibited no toxicity observed in any precursor after 72 h regardless the concentration.

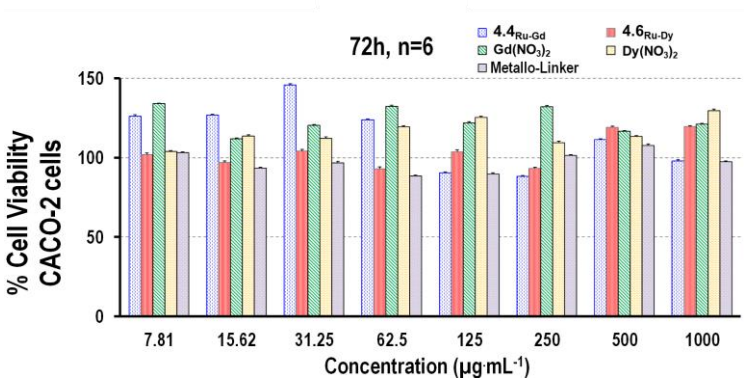

Figure A4.11. The cell viability of Caco-2 cells after being incubated with compounds **4.4** and **4.6** and precursors (metalloligand and metallic salts) for 72 h at various MOF concentrations.

Appendix 5

Supporting information of Chapter 5

A5.1 Experimental section. General instrumentation

Elemental analyses (C, H, N) were performed on a Leco CHNS-932 microanalyser.

IR spectra of the ligand and prepared coordination compound were collected in the region 400-4000 cm^{-1} on a Nicolet 6700 FTIR (Fourier transform infrared) spectrophotometer (Thermo Phisher Scientific, TX, USA) KBr pellets.

Thermogravimetric analysis (TG/DTA) were performed on a TG-Q500 TA Instruments thermal analyser from room temperature to 800 °C under a synthetic air atmosphere (79 % N_2/21 % O_2) at a heating rate of 10 °C min^{-1}.

X-ray powder diffraction (XRPD) patterns were collected at 25 °C on a Phillips X'PERT powder diffractometer with Cu-Kα radiation (λ = 1.5418 Å) over the range 5º < 2θ < 50º with a step size of 0.02º and an acquisition time of 2.5 s per step. Indexation of the diffraction profiles were made by means of the FULLPROF program (pattern- matching analysis) based on the space group and the cell parameters found by single crystal X-ray diffraction.

Magnetic susceptibility measurements were performed on polycrystalline samples of the complexes with a Quantum Design SQUID MPMS-7T susceptometer at an applied magnetic field of 1000 G. The susceptibility data were corrected for diamagnetism estimated from Pascal's tables.[6] the temperature-independent paramagnetism and magnetisation of the sample holder. The ac measurements were performed on a physical property measurement system quantum design model 6000 magnetometer under a 3.5 G ac field and frequencies ranging from 60 to 10000 Hz.

Photoluminescence measurements at low temperature were done in an Edinburgh Instruments FLS920 spectrometer using a close cycle helium cryostat enclosed, in an applied vacuum (10^{-7} bar). For steady state measurements in the UV-Vis range an IK3552R-G HeCd continuous laser (325 nm) was used as excitation source, whereas a Müller-Elektronik-Optik SVX1450 Xe lamp was employed to collect the excitation spectra. LDH-P-C-370 laser diode of PicoQuant was employed for recording the decay curves corresponding to the lifetimes of ns range.

MRI scans were carried out in a preclinical 7-T magnet (Agilent, Palo Alto, CA, USA) interfaced to Avance III electronics, using a quadrature transmit-receive coil (Bruker, Ettlingen, Germany). T_1 values were estimated from images acquired using the rapid acquisition with relaxation enhancement (RARE) sequence with inversion recovery (IT = 50, 200, 400, 800, 1500, 3000, 5500, 8000, 12,000 ms, TE = 7.0 ms, echo train length 2, data matrix size 128 × 64, field of view 30 × 15 mm^2, slice thickness = 3 mm, 1 scan).

A5.2 Chemical characterization

A5.2.1 Elemental Analysis

Table A5.1 Elemental analysis of compound **5.1**-**5.14**.

Compound	Formula	Molecular weight	Calc.	Found.
5.1	$C_{86}H_{72}Cl_{12}Pr_2N_6O_{16}$	2152.8	C: 47.98; H: 3.37; Cl: 19.76; Pr: 13.09; N: 3.90; O: 11.89;	C: 48.01; H: 3.35; Cl: 19.82; Pr: 13.10; N: 3.92; O: 11.90;
5.2	$C_{86}H_{72}Cl_{12}Nd_2N_6O_{16}$	2159.5	C: 47.83; H: 3.36; Cl: 19.70; Nd: 13.36; N: 3.89; O: 11.85;	C: 47.80; H: 3.42; Cl: 19.71; Nd: 13.34; N: 3.94; O: 11.86;
5.3	$C_{86}H_{72}Cl_{12}Sm_2N_6O_{16}$	2171.8	C: 47.56; H: 3.34; Cl: 19.59; Sm: 13.85; N: 3.87; O: 11.79;	C: 47.54; H: 3.32; Cl: 19.62; Sm: 13.82; N: 3.89; O: 11.83;
5.4	$C_{86}H_{72}Cl_{12}Eu_2N_6O_{16}$	2174.9	C: 47.49; H: 3.34; Cl: 19.56; Eu: 13.97; N: 3.86; O: 11.77;	C: 47.49; H: 3.36; Cl: 19.58; Eu: 14.01; N: 3.87; O: 11.78;
5.5	$C_{86}H_{72}Cl_{12}Gd_2N_6O_{16}$	2185.5	C: 47.26; H: 3.32; Cl: 19.47; Gd: 14.39; N: 3.85; O: 11.71;	C: 47.24; H: 3.30; Cl: 19.51; Gd: 14.40; N: 3.86; O: 11.71;
5.6	$C_{86}H_{72}Cl_{12}Tb_2N_6O_{16}$	2188.8	C: 47.19; H: 3.32; Cl: 19.44; Tb: 14.52; N: 3.84; O: 11.70;	C: 47.20; H: 3.35; Cl: 19.46; Tb: 14.50; N: 3.86; O: 11.71;
5.7	$C_{86}H_{72}Cl_{12}Dy_2N_6O_{16}$	2196.0	C: 47.04; H: 3.30; Cl: 19.37; Dy: 14.80; N: 3.83; O: 11.66;	C: 47.14; H: 3.31; Cl: 19.42; Dy: 14.81; N: 3.84; O: 11.68;
5.8	$C_{86}H_{72}Cl_{12}Ho_2N_6O_{16}$	2200.8	C: 46.93; H: 3.30; Cl: 19.33; Ho: 14.99; N: 3.82; O: 11.63;	C: 46.96; H: 3.32; Cl: 19.42; Ho: 14.98; N: 3.81; O: 11.62;
5.9	$C_{86}H_{72}Cl_{12}Er_2N_6O_{16}$	2205.5	C: 46.83; H: 3.29; Cl: 19.29; Er: 15.17; N: 3.81; O: 11.61;	C: 46.86; H: 3.31; Cl: 19.26; Er: 15.22; N: 3.81; O: 11.66;
5.10	$C_{86}H_{72}Cl_{12}Tm_2N_6O_{16}$	2208.9	C: 46.76; H: 3.29; Cl: 19.26; Tm: 15.30; N: 3.80; O: 11.59;	C: 46.82; H: 3.30; Cl: 19.26; Tm: 15.31; N: 3.85; O: 11.62;
5.11	$C_{86}H_{72}Cl_{12}Yb_2N_6O_{16}$	2217.1	C: 46.59; H: 3.27; Cl: 19.19; Yb: 15.61; N: 3.79; O: 11.55;	C: 46.63; H: 3.32; Cl: 19.22; Yb: 15.60; N: 3.82; O: 11.54;
5.12	$C_{88}H_{76}Cl_{12}Gd_2N_6O_{16}$	2213.4	C: 47.75; H: 3.46; Cl: 19.22; Gd: 14.21; N: 3.80; O: 11.56;	C: 47.76; H: 3.49; Cl: 19.26; Gd: 14.25; N: 3.84; O: 11.63;
5.13	$C_{84}H_{74}Cl_{12}Gd_2N_6O_{16}$	2163.5	C: 46.63; H: 3.45; Cl: 19.66; Gd: 14.54; N: 3.88; O: 11.83;	C: 46.68; H: 3.45; Cl: 19.65; Gd: 14.55; N: 3.88; O: 11.81;
5.14	$C_{80}H_{160}Cl_4Fe_2N_{32}O_{48}$	2591.9	C: 37.07; H: 6.22; Cl: 5.47; Fe: 4.31; N: 17.29; O: 29.63;	C: 37.10; H: 6.25; Cl: 5.49; Fe: 4.33; N: 17.30; O: 29.63;

A5.2.2 FT-IR spectroscopy

Derived by their isostructural nature, compounds **5.1**-**5.11** display very similar FT-IR spectra, that is **5.5$_{Gd}$** was selected as representative material and compare it with the rest gadolinium-based counterparts, **5.12** and **5.13** materials. When examining FT-IR spectrum in detail from higher to smaller frequency, compound **5.11-5.13** display a narrow peak (not clearly visible in all compounds spectra) at around 3653 cm^{-1} attributed to the N-H stretching vibration of amine group. which is practically hided below the intense broad band around 3404 cm^{-1} attributed to O–H bond vibration corresponding to the carboxylate group of the of diclofenac free ligand. At lower frequency, a set of sharp and of medium intensity bands that corresponds to aromatic ring's C–H bond vibrations of the ligand are visible between 3373 cm^{-1} and 3289 cm^{-1}. The following intense vibrations located in 1589–1442 cm^{-1} region are attributed to both the asymmetric stretching vibrations of the carboxylate groups and the aromatic C–C bonds. Moving to lower range of 1373–1268 cm^{-1} symmetric stretching vibrations of the carboxylate groups appear in the spectrum. The remaining bands that are found at lower frequency can be attributed to the distortions originated in the aromatic ring and the carboxylate groups of the ligands.

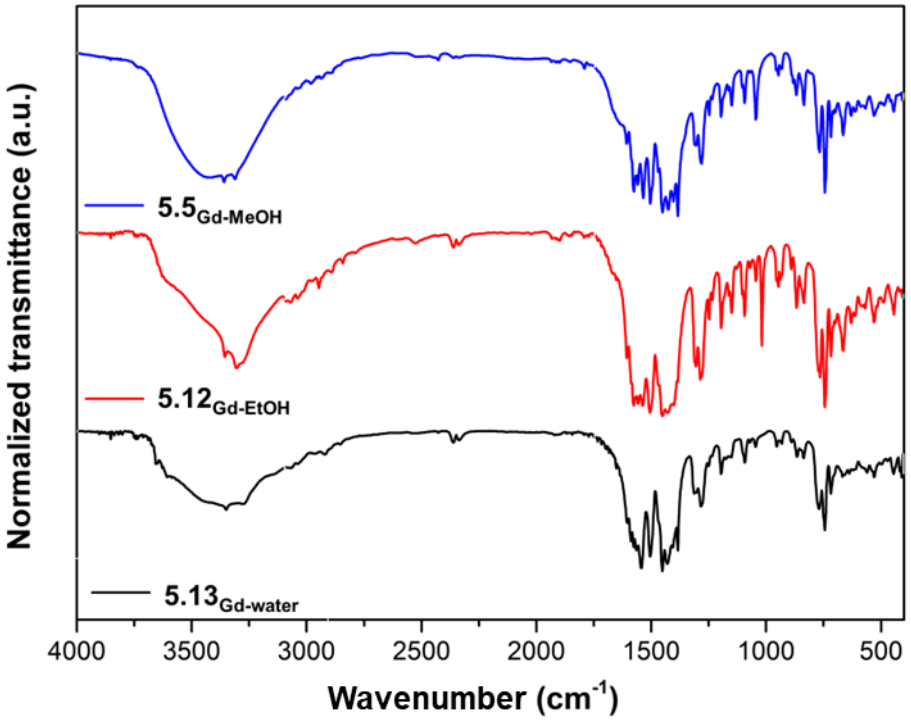

Figure A5.1. Infrared spectra of the ligand and compound **5.5** and **5.12-5.13.**

A5.3 Crystallographic data

Table A5.2. Crystallographic data and structure refinement details of compound **5.7**, **5.12** and **5.14**.

Compound	**5.7_{Dy}**	**$5.12_{Gd\text{-}EtOH}$**	**5.14_{Fe}**
Formula	$C_{86}H_{72}Cl_{12}Dy_2N_6O_{16}$	$C_{88}H_{76}Cl_{12}Gd_2N_6O_{16}$	$C_{80}H_{160}Cl_4Fe_2N_{32}O_{48}$
M_r	2195.9	2213.4	2591.89
Crystal system	monoclinic	Monoclinic	Triclinic
Space group (no.)	$P2_1/c$	$P2_1/c$	P-1
a(Å)	9.7378(5)	9.7965(18)	15.800
b(Å)	33.4196(17)	33.592(6)	17.792
c(Å)	13.9653(6)	14.138(3)	23.245
α(°)	90	90	82.07
β(°)	105.6090(10)	105.968(3)	83.95
γ(°)	90	90	83.64
V(Å^3)	4377.2(4)	4473.1(14)	6454.7
Z	2	2	2
ρ_{calc} g/cm^3	1.666	1.643	1.334
μ/mm^{-1}	2.130	1.897	0.400
F(000)	2188.0	2212.0	2736.0
Crystal size/mm^3	0.24 × 0.15 × 0.13	0.21 × 0.16 × 0.14	0.18 × 0.13 × 0.09
Radiation	MoKα (λ = 0.71073)	MoKα (λ = 0.71073)	MoKα (λ = 0.71073)
2θ range for data collection/°	4.51 to 57.632	2.424 to 47.666	4.434 to 58.022
Index ranges	-13 ≤ h ≤ 13, -45 ≤ k ≤ 45, -18 ≤ l ≤ 16	-10 ≤ h ≤ 11, -38 ≤ k ≤ 29, -15 ≤ l ≤ 13	-21 ≤ h ≤ 20, -24 ≤ k ≤ 24, -31 ≤ l ≤ 31
Reflections collected	105775	21339	203609
Independent reflections	11357 [R_{int} = 0.1950, R_{sigma} = 0.1366]	6764 [R_{int} = 0.0853, R_{sigma} = 0.0941]	32160 [R_{int} = 0.0962. R_{sigma} = 0.0745]
Data/restraints/parameters	11357/0/551	6764/6/560	32160/0/1408
Goodness-of-fit on F^2	1.064	1.033	0.975
Final R indexes [I>=2σ (I)]	R_1 = 0.0655, wR_2 = 0.0654	R_1 = 0.0518, wR_2 = 0.1079	R_1 = 0.1065, wR_2 = 0.2750
Final R indexes [all data]	R_1 = 0.1350, wR_2 = 0.0768	R_1 = 0.0755, wR_2 = 0.1240	R_1 = 0.1762, wR_2 = 0.3349
Largest diff. peak/hole / e Å^{-3}	1.02/-1.54	1.33/-1.49	2.87/-2.04

Table A5.3. Table of the selected bond lengths (Å) for compound **5.7, 5.12** and **5.14.**

5.7_{Dy}			**$5.12_{Gd\text{-}EtOH}$**			**5.14_{Fe}**		
Atom	**Atom**	**Length/Å**	**Atom**	**Atom**	**Length/Å**	**Atom**	**Atom**	**Length/Å**
Dy1	O1B	2.451(3)	Gd1	O2C	2.366(4)	Fe1	O1G	1.908(4)
Dy1	O1C	2.442(3)	Gd1	O2C1	2.564(4)	Fe1	O1E	2.027(4)
Dy1	O2A	2.429(3)	Gd1	O1A	2.438(4)	Fe1	O1B	2.009(5)
Dy1	O2B	2.490(3)	Gd1	O1B	2.462(4)	Fe1	O1C1	2.002(5)
Dy1	O1A	2.413(3)	Gd1	O1C1	2.466(5)	Fe1	O1A	2.015(5)
Dy1	O1M	2.375(3)	Gd1	O1E	2.395(4)	Fe1	O1H	2.074(4)
Dy1	O1W	2.362(3)	Gd1	O2B	2.520(4)	Fe2	O2E	2.041(4)
Dy1	O2C	2.549(3)	Gd1	O2A	2.464(4)	Fe2	O1G	1.890(5)
Dy1	O2C1	2.327(3)	Gd1	O1W	2.392(4)	Fe2	O1G1	2.071(5)
O2C	Dy11	2.327(3)	O2C	Gd11	2.564(4)	Fe2	O1D	2.022(5)
11-x,-y,-z			O1C	Gd11	2.466(5)	Fe2	O1F	2.011(5)
			1-1-x,-y,1-z			Fe2	O2A	2.030(5)
						Fe3	O1G	1.936(5)
						Fe3	O2D	1.999(7)
						Fe3	O2F	2.033(5)
						Fe3	O1I	2.077(6)
						Fe3	O2B	2.021(5)
						Fe3	O2C	2.008(6)

Table A5.4. Table of the selected angles (º) for compound **5.7**, **5.12** and **5.14.**

5.7_{Dy}				**$5.12_{Gd\text{-}EtOH}$**				**5.14_{Fe}**			
Atom	**Atom**	**Atom**	**Angle/˚**	**Atom**	**Atom**	**Atom**	**Angle/˚**	**Atom**	**Atom**	**Atom**	**Angle/°**
O1B	Dy1	O2B	52.86(10)	O2C	Gd1	O2C^{1}	67.54(17)	O1G	Fe1	O1E	92.44(18)
O1B	Dy1	O2C	90.63(10)	O2C	Gd1	O1A	105.22(15)	O1G	Fe1	O1B	93.61(19)
O1C	Dy1	O1B	71.74(11)	O2C	Gd1	O1B	128.50(15)	O1G	Fe1	O1C1	98.5(2)
O1C	Dy1	O2B	99.99(11)	O2C	Gd1	O1C^{1}	116.30(15)	O1G	Fe1	O1A	95.32(19)
O1C	Dy1	O2C	51.87(10)	O2C	Gd1	O1E	75.12(15)	O1G	Fe1	O1H	179.0(2)
O2A	Dy1	O1B	122.16(10)	O2C	Gd1	O2B	76.68(15)	O1E	Fe1	O1H	87.63(18)
O2A	Dy1	O1C	142.15(10)	O2C	Gd1	O2A	83.33(15)	O1B	Fe1	O1E	172.80(19)
O2A	Dy1	O2B	116.46(11)	O2C	Gd1	O1W	154.29(15)	O1B	Fe1	O1A	91.2(2)
O2A	Dy1	O2C	145.89(10)	O1A	Gd1	O2C^{1}	149.42(15)	O1B	Fe1	O1H	86.39(18)
O2B	Dy1	O2C	74.15(10)	O1A	Gd1	O1B	71.39(15)	O1C1	Fe1	O1E	84.34(19)
O1A	Dy1	O1B	71.04(10)	O1A	Gd1	O1C^{1}	136.26(15)	O1C1	Fe1	O1B	90.9(2)
O1A	Dy1	O1C	136.94(11)	O1A	Gd1	O2B	74.47(15)	O1C1	Fe1	O1A	165.80(19)
O1A	Dy1	O2A	53.70(11)	O1A	Gd1	O2A	53.69(15)	O1C1	Fe1	O1H	82.43(18)
O1A	Dy1	O2B	73.60(11)	O1B	Gd1	O2C^{1}	89.75(15)	O1A	Fe1	O1E	92.08(19)
O1A	Dy1	O2C	147.71(10)	O1B	Gd1	O1C^{1}	72.35(15)	O1A	Fe1	O1H	83.70(17)
O1M	Dy1	O1B	147.21(10)	O1B	Gd1	O2B	52.44(14)	O2E	Fe2	O1G1	83.86(19)
O1M	Dy1	O1C	77.53(11)	O1B	Gd1	O2A	123.12(16)	O1G	Fe2	O2E	94.63(18)
O1M	Dy1	O2A	77.21(11)	O1C^{1}	Gd1	O2C^{1}	51.57(14)	O1G	Fe2	O1G1	178.0(2)
O1M	Dy1	O2B	146.88(10)	O1C^{1}	Gd1	O2B	101.44(15)	O1G	Fe2	O1D	96.2(2)
O1M	Dy1	O1A	130.23(11)	O1E	Gd1	O2C^{1}	77.56(14)	O1G	Fe2	O1F	94.1(2)
O1M	Dy1	O2C	79.00(10)	O1E	Gd1	O1A	130.88(15)	O1G	Fe2	O2A	94.7(2)
O1W	Dy1	O1B	77.62(10)	O1E	Gd1	O1B	146.42(16)	O1D	Fe2	O2E	169.0(2)
O1W	Dy1	O1C	72.93(10)	O1E	Gd1	O1C^{1}	75.48(15)	O1D	Fe2	O1G1	85.4(2)
O1W	Dy1	O2A	76.32(10)	O1E	Gd1	O2B	146.35(15)	O1D	Fe2	O2A	87.2(2)
O1W	Dy1	O2B	128.64(11)	O1E	Gd1	O2A	78.22(15)	O1F	Fe2	O2E	86.9(2)
O1W	Dy1	O1A	78.63(11)	O2B	Gd1	O2C^{1}	74.96(14)	O1F	Fe2	O1G1	84.5(2)
O1W	Dy1	O1M	82.77(10)	O2A	Gd1	O2C^{1}	145.95(14)	O1F	Fe2	O1D	94.1(2)
O1W	Dy1	O2C	124.28(10)	O2A	Gd1	O1C^{1}	141.05(15)	O1F	Fe2	O2A	170.9(2)
O2C1	Dy1	O1B	128.13(10)	O2A	Gd1	O2B	116.23(15)	O2A	Fe2	O2E	90.15(19)
O2C1	Dy1	O1C	117.04(11)	O1W	Gd1	O2C^{1}	122.93(15)	O2A	Fe2	O1G1	86.6(2)
O2C1	Dy1	O2A	83.42(10)	O1W	Gd1	O1A	77.02(15)	O1G	Fe3	O2D	95.2(2)
O2C1	Dy1	O2B	75.65(10)	O1W	Gd1	O1B	76.89(15)	O1G	Fe3	O2F	95.3(2)
O2C1	Dy1	O1A	102.79(11)	O1W	Gd1	O1C^{1}	71.64(15)	O1G	Fe3	O1I	176.2(2)
O2C1	Dy1	O1M	76.36(10)	O1W	Gd1	O1E	84.15(15)	O1G	Fe3	O2B	92.5(2)
O2C1	Dy1	O1W	153.63(10)	O1W	Gd1	O2B	127.39(14)	O1G	Fe3	O2C	94.6(2)
O2C1	Dy1	O2C	67.38(11)	O1W	Gd1	O2A	77.59(15)	O2D	Fe3	O2F	89.0(3)

Dy1[1]	O2C	Dy1	112.62(11)	Gd1	O2C	Gd1[1]	112.46(17)	O2D	Fe3	O1I	87.6(3)
[1]1-x,-y,-z				[1]-1-x,-y,1-z				O2D	Fe3	O2B	85.6(2)
								O2D	Fe3	O2C	170.1(2)
								O2F	Fe3	O1I	87.3(2)
								O2B	Fe3	O2F	170.8(2)
								O2B	Fe3	O1I	85.1(2)
								O2C	Fe3	O2F	88.3(3)
								O2C	Fe3	O1I	82.8(3)
								O2C	Fe3	O2B	95.8(3)
								Fe1	O1G	Fe3	119.1(2)
								Fe2	O1G	Fe1	120.7(2)
								Fe2	O1G	Fe3	120.2(2)

Table A5.5. Structural parameters of hydrogen bonds (Å. °) in compound **5.7$_{Dy}$.**[a]

D–H···A[b]	***D–H***	***H···A***	***D···A***	***D–H···A***
O1w–H1wa···O1A(i)	0.85	2.02	2.830(5)	159.7
O1w–H1wb···O1B(i)	0.85	1.99	2.743(4)	145.7

[a]Symmetry codes: (i) –x. –y. –z. [b]D: donor. A: acceptor

.

A5.4 Powder X-ray diffraction analysis

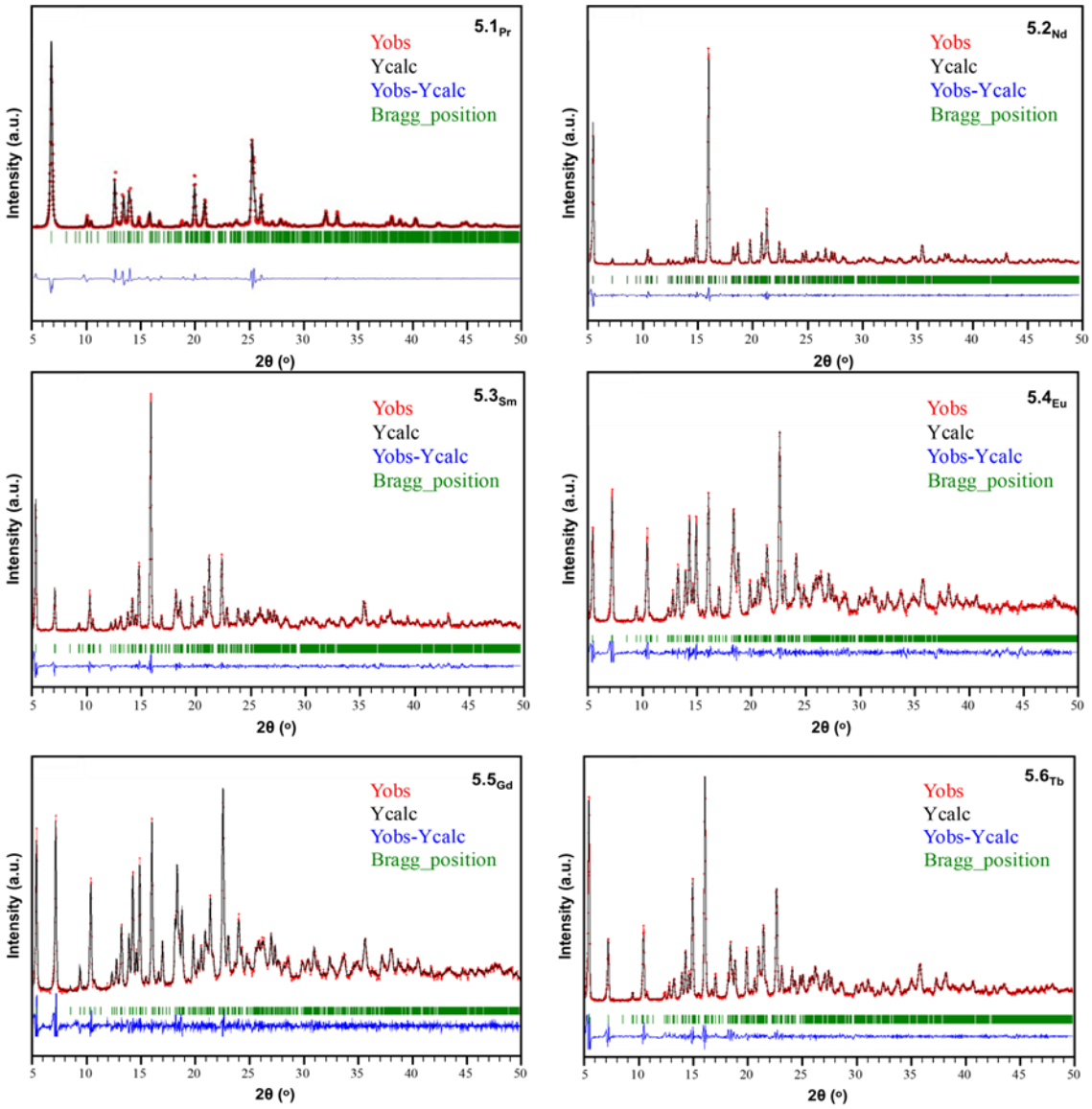

Figure A5.2. Figure of the pattern matching analysis and experimental PXRD for complexes **5.1**-**5.6**.

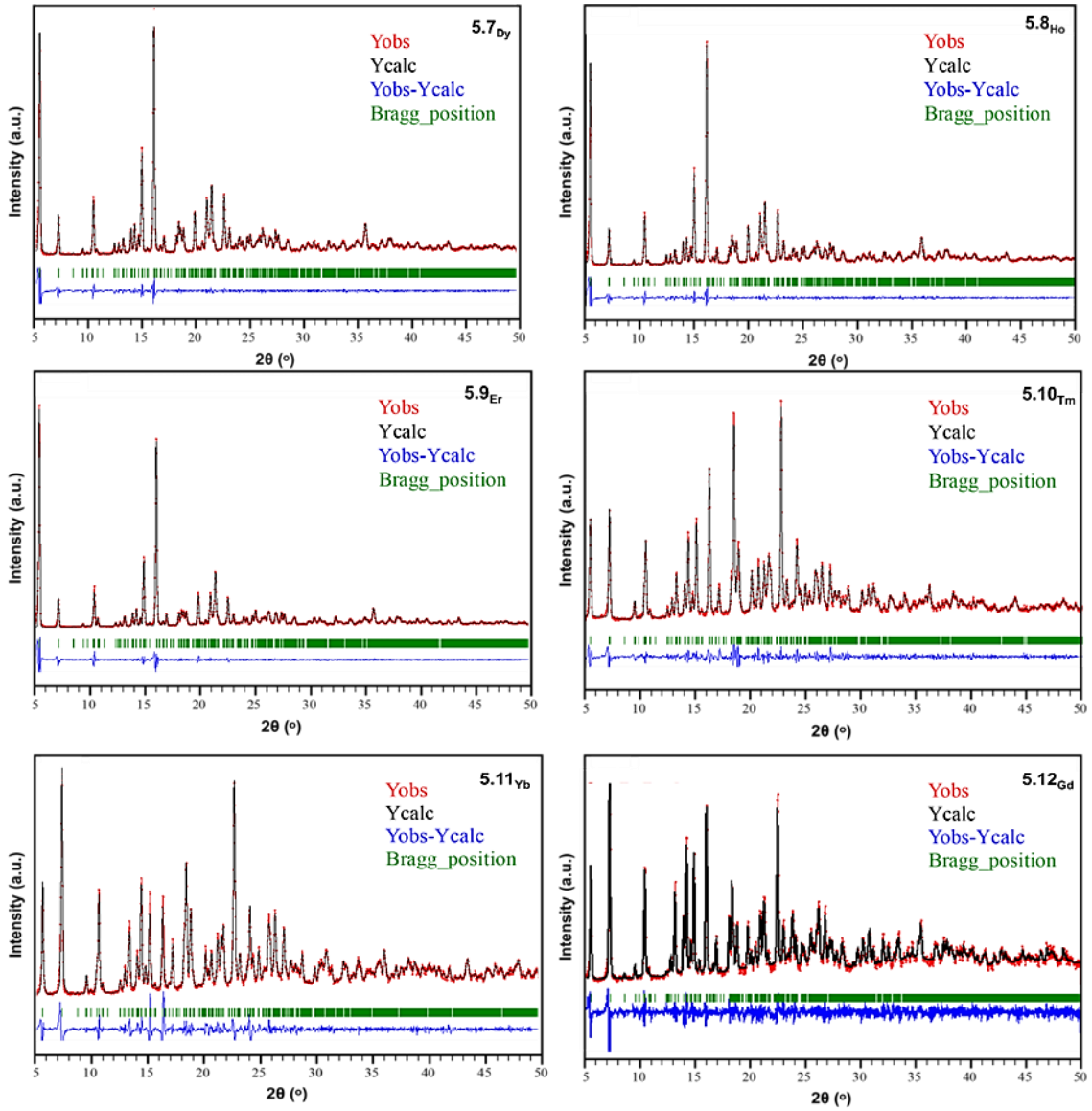

Figure A5.3. Figure of the pattern matching analysis and experimental PXRD for complexes **5.7**-**5.12**.

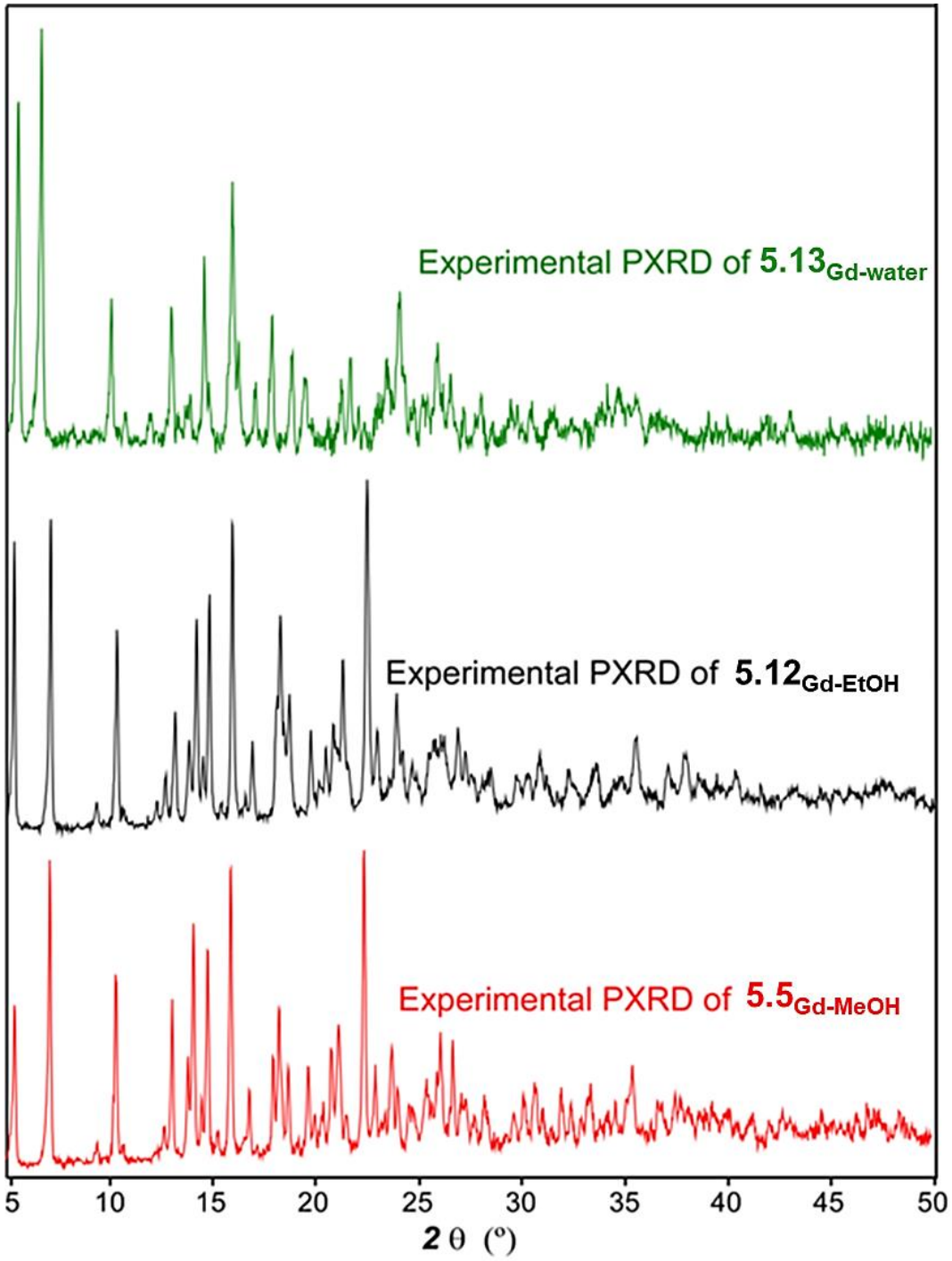

Figure A5.4. Figure of the pattern matching analysis and experimental PXRD for gadolinium-based complexes **5.5** and **5.12-5.13**.

A5.5 Continuous Shape Measurements

CShMs for the coordination environment of **5.7$_{Dy}$**, **5.12$_{Gd\text{-}EtOH}$** and **5.14$_{Fe}$**. The lowest SHAPE values for each ion are shown highlighted in grey, indicating best fits.

Table A5.6. Table of the continuous Shape Measurements for the LnO_9 coordination environment.

EP-9	D_{9h}	Enneagon
OPY-9	C_{8v}	Octagonal pyramid
HBPY-9	D_{7h}	Heptagonal bipyramid
JTC-9	C_{3v}	Johnson triangular cupola J3
JCCU-9	C_{4v}	Capped cube J8
CCU-9	C_{4v}	Spherical-relaxed capped cube
JCSAPR-9	C_{4v}	Capped square antiprism J10
CSAPR-9	C_{4v}	Spherical capped square antiprism
JTCTPR-9	D_{3h}	Tricapped trigonal prism J51
TCTPR-9	D_{3h}	Spherical tricapped trigonal prism
JTDIC-9	C_{3v}	Tridiminished icosahedron J63
HH-9	C_{2v}	Hula-hoop
MFF-9	C_s	Muffin

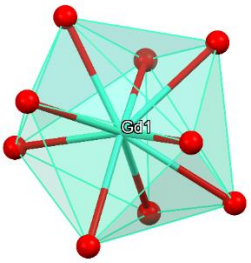

Compound	JCSAPR-9	CSAPR-9	TCTPR-9	MFF-9
5.7$_{Dy}$	3.594	2.497	2.653	**2.228**
5.12$_{Gd\text{-}EtOH}$	3.577	2.526	2.591	**2.423**

Table A5.7. Table of the continuous Shape Measurements for the FeO_6 coordination environment.

HP-6	D_{6h}	Hexagon
PPY-6	C_{5v}	Pentagonal pyramid
OC-6	O_h	Octahedron
TPR-6	D_{3h}	Trigonal prism
JPPY-6	C_{5v}	Johnson pentagonal pyramid J2

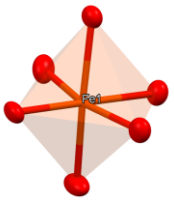

Compound	HP-6	PPY-6	OC-6	TPR-6	JPPY-6
5.14$_{Fe}$	32.208	27.451	**0.279**	14.722	31.232

A5.6 Thermal analysis

Thermogravimetric analyses have been performed over polycrystalline sample in compounds **5.5, 5.12-5.13** in order to check the stability of the products. The TG curves show three main steps of weight loses. The first steps concern to the release of coordinated solvent molecules which are released from room temperature up to 160 ºC. The second step refers to the decomposition of the ligands which involves the collapse of the crystal structure, evolving to Gd_2O_3 obtained at 800 ºC as the final residue.

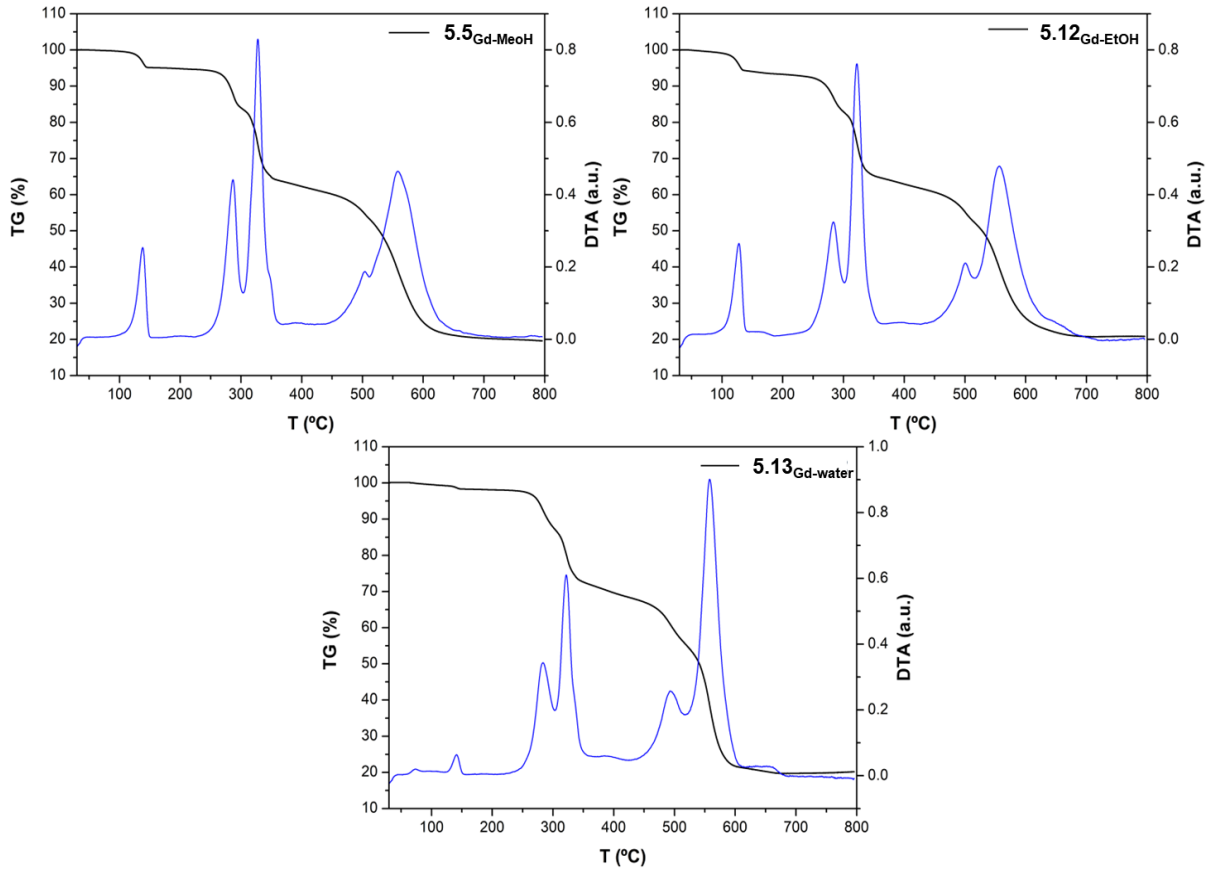

Figure A5.5. Figure of TG analysis of compound **5.5**$_{Gd\text{-}MeOH}$, **5.12**$_{Gd\text{-}EtOH}$ and **5.13**$_{Gd\text{-}water}$.

A5.7 Additional views of the structure

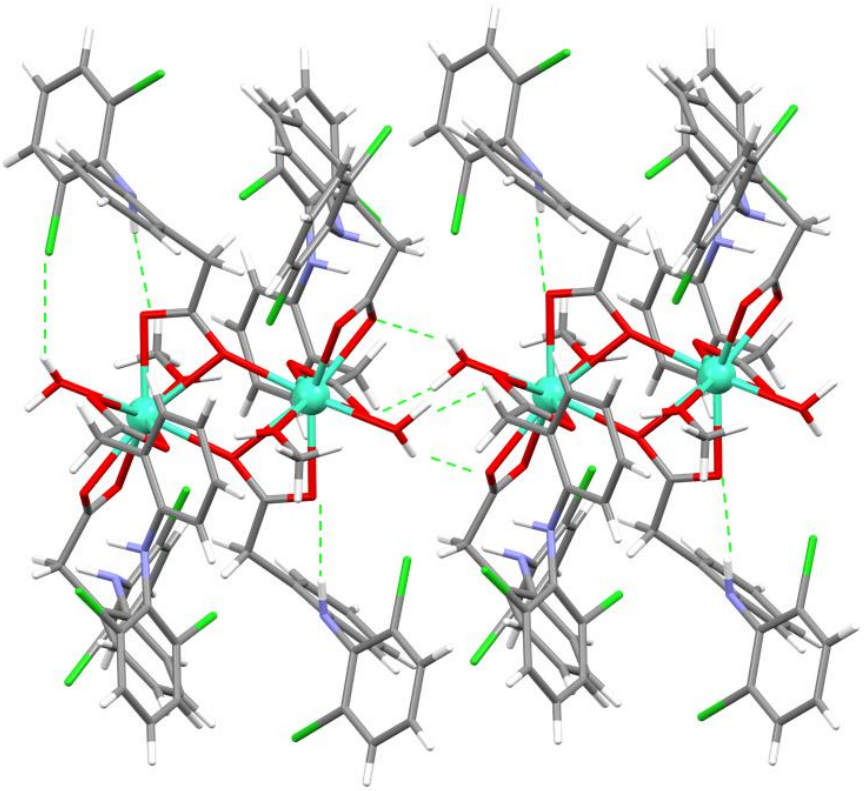

Figure A5.6. Most representative intermolecular interactions: H bonds found in compound **5.6$_{Dy}$** are highlighted in green.

A5.8 Magnetic properties

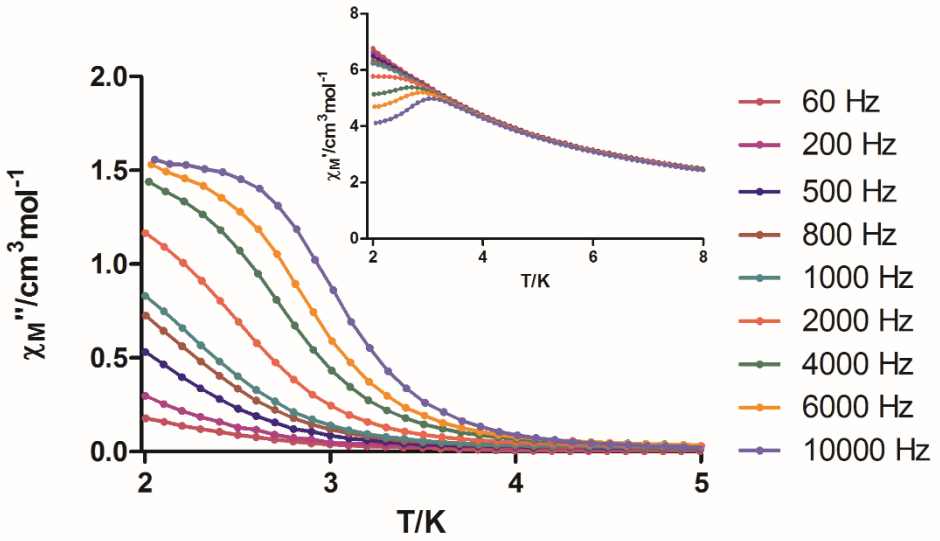

Figure A5.7. Temperature dependence of out-of-phase components of the ac susceptibility in a dc applied field of 1000 Oe for **5.7**$_{Dy}$.

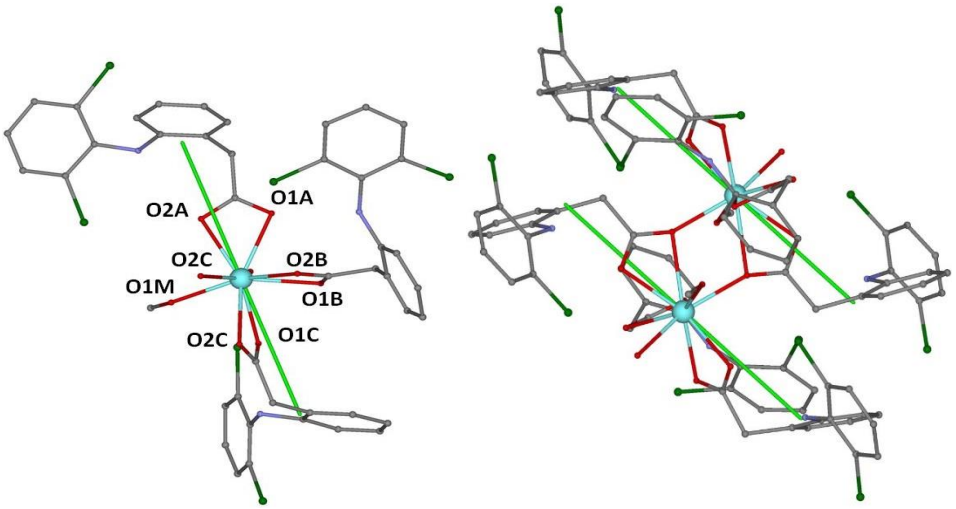

Figure A5.8. Theoretical orientation of the magnetic moments (green line) for Dy^{3+} ions in **5.7**$_{Dy}$. Left the asymmetric unit, in right the coordination compound.

A5.9 Photoluminescent properties

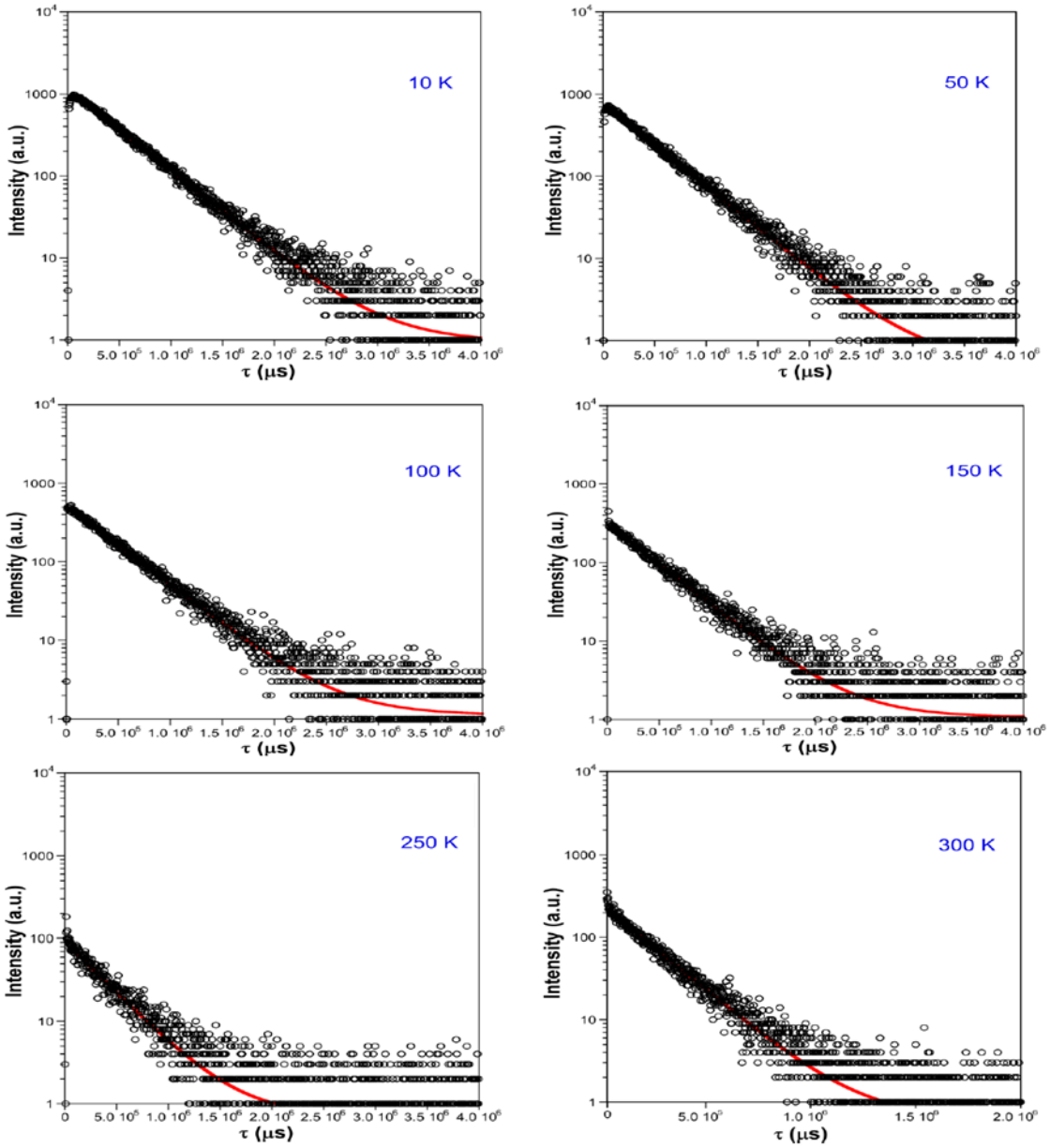

Figure A5.9. $^5D_0$ decay curves monitoring the emissions at 619 nm with the excitations selected at 325 nm, respectively for **5.4$_{Eu}$** at various temperatures; the solid red lines are the best fits using first-order decay functions, $y = y_0 + A_1 \cdot \exp(-x/\boldsymbol{\tau_1})$.

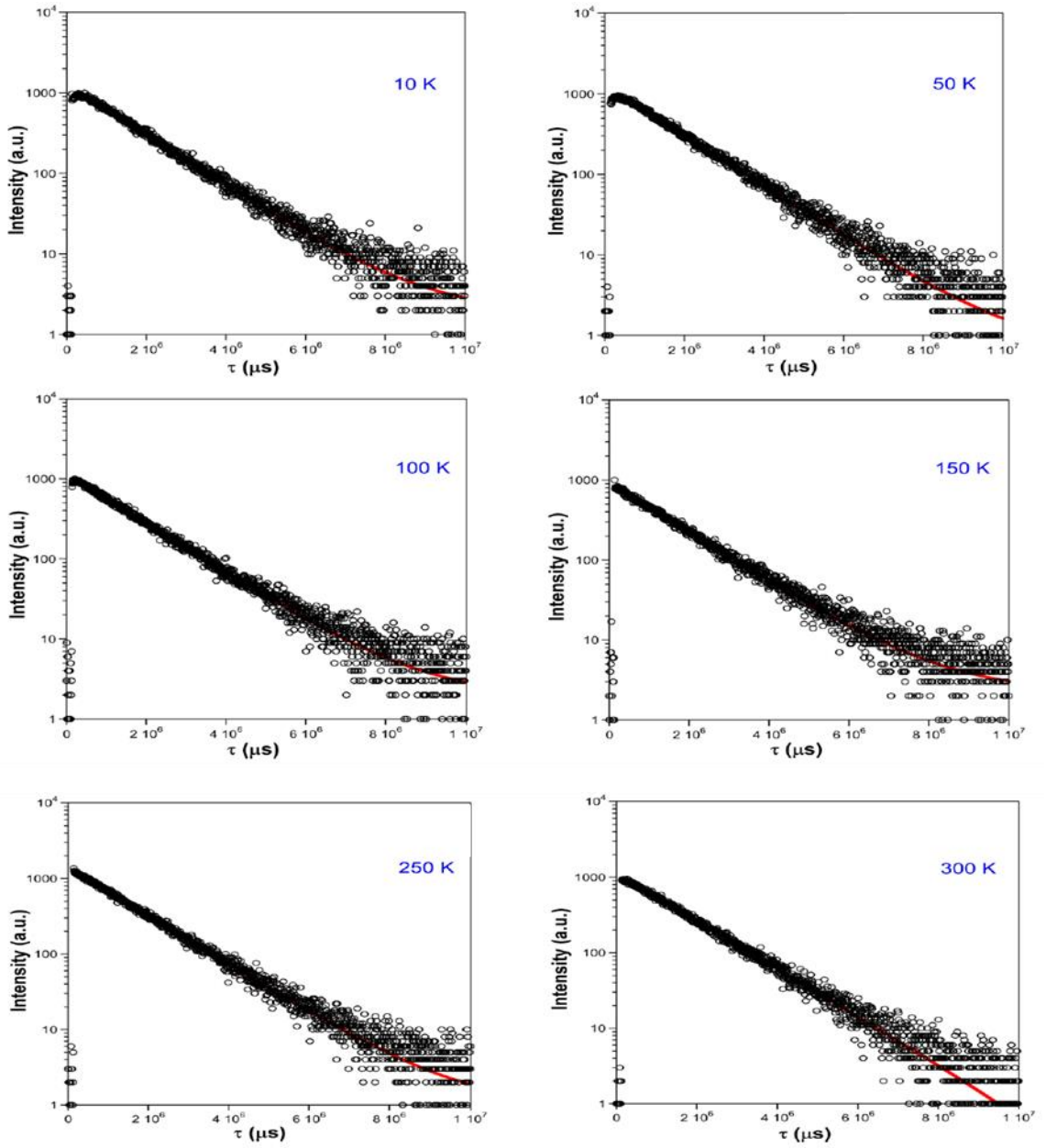

Figure A5.10. $^5D_4$ decay curves monitoring the emissions at 546 nm with the excitations selected at 325 nm, respectively for **5.6$_{Tb}$** at various temperatures; the solid red lines are the best fits using first-order decay functions, $y = y_0 + A_1 \cdot \exp(-x/\boldsymbol{\tau_1})$.

A5.10 TD-DFT calculations

Table A5.8. Calculated main excitation energies (nm) and singlet electronic transitions and associated oscillator strengths of diclofenac molecule in gas phase.

Calcd. λ (nm)	Exp. λ (nm)	Significant contributions	Osc. strength (a.u.)
213	220	HOMO – 6 → LUMO (32%) HOMO – 3 → LUMO + 4 (51%) HOMO – 4 → LUMO + 3 (8%)	0.1681
221	220	HOMO – 6 → LUMO (23%) HOMO – 5 → LUMO + 1 (47%) HOMO – 3 → LUMO + 4 (22%)	0.0538
310	330	HOMO – 3 → LUMO + 1 (91%) HOMO – 2 → LUMO + 4 (4%)	0.1303
321	330	HOMO – 2 → LUMO + 3 (82%) HOMO – 3 → LUMO + 1 (4%) HOMO – 2 → LUMO + 4 (3%)	0.0407

Table A5.9. Calculated main emission energies (nm) and singlet electronic transitions and associated oscillator strengths of diclofenac molecule in gas phase.

Calcd. λ (nm)	Exp. λ (nm)	Significant contributions	Osc. strength (a.u.)
370	386	HOMO – 3 ← LUMO + 1 (96%)	0.0844
365	386	HOMO – 3 ← LUMO + 1 (96%)	0.0681
486	462	HOMO – 2 ← LUMO + 1 (94%) HOMO ← LUMO + 2 (5%)	0.0099

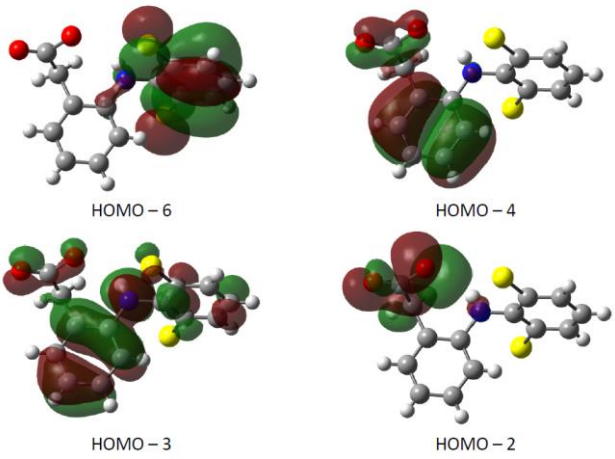

Figure A5.11. Highly Occupied Molecular Orbitals of diclofenac molecule involved in the singlet excitation transitions.

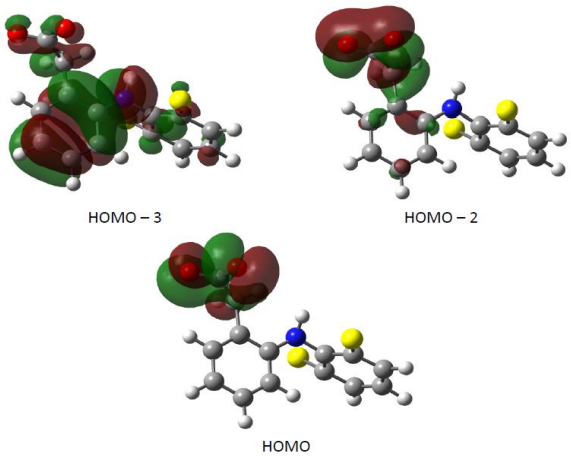

Figure A5.12. Highly Occupied Molecular Orbitals of diclofenac molecule involved in the singlet emission transitions.

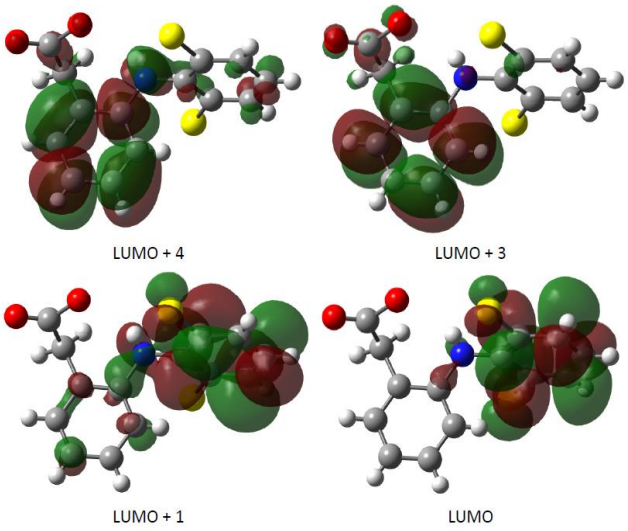

Figure A5.13. Lowest Unoccupied Molecular Orbitals of diclofenac molecule involved in the singlet excitation transitions.

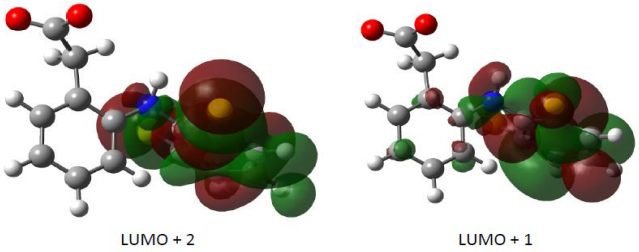

Figure A5.14. Lowest Unoccupied Molecular Orbitals of diclofenac molecule involved in the singlet emission transitions**.**

A5.11 Encapsulation in liposomes and characterization

Physical-chemical characterization was performed by dynamic light scattering (DLS) and the determination of metal content using inductively coupled plasma mass spectrometer (ICP-MS).

A5.11.1 Liposomes characterization: DLS and Z potential

Table A5.10. Characterization of liposomes.

Parameter	Gd-liposomes	Eu-liposomes	Fe-liposomes
Z potential (±SD) /mV	3.27 ± 5.90	3.17 ± 5.29	6.20 ± 6.14
Polydispersity index (±SD) /nm	0.177	0.192	0.091
Size distribution–Intensity (±SD) /nm	119.4 ± 34.7	130.5 ± 47.7	122.0 ± 38.8
Size distribution–Volume (±SD) /nm	103.9 ± 34.6	108.7 ± 47.3	104.0 ± 38.2
Size distribution–Number (±SD) /nm	83.2 ± 22.9	81.5 ± 23.2	78.1 ± 24.5

A5.11.2 Quantification of metal content by ICP-MS

Table A5.11. Metal content determined by ICP-MS.

Liposomes	Gd content in mgL^{-1}	Eu content in mgL^{-1}	Fe content in mgL^{-1}
	0.00001 (1.70 mM)	0.00001 (1.70 mM)	0.003 (169.6 mM)

A5.11.3 Determination of phosphates by Rouser method

Rouser method was applied to determine the lipid concentration transformed into liposomes from the initial phosphate concentration. For that purpose, phosphate free buffers were required for lipid rehydration process. In view of the synthetic problems encountered when directly rehydrating liposomes with HEPES or HPLC water, we decided to rehydrate with PBS and subsequently exchange solvent by washing several times with phosphate-free buffers. Additionally, as reference material we performed the same procedure with PBS buffer and exchange it with HEPES and HPLC water.

Table A5.12. Phosphate concentration in mM for Gd, Eu and Fe liposomes after being rehydrated with PBS and solvent exchange procedure was performed for liposomes and the buffer. Exhibited results are averages of the triplicated data.

Phosphate concentration/ mM	Gd-liposomes	Fe-liposomes
HEPES blank	2.30	3.90
$Liposomes_{HEPES}$	65.03	50.03
HPLC water blank	2.77	3.60
$Liposomes_{HPLC}$	50.39	59.80

In view of the obtained results, it can be concluded that the approach to exchange liposome's rehydration solvent by centrifugation was efficient and we successfully performed it, since as it is summarized in Table A5.9 the phosphate concentration in reference or blank material was practically negligible.

Appendix 6

Supporting information of Chapter 6.A1

A6.1 Experimental section. General instrumentation

Elemental analyses (EA) of synthetized novel catalyst compound **Y/Eu-MOF** performed on an Elementar vario EL cube in the CHN mode.

IR (ATR) spectra of 3-amino-4-hydroxybenzoic acid ligand and compound **Y/Eu-MOF** collected in the region 400–4000 cm^{-1} on a Nicolet 6700 FTIR (Fourier transform infrared) spectrophotometer (Thermo Phisher Scientific, TX, USA) KBr pellets.

NMR measurements: NMR spectra were measured in a Bruker Avance III 300 spectrometer equipped with a direct double SmartProbe BBFO 1H/BB(19F) probe. Chemical shifts are reported in parts per million (ppm) relative to residual solvent peak ($CDCl_3$, ^1H: 7.26 ppm; 13C: 77.16 ppm). Coupling constants are reported in Hertz. Multiplicity is reported with the usual abbreviations (s: singlet, bs: broad singlet, d: doublet, dd: doublet of doublets, ddd: doublet of doublet of doublets, t: triplet, td: triplet of doublets, q: quartet, dq: doublet of quartet, p: pentet, sex: sextet, hept: heptet, m: multiplet). Quantitative NMR acquisition parameters. ^1H NMR determination of product conversion was carried out by comparing signals arising from both CH of aldehyde or CH_3 of ketone **1** and products **2**, **3** or **4**. The standard acquisition parameters were one-dimensional pulse sequence which includes a 30º flip angle (Bruker zg30), recycle time (D1 = 30 s), time domain (TD = 27k), number of scans (NS = 32), acquisition time (AQ = 2.05 s), transmitter (frequency) offset (O1P = 6.0 ppm), and spectral width (SW = 22.0 ppm).

ICP-AES analysis of catalyst $\mathbf{6.1_{Y\text{-}Eu}}$ was conducted in Horiba Yobin Yvon Activa atomic emission spectrometer equipped with a glass and Teflon nebulizer system, which enables samples from acidic digestion to be determined using HF. This equipment also provides the option of coupling a hydride generation system which enables elements such as As, Hg and Sb,.etc. to be determined, in very low levels of concentration (ppb). The equipment is controlled by a control computer with Activa Analyst 5.4 software, which enables it to interact with the equipment at all times. It permits sequential multi-elemental analysis and also enables numerous analytical requirements to be met due to the large linear interval that characterizes this technique, which in turn facilitates the analysis of majority and minority elements.

SEM-EDX, Scanning Electron Microscopy (SEM Leo 1430 VP) with microanalysis of elements (EDX): Scanning electron microscopy, SEM Leo 1430VP, linked to a system for the microanalysis of elements via energy-dispersive X-ray spectroscopy, Inca 350, version 17 (hereinafter, SEM-EDX). Scanning electron microscopy enables the identification of elements with low atomic numbers, including carbon.

X-ray Diffraction Data Collection and Structure Determination. Single-crystal diffraction data were collected at 100(2) K on a Bruker X8 APEX II and Bruker D8 Venture with a Photon detector equipped with graphite monochromated MoKα radiation (λ = 0.71073 Å). The data reduction was performed with the APEX2 software[37] and corrected for absorption using

SADABS.[2] These structures were solved by direct methods using the SHELXT program[38] and refined by full-matrix least-squares of F2 including all reflections with SHELXL-2018/3 program.[39] All calculations for these structures were performed using the WINGX crystallographic software package.[4]

Powder X-ray diffractions (XRPD) patterns were collected on a Philips X'PERT powder diffractometer with Cu Kα radiation (λ = 1.5418 Å) over the range of $5 < 2\theta < 50°$ with a step size of 0.02° and an acquisition time of 2.5 s per step at 25 °C. Indexation of the diffraction profiles were carried out using the FULLPROF program,[1] on the basis of the space group and cell parameters found for isostructural compounds by single crystal X-ray diffraction.

A6.2 Chemical characterization

A6.2.1 Elemental Analysis

Table A6.1. Elemental analysis of compound **6.1**.

Compound	Formula	Molecular weight	Calc.	Found.
6.1	$C_{78}H_{115}N_{18}O_{36}Y_{3.5}Eu_{1.5}$	2419.98	C: 38.71; H: 4.79; N: 10.42; O: 23.80; Y: 12.86; Eu: 9.42	C: 38.76; H: 4.83; N: 10.44; O: 23.81; Y: 12.88; Eu: 9.46

A6.2.2 Determination of the metal content by ICP-AES

Table A6.2. Determination of the metal content by ICP and Y to Eu relationship.

Compound	Y content in mgL^{-1}	Eu content in mgL^{-1}	Y to Eu relationship
6.1$_{Y\text{-}Eu}$	1672 (18.8 mM)	1268 (8.34 mM)	± 2.25 ~ 2.33

A6.2.3 FT-IR spectroscopy

FTIR spectrum of **Y/Eu-MOF** display a narrow peak at around 3617 cm^{-1} attributed to the N–H stretching vibration of the amine group of 3-amino-4-hydroxbenzoate ligand. Also, an intense and broad band attributable to O–H bond of free ligand along with a set of weak bands between 3325 and 2917 cm^{-1} corresponding to the C–H vibrations of the aromatic ring of the 3-amino-4-hydroxybenzoate ligand are visible in the spectrum. Peaks in 1683–1408cm^{-1} region are associated with asymmetric stretching vibrations of the carboxylate groups and the aromatic C–C and C–N bonds. The group of signals at lower range, 1390–1263 cm^{-1}, can be linked to symmetric stretching vibrations of the carboxylate groups. Remaining bands found at lower frequencies originated by distortions in the aromatic and carboxylate group of the ligand. Note that vibrational bands M–O and M–N bonds are observed below 660 cm^{-1}.

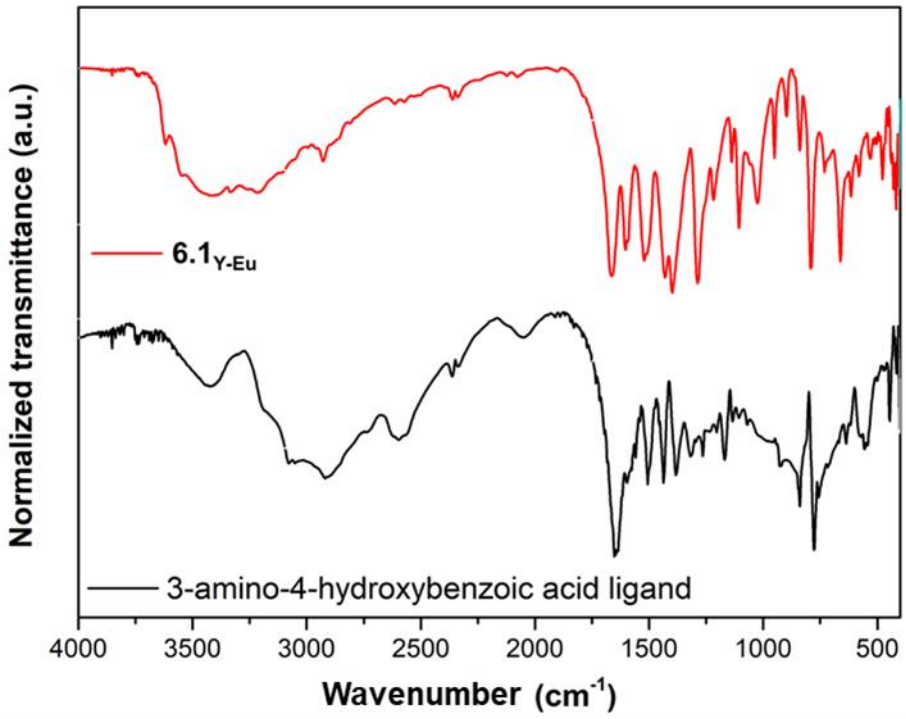

Figure A6.1. Figure of the infrared spectra of the ligand and Y/Eu-MOF.

A6.3 Crystallographic data

Table A6.3. Crystallographic data and structure refinement details of compound **6.1$_{Y\text{-}Eu}$**.

Compound	**6.1$_{Y\text{-}Eu}$**
Formula	$C_{78}H_{115}N_{18}O_{36}Y_{3.5}Eu_{1.5}$
M_r	2419.98
Crystal system	hexagonal
Space group (no.)	*$P6_3/m$ (176)*
a(Å)	15.8510(3)
b(Å)	15.8510(3)
c(Å)	16.8255(7)
α(°)	90
β(°)	90
γ(°)	120
V(Å^3)	3661.1(2)
Z	2
ρ_{calc}g/cm^3	2.193
μ/mm^{-1}	4.130
F(000)	2454.0
Crystal size/mm^3	0.658 × 0.167 × 0.103
Radiation	MoKα (λ = 0.71073)
2θ range for data collection/°	5.14 to 54.952
Index ranges	-18 ≤ h ≤ 20, -20 ≤ k ≤ 20, -21 ≤ l ≤ 21
Reflections collected	72657
Independent reflections	2898 [R_{int} = 0.0886, R_{sigma} = 0.0238]
Data/restraints/parameters	2898/0/123
Goodness-of-fit on F^2	1.127
Final R indexes [I>=2σ (I)]	R_1 = 0.0276, wR_2 = 0.0889
Final R indexes [all data]	R_1 = 0.0341, wR_2 = 0.0922
Largest diff. peak/hole / e Å^{-3}	0.75/-0.52

Table A6.4. Table of the selected bond lengths (Å) and angles (°) for compound **6.1$_{Y\text{-}Eu}$**.

Atom	Atom	Length/Å
Eu1	Eu1^{2}	3.5335(7)
Eu1	Y2	3.9093(3)
Eu1	Y2^{3}	3.9093(3)
Eu2	Y1	3.9093(3)
N1	Eu1	2.507(3)
N1	Y1	2.507(3)
O1	Eu2	2.341(2)
O1	Y1	2.512(2)
O1	Eu1	2.512(2)
O1	Y2	2.341(2)
O2	Y2^{1}	2.419(2)
O3	Y2^{1}	2.428(2)
O4	Eu1	2.3830(19)
O4	Eu1^{2}	2.3831(19)
O4	Y2	2.321(3)
O4	Eu2	2.321(3)
O4	Y1	2.3830(19)
O5	Y2	2.332(3)
O5	Eu2	2.332(3)

^{1}+y, -x+y, 1-z; ^{2}+x, +y,1/2-z; ^{3}1-y; +x-y, +z

Atom	Atom	Atom	Angle/˚	Atom	Atom	Atom	Angle/˚	Atom	Atom	Atom	Angle/˚
Eu1^{4}	Eu1	Y2	63.133(5)	O1^{3}	Eu1	Y2^{2}	135.14(5)	O4	Eu2	Y1	34.30(4)
Eu2	O1	Y1	107.28(8)	O1^{3}	Y1	Eu2	97.73(5)	O4	Y1	N1^{3}	89.48(8)
Eu2	O4	Y1	112.41(8)	O1^{4}	Y2	O1	101.22(10)	O4	Y1	N1^{2}	142.66(9)
N1	Eu1	N1^{3}	81.02(10)	O1^{4}	Y2	O2^{5}	145.35(7)	O4	Y1	N1	133.23(9)
N1	Eu1	O1	65.68(8)	O1^{4}	Y2	O2^{6}	82.25(7)	O4	Y1	O1^{3}	74.26(8)
N1	Eu1	O1^{2}	68.90(8)	O1^{4}	Y2	O3^{6}	87.22(7)	O4	Y1	O1	68.16(8)
N1	Eu1	O1^{3}	137.57(8)	O1^{4}	Y2	O3^{5}	159.46(7)	O4	Y1	O1^{2}	132.92(7)
N1	Eu1	Eu1^{4}	131.40(7)	O1^{4}	Y2	Eu1^{4}	37.84(5)	O4	Y1	Eu2	33.29(6)
N1	Eu1	Y2^{2}	77.87(6)	O1^{4}	Y2	Eu1	84.77(5)	O4^{2}	Eu1	N1^{2}	133.23(9)
N1	Eu1	Y2	100.22(6)	O1^{4}	Eu2	O1	101.22(10)	O4^{2}	Eu1	N1^{3}	142.66(9)
N1	Y1	N1^{3}	81.02(10)	O1^{4}	Eu2	O2^{6}	82.25(7)	O4^{2}	Eu1	N1	89.48(8)
N1	Y1	O1	65.68(8)	O1^{4}	Eu2	O2^{5}	145.35(7)	O4^{2}	Eu1	O1^{2}	68.16(8)
N1	Y1	O1^{2}	68.90(8)	O1^{4}	Eu2	O3^{5}	159.46(7)	O4^{2}	Eu1	O1^{3}	132.92(7)
N1	Y1	O1^{3}	137.57(8)	O1^{4}	Eu2	O3^{6}	87.22(7)	O4^{2}	Eu1	O1	74.26(8)
N1	Y1	Eu2	100.22(6)	O1^{4}	Eu2	Y1	84.77(5)	O4^{2}	Eu1	O4	71.06(8)
N1^{2}	Eu1	N1^{3}	81.02(10)	O2^{5}	Y2	O2^{6}	76.55(11)	O4^{2}	Eu1	O4^{3}	71.06(8)
N1^{2}	Eu1	N1	81.02(10)	O2^{5}	Y2	O3^{5}	53.83(7)	O4^{2}	Eu1	Eu1^{4}	42.15(5)
N1^{2}	Eu1	O1^{3}	68.90(8)	O2^{5}	Y2	O3^{6}	101.49(8)	O4^{2}	Eu1	Y2	68.37(7)
N1^{2}	Eu1	O1	137.58(8)	O2^{5}	Y2	Eu1^{4}	109.74(5)	O4^{2}	Eu1	Y2^{2}	33.29(6)
N1^{2}	Eu1	O1^{2}	65.68(8)	O2^{5}	Y2	Eu1	77.16(5)	O4^{2}	Y1	N1	89.48(8)
N1^{2}	Eu1	Eu1^{4}	131.40(7)	O2^{5}	Eu2	O2^{6}	76.55(11)	O4^{2}	Y1	N1^{3}	142.66(9)
N1^{2}	Eu1	Y2^{2}	100.22(6)	O2^{5}	Eu2	O3^{5}	53.83(7)	O4^{2}	Y1	N1^{2}	133.23(9)
N1^{2}	Eu1	Y2	158.35(6)	O2^{5}	Eu2	O3^{6}	101.49(8)	O4^{2}	Y1	O1	74.26(8)

N1^{2}	Y1	N1^{3}	81.02(10)	O2^{5}	Eu2	Y1	77.16(5)	O4^{2}	Y1	O1^{2}	68.16(8)
N1^{2}	Y1	N1	81.02(10)	O2^{6}	Y2	O3^{6}	53.83(7)	O4^{2}	Y1	O1^{3}	132.92(7)
N1^{2}	Y1	O1^{3}	68.90(8)	O2^{6}	Y2	O3^{5}	101.49(8)	O4^{2}	Y1	O4^{3}	71.06(8)
N1^{2}	Y1	O1^{2}	65.68(8)	O2^{6}	Y2	Eu1^{4}	77.16(5)	O4^{2}	Y1	O4	71.06(8)
N1^{2}	Y1	O1	137.58(8)	O2^{6}	Y2	Eu1	109.74(5)	O4^{2}	Y1	Eu2	68.37(7)
N1^{2}	Y1	Eu2	158.35(6)	O2^{6}	Eu2	O3^{5}	101.49(8)	O4^{3}	Eu1	N1^{3}	133.23(9)
N1^{3}	Eu1	O1^{3}	65.68(8)	O2^{6}	Eu2	O3^{6}	53.83(7)	O4^{3}	Eu1	N1	142.66(9)
N1^{3}	Eu1	O1	68.90(8)	O2^{6}	Eu2	Y1	109.74(5)	O4^{3}	Eu1	N1^{2}	89.48(9)
N1^{3}	Eu1	O1^{2}	137.58(8)	O3^{5}	Y2	Eu1	112.25(5)	O4^{3}	Eu1	O1^{2}	74.26(8)
N1^{3}	Eu1	Eu1^{4}	131.40(7)	O3^{5}	Y2	Eu1^{4}	162.69(5)	O4^{3}	Eu1	O1	132.92(7)
N1^{3}	Eu1	Y2	77.86(6)	O3^{5}	Eu2	Y1	112.25(5)	O4^{3}	Eu1	O1^{3}	68.16(8)
N1^{3}	Eu1	Y2^{2}	158.35(6)	O3^{6}	Y2	O3^{5}	79.17(11)	O4^{3}	Eu1	O4	71.07(8)
N1^{3}	Y1	O1	68.90(8)	O3^{6}	Y2	Eu1	162.69(5)	O4^{3}	Eu1	Eu1^{4}	42.15(5)
N1^{3}	Y1	O1^{3}	65.68(8)	O3^{6}	Y2	Eu1^{4}	112.25(5)	O4^{3}	Eu1	Y2^{2}	68.37(7)
N1^{3}	Y1	O1^{2}	137.58(8)	O3^{6}	Eu2	O3^{5}	79.17(11)	O4^{3}	Eu1	Y2	101.50(6)
N1^{3}	Y1	Eu2	77.86(6)	O3^{6}	Eu2	Y1	162.69(5)	O4^{3}	Y1	N1^{2}	89.48(9)
O1	Eu1	O1^{3}	119.971(3)	O4	Eu1	N1^{3}	89.48(8)	O4^{3}	Y1	N1	142.66(9)
O1	Eu1	Eu1^{4}	90.97(5)	O4	Eu1	N1	133.23(9)	O4^{3}	Y1	N1^{3}	133.23(9)
O1	Eu1	Y2^{2}	97.73(5)	O4	Eu1	N1^{2}	142.66(9)	O4^{3}	Y1	O1^{3}	68.16(8)
O1	Eu1	Y2	34.88(5)	O4	Eu1	O1	68.16(8)	O4^{3}	Y1	O1	132.92(7)
O1	Y2	O2^{6}	145.35(7)	O4	Eu1	O1^{2}	132.92(7)	O4^{3}	Y1	O1^{2}	74.26(8)
O1	Y2	O2^{5}	82.25(7)	O4	Eu1	O1^{3}	74.26(8)	O4^{3}	Y1	O4	71.07(8)
O1	Y2	O3^{6}	159.46(7)	O4	Eu1	Eu1^{4}	42.15(5)	O4^{3}	Y1	Eu2	101.50(6)
O1	Y2	O3^{5}	87.22(7)	O4	Eu1	Y2	33.29(6)	O5	Y2	O1^{4}	79.84(7)
O1	Y2	Eu1	37.84(5)	O4	Eu1	Y2^{2}	101.50(6)	O5	Y2	O1	79.84(7)

O1	Y2	Eu1[4]	84.77(5)	O4	Y2	O1	72.14(7)	O5	Y2	O2[6]	134.13(7)
O1	Eu2	O2[5]	82.25(7)	O4	Y2	O1[4]	72.14(7)	O5	Y2	O2[5]	134.13(7)
O1	Eu2	O2[6]	145.35(7)	O4	Y2	O2[5]	76.39(8)	O5	Y2	O3[6]	83.34(9)
O1	Eu2	O3[6]	159.46(7)	O4	Y2	O2[6]	76.39(8)	O5	Y2	O3[5]	83.34(9)
O1	Eu2	O3[5]	87.22(7)	O4	Y2	O3[6]	128.40(7)	O5	Y2	Eu1	110.21(8)
O1	Eu2	Y1	37.84(5)	O4	Y2	O3[5]	128.40(7)	O5	Y2	Eu1[4]	110.21(8)
O1	Y1	O1[3]	119.971(3)	O4	Y2	O5	134.95(11)	O5	Eu2	O1[4]	79.84(7)
O1	Y1	Eu2	34.88(5)	O4	Y2	Eu1[4]	34.30(4)	O5	Eu2	O1	79.84(7)
O1[2]	Eu1	O1	119.972(3)	O4	Y2	Eu1	34.30(4)	O5	Eu2	O2[6]	134.13(7)
O1[2]	Eu1	O1[3]	119.971(3)	O4	Eu2	O1[4]	72.14(7)	O5	Eu2	O2[5]	134.13(7)
O1[2]	Eu1	Eu1[4]	90.97(5)	O4	Eu2	O1	72.14(7)	O5	Eu2	O3[6]	83.34(9)
O1[2]	Eu1	Y2[2]	34.88(5)	O4	Eu2	O2[6]	76.39(8)	O5	Eu2	O3[5]	83.34(9)
O1[2]	Eu1	Y2	135.14(5)	O4	Eu2	O2[5]	76.39(8)	O5	Eu2	Y1	110.21(8)
O1[2]	Y1	O1[3]	119.971(3)	O4	Eu2	O3[5]	128.40(7)	Y2	O1	Eu1	107.28(8)
O1[2]	Y1	O1	119.972(3)	O4	Eu2	O3[6]	128.40(7)	Y2	O4	Eu1	112.41(8)
O1[2]	Y1	Eu2	135.14(5)	O4	Eu2	O5	134.95(11)	Y2[2]	Eu1	Y2	101.165(7)
O1[3]	Eu1	Eu1[4]	90.97(5)								
O1[3]	Eu1	Y2	97.73(5)								

[1]+y,-x+y,1-z; [2]1-y,+x-y,+z; [3]1+y-x,1-x,+z; [4]+x,+y,1/2-z; [5]-y+x,+x,1-z; [6]-y+x,+x,-1/2+z

A6.4 Powder X-ray diffraction analysis

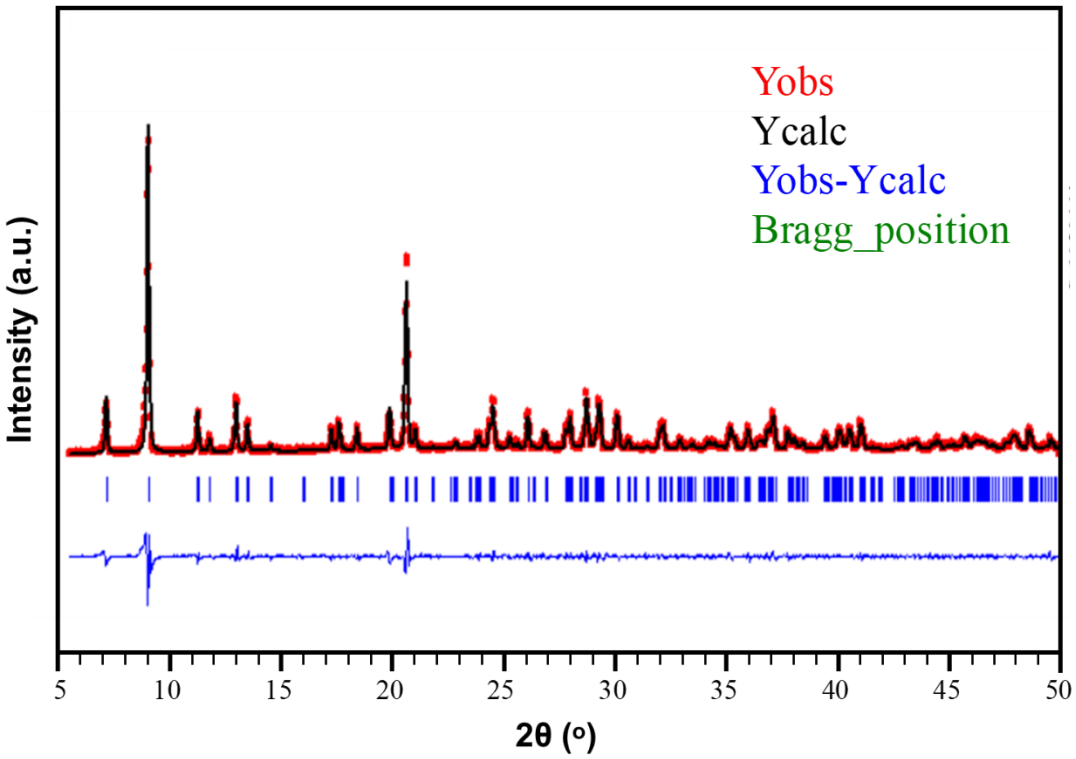

Figure A6.2. Figure of the pattern matching analysis and experimental PXRD for Y/Eu-MOF.

A6.5 Continuous Shape Measurements

CShMs for the coordination environment of **6.1$_{Y\text{-}Eu}$**. The lowest SHAPE values for each ion is shown highlighted in grey, indicating best fits.

Table A6.5. Table of the continuous Shape Measurements for the MN_3O_6 coordination environment.

EP-9	D_{9h}	Enneagon
OPY-9	C_{8v}	Octagonal pyramid
HBPY-9	D_{7h}	Heptagonal bipyramid
JTC-9	C_{3v}	Johnson triangular cupola J3
JCCU-9	C_{4v}	Capped cube J8
CCU-9	C_{4v}	Spherical-relaxed capped cube
JCSAPR-9	C_{4v}	Capped square antiprism J10
CSAPR-9	C_{4v}	Spherical capped square antiprism
JTCTPR-9	D_{3h}	Tricapped trigonal prism J51
TCTPR-9	D_{3h}	Spherical tricapped trigonal prism
JTDIC-9	C_{3v}	Tridiminished icosahedron J63
HH-9	C_{2v}	Hula-hoop
MFF-9	C_s	Muffin

Complex	JCSAPR-9	CSAPR-9	JTCTPR-9	TCTPR-9	MFF-9
M1	2.342	1.370	1.958	**0.666**	2.050

Table A6.6. Table of the continuous Shape Measurements for the MO_8 coordination environment.

OP-8	D_{8h}	Octagon
HPY-8	C_{7v}	Heptagonal pyramid
HBPY-8	D_{6h}	Hexagonal bipyramid
CU-8	O_h	Cube
SAPR-8	D_{4d}	Square antiprism
TDD-8	D_{2d}	Triangular dodecahedron
JGBF-8	D_{2d}	Johnson - Gyrobifastigium (J26)
JETBPY-8	D_{3h}	Johnson - Elongated triangular bipyramid (J14)
JBTP-8	C_{2v}	Johnson - Biaugmented trigonal prism (J50)
BTPR-8	C_{2v}	Biaugmented trigonal prism
JSD-8	D_{2d}	Snub disphenoid (J84)
TT-8	T_d	Triakis tetrahedron
ETBPY-8	D_{3h}	Elongated trigonal bipyramid

Complex	SAPR-8	TDD-8	JBTPR-8	BTPR-8	JSD-8
M2	2.703	**2.693**	3.668	3.234	5.526

A6.6 Scanning Electron Microscopy

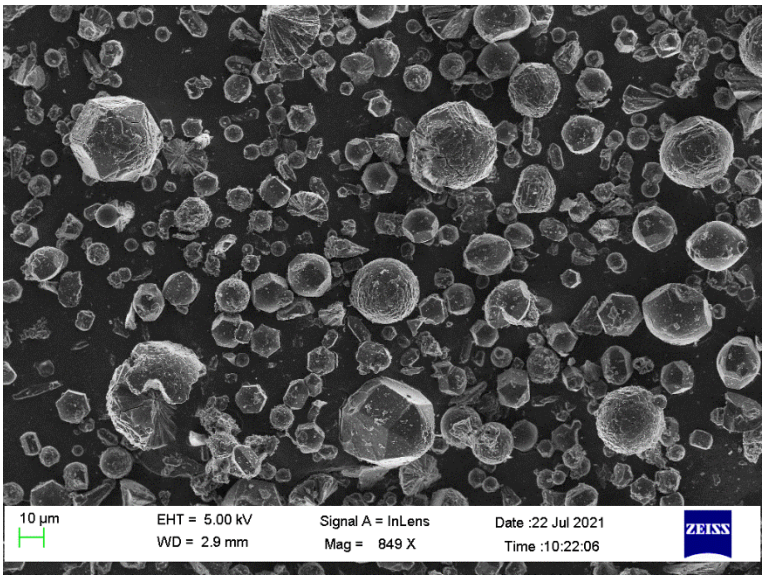

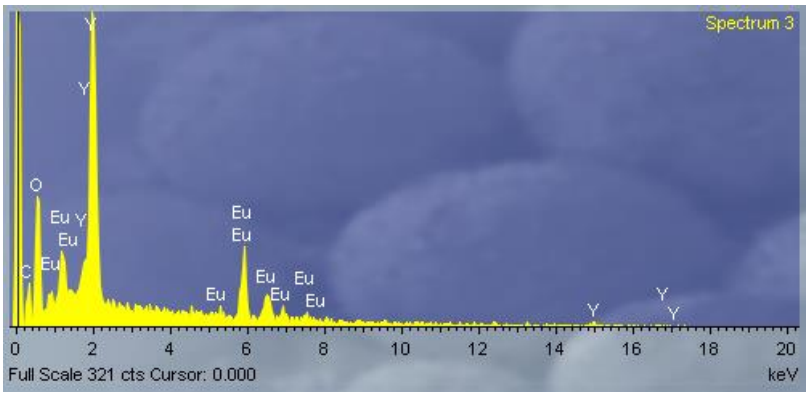

Spectrum	Weight% **O** K_SERIES	Weight% **Y** L_SERIES	Weight% **Eu** L_SERIES	Weight% Total	Atomic% **O** K_SERIES	Atomic% **Y** L_SERIES	Atomic% **Eu** L_SERIES
Spectrum 3	35.707	41.004	21.526	98.237	78.733	16.27	4.997

Figure A6.3. SEM and EDS mapping of bulk material of Y/Eu-MOF.

A6.7 Optimization of the hydroboration reaction conditions

Table A6.7. Optimization of the reaction conditions in the hydroboration reaction.[a]

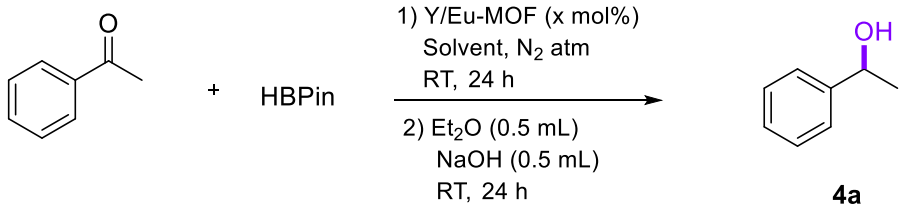

4a

Entry	Y/Eu-MOF (x mol%)	Solvent	Conversion (%)[b]
1	0.35	-	71
2	0.35	PhMe	13
3	0.35	THF	25
4	0.35	DCM	9
5	0.35	CH_3CN	4
6	0.5	-	95
7	0.75	-	95
8	1.1	-	92

[a] Reaction carried out using acetophenone (28 µL, 0.25 mmol), HBPin (40 µL, 0.275 mmol) in 0.5 mL of the corresponding solvent at room temperature and under nitrogen inert atmosphere during 24 h. [b] Conversions (relative to acetophenone) determined by ^{1}H NMR of the reaction crude.

A6.8 Characterization Data of Products

Cyanosilylated carbonyl compounds catalysed by 6.1$_{Y\text{-}Eu}$

2-Phenyl-2-((trimethylsilyl)oxy)acetonitrile (2a). This product has been previously reported.[10] ^{1}H NMR (300.13 MHz, $CDCl_3$): δ 7.50–7.35 (m, 5H, ArH), 5.50 (s, 1H, *CH*CN), 0.23 (s, 9H, TMS) ppm. ^{13}C NMR (75.48 MHz, $CDCl_3$): δ 136.2 (C_{ipso}), 129.3(ArCH), 128.9 (ArCH), 126.3 (ArCH), 119.1 (CN), 63.6 (CH), -0.29 (TMS) ppm.

2-(4-Methoxyphenyl)-2-((trimethylsilyl)oxy)acetonitrile (2b). This product has been previously reported.[12] ^{1}H NMR (300.13 MHz, $CDCl_3$): δ 7.38 (d, *J* = 8.6 Hz, 2H, ArH), 6.92 (d, *J* = 8.6 Hz, 2H, ArH), 5.43 (s, 1H, *CH*CN), 3.82 (s, 3H, OMe), -0.21 (s, 9H, TMS) ppm. ^{13}C NMR (75.48 MHz, $CDCl_3$): δ 160.3 (C_{ipso}), 128.3 (C_{ipso}), 127.9 (ArCH), 119.3 (CN), 114.2 (ArCH), 63.3 (CH), 55.3 (OCH_3), -0.24 (TMS) ppm.

2-(4-Chlorophenyl)-2-((trimethylsilyl)oxy)acetonitrile (2c). This product has been previously reported.[14] ^{1}H NMR (300.13 MHz, $CDCl_3$): δ 7.45–7.40 (m, 5H, ArH), 5.49 (s, 1H, *CH*CN), 0.26 (s, 9H, TMS) ppm. ^{13}C NMR (75.48 MHz, $CDCl_3$): δ 135.3 (C_{ipso}), 134.8 (C_{ipso}), 129.1 (ArCH), 127.7 (ArCH), 118.8 (CN), 63.0 (CH), -0.30 (TMS) ppm.

2-(Pyridin-2-yl)-2-((trimethylsilyl)oxy)acetonitrile (2d). This product has been previously reported.[15] ^{1}H NMR (300.13 MHz, $CDCl_3$): δ 8.60–8.55 (m, 1H, ArH), 7.79 (dt, *J* = 7.7, 1.7 Hz, 1H, ArH), 7.59 (d, *J* = 7.7 Hz, 1H, ArH), 7.35–7.25 (m, 1H, ArH), 5.58 (s, 1H, *CH*CN), 0.26 (s, 9H, TMS) ppm. ^{13}C NMR (75.48 MHz, $CDCl_3$): δ 155.4 (C_{ipso}), 149.3 (ArCH), 137.5(ArCH), 124.0 (ArCH), 120.5 (ArCH), 118.6 (CN), 65.1 (CH), -0.37 (TMS) ppm.

2-((Trimethylsilyl)oxy)butanenitrile (2e). This product has been previously reported.[17] ^{1}H NMR (300.13 MHz, $CDCl_3$): δ 4.34 (t, *J* = 6.3 Hz, 1H, CH), 1.85–1.75 (m, 2H, CH_2), 1.04 (t, *J* = 7.4 Hz, 3H, CH_3), 0.21 (s, 9H, CH_3 x 3) ppm. ^{13}C NMR (75.48 MHz, $CDCl_3$): δ 119.9 (CN), 62.7 (CH), 29.6 (CH_2), 8.9 (CH_3), 0.4 (TMS) ppm.

2-Phenyl-2-((trimethylsilyl)oxy)propanenitrile (3a). This product has been previously reported.[19] ^{1}H NMR (300.13 MHz, $CDCl_3$): δ 7.60–7.50 (m, 2H, ArH), 7.45–7.30 (m, 3H, ArH), 1.86 (s, 3H, CH_3), 0.18 (s, 9H, TMS) ppm. ^{13}C NMR (75.48 MHz, $CDCl_3$): δ 142.0 (C_{ipso}), 128.68 (ArCH), 128.66 (ArCH), 124.6 (ArCH), 121.6 (CN), 71.6 (C), 33.5 (CH_3), 1.03 (TMS) ppm.

2-(4-Methoxyphenyl)-2-((trimethylsilyl)oxy)propanenitrile (3b). This product has been previously reported.[22] ^{1}H NMR (300.13 MHz, $CDCl_3$): δ 7.46 (d, *J* = 8.7 Hz, 2H, ArH), 6.91 (d, *J* = 8.7 Hz, 2H, ArH), 3.82 (s, 3H, OMe), 1.85 (s, 3H, CH_3), 0.16 (s, 9H, TMS) ppm. ^{13}C NMR (75.48 MHz, $CDCl_3$): δ 159.7 (C_{ipso}), 133.9 (C_{ipso}), 126.0 (ArCH), 121.7 (CN), 113.8 (ArCH), 71.2 (C), 55.2 (OCH_3), 33.3 (CH_3), 1.00 (TMS) ppm.

2-(4-Chlorophenyl)-2-((trimethylsilyl)oxy)propanenitrile (3c). This product has been previously reported.[22] ^{1}H NMR (300.13 MHz, $CDCl_3$): δ 7.48 (d, *J* = 8.5 Hz, 2H, ArH), 7.37 (d, *J* = 8.5 Hz, 2H, ArH), 1.83 (s, 3H, CH_3), 0.19 (s, 9H, TMS) ppm. ^{13}C NMR (75.48 MHz, $CDCl_3$): δ 140.6 (C_{ipso}), 134.5 (C_{ipso}), 128.8 (ArCH), 126.0 (ArCH), 121.2 (CN), 71.0 (C), 33.4 (CH_3), 1.00 (TMS) ppm.

2-(2,4-Difluorophenyl)-2-((trimethylsilyl)oxy)propanenitrile (3d). This product has been previously reported.[28] ^{1}H NMR (500.13 MHz, $CDCl_3$): δ 7.56 (td, *J* = 8.8, 6.4 Hz, 1H, ArH), 6.95–6.90 (m, 1H, ArH), 6.86 (ddd, *J* = 11.1, 8.8, 2.5 Hz, 1H, ArH), 1.92 (s, 3H, CH_3), 0.27 (s, 9H, TMS) ppm. ^{13}C NMR (125.77 MHz, $CDCl_3$): δ 163.2 (dd, *J* = 250.8, 12.0 Hz, C_{ipso}-F), 159.4 (dd, *J* = 252.5, 12.0 Hz, C_{ipso}-F), 127.8 (dd, *J* = 9.7, 4.3 Hz, ArCH), 125.0 (dd, *J* = 11.2, 3.9 Hz, C_{ipso}-F), 120.4 (CN), 111.2 (d, *J* = 21.2 Hz, ArCH), 104.9 (t, *J* = 25.6 Hz, ArCH), 68.0 (d, *J* = 2.0 Hz, C), 30.8 (d, *J* = 2.9 Hz, CH_3), 1.08 (TMS) ppm.

2-(Pyridin-2-yl)-2-((trimethylsilyl)oxy)propanenitrile (3e). This product has been previously reported.[29] ^{1}H NMR (300.13 MHz, $CDCl_3$): δ 8.62 (d, *J* = 4.7 Hz, 1H, ArH), 7.77 (t, *J* = 7.8 Hz, 1H, ArH), 7.60 (d, J = 7.8 Hz, 1H, ArH), 7.30–7.25 (m, 1H, ArH), 1.93 (s, 3H, CH_3), 0.26 (s, 9H, TMS) ppm. ^{13}C NMR (75.48 MHz, $CDCl_3$): δ 160.0 (C_{ipso}), 149.0 (ArCH), 137.2 (ArCH), 123.4 (ArCH), 121.3 (CN), 118.9 (ArCH), 72.9 (C), 31.2 (CH_3), 1.06 (TMS) ppm.

2-Methyl-2-((trimethylsilyl)oxy)butanenitrile (3f). This product has been previously reported.[22] ^{1}H NMR (300.13 MHz, $CDCl_3$): δ 1.85–1.65 (m, 2H, CH_2), 1.55 (s, 3H, CH_3), 1.04 (t, *J* = 7.4 Hz, 3H, CH_3CH_2), 0.23 (s, 9H, TMS) ppm. ^{13}C NMR (75.48 MHz, $CDCl_3$): δ 121.9 (CN), 70.2 (C), 36.4 (CH_2), 28.4 (CH_3), 8.6 (CH_3), 1.21 (TMS) ppm.

1-((Trimethylsilyl)oxy)cyclohexane-1-carbonitrile (3g). This product has been previously reported.[22] ^{1}H NMR (300.13 MHz, $CDCl_3$): δ 2.10–2.00 (m, 2H, CH_2), 1.75–1.70 (m, 2H, CH_2), 1.70–1.45 (m, 6H, CH_2 x 3), 1.30–1.20 (m, 2H, CH_2), 0.23 (s, 9H, TMS) ppm. ^{13}C NMR (75.48 MHz, $CDCl_3$): δ 121.9 (CN), 70.6 (C), 39.3 (CH_2), 24.5 (CH_2), 22.6 (CH_2), 1.38 (TMS) ppm.

Hydroborated carbonyl compounds catalysed by 6.1$_{Y\text{-}Eu}$

1-Phenylethan-1-ol (**4a**). This product has been previously reported.[40] ^{1}H NMR (300.13 MHz, $CDCl_3$): δ 7.30–7.20 (m, 5H, ArH), 4.82 (q, *J* = 6.5 Hz, 1H, CH), 1.83 (br s, 1H, OH), 1.42 (d, *J* = 6.5 Hz, 3H, CH_3) ppm. ^{13}C NMR (75.48 MHz, $CDCl_3$): δ 145.8 (C_{ipso}), 128.5 (ArCH), 127.5 (ArCH), 125.3 (ArCH), 70.4 (CH), 25.1 (CH_3) ppm.

1-(4-Isobutylphenyl)ethan-1-ol (**4b**). This product has been previously reported.[41] ^{1}H NMR (400 MHz, CDCl3): δ 7.27 (d, *J* = 8.0 Hz, 2H, ArH), 7.12 (d, *J* = 8.0 Hz, 2H, ArH), 4.86 (q, *J* = 6.4 Hz, 1H, CH), 2.46 (d, *J* = 7.2 Hz, 2H, CH_2), 2.12 (br s, 1H, OH), 2.00–1.75 (m, 1H, CH),

1.48 (d, *J* = 6.5 Hz, 3H, C*H*$_3$CHOH), 0.90 (d, *J* = 6.4 Hz, 6H, CH_3 x 2). ^{13}C NMR (75.48 MHz, $CDCl_3$): δ 143.0, 141.0, 129.2, 125.2, 70.3, 45.1, 30.2, 25.0, 22.4 ppm.

1-(4-Methoxyphenyl)ethan-1-ol (**4c**). This product has been previously reported.[40] ^{1}H NMR (300.13 MHz, $CDCl_3$): δ 7.30 (d, *J* = 8.6 Hz, 2H, ArH), 6.88 (d, *J* = 8.6 Hz, 2H, ArH), 7.85 (q, *J* = 6.5 Hz, 1H, CH), 3.8 (s, 3H, MeO), 1.48 (d, *J* = 6.5 Hz, 3H, CH_3) ppm. ^{13}C NMR (75.48 MHz, $CDCl_3$): δ 159.0 (C_{ipso}), 138.0 (C_{ipso}), 130.6 (ArCH), 113.6 (ArCH), 70.0 (CH), 55.2 (OMe), 25.0 (CH_3) ppm.

1-(4-Chlorophenyl)ethan-1-ol (**4d**). This product has been previously reported.[40] ^{1}H NMR (300.13 MHz, $CDCl_3$): δ 7.30–7.25 (m, 5H, ArH), 4.88 (q, *J* = 6.5 Hz, 1H, CH), 1.85 (br s, 1H, OH), 1.47 (d, *J* = 6.5 Hz, 3H, CH_3) ppm. ^{13}C NMR (75.48 MHz, $CDCl_3$): δ 144.2 (C_{ipso}), 133.0 (C_{ipso}), 128.6 (ArCH), 126.8 (ArCH), 69.7 (CH), 25.2 (CH_3) ppm.

1-(3-Chlorophenyl)ethan-1-ol (4e). This product has been previously reported.[42] ^{1}H NMR (300.13 MHz, $CDCl_3$): δ 7.40–7.35 (m, 1H, ArH), 7.30–7.25 (m, 3H, ArH), 4.91 (q, *J* = 6.4 Hz, 1H, CH), 1.83 (br s, 1H, OH), 1.51 (d, *J* = 6.4 Hz, 3H, CH_3) ppm. ^{13}C NMR (75.48 MHz, $CDCl_3$): δ 147.8 (C_{ipso}), 134.4 (C_{ipso}), 129.8 (ArCH), 127.6 (ArCH), 125.6 (ArCH), 123.5 (ArCH), 69.8 (CH), 25.3 (CH_3) ppm.

1-(2-Chlorophenyl)ethan-1-ol (4f). This product has been previously reported.[42] ^{1}H NMR (300.13 MHz, $CDCl_3$): δ 7.61 (d, *J* = 7.7 Hz, 1H, ArH), 7.35–7.30 (m, 2H, ArH), 7.25–7.20 (m, 1H, ArH), 5.31 (q, *J* = 6.4 Hz, 1H, CH), 2.2 (br s, 1H, OH), 1.51 (d, *J* = 6.4 Hz, 3H, CH_3) ppm. ^{13}C NMR (75.48 MHz, $CDCl_3$): δ 143.0 (C_{ipso}), 131.6 (C_{ipso}), 129.4 (ArCH), 128.3 (ArCH), 127.2 (ArCH), 126.4 (ArCH), 66.9 (CH), 23.5 (CH_3) ppm.

1-(2,4-Difluorophenyl)ethan-1-ol (4g). This product has been previously reported.[43] ^{1}H NMR (300.13 MHz, $CDCl_3$): δ 7.55-7.45 (m, 1H, ArH), 6.95-6.85 (m, 1H, ArH), 6.85-6.75 (m, 1H, ArH), 5.25-5.10 (m, 1H, CH), 1.52 (d, J = 6.5 Hz, 3H, CH_3) ppm. ^{13}C NMR (75.48 MHz, $CDCl_3$): δ 162.1 (dd, *J* = 247.8, 12.2 Hz), 159.6 (dd, *J* = 248.1, 11.9 Hz), 128.6 (dd, *J* = 13.7, 3.8 Hz), 127.5 (dd, *J* = 9.5, 6.5 Hz), 111.2 (dd, *J* = 20.9, 3.5 Hz), 103.6 (t, *J* = 25.4 Hz), 63.9 (d, *J* = 2.5 Hz), 24.0 ppm. ^{19}F-NMR ($CDCl_3$, 282.37 MHz): δ -112.1 (d, *J* = 6.6 Hz), -116.1 (d, *J* = 7.1 Hz) ppm.

2,2,2-Trifluoro-1-(4-fluorophenyl)ethan-1-ol (**4h**): This product has been previously reported.[44] ^{1}H NMR (300.13 MHz, $CDCl_3$): δ 7.55–7.45 (m, 2H, ArH), 7.15–7.10 (m, 2H, ArH), 5.15–5.00 (m, 1H, CH), 2.78 (br s, 1H, OH) ppm. ^{13}C NMR (75.48 MHz, $CDCl_3$): δ 163.4 (d, $^1J_{C\text{-}F}$ = 248.4 Hz), 129.8 (C_{ipso}), 129.3 (d, $^3J_{C\text{-}F}$ = 8.3 Hz), 124.1 (q, $^1J_{C\text{-}F}$ = 282.2 Hz), 115.6 (d, $^2J_{C\text{-}F}$ = 21.5 Hz), 72.1 (q, $^2J_{C\text{-}F}$ = 32.1 Hz) ppm. ^{19}F-NMR ($CDCl_3$, 282.5 MHz): δ -78.6 (d, *J* = 6.1 Hz, 3F), -111.9 (m, 1F) ppm.

1-(Pyridin-2-yl)ethan-1-ol (4i). This product has been previously reported.[45] ^{1}H NMR (300.13 MHz, $CDCl_3$): δ 8.55 (d, *J* = 4.8 Hz, 1H, ArH), 7.75–7.65 (m, 1H, ArH), 7.30 (d, *J* = 8.1 Hz, 1H, ArH), 7.30–7.20 (m, 1H, ArH), 4.91 (q, *J* = 6.5 Hz, 1H, CH), 4.35 (br s, 1H, OH), 1.52 (d, *J* = 6.5 Hz, 3H, CH_3) ppm. ^{13}C NMR (75.48 MHz, $CDCl_3$): δ 163.0 (C_{ipso}), 148.1 (ArCH), 136.8 (ArCH), 122.2 (ArCH), 119.8 (ArCH), 68.8 (CH), 24.25 (CH_3) ppm.

Diphenylmethanol (4j): This product has been previously reported.[41] ^{1}H NMR (400 MHz, CDCl3): δ 7.45-7.25 (m, 10 H, Ar-H), 5.87 (s, 1 H, CH), 2.52 (s, 1 H, OH) ppm. ^{13}C NMR (75.48 MHz, $CDCl_3$): δ 143.8 (C_{ipso}), 128.5 (ArCH), 127.6 (ArCH), 126.5 (ArCH), 76.2 (CH) ppm.

(*E*)-1,3-Diphenylprop-2-en-1-ol (4k): This product has been previously reported.[46]^{1}H NMR (300.13 MHz, $CDCl_3$): δ 7.55–7.20 (m, 10H, ArH), 6.73 (d, *J* = 15.9 Hz, 1H, C*H*-Ph), 6.42 (dd, *J* = 15.9, 6.5 Hz, 1H, C*H*=CH-Ph), 5.42 (d, *J* = 6.5 Hz, 1H, CH-OH), 2.19 (br s, 1H, OH) ppm. ^{13}C NMR (75.48 MHz, $CDCl_3$): δ 124.7 (C_{ipso}), 136.5 (C_{ipso}), 131.5, 130.5, 128.6 (ArCH), 128.5 (ArCH), 127.76, 127.74 (ArCH), 126.6 (ArCH), 126.3, 75.1 (CH) ppm.

Butan-2-ol (4m). This product has been previously reported.[47] ^{1}H NMR (300.13 MHz, $CDCl_3$): δ 3.75–3.70 (m, 1H, CH), 1.67 (br s, 1H, OH), 1.50–1.45 (m, 2H, CH_2), 1.18 (d, *J* = 6.2 Hz, 3H, C*H*$_3$-CH), 0.93 (t, *J* = 7.5 Hz, 3H, C*H*$_3$-CH_2) ppm. ^{13}C NMR (75.48 MHz, $CDCl_3$): δ 69.4 (CH), 32.0 (CH_2), 22.8 (CH_3), 9.9 (CH_3) ppm.

Cyclohexanol (4n): This product has been previously reported.[48,49] ^{1}H NMR (300.13 MHz, $CDCl_3$): δ 3.70–3.55 (m, 1H, CH), 2.05 (br s, 1H, OH), 2.00–1.85 (m, 2H, CH_2), 1.80–1.65 (m, 2H, CH_2), 1.60–1.45 (m, 2H, CH_2), 1.40–1.20 (m, 4H, CH_2 x 2) ppm. ^{13}C NMR (75.48 MHz, $CDCl_3$): δ 70.3 (CH), 35.5 (CH_2), 25.4 (CH_2), 24.1 (CH_2) ppm.

1,2,3,4-Tetrahydronaphthalen-1-ol (4o): This product has been previously reported.[41] ^{1}H NMR (300.13 MHz, $CDCl_3$): δ 7.50–7.40 (m, 1 H, ArH), 7.30–7.05 (m, 3 H, ArH), 4.85–4.75 (m, 1 H, C*H*-OH), 2.90–2.70 (m, 2 H, CH_2), 2.10–1.70 (m, 5 H, CH_2 x 2, CH) ppm. ^{13}C NMR (75.48 MHz, $CDCl_3$): δ 138.8 (C_{ipso}), 137.1 (C_{ipso}), 129.0 (ArCH), 128.7 (ArCH), 127.6 (ArCH), 126.2 (ArCH), 68.1 (CH), 32.3 (CH_2), 29.2 (CH_2), 18.8 (CH_2) ppm.

(1*r*,3*r*,5*r*,7*r*)-Adamantan-2-ol (4p): This product has been previously reported. ^{1}H NMR (300.13 MHz, $CDCl_3$): δ 3.95-3.85 (m, 1H, CH), 2.50–1.50 (m, 15H) ppm. ^{13}C NMR (75.48 MHz, $CDCl_3$): δ 74.5 (CH), 37.5 (CH_2), 36.2 (CH_2), 34.5 (CH), 31.0 (CH_2), 27.5 (CH), 27.0 (CH) ppm.

A6.9 Catalyst recyclability

Recyclability of the catalyst in the cyanosilylation reaction: In a 1 mL vial with a septum screw capped equipped with a stirring bar, the catalysts **Y/Eu-MOF** (6.4 mg, 0.5 mol%) were weighed. Then, the corresponding amount of acetophenone (56 µL, 0.5 mmol) followed by TMSCN (68 µL, 0.55 mmol, 1.1 equiv.) were added and the reaction was stirred under inert N_2 atmosphere at room temperature overnight. After this time, 1.5 mL of DCM was added to the reaction mixture and transferred to a centrifuge tube for the separation of the catalyst. The centrifugation of the mixture was carried out at 12300 rpm during 5 min. After that, the solution was eliminated, and the catalyst was washed with DCM (2 x 1.5 mL). Later on, the catalyst was dried under vacuum and reused in the next cycle of the reaction with the same reaction conditions previously described.

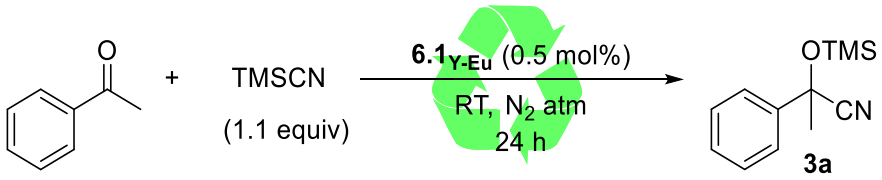

Scheme A6.1. Reaction conditions used for the study of recyclability of Y/Eu-MOF catalysts in the cyanosilylation reaction.

Recyclability of the catalyst in the hydroboration reaction: In a 1 mL vial with a septum screw capped equipped with a stirring bar, the catalysts **Y/Eu-MOF** (9.2 mg, 0.5 mol%) were weighed. Then, the corresponding amount of acetophenone (84 µL, 0.75 mmol) followed by HBPin (120 µL, 0.825 mmol, 1.1 equiv.) were added and the reaction was stirred under inert N_2 atmosphere at room temperature overnight. After this time, 1.5 mL of DCM was added to the reaction mixture and transferred to a centrifuge tube for the separation of the catalyst. The centrifugation of the mixture was carried out at 12300 rpm during 5 min. After that, the solution was eliminated, and the catalyst was washed with DCM (2 x 1.5 mL). Later on, the catalyst was dried under vacuum and reused in the next cycle of the reaction with the same reaction conditions previously described.

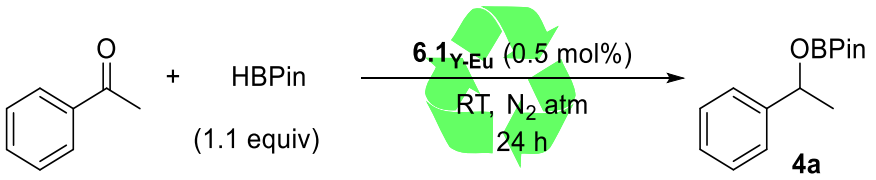

Scheme A6.2. Reaction conditions used for the study of recyclability of Y/Eu-MOF catalysts in the hydroboration reaction.

A6.10 Leaching test

Leaching test: after the first and second reaction of the recyclability test was complete in the hydroboration reaction, the reaction was centrifuged and the supernatant was filtered through a plug of celite and dried under vacuum. Later, 1-(pyridin-2-yl)ethan-1-one (86 µL, 0.75 mmol) and HBPin (120 µL, 0.825 mmol, 1.1 equiv.) were added to the crude of the corresponding reaction cycle and the reaction was stirred under inert N2 atmosphere at room temperature during 24 h. After that time, an aliquot was analysed by ^{1}H NMR obtaining in 38 % and 13 % of product **4j**, corroborating that the leaching of Y or Eu take place.

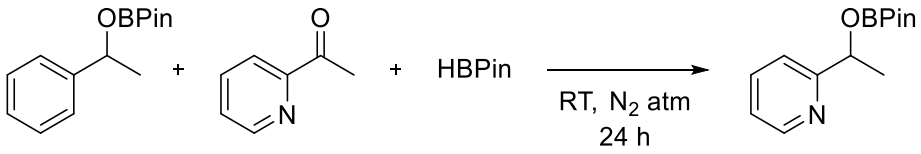

Scheme A6.3. Leaching test carried out after the first and second cycle.

A6.11 TOF of 6.1$_{Y\text{-}Eu}$

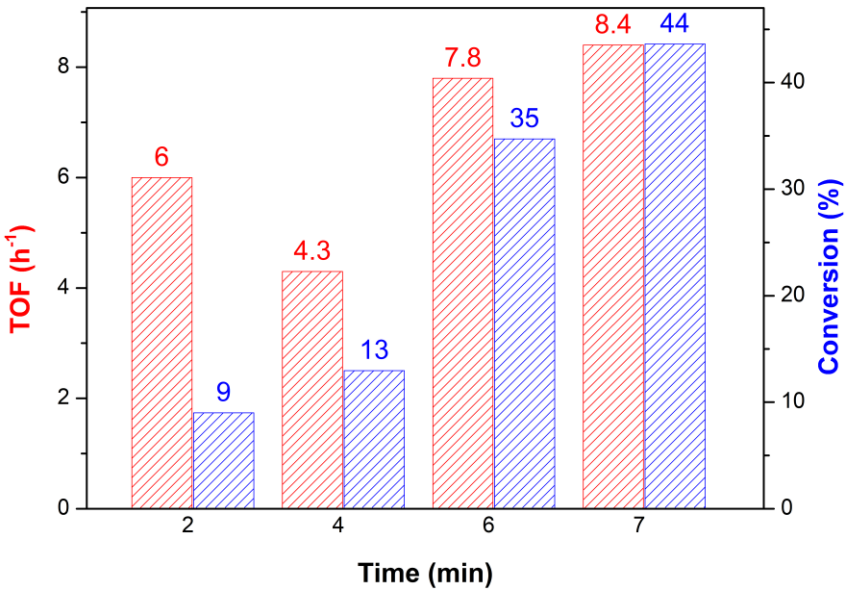

Figure A6.4. Analysis of the TOF (h^{-1}) obtained in the cyanosilylation reaction of acetophenone at different times of reaction with **6.1**$_{Y\text{-}Eu}$ (0.5 mol%) with the optimized reaction conditions.

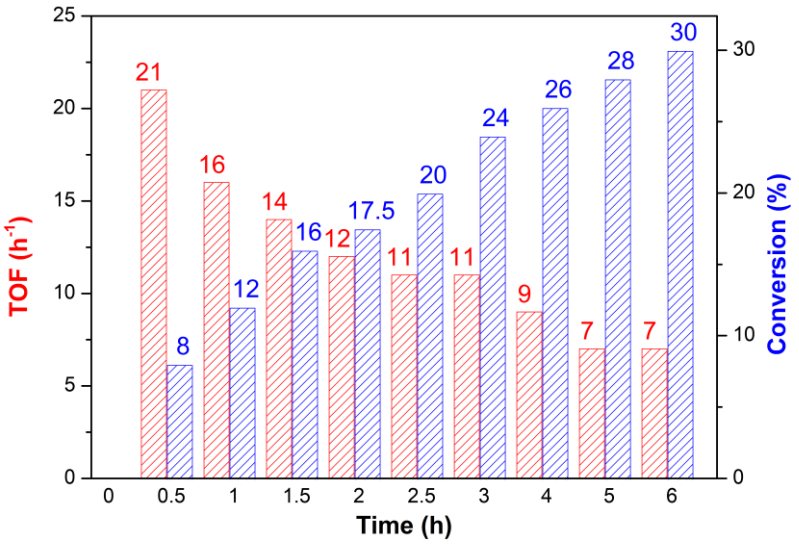

Figure A6.5. Analysis of the TOF (h^{-1}) obtained in the hydroboration reaction acetophenone at different times of reaction with **6.1**$_{Y\text{-}Eu}$ (0.5 mol%) with the optimized reaction conditions.

Reference of appendixes

1. J. Rodríguez-Carvajal FULLPROF 2000,version 2.5d,. *FULLPROF 2000,version 2.5d, Lab. Léon Brillouin (CEA-CNRS), Cent. d'Études Saclay, Gif sur Yvette Cedex, Fr.* 2000.

2. Sheldrick, G.M. SADABS 1996, Program for Empirical Adsorption Correction.

3. Altomare, A.; Burla, M.C.M.C.; Camalli, M.; Cascarano, G.L.G.L.; Giacovazzo, C.; Guagliardi, A.; Moliterni, A.G.G.A.G.G.; Polidori, G.; Spagna, R.; IUCr SIR97: a new tool for crystal structure determination and refinement. *urn:issn:0021-8898* **1999**, *32*, 115–119, doi:10.1107/S0021889898007717.

4. Farrugia, L.J. WinGX and ORTEP for Windows: An update. *J. Appl. Crystallogr.* **2012**, *45*, 849–854, doi:10.1107/S0021889812029111.

5. Farrugia, L.J.; IUCr WinGX suite for small-molecule single-crystal crystallography. *urn:issn:0021-8898* **1999**, *32*, 837–838, doi:10.1107/S0021889899006020.

6. A. Earnshaw *Introduction to Magnetochemistry*; Academic P.; London, 1968;

7. Chilton, N.F.; Collison, D.; McInnes, E.J.L.L.; Winpenny, R.E.P.P.; Soncini, A. An electrostatic model for the determination of magnetic anisotropy in dysprosium complexes. *Nat. Commun.* **2013**, *4*, 1–7, doi:10.1038/ncomms3551.

8. Herdes, C.; Sarkisov, L. Computer Simulation of Volatile Organic Compound Adsorption in Atomistic Models of Molecularly Imprinted Polymers. *Langmuir* **2009**, *25*, 5352–5359, doi:10.1021/LA804168B.

9. Sarkisov, L.; Harrison, A. Computational structure characterisation tools in application to ordered and disordered porous materials. *Mol. Simul.* **2011**, *37*, 1248–1257, doi:10.1080/08927022.2011.592832.

10. Thavornpradit, S.; Killough, J.M.; Bergbreiter, D.E. Minimizing solvent waste in catalytic reactions in highly recyclable hydrocarbon solvents. *Org. Biomol. Chem.* **2020**, *18*, 4248–4256, doi:10.1039/d0ob00734j.

11. Zhu, C.; Tang, H.; Yang, K.; Wu, X.; Luo, Y.; Wang, J.; Li, Y. A urea-containing metal-organic framework as a multifunctional heterogeneous hydrogen bond-donating catalyst. *Catal. Commun.* **2020**, *135*, 105837, doi:10.1016/j.catcom.2019.105837.

12. Wang, W.; Luo, M.; Yao, W.; Ma, M.; Pullarkat, S.A.; Xu, L.; Leung, P.H. Catalyst-free and Solvent-free Cyanosilylation and Knoevenagel Condensation of Aldehydes. *ACS Sustain. Chem. Eng.* **2019**, *7*, 1718–1722, doi:10.1021/acssuschemeng.8b05486.

13. North, M.; Omedes-Pujol, M.; Young, C. Kinetics and mechanism of the racemic addition of trimethylsilyl cyanide to aldehydes catalysed by Lewis bases. *Org. Biomol. Chem.* **2012**, *10*, 4289–4298, doi:10.1039/c2ob25188d.

14. Gu, J.Z.; Wan, S.M.; Kirillova, M. V.; Kirillov, A.M. H-Bonded and metal(II)-organic architectures assembled from an unexplored aromatic tricarboxylic acid: structural variety and functional properties. *Dalton Trans.* **2020**, *49*, 7197–7209, doi:10.1039/d0dt01261k.

15. Wu, W.B.; Zeng, X.P.; Zhou, J. Carbonyl-Stabilized Phosphorus Ylide as an Organocatalyst for Cyanosilylation Reactions Using TMSCN. *ACS Appl. Mater. Interfaces* **2020**, *85*, doi:10.1021/acs.joc.9b03347.

16. Zhang, Z.; Chen, J.; Bao, Z.; Chang, G.; Xing, H.; Ren, Q. Insight into the catalytic properties and applications of metal-organic frameworks in the cyanosilylation of

aldehydes. *RSC Adv.* **2015**, *5*, 79355–79360, doi:10.1039/c5ra13102b.

17. Sharma, M.K.; Singh, D.; Mahawar, P.; Yadav, R.; Nagendran, S. Catalytic cyanosilylation using germylene stabilized platinum(II) dicyanide. *Dalton Trans.* **2018**, *47*, 5943–5947, doi:10.1039/c8dt00043c.

18. Wang, W.; Luo, M.; Li, J.; Pullarkat, S.A.; Ma, M. Low-valent magnesium(I)-catalyzed cyanosilylation of ketones. *Chem. Commun.* **2018**, *54*, 3042–3044, doi:10.1039/c8cc00826d.

19. Harinath, A.; Bhattacharjee, J.; Nayek, H.P.; Panda, T.K. Alkali metal complexes as efficient catalysts for hydroboration and cyanosilylation of carbonyl compounds. *Dalton Trans.* **2018**, *47*, 12613–12622, doi:10.1039/c8dt02032a.

20. Sakai, T.; Miyata, K.; Tsuboi, S.; Takeda, A.; Utaka, M.; Torii, S. A convenient reductive removal of benzylic hydroxyl and trimethylsilyloxyl groups with Me_3SiCl-NaI-MeCN reagent. *Bull. Chem. Soc. Jpn.* **1989**, *62*, 3537–3541, doi:10.1246/bcsj.62.3537.

21. Strappaveccia, G.; Lanari, D.; Gelman, D.; Pizzo, F.; Rosati, O.; Curini, M.; Vaccaro, L. Efficient synthesis of cyanohydrin trimethylsilyl ethers via 1,2-chemoselective cyanosilylation of carbonyls. *Green Chem.* **2013**, *15*, 199–204, doi:10.1039/c2gc36442e.

22. Garnes-Portolés, F.; Rivero-Crespo, M.Á.; Leyva-Pérez, A. Nanoceria as a recyclable catalyst/support for the cyanosilylation of ketones and alcohol oxidation in cascade. *J. Catal.* **2020**, *392*, 21–28, doi:10.1016/j.jcat.2020.09.032.

23. Song, J.J.; Gallou, F.; Reeves, J.T.; Tan, Z.; Yee, N.K.; Senanayake, C.H. Activation of TMSCN by N-heterocyclic carbenes for facile cyanosilylation of carbonyl compounds. *J. Org. Chem.* **2006**, *71*, 1273–1276, doi:10.1021/jo052206u.

24. Kolocouris, A.; Koch, A.; Kleinpeter, E.; Stylianakis, I. 2-Substituted and 2,2-disubstituted adamantane derivatives as models for studying substituent chemical shifts and C-Hax···Yax cyclohexane contacts - results from experimental and theoretical NMR spectroscopic chemical shifts and DFT structures. *Tetrahedron* **2015**, *71*, 2463–2481, doi:10.1016/j.tet.2015.01.044.

25. Jia, Y.; Zhao, S.; Song, Y.F. The application of spontaneous flocculation for the preparation of lanthanide-containing polyoxometalates intercalated layered double hydroxides: highly efficient heterogeneous catalysts for cyanosilylation. *Appl. Catal. A Gen.* **2014**, *487*, 172–180, doi:10.1016/j.apcata.2014.09.005.

26. Wang, F.; Wei, Y.; Wang, S.; Zhu, X.; Zhou, S.; Yang, G.; Gu, X.; Zhang, G.; Mu, X. Synthesis, characterization, and reactivity of lanthanide amides incorporating neutral pyrrole ligand. Isolation and characterization of active catalyst for cyanosilylation of ketones. *Organometallics* **2015**, *34*, 86–93, doi:10.1021/om500924q.

27. Zhu, Y.; Wang, Y.; Liu, P.; Xia, C.; Wu, Y.; Lu, X.; Xie, J. Two chelating-amino-functionalized lanthanide metal-organic frameworks for adsorption and catalysis. *Dalton Trans.* **2015**, *44*, 1955–1961, doi:10.1039/c4dt02048k.

28. Sternberg, Jeffrey Arthur; Adams, J.B. EP0503798A1_Original_document_20210421152633.pdf 1992, 120.

29. Nie, Y.M.; Li, S.H.; Lin, M.Y.; Yan, J. A micro-environment tuning approach for enhancing the catalytic capabilities of lanthanide containing polyoxometalate in the cyanosilylation of ketones. *Chem. Commun.* **2020**, *56*, 3809–3812, doi:10.1039/d0cc01216e.

30. Matsukawa, S.; Kimura, J. TBD-catalyzed cyanosilylation of aldehydes and ketones. *Synth. Commun.* **2016**, *46*, 1947–1952, doi:10.1080/00397911.2016.1241884.

31. Echenique-Errandonea, E.; Pérez, J.M.; Rojas, S.; Cepeda, J.; Seco, J.M.; Fernández, I.; Rodríguez-Diéguez, A. A novel yttrium-based metal-organic framework for the efficient solvent-free catalytic synthesis of cyanohydrin silyl ethers. *Dalton Trans.* **2021**, *50*, 11720–11724, doi:10.1039/d1dt01953h.

32. Øien, S.; Agostini, G.; Svelle, S.; Borfecchia, E.; Lomachenko, K.A.; Mino, L.; Gallo, E.; Bordiga, S.; Olsbye, U.; Lillerud, K.P.; et al. Probing reactive platinum sites in UIO-67 zirconium metal-organic frameworks. *Chem. Mater.* **2015**, *27*, 1042–1056, doi:10.1021/cm504362j.

33. Zhang, L.; Cao, Q.; Gao, F.; Dong, Y.; Li, X. Self-Supported Rhodium Catalysts Based on a Microporous Metal-Organic Framework for Polymerization of Phenylacetylene and Its Derivatives. **2020**.

34. Matthews, C.J.; Elsegood, M.R.J.; Bernardinelli, G.; Clegg, W.; Williams, A.F. Crystal structures of dicarboxy-2,2′-bipyridyl complexes: the role of hydrogen bonding and stacking interactions. *Dalton Trans.* **2004**, 492–497, doi:10.1039/B314539E.

35. Zhou, M.; Robertson, G.P.; Roovers, J. Comparative study of ruthenium(II) tris(bipyridine) derivatives for electrochemiluminescence application. *Inorg. Chem.* **2005**, *44*, 8317–8325, doi:10.1021/IC0510112/SUPPL_FILE/IC0510112SI20050621_035054.PDF.

36. Lea, T. Caco-2 Cell Line. *Impact Food Bioact. Heal. Vitr. Ex Vivo Model.* **2015**, 103–111, doi:10.1007/978-3-319-16104-4_10.

37. Bruker Apex2, B.A.I. Bruker Apex2, Bruker AXS Inc. 2004.

38. Sheldrick, G.M. A short history of SHELX. *Acta Crystallogr. Sect. A Found. Crystallogr.* **2008**, *64*, 112–122, doi:10.1107/S0108767307043930.

39. Sheldrick, G.M. Crystal structure refinement with SHELXL. *Acta Crystallogr. Sect. C Struct. Chem.* **2015**, *71*, 3–8, doi:10.1107/S2053229614024218.

40. Yadav, S.; Vijayan, P.; Yadav, S.; Gupta, R. Ruthenium complexes of phosphine-amide based ligands as efficient catalysts for transfer hydrogenation reactions. *Dalton Trans.* **2021**, *50*, 3269–3279, doi:10.1039/d0dt04401f.

41. Song, H.T.; Ding, W.; Zhou, Q.Q.; Liu, J.; Lu, L.Q.; Xiao, W.J. Photocatalytic Decarboxylative Hydroxylation of Carboxylic Acids Driven by Visible Light and Using Molecular Oxygen. *J. Org. Chem.* **2016**, *81*, 7250–7255, doi:10.1021/acs.joc.6b01360.

42. Luo, N.; Zhong, Y.; Liu, J.T.; Ouyang, L.; Luo, R. An Efficient Hydration and Tandem Transfer Hydrogenation of Alkynes for the Synthesis of Alcohol in Water. *Synth.* **2020**, *52*, 3439–3445, doi:10.1055/s-0040-1707233.

43. Call, A.; Casadevall, C.; Acuña-Parés, F.; Casitas, A.; Lloret-Fillol, J. Dual cobalt-copper light-driven catalytic reduction of aldehydes and aromatic ketones in aqueous media. *Chem. Sci.* **2017**, *8*, 4739–4749, doi:10.1039/c7sc01276d.

44. van der Born, D.; Herscheid, J.D.M.; Orru, R.V.A.; Vugts, D.J. Efficient synthesis of [18F]trifluoromethane and its application in the synthesis of PET tracers. *Chem. Commun.* **2013**, *49*, 4018–4020, doi:10.1039/c3cc37833k.

45. Bhattacharya, P.; Krause, J.A.; Guan, H. Iron hydride complexes bearing phosphinite-

based pincer ligands: Synthesis, reactivity, and catalytic application in hydrosilylation reactions. *Organometallics* **2011**, *30*, 4720–4729, doi:10.1021/om2005589.

46. Nardi, M.; Sindona, G.; Costanzo, P.; Oliverio, M.; Procopio, A. Eco-friendly stereoselective reduction of α,β-unsaturated carbonyl compounds by Er(OTf)3/NaBH4 in 2-MeTHF. *Tetrahedron* **2015**, *71*, 1132–1135, doi:10.1016/j.tet.2014.12.005.

47. Clarke, Z.E.; Maragh, P.T.; Dasgupta, T.P.; Gusev, D.G.; Lough, A.J.; Abdur-Rashid, K. A family of active iridium catalysts for transfer hydrogenation of ketones. *Organometallics* **2006**, *25*, 4113–4117, doi:10.1021/om060049z.

48. Sánchez-Rodríguez, E.P.; Fragoso-Medina, A.J.; Ramírez-Meneses, E.; Gouygou, M.; Ortega-Alfaro, M.C.; López-Cortés, J.G. [N,P]-pyrrole-phosphine ligand: An efficient and robust ligand for Ru-catalyzed transfer hydrogenation microwave-assisted reactions. *Catal. Commun.* **2018**, *115*, 49–54, doi:10.1016/j.catcom.2018.07.009.

49. Consiglio, G.B.; Queval, P.; Harrison-Marchand, A.; Mordini, A.; Lohier, J.-F.; Delacroix, O.; Gaumont, A.-C.; Gérard, H.; Maddaluno, J.; Oulyadi, H. Ph 2 P (BH 3) Li : From Ditopicity to Dual Reactivity. *J. Am. Chem. Soc.* **2011**, *133*, 6472–6480.